IN SEARCH OF CLEARER SKIES? LINKING PLANETARY AEROSOLS FROM THE LABORATORY TO MODELS

by
Sarah E. Moran

A dissertation submitted to The Johns Hopkins University in conformity with the requirements for the degree of Doctor of Philosophy

Baltimore, Maryland
June 2021

Abstract

"We are dreamers, shapers, singers, and makers. We study the mysteries of laser and circuit, crystal and scanner, holographic demons and invocations of equations. These are the tools we employ and we know many things"

– J. Michael Straczynski, *The Geometry of Shadows, Babylon 5*

In this dissertation, I integrate atmospheric modeling and laboratory characterization of clouds and hazes for temperate sub-Neptune exoplanets and Neptune's moon, Triton. I draw on advances in laboratory atmospheric experiments for the Solar System and in modeling for exoplanets, where previously a gap existed between the two. My work continues this laboratory characterization of exoplanet and Triton-like hazes, then ties this information to modeling of diverse worlds. These data are amenable for comparison to observations of exoplanet atmospheres in transmission and reflected light, as well as from potential future missions to the outer Solar System.

The first chapter puts upper limits on the cloud and haze contents of the TRAPPIST-1 planets. Transmission spectroscopy performed with Hubble (HST) suggests these planets do not possess clear hydrogen atmospheres. I reassess this conclusion with updated masses and expand the analysis to include metallicity, cloud top pressure, and haze scattering. I connect laboratory results of particle size and production rate for exoplanet hazes to a one-dimensional atmospheric model, obtaining a physically-based estimate of haze scattering cross sections. I find larger haze scattering cross sections than supported by laboratory measurements are needed in H_2-rich atmospheres for

TRAPPIST-1 d, e, and f to match the HST data. By modeling a cloud deck and high metallicity atmospheres, I also determine that either H_2-rich atmospheres with high altitude clouds (<12mbar) or that metallicities of at least 60x solar with tropospheric (0.1 bar) clouds are required to match HST data. My results therefore suggest secondary atmospheres for the TRAPPIST-1 planets.

The second chapter delves specifically into the chemistry of the laboratory-made exoplanet hazes themselves. I use very high resolution mass spectrometry to measure the chemical components of solid particles produced in atmospheric chamber experiments for exoplanet atmospheres with hydrogen-, water-, and carbon dioxide-rich atmospheres at 300, 400, and 600 K. I detect many complex molecular species with general chemical formulas $C_wH_xO_yN_z$, including oxygen ratios of up to 20%, an order of magnitude greater than that assumed in typical exoplanet haze models. I also find molecular formulas of prebiotic interest in the data, including those for a variety of amino acids, nucleotide bases, and several sugar derivatives. Additionally, the exoplanetary haze analogues exhibit diverse solubilities, which provides insight into their further alteration and evolution in exoplanetary atmospheres.

The final portion of this thesis centers on the physicochemical properties of laboratory hazes produced for a Triton-like atmosphere. Triton conditions have commonalities to the best characterized Titan tholin, yet include larger amounts of carbon monoxide, allowing for a deeper examination of the role of oxygen-bearing molecules on haze properties. Using Fourier Transform Infrared Spectroscopy, I measure the spectra of the analog hazes and measure their composition with high resolution mass spectrometry. When carbon monoxide dominates over methane in the initial gas mixture, oxygen content of the solid particles greatly increases, with observable effects in the near-infrared spectra of the material. These Triton results emphasize the importance of understanding trace species in the pathway to haze formation, particularly regarding the role of carbon-carrier and oxygen-carrier species.

Thesis Committee

Primary Readers

Dr. Sarah M. Hörst (Primary Advisor)
Associate Professor
Department of Earth & Planetary Sciences
Hopkins Extreme Materials Institute
Johns Hopkins University Krieger School of Arts & Sciences

Dr. David K. Sing
Bloomberg Distinguished Professor
Departments of Earth & Planetary Sciences, Physics & Astronomy
Johns Hopkins University Krieger School of Arts & Sciences

Alternate Readers

Dr. Nikole K. Lewis (Secondary Advisor)
Assistant Professor, Deputy Director
Department of Astronomy, Carl Sagan Institute
Cornell University

Dr. Sabine Stanley
Bloomberg Distinguished Professor
Department of Earth & Planetary Sciences; Space Exploration Sector
Johns Hopkins University Krieger School of Arts & Sciences;
Johns Hopkins University Applied Physics Laboratory

Dedicated to that little voice of doubt

in my head that kept saying to give up.

Showed you.

Acknowledgements

"Journey before Destination"

– Brandon Sanderson, *The Stormlight Archive*

"You are what your creators and experiences have made you, like every other being in this universe. Accept that and be done."

– N.K. Jemison, *The Hundred Thousand Kingdoms*

This work is the result of dozens of individuals who have shaped me, supported me, and inspired me. To recognize a few in particular... I thank my teachers throughout the years, especially Therese Keirsey (5th grade science), who first truly recognized my love of space and of writing and nurtured that love, Christine Russell (middle school science), whose enthusiasm for my enthusiasm and excellent teaching set the stage for so much more, Mary Rietbrock (high school chemistry), who taught me about colloids and suspensions and forever changed the way I view a sunset, Magistra Sue Marquis (high school Latin), whose joy of teaching and grounding in the classics made me the goth nerd I am today, Shana Prentiss (high school drama) whose recognition of my techformance abilities gave me the tools to eventually thrive in the lab and in science communication, and Stephen Himes and Kelly Fast (high school English), who taught me to write in a way that's (hopefully) thoughtful, direct, and still pleasing to the ear.

I thank my undergraduate professors and mentors, especially Laura Kay, my undergraduate advisor, who has cheered me on, offered advice, and modeled the kind of badass scientist I hope to be one day. I also thank Kyle Dawson and Marcel Agüeros,

without whom I would not have had the courage to apply to graduate school that second time. I thank the Physics and Astro majors of Barnard College, class of 2015 – you inspire me, challenge me, and I'm so proud of each of us. Keep giving 'em hell, y'all.

I acknowledge that the bulk of this work was done on traditional and unceded land of the Piscataway People, and I honor and mourn the plight and persecution by settler colonialists that has driven them from their home. I also acknowledge that Baltimore City is rife with other racial injustices, especially against its Black residents, and Johns Hopkins in particular has greatly played a part in perpetuating those wrongs. I hope that by recognizing these wrongs, I and the institutions I am part of can begin to reckon and right this history.

I thank the whole of the EPS department, for creating an environment to do science that's supportive, fun, and doesn't take itself too seriously (most of the time). I especially thank all of my committee members past and present, Darryn Waugh, Sabine Stanley, Nikole Lewis, and David Sing. Extra thanks to Darryn for taking me on in the beginning and being happy to see me jump for distant shores, and to David for treating me as an adopted group member from the moment of his arrival at JHU. Thanks to my officemates, source of endless jokes and derivations and general commiseration – Chi Yan, (honorarily) Mariah Baker and Joe Serigano, Michael Radke, Bryné Hadnott, Andrew Annex, and Kristin Showalter Sotzen. To my planetary seminar folks not previously mentioned – Miché Aaron, Regu Angappan, Jamie Miller, Mayuri Sadhasivan, Maddy Turner, and everyone else – thanks for making Fridays exactly as ridiculous as they should be. Special thanks to the Tuesday night Trivia/Sunday brunch crew – Eric Yee, Naomi and Tim Becker, Joe and Rae Browning-Hanson, Junellie González Quiles, Tyler Perez, Freya George, Simon Matthews, Mary Lonsdale, Andrew Annex, Allie Blanchette, and the rest of the irregulars for reminding me to stop and laugh.

To the Hörst Group past and present, Xinting Yu, Chao He, Marcella Yant, Joe Serigano (again), Bryné Hadnott (again), Ashley Lindalia Walker, Amy Wetsch, Chelsea Conrad, and especially my cohort-members Michael Radke and Kristin Showalter Sotzen (again) – I'm endlessly grateful to have done this grad school thing with you all by my side and can't imagine it any other way.

To the roommates I've had in Baltimore who have made a house a home – Anna Marie MacInnis and Eric Yee (again) – your late night chats, love of cats, and shopping addictions to rival my own was a balm in times of stress. Thanks also to my planet frandzzzzzzz, Michael Radke (again?! Come on, Michael, be less helpful) and Zafar Rustamkulov, whose conversation and memes got me through a year of COVID-separation in a way no one else could.

Thanks to the group at IPAG – Véronique Vuitton, Cédric Wolters, Laurène Flandinet, and François-Régis Orthous-Daunay – for letting me loose in your lab, showing me the ins and outs of the Orbitrap, and generally for teaching me more about organic chemistry than this astro major ever expected to learn. Your generosity and expertise know no bounds.

Thanks to the folks at the Space Studies Board of the National Academies of Sciences, Engineering and Medicine – especially Mia Brown, Dan Nagasawa, Art Charo, and Abby Sheffer, along with my fellow interns Jordan McKaig and Osase Omoruyi – for expanding my astronomical worldview and broadening my understanding of what it means to do science.

Thanks also to the STARGATE collaboration for turning me from a nervous first year grad student into something like a scientist. Special thanks to the OGs Kevin Stevenson, Jonathan Fraine, and Jeff Valenti, who treated me like a grown-up scientist from the first and did more for my confidence than I could ever explain, and to the veritable powerhouses of postdocs (former and current) who I look up to, depend upon, and am more grateful to than I could ever say: Natasha Batalha, Hannah Wakeford

(+ Tom), Laura Mayorga, and Erin May.

To my advisors, Sarah Hörst and Nikole Lewis, who have challenged me, altered me, supported me, and both shown me the way and also how to make my own. Your scientific and professional guidance infused with care, kindness, toughness, and insight is unmatched. Thank you for pulling me through my crises of faith and keeping me away from the edge. Thank you for showing me the kind of scientists I want to be. Thanks to Sarah for taking me on when space was tight and being generally goddamn inspiring, and to Nikole for taking me on when I wandered in unannounced and being a steady voice of reason when I needed one most.

I thank the soundtracks that kept me writing and coding when I didn't wanna anymore, but especially Alan Menken, Janelle Monáe, Beyoncé, Elton John, Muse, and the cast of Hadestown. I thank my childhood friends for keeping my head too far out of the clouds and mostly tethered to the ground – Hannah Longstreet Bonello, Jamie Gangl Varney, and Ryan Tucker. To the JHU Rec Yoga instructors Amber, Myriam, Charlotte, and Elena – thank you for helping me find an outlet for my stress and worry and teaching me to, for once, really truly breathe. To Lisa Green-Cudek, thank you for giving me a space for ballet, a balm for the soul. Thank you to my dearest friends for always offering a listening ear, plying me with musicals and movies and laughter when I needed them most, and generally being an incredibly awe-inspiring group of human beings – Ray Rayburn, Alysa Turner, Libby O'Neil, Nora Rose, César San Miguel, and Jess Spake.

Finally, I thank my family members who have believed in me most and who have given me the world(s) so I can look at all the others. Thanks to my extended family who have supported my dreams and always ask all the right questions. Especially thanks to my grandparents, Nancy Grossman, and those who are gone, Ray and Lorraine Sawicki and Charlie Grossman. Thanks also to my aunts Kathleen Blanton (and cousin Liz) and Joan Sawicki for somehow always knowing when I needed a kind

or funny message to keep me going. To my parents – Nancy Moran, who taught me that with intellect comes the responsibility to do good and to jump for the fantastical before the boring; Charlie Moran, who first taught me to love the skies and stars; and Charyl Moran, who taught me to share kindness whenever I could. To my sister, Rachel Moran, whose good humor, utter weirdness, and killer smarts never cease to amaze and without whom I'd be someone else entirely (someone much more boring).

And finally (no really, finally) to my kitty cats, Set and Zorya, who are the very best science and writing buddies anyone could ever have and who remind me that really nothing is more important than food and snuggles, hang the rest. And the very most thanks to my fiancé, Ben Patterson, who has seen all the best and all the worst, who has committed to following me to the ends of this Earth and all the worlds beyond, and without whom I'd be so much less free and flying. I love you, and I truly could not have done this without you (but still only I get to be Doctor, sorry not sorry).

Contents

List of Tables

List of Figures

Chapter 1

Introduction

"If you wish to make an apple pie from scratch, you must first invent the universe."

– Carl Sagan, *Cosmos*

1.1 Foreword

Where to start? How does one sum up five years' worth of work that took turns and stops and starts? No one expects a Global Pandemic[1]. The fourth chapter of this work, intended to continue the previous chapters' focus on exoplanets, instead is now concerned with Triton, Neptune's largest moon. As such, this introduction, which once would have been a "streamlined"[2] discussion of our current understanding about exoplanet aerosols, now must rise to the task of linking exoplanet atmospheres to that of a small, cold outer moon whose atmosphere is so tenuous that we aren't sure whether it persists across its whole year. Forgive me if I aim too high and miss. Yet, we must try, so here goes nothing...[3]

[1] Or the Spanish Inquisition

[2] unlikely

[3] It should be noted that this chapter is the only one that will never be published. No one reads dissertations anyway, right? My inner voice of snarky asides therefore has been allowed to run free, but I have done my best to relegate these to footnotes.

1.2 Planetary Atmospheres Near and Far

All kinds of star systems have been found to have planets, from our own Sun to binary systems to brown and red dwarf stars to white dwarfs to pulsars. The presence of hot Jupiters and now mini-Neptune and super-Earth type planets has revolutionized our understanding of planet formation and star system structure. We went from not knowing for certain if any planets existed outside our Solar System to being able to statistically say that stars, on average, have at least one planet (Fressin et al., 2013). In only 30 years, the field of exoplanets has gone from merely theoretical to bursting with new discoveries. In light of this overload of new exoplanetary data, the atmospheres of distant worlds are within our grasp through models and through spectroscopic observations.

This work all depends on our understanding of the radiative transfer processes within these atmospheres, which depends in turn on composition, particle size, cloud properties and locations, and our ability to model these aspects of the atmosphere in computationally reasonable ways. Furthermore, all of these properties have profound implications for planetary habitability, from determining the surface temperature and allowing liquid water (or other molecular species that could enable life to prosper) to protecting the surface from harmful radiation. Due to the many uncertainties in the above quantities, experimental work provides a way forward to both provide data where it is lacking and inform the data that comes down from telescopic observations. These experiments are only beginning – much analysis remains; more phase space awaits [4].

At the same time, our own Solar System teems with a fascinating diversity of worlds, from terrestrial planets to gas giants to moons with oceans under the surface. The detailed physics and chemistry we can obtain from our own cosmic backyard has

[4] Yay for job security?

much to teach us about the workings of planetary atmospheres, and only by putting together our ideas about the formation and evolution of Solar System planets *and* exoplanets can we hope to know the workings of planets as a whole.

In both our Solar System as well as for exoplanets, initial results powerfully show that experimental work is paramount to understanding future model and observational data in the upcoming era of JWST, large ground based telescopes, future space-based missions, and further Solar System exploration. Our galactic neighborhood grows ever more crowded with potential worlds, and all techniques must work in concert with each other to understand them, near and far.

1.2.1 Atmospheric Origins

Broadly speaking, atmospheres can be broken down into two types, primary and secondary atmospheres. Primary atmospheres are those that are directly accreted from the protoplanetary disk, and are largely comprised of molecular hydrogen and helium, with lesser contributions from other refractories and volatiles, the exact compositions of which are set by the snowlines of each species and evolve with time and location within the disk. The composition of the primary atmosphere, and its C/O ratio in particular, is therefore often treated as a tracer for the location of the planet's formation, though both planetary migration and chemical evolution over the timescale of atmospheric accretion complicate this simple picture (Eistrup et al., 2018). If a planet loses its primary atmosphere – whether due to thermal or hydrodynamic escape, impact erosion, or otherwise – a secondary atmosphere can be generated by volcanic outgassing (e.g., Kite & Barnett, 2020) or cometary impacts (e.g., Zahnle et al., 2020).

Recent work also suggests that there may be a universal control on whether or not a world – within the Solar System or beyond it – maintains an atmosphere, as determined mainly by the balance between instellation and its escape velocity, a concept known

as the "cosmic shoreline[5]" (Zahnle & Catling, 2017); see Figure 1.1. However, such a relation does not tell us whether an atmosphere is thick or thin, primary or secondary. This dichotomy is made more pressing by the fact that the most common planet archetype, sub-Neptunes, appear to be made up of two populations, super-Earths and mini-Neptunes, with a so-called Radius Gap of fewer planets around 1.6 $R_\oplus$ (Fulton & Petigura, 2018; Fulton et al., 2017). This transition in planetary radius could occur through escape of the original, primary atmosphere by photoevaporation or other thermal escape processes or be the natural result of planetary formation (Cloutier & Menou, 2019; Gupta & Schlichting, 2019); see Figure 1.2. Knowing the atmospheric composition could offer a window into a planet's formation and evolutionary history, breaking the degeneracy between these two processes, yet for the vast majority of planets outside our Solar System, our mass and radius measurements are not yet precise enough to constrain even the planet's bulk composition (e.g., Damasso et al., 2018), much less its atmosphere (Batalha et al., 2019).

A multitude of processes clearly shape a planetary atmosphere (overviewed in Figure 1.3) after its formation, including instellation from the host star, atmospheric escape, photochemical and disequilibrium processes in the upper atmospheric layers to dynamics, mixing, and chemical equilibrium at depth for thick atmospheres, or atmosphere-surface interactions for thin atmospheres. The challenge for both astronomers and planetary scientists is to determine which process(es) dominates a particular atmosphere to produce the observed or modeled planet.

1.2.2 Measuring Atmospheres

For worlds of the Solar System, our options to measure the composition and dynamics of atmospheres rely primarily on imaging both from Earth or from flybys/orbital missions, with lesser contributions from solar occultations or, when we're lucky[6], *in*

[5]Sometimes astronomers/planetary scientists can be poetic.
[6]or NASA is especially motivated

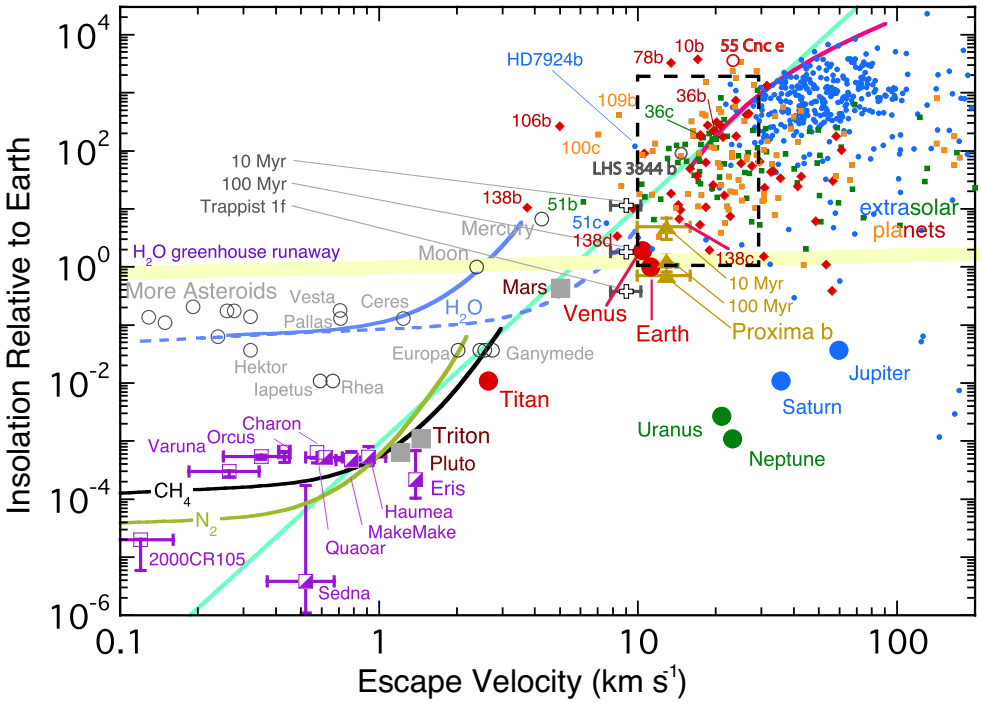

Figure 1.1. The "cosmic shoreline", as proposed in Zahnle and Catling (2017), showing the worlds of the Solar System (colored shapes) and exoplanets (blue circles) with and without atmospheres. Adapted from Zhang (2020).

situ probes. An excellent example of the power of a solar occultation is shown in Figure 1.4. The shape of the lightcurve allows us to observe that Pluto has an atmosphere while Charon does not – the dropoff in flux as Pluto's atmosphere absorbs sunlight is gradual as the atmosphere becomes more and more optically thick, creating a sloped lightcurve before it flattens out, while the flux dropoff from Charon is sharp and immediate as the solid, atmosphere-less body blocks our view of the sun.

Exoplanet transits offer a similar viewing geometry, and if we had the same kind of time and spatial resolution as a flyby, we could perform a similar measurement to detect whether or not a particular planet has an atmosphere. Transmission spectroscopy,

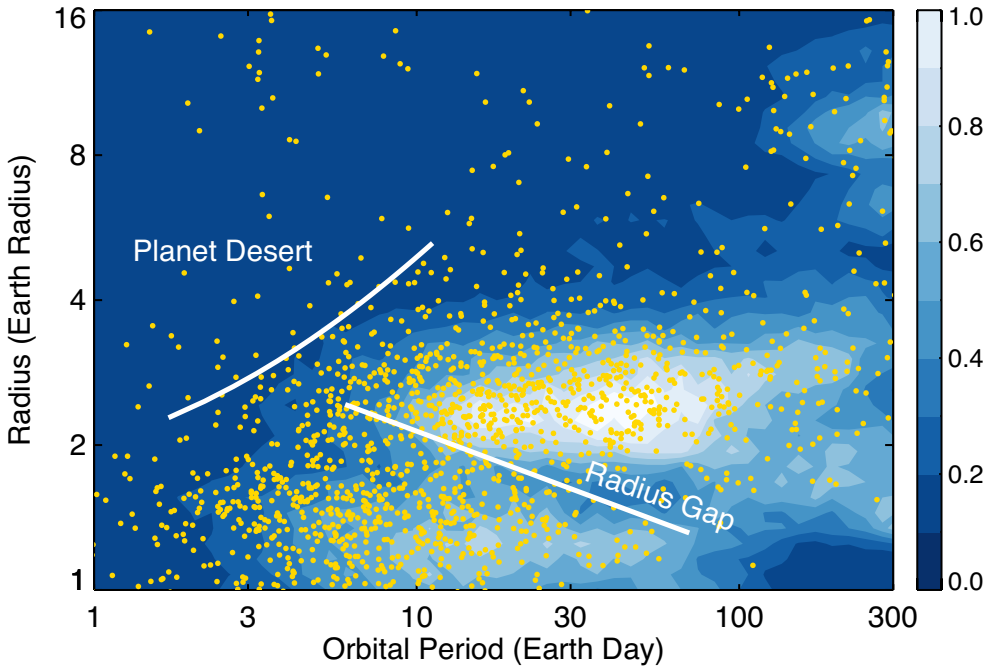

Figure 1.2. The Radius Valley (Fulton et al., 2017), suggesting that sub-Neptune worlds are the most populous in the galaxy with a dearth of planets around 1.6 $R_\oplus$. This valley could form by photoevaporation driving mini-Neptunes into super-Earths (Owen & Wu, 2016). Adapted from Zhang (2020).

by splitting the light up by wavelength, allows us to infer the presence of particular molecular absorbers, enabling atmospheric detections. A schematic of transmission spectroscopy is found in Figure 1.5.

In addition to transmission spectroscopy, exoplanet atmospheres can also be observed through emission spectroscopy, where light directly radiated away by the planet is inferred when the planet is in secondary eclipse with its host star, and from direct imaging, where light reflected directly off the planet is detected. While these latter two techniques have much to teach us about exoplanet atmospheres and their aerosols, here I focus primarily on transmission spectroscopy given its prevalence of use.

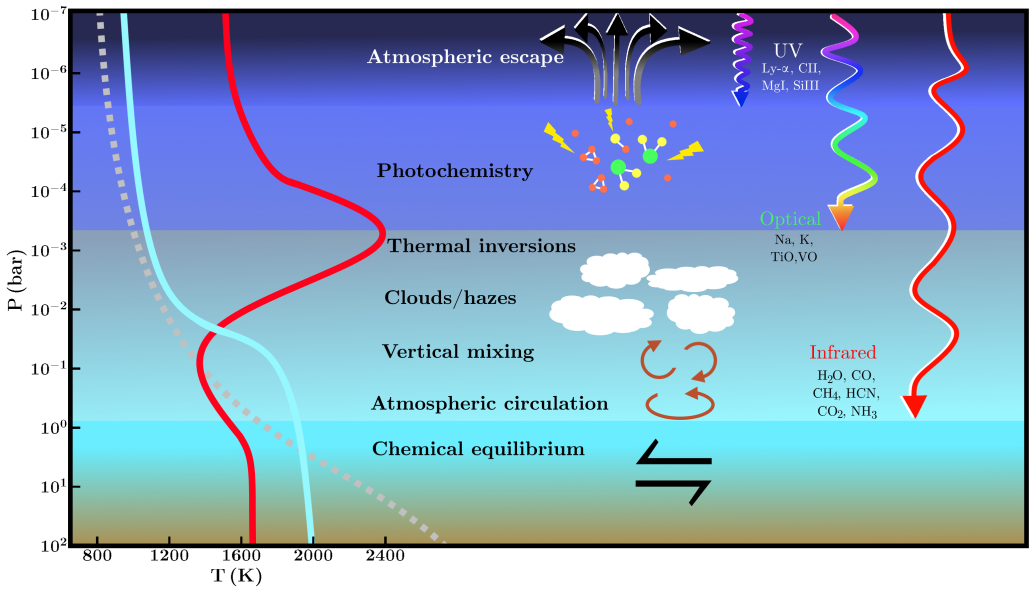

Figure 1.3. An overview of the processes at work in planetary atmospheres and the wavelengths that penetrate each depth of the atmosphere. A subset of elemental and molecular species which can be probed at these wavelengths and temperature profiles of a highly irradiated planet with a temperature inversion (red), without a temperature inversion (blue), and a poorly irradiated planet (grey, dashed) are also shown. Adapted from Madhusudhan (2019).

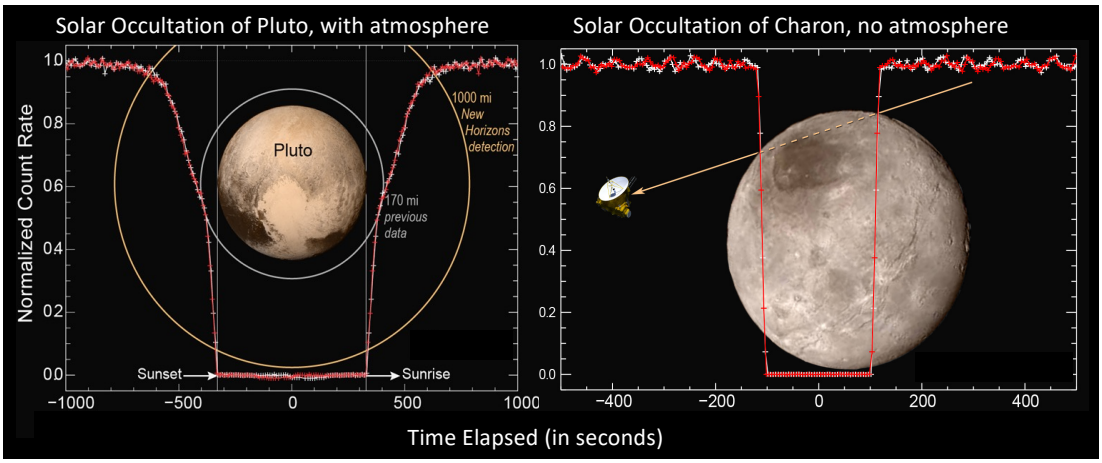

Figure 1.4. A solar occultation of Pluto (right) and its moon Charon (left), from the New Horizons flyby. Flux is shown as a function of time. The shape of the lightcurve shows the presence of an atmosphere vs a world with none. Image credits: NASA/JHUAPL/SwRI

.

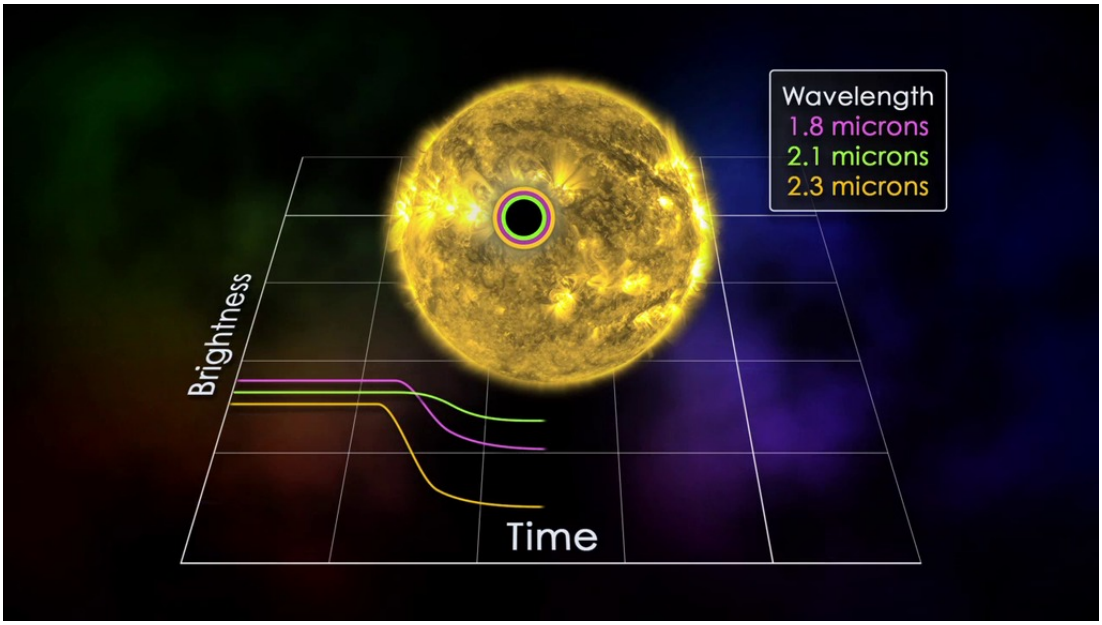

Figure 1.5. A exoplanet transit depth lightcurve, divided by wavelength. At certain wavelengths, the atmosphere is more optically thick and less light is transmitted. Image credits: NASA's Goddard Space Flight Center

.

1.3 Aerosols: Clouds, Hazes, and Tholins

Before we delve into a discussion of the observational evidence for aerosols[7,8] across a diversity of atmospheres, it is instructive to be abundantly clear[9] about the usage of terms. As in Gao et al. (2021), which was itself inspired by Hörst (2016), I use throughout this work the terms "clouds" and "hazes" in the following way: Clouds are particles suspended in the atmosphere that are generated purely through condensation. That is, a temperature-pressure differential forces vapor into solid or liquid particles. In most cases, this process requires moist convective action in the atmosphere, as vapor is lofted to higher (and therefore cooler) altitudes. For hazes, I imply particles

[7]For planetary scientists. if you ask an Earth climate scientist about this, as I did once during a department social hour, your head will hurt.

[8]Writing your dissertation on aerosols during a Global Pandemic^{TM} that is primarily trasmitted by aerosols and which literally forced a reckoning between physical aerosol scientists and infectious disease scientists – https://www.wired.com/story/the-teeny-tiny-scientific-screwup-that-helped-covid-kill/ – is a trip, let me tell you.

[9]Ha!

that are the result of a chemical, and more specifically usually *photo*chemical, process. Incident stellar light breaks apart the constituent gases of the atmosphere, which form ions and radicals that subsequently continue reacting until solid particles of increasing complexity are produced. This process begins naturally then at the top of the atmosphere, or at the depth at which stellar photons are able to penetrate. In this sense, clouds can be thought of as a "bottom-up" phenomena while hazes are more "top-down". Figure 1.6 shows all the major known condensate cloud species temperature-pressure dependencies, along with the atmospheric temperature-pressure profiles of Solar System worlds and a handful of extrasolar worlds and brown dwarfs.

While in some sense these definitions are rather rigid, implying a *physical* underpinning for clouds and a *chemical* underpinning for hazes, the truth is likely murkier[10]. In some cases, the condensable gas in an atmosphere can only form through a chemical reaction, as occurs with the sulfuric acid clouds of Venus. In other cases, hazes themselves may act a seed particles, or cloud condensation nuclei, upon which a cloud may eventually form (e.g., Gao & Benneke, 2018; Yu et al., 2020). Atmospheric dynamics may drive both gases and particles out of equilibrium where they initially form, complicating the simplistic "bottom-up" and "top-down" picture I've painted. Nevertheless, these definitions offer a useful framework for understanding the mechanisms behind aerosol formation on a variety of diverse worlds.

In contrast to these real substances found in planetary atmospheres, we next turn to the definition of "tholin". First coined by Carl Sagan and Bishun Khare in 1979[11], *tholin* refers to the solids or residues produced when gas or ice mixtures are subjected to UV, X-ray, or other energetic discharges which kickstart chemical reactions. These tholins are therefore meant to represent our best guess of the results of a particular planetary atmospheric or surface condition or process, but tholin is *not* the actual

[10] or hazier, if you will

[11] I think *star tar* is better, but they didn't ask me.

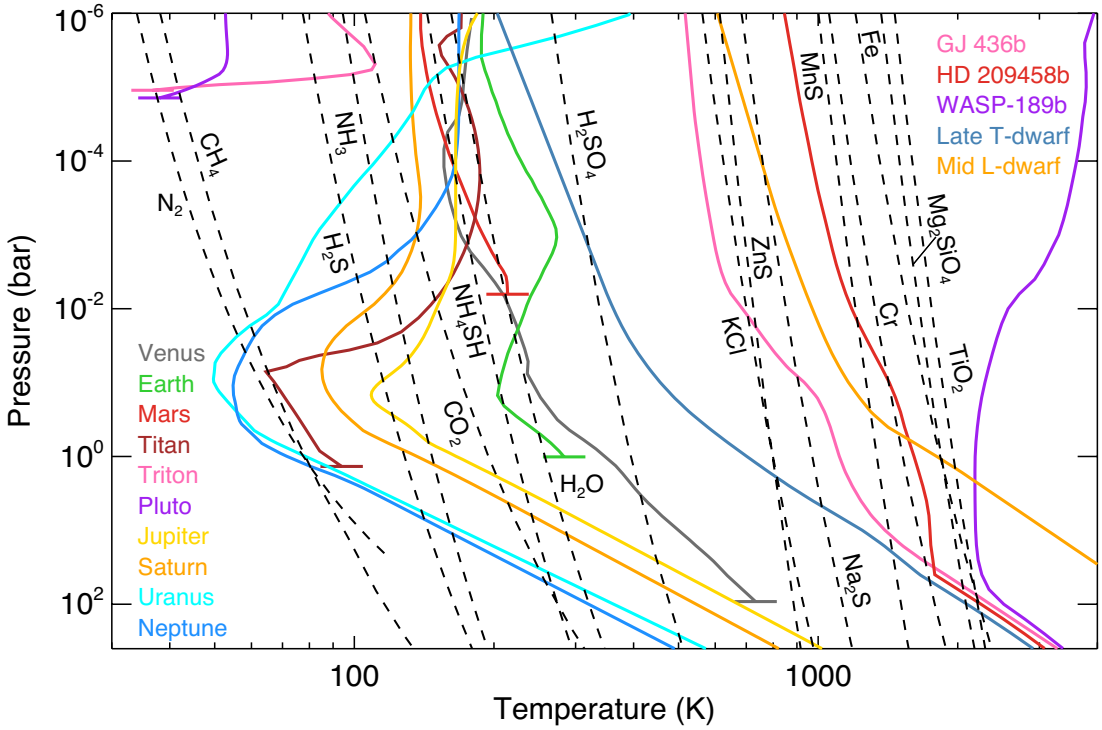

Figure 1.6. Temperature-pressure profiles for all major atmosphere-having Solar System worlds, along with a subset of those for exoplanets and brown dwarfs. GJ 436 b is a sub-Neptune, HD 209458 b a "typical" hot Jupiter, and WASP-189 b an ultra-hot Jupiter. The dashed lines show condensation curves of major expected and observed cloud species. Solar metallicity abundances are assumed for most condensates. Note that these cloud curves are metallicity dependent and since they assume solar metallicity, Venus' temperature-pressure profile does not cross the condensation curve of H_2SO_4 in this schematic at the actual location clouds form on Venus. Additionally, Venus' sulfuric acid clouds are also likely not pure H_2SO_4, but contain some percentage of water as well, depressing the condensation temperature. Adapted from Zhang (2020).

substance that swirls about a planetary atmosphere or coats an icy surface. We use tholins, and the laboratory generally, to better understand the physical and chemical processes and properties of aerosols on other worlds, but until a mission can directly sample this aerosol material[12], we cannot be sure how close our experiments come to reality. While particular properties of specific tholins may match certain observations better than others, we still must always caution that tholins are a laboratory substance, not a real aerosol.

[12] cough–*Dragonfly*–cough

1.4 Observational Evidence for Planetary Aerosols

Many of the exoplanets that host atmospheres have muted transmission spectra (Pont et al., 2008; Wakeford et al., 2019b), indicative of significant and as of yet unconstrained opacity sources in their atmospheres. Aerosols, i.e., clouds and hazes, are a potential explanation for this observational feature. In fact, the very first hot Jupiter exoplanet transmission spectrum showed a weaker sodium feature than expected from a clear sky, solar metallicity atmospheric model (Charbonneau et al., 2002), which could be explained by a high altitude aerosol layer. Since then, muted spectral features have been detected in dozens of atmospheres. Either clouds or hazes in these atmospheres, or some combination thereof, have been invoked to explain the observed spectra of these exoplanets (e.g., Dragomir et al., 2015; Knutson et al., 2014b; Kreidberg et al., 2014a; Sing et al., 2016). Given the ubiquity of clouds and hazes on every world across our own Solar System, aerosols on extrasolar worlds should be expected, not surprising[13]. In fact, the first theoretical studies of hot Jupiters did indeed include cloud treatments (e.g, Brown, 2001; Hubbard et al., 2001; Seager & Sasselov, 2000), but subsequent work then ignored clouds for nearly the next decade.

In the Solar System, evidence for aerosols often comes from imaging, where we see for example the alternating bands of bright and darkly colored clouds on Jupiter or short-lived bright white clouds on Neptune. On hazier worlds, we often see enhancements in blue scattered light in the upper atmosphere, as on Pluto (see Figure 1.7) or Titan. Titan's thick haze in the atmosphere eventually becomes optically thick and gives the moon its characteristic orange color in visible wavelengths.

The more detailed information we gain from spectroscopic studies of Solar System atmospheres can tell us about the particle size and shape, but spectra are often all we have to go on for exoplanet atmospheres, wherein the whole planet is reduced to the

[13] and yet

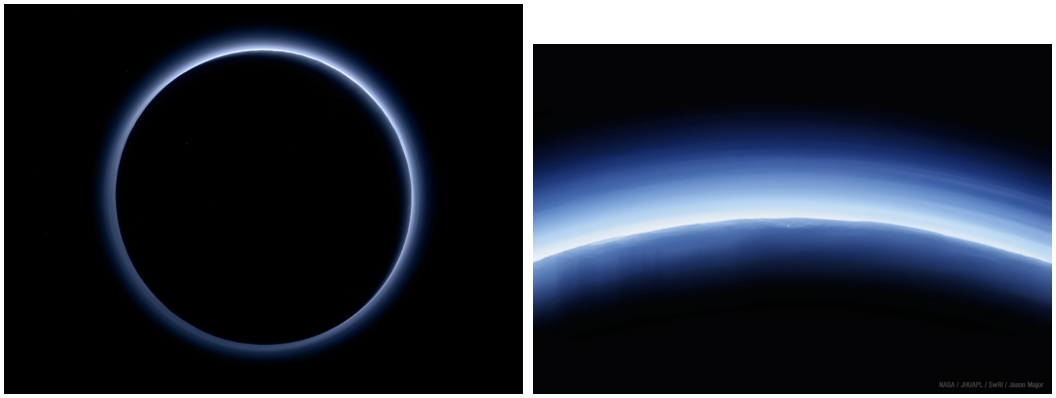

Figure 1.7. Pluto's haze layers, which because of their small particle sizes, are dominated by Rayleigh scattering and appear a serene blue. Image credits: NASA/JHUAPL/SwRI/-Jason Major

.

dimming of light over the course of a planetary transit. A first evidence of diversity in *exo*planetary atmospheres, as is clear exists in the Solar System from the vibrant range of colors and shapes we see, was strongly shown in the collection of hot Jupiter transmission spectra from the PanCET (PanChromatic Exoplanet Treasury) program from Hubble observations, as displayed in Figure 1.8.

There, Sing et al. (2016) showed a continuum of cloudy to clear atmospheres, with increased slopes toward the blue, indicative of smaller, high altitude particles, and weakened features in the infrared around the water band at 1.4μm. The very best evidence for aerosols in a sub-Neptune atmosphere came with the mini-Neptune GJ 1214 b. Its infrared spectrum was measured to extremely high precision with Hubble, disproving a clear solar metallicity atmosphere, a clear water atmosphere, or a clear methane atmosphere, as shown in Figure 1.9. Given its mass and radius, its bulk composition dictates it must be made mostly of hydrogen and helium, yet the measured transmission spectrum is devoid of any molecular features. This was smoking gun evidence that either clouds or hazes (or both) were present in the atmosphere and dramatically altering our telescopic observations. This planet set off a plethora of studies to explain how and what kinds of clouds and hazes could cause the observed

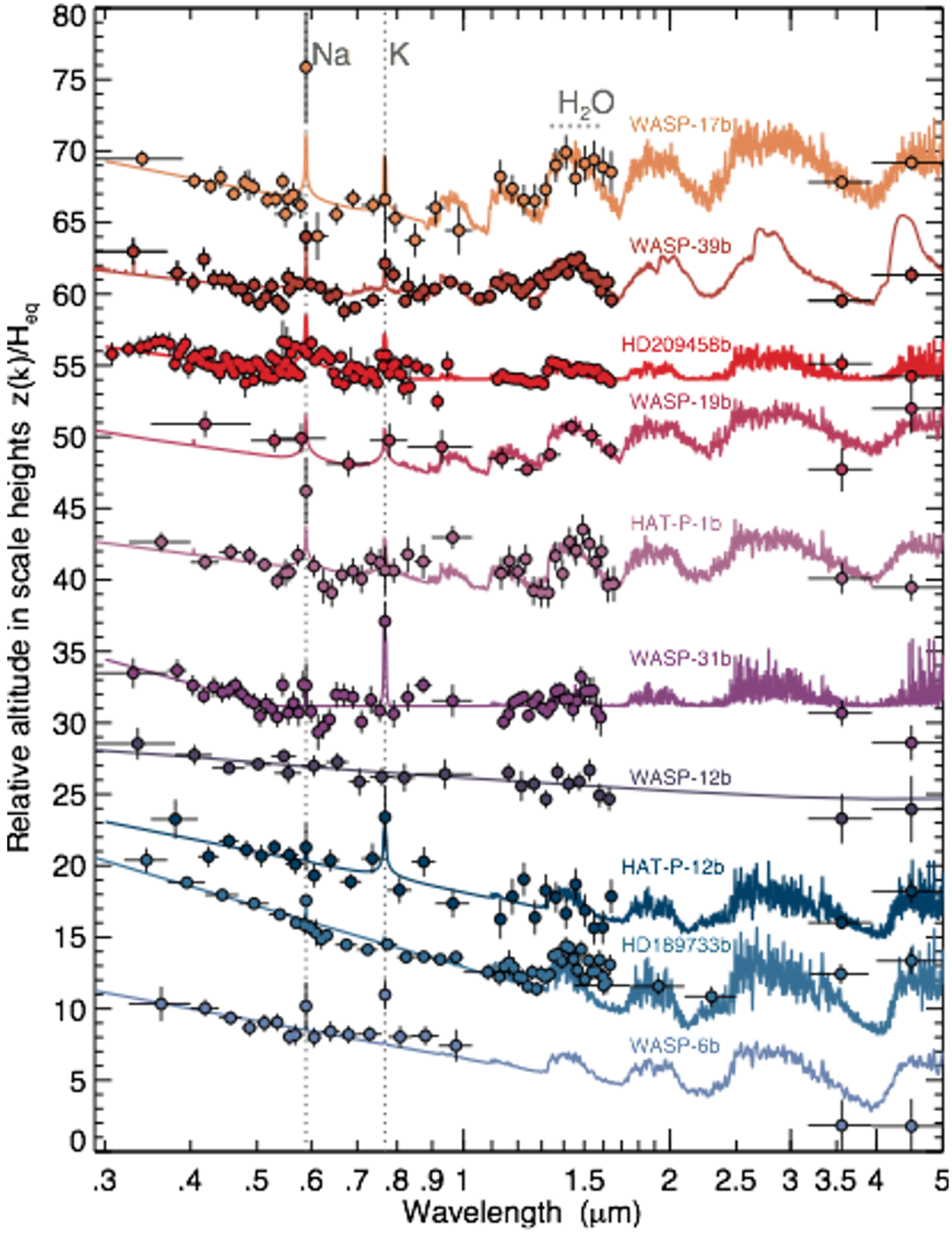

Figure 1.8. The wide diversity of aerosol conditions for a range of hot Jupiter atmospheres, as observed by Hubble. Adapted from Sing et al. (2016).

spectrum (e.g., Charnay et al., 2015; Gao & Benneke, 2018; Miller-Ricci Kempton et al., 2012; Morley et al., 2013; Ohno & Okuzumi, 2018).

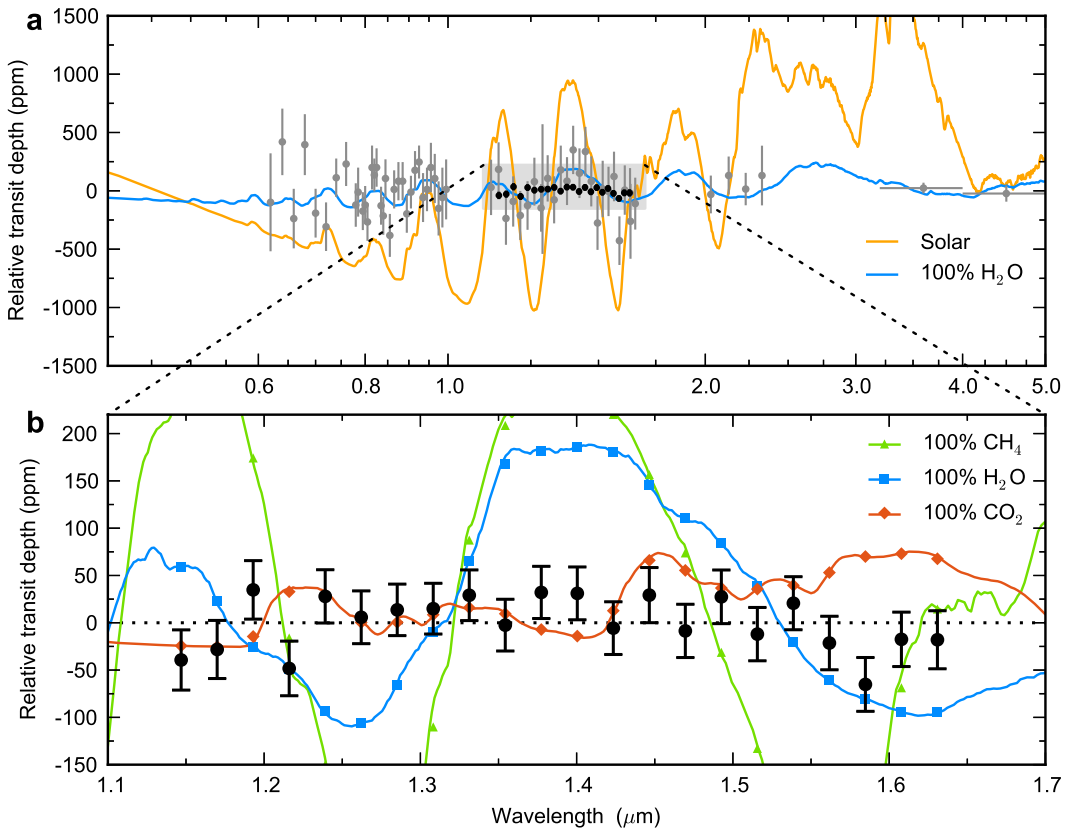

Figure 1.9. Hubble observations of GJ 1214 b. Aerosols must be present in the planetary atmosphere to explain the flatness of the measured transmission spectrum of this mini-Neptune. Adapted from Kreidberg et al. (2014a).

As additional sub-Neptunes amenable to atmospheric characterization have been found and their atmospheres measured, clouds and hazes have been observed to be just a ubiquitous beyond the Solar System as inside it. A very tentative trend has been put forward with the half dozen sub-Neptune planets thus characterized, which suggests, as for hot Jupiters (Gao et al., 2020), that a strong compositional trend exists wherein planetary atmospheres colder than ∼800 K are dominated by photochemical hazes. Crossfield and Kreidberg (2017) suggested this is due to the stronger methane mixing ratios that exist under chemical equilibrium at these temperatures. In Figure 1.10, this tentative trend is shown, with the height of the water feature increasing as a function of increasing temperature. Because spectroscopic measurements of sub-Neptunes are

currently mainly limited to the wavelength coverage and transit depth precisions of Hubble, whether this trend will persist with more planets and at all wavelengths, such as those covered by JWST, remains to be seen.

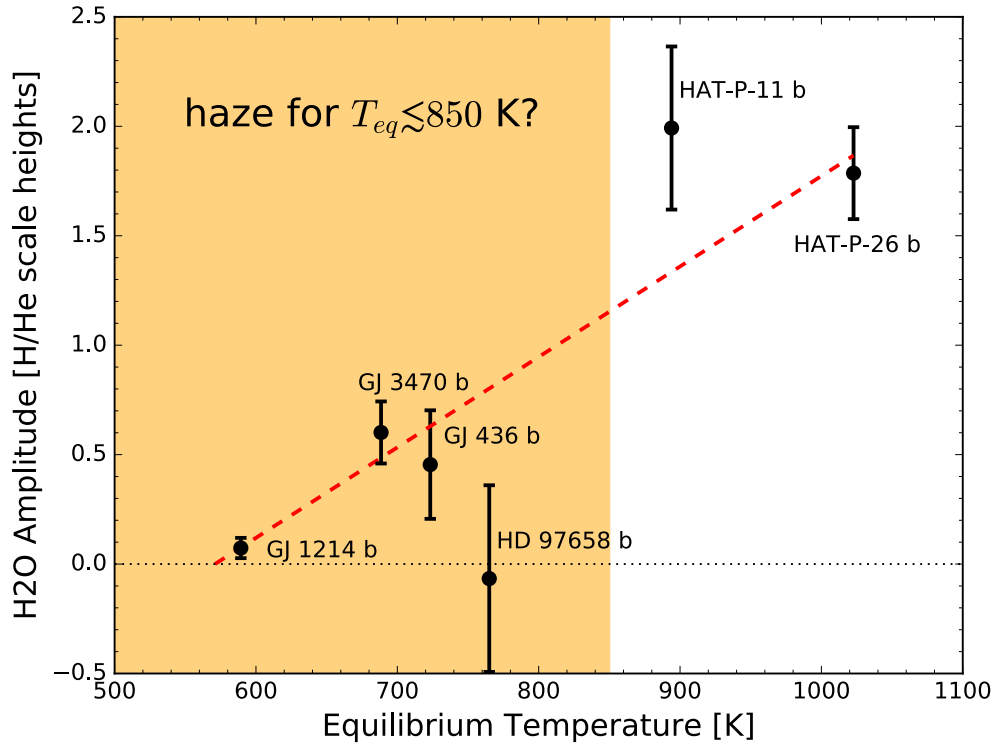

Figure 1.10. An extremely tentative trend of exoplanet haziness with temperature, suggesting that hazier planets are those with temperatures below 800 K. Adapted from Crossfield and Kreidberg (2017).

1.5 Modelling Planetary Atmospheric Aerosols

When attempting to explain the observed contributions of aerosols near and far, the accuracy and efficiency of models depends on the parameterization and simulation of the relevant physical processes. There must be a subtle balance between simplifying the physical equations and resolution so the computational expense is reasonable while still maintaining clear and meaningful results.

1.5.1 Types of Models

The way atmospheric models treat aerosols varies greatly in complexity, with the level of detail in approximating the aerosol's effect on the atmosphere dependent on the exact question we're trying to answer. In the simplest[14] of cases, a highly parameterized model is usually used for the computationally intensive process of atmospheric retrievals. In this case, aerosols are usually treated as a gray cloud absorbing completely at some atmospheric pressure level or as enhanced Rayleigh scattering through either a multiplicative amplitude factor or a higher order power than the 4 used in a true Rayleigh scattering case (e.g., Goyal et al., 2018); see further examples in Gao et al. (2021). Increasing in complexity, spherical particles treated by Mie theory, spatially distributed aerosols, or a few different compositions of aerosol have often been included in retrievals (Barstow, 2020; Gao et al., 2021). A review of the various implementations reveals that while we cannot determine the specific properties of the aerosol with current retrieval efforts, the ultimate effect on the atmosphere overall does not depend on the particular aerosol implementation (Barstow, 2020).

Moving to slightly less parameterized methods, radiative-convective models calculate the temperature and pressure at which a cloud will condense (see Figure 1.6 for examples of these), but do not nescessarily account for the microphysical processes that dictate whether a cloud will actually form. The widely used Ackerman and Marley (2001) – often called "Eddysed" – is frequently used in forward modeling (e.g., Morley et al., 2015) and generates cloud particle distributions by invoking radiative-convective equilibrium and essentially balancing whether a particle can stay aloft or whether it sediments out of the atmosphere. `Eddysed` includes vertical mixing and can treat multiple cloud species at once as long as the optical properties are known. Photochemical models attempt to generate hazes from the initial gaseous

[14] or most complex?

contents of the atmosphere (Hu & Seager, 2014; Kawashima & Ikoma, 2019), but rely implicitly on our knowledge of the relevant chemical reactions[15]. Some pseudo-photochemical models use a "haze efficiency" parameter, where some fraction of a subset of photochemically active gases[16] are agnostically prescribed to end up as haze particles (Morley et al., 2013), the properties of which depend on the particular implementation. Microphysical models are used to kinetically calculate the number, particle size distribution, particle shape, and extent of aerosols. To do this, they calculate the production rate of particles based on their nucleation efficiencies, which in turn are generated from the number density of cloud condensation nuclei and the composition and material properties of the cloud species in question. Various microphysical models exist for use in planetary and exoplanetary aerosols, but some of the more well-known are `CARMA` (e.g., Gao & Benneke, 2018) and `DRIFT` (Helling, 2019), whose heritage come from rather opposite ends of astronomy and planetary science, with the former being developed from Earth-based models and the latter from gas-grain chemistry of molecular clouds.

Finally, in even further complexity, some models treat the full extent of atmospheric mixing through turbulence and diffusive mixing in 3-D GCMs once aerosols are generated in the model. However, these models are somewhat beyond the scope of this thesis and the work it contains, so I direct the reader to a review of these found in Gao et al. (2021)[17].

1.5.2 Radiative Transfer in Atmospheric Models

Cloud and haze properties that affect radiative flux are complex. Thermal emission requires knowledge of the emissivity and temperature of the aerosol particles, while vertical fluxes throughout the atmosphere depend on aerosol particle cross-sections,

[15] which are, to say the least, underconstrained
[16] spoiler: it's almost always methane and its initial photochemical products
[17] this section is already too long and we have to move on.

their scattering phase function, and the albedo for each species in the atmospheric composition for which clouds can form. Additionally, aerosol temporal and spatial evolution is governed by many other processes. Nucleation is the microscopic description of the process by which the gases in the atmosphere condense, for example through collisions of particles in the vapor phase into larger molecules. Evaporation, diffusion, precipitation, and coalescence all also affect the cloud dynamics (Marley et al., 2013).

Due to the lack of observational constraints, the first of many exoplanet atmospheric models treated cloud effects in an extremely simplified manner, by merely accounting for a cloud's influence as a modified surface albedo. A reference case is obtained by adjusting the surface albedo to obtain the mean surface temperature of an Earth-like system. The adjusted surface albedo found to match the observed surface temperature of Earth is then used in all further model calculations, assuming that the net effect of clouds on the climate is captured without regard to cloud composition, size, or optical properties such as scattering or optical thickness (Marley et al., 2013). This method is extremely crude, and cannot be used in cases that significantly deviate from the reference used (usually Earth), as ought to be the case more often than not given the great diversity of planetary atmospheres and their constituents. Less simple models may try to include cloud effects where the particular properties of the clouds are known or have been studied. In the case of water clouds, the microphysics have been developed for Earth models, and mean cloud properties under different atmospheric conditions can be folded in. Still, assumptions about the distribution of cloud condensation nuclei must be made (Gao et al., 2021; Marley et al., 2013).

Specific radiative properties of each atmospheric component must be computed, which means a hierarchy of models are frequently necessary to achieve each coefficient used in a given atmosphere. The atmospheric components of a given atmosphere are determined through spectroscopy, where specific absorption lines denote particular gases. However, planetary atmospheres typically have hundreds of thousands of lines

and features, and the model must determine absorption coefficients for each gas at specific temperature and pressure. Alone, this is already computationally expensive. This is complicated by the fact that there can be huge uncertainties in the exact behavior of absorption features: multiple transitions to non-quantized upper states can create a continuum instead of distinct line features, molecular collisions behave differently than single molecules creating new additional spectral lines, and so on. Some of these collisions may be very rapid, which leads to very wide lines which can overlap and create a continuum rather than individual features (Forget & Lebonnois, 2013).

Several methods for dealing with the radiative transfer problem exist. The simplest is called the gray gas radiative transfer scheme, in which the radiative transfer is simply assumed not to be wavelength dependent[18], and the absorption coefficient is constant across all wavelengths of incoming radiation. Sometimes this is extended to a "semi-gray" regime where shortwave and longwave radiation are treated separately (e.g., Koll & Abbot, 2016). These approximations work fairly well for global means, but absolutely cannot capture many specifics, such as cloud or haze effects. The next approach is called a two-stream approximation, where the radiative flux is broken into an upward stream and a downward stream, instead of having to account for scattering in each direction. For application in planetary atmospheres, the consequence of the two stream approximation is often that one absorption coefficient is used at longer, thermal radiation wavelengths and another approximation is used at shorter wavelengths, as in the semi-gray gas case, but with a slightly more complicated parametrization to represent strong forward scattering by small particles at shorter wavelengths (e.g., Forget & Lebonnois, 2013).

Another approach would be a line-by-line algorithm, wherein the monochromatic equation of radiative transfer is solved at a given wavelength for known lines one by

[18] an utterly incorrect assumption!

one. Databases of spectroscopic molecular absorption information exist for Earth, but the full range of temperature and pressure space to cover Solar System and exoplanet regimes does not. Several databases are actively tackling this problem for other worlds, such as the most frequently used for exoplanets, HITRAN (Gordon et al., 2017) and its offshoot for significantly high temperature atmospheres, HITEMP, and ExoMol (Chubb et al., 2021; Tennyson & Yurchenko, 2012). The parameters in HITRAN and ExoMol are a mixture of direct observations, theoretical calculations which result from quantum-mechanical solutions, and semi-empirical values. Different line lists offer slightly different values of the molecular absorption depending on their accuracy and applicability to a particular atmosphere given temperature and pressure conditions, and thus the choice of line list for a model can have great repercussions in interpreting data (e.g., Madhusudhan, 2019).

A line-by-line calculation is heavily taxing computationally, so many models, particularly already complex ones like Global Circulation Models (GCMs) typically use instead band models, which integrate radiative flux with respect to wavelength over many different lines and attempt to statistically represent the behavior of photons within bandwidths. In this sense, band models are somewhere between a line-by-line and two-stream model. Finally, the most widely used development in radiative transfer algorithms, which is oft used for forward modeling – the subject of Chapter 2 – is the correlated-k distribution technique. In the correlated-k approach, individual absorption intensities derived from a line-by-line spectrum at given temperature and pressure are used to derive probability density distributions at a given resolution (Lacis & Oinas, 1991). In effect, this treats opacity as correlated[19] throughout the atmosphere, and it is generally considered quite accurate while tractable computationally (Leconte, 2021; Zhang et al., 2020).[20]

[19]hence the name

[20]I would like to personally shout out Zhang et al. (2020) for their excellent description of the correlated-k method that was the first to ever make intuitive sense to me. Any failure to translate that here is the fault of mine alone.

Clearly, the addition of a more realistic radiative transfer scheme allows more situations to be probed, and despite the computational cost provides valuable understanding to the conditions and will be paramount to teasing out the possible conditions, including habitability, of exoplanets. However, especially in the case of the new regime of mini-Neptunes and super-Earths, we have little understanding of the wavelength specific behaviors of any atmospheric hazes or clouds, or even what the major atmospheric constituents might be. While a few of these are included in HITRAN, for example, they are a tiny fraction of what likely exists out in the universe. To that end, we must turn to laboratory experiments to begin to probe the possible phase space in order to provide predictions upon which models can rest.

1.6 Experimental Approaches in Planetary Hazes

[21] The vast majority of laboratory experiments investigating hazes have been performed for Titan's atmosphere, though in many ways tholin experiments have heritage back to the Miller-Urey (Miller, 1953; Miller & Urey, 1959) "primordial soup" experiments investigating prebiotic synthesis on the Early Earth. For Titan experiments, gas mixtures primarily are made up of N_2/CH_4 and are performed at room temperature (<300 K) or colder. Such experiments have been performed since the 1970s, even in advance of the Voyager spacecraft's visit to the Saturn system, given the ample evidence for Titan's aerosol layer from remote sensing (e.g., Bar-Nun & Podolak, 1979). Our current knowledge of exoplanet aerosols is in some sense therefore mirroring this history of Titan aerosol work. An excellent in-depth review discussing the effect of the particular energy source, gas mixture, temperature, and experimental set-up on the resulting composition, structure, and optical properties of the solid and the composition and yield of gas phase products for Titan experiments in particular is

[21] Full disclosure, much of this section is adapted from the laboratory section of a recent review of exoplanet aerosols, of which I am a coauthor: Gao et al. (2021). I have expanded upon that section in all its messy glory for this introductory chapter of my thesis.

found in Cable et al. (2012). I discuss the relevant prior experiments for Triton at more length in Chapter 4, but here I focus primarily on the newer generation of exoplanet experiments that have been performed in the last several years.

In general, haze analogue experiments involve exposing various gas mixtures in a chamber under vacuum to an energy source, which dissociates and ionizes molecules that can then recombine and grow into larger haze particles. Initial experiments cover a variety of possible atmospheres and temperatures, from those of hot Jupiters to temperate terrestrial planets. Each laboratory is distinct in its choice of temperature, pressure, and composition phase space, as well as in its technical practicalities such as the gas flow rate and the choice and power of energy source(s). Since only a handful of exoplanet focused experiments have yet been performed, due caution must be taken when drawing larger trends out of their results. This is yet another area where Solar System experiments can offer great insight since they have had much more time to pursue the specifics of any tentative trends exposed by these exoplanet experiments. Additionally, since as discussed above, the true atmospheric constituents of exoplanets are very poorly constrained, gas mixtures in these experiments is either based on equilibrium model predictions or extrapolations of Solar System compositional regimes.

Fleury et al. (2019) performed a study for a hot Jupiter-like atmosphere by running an experiment of H_2 and 0.3% CO at temperatures of 600 K to 1500 K. They exposed this mixture to a UV lamp giving off Lyα, 121.6 nm photons to simulate the photochemistry of the upper atmosphere. No solid aerosol material was observed for most of their temperature range except at 1473 K and after very long UV exposure times, though contamination by the ambient atmosphere influenced their results. In the PHAZER laboratory at JHU, upon which the work of this dissertation is primarily focused[22], He et al. (2018a) and He et al. (2018b), He et al. (2020a), He et al. (2020b), Hörst et al. (2018a) have conducted a series of experiments targeting hazes in

[22]Meaning I have excised discussion of my own results to Chapter 3

mini-Neptunes and rocky planets with temperatures between 300 and 800 K. The gas mixtures chosen for this series of sub-Neptune atmospheres are dominated by H_2, H_2O, and CO_2, with varying amounts of CH_4, CO, NH_3, N_2, and H_2S, as determined by equilibrium chemistry calculations at metallicities from 100× to 10000× solar. Both plasma discharge and UV energy sources were used, mimicking stellar photons for the latter and a more generalized "energetic upper atmosphere" for the former.

These sub-Neptune experiments showed that increasing H_2 tended to decrease aerosol particle production, while the water-dominated atmospheres actually produced more haze than Titan experiments, suggesting that some temperate terrestrial atmospheres may be extremely hazy (He et al., 2018a; Hörst et al., 2018a). The visible appearance of these haze materials are highly diverse, as shown in Figure 1.11, implying that the resulting optical properties and influence of photochemical hazes on spectra will be equally diverse. This result also suggested accompanying diversity in exoplanet haze compositions (the subject of Chapter 3 of this work) would vary greatly as well. In addition, the inclusion of sulfur species appears to dramatically increase haze production in terrestrial-like CO_2 atmospheres, which results in organosulfur haze compositions (He et al., 2020a; Vuitton et al., 2021). Organosulfur hazes are in contrast to the elemental sulfur species, such as S_8, that have been predicted by some photochemical models (Hu & Seager, 2014; Zahnle et al., 2016), underscoring the importance of laboratory work in concert with modeling approaches. Another study examined $N_2/CH_4/H_2S$ gas mixtures (Reed et al., 2020) and also produced organosulfur haze materials, hinting that oxygen-bearing species are not essential to the production of organosulfur hazes, opening the possibility for their presence in more reducing atmospheres. Gas phase compositions from the mini-Neptune and super-Earth experiments include a substantial abundance of organic species (He et al., 2019), the implications for which I explore further in Chapter 3. Previous more oxidizing Solar System gas mixture experiments, mostly focused on the atmospheric

chemistry of the Early Earth, demonstrated that oxygen is readily integrated into the haze particles along with nitrogen and carbon (Hasenkopf et al., 2010; Hörst & Tolbert, 2014; Trainer et al., 2006; Ugelow et al., 2018), which is also borne out further in Chapter 3 and 4 of this dissertation.

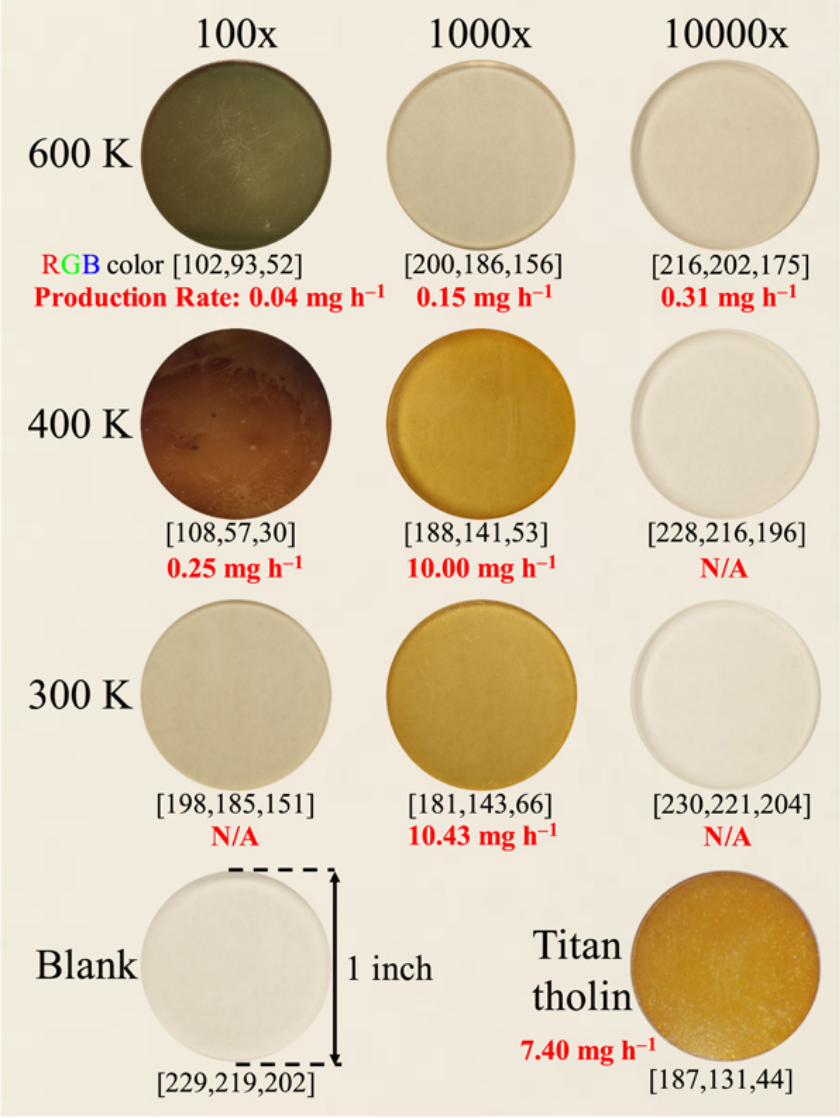

Figure 1.11. Laboratory hazes made from hydrogen-rich, water-rich, and carbon dioxide-rich atmospheres from 300 K to 600 K show significant variance in visible color, hinting at observable differences for future telescope observations of exoplanet aerosols. Adapted from He et al. (2018b).

Critically, exoplanet aerosol experiments have demonstrated that methane, long used in the exoplanet literature as an essential component of haze formation (e.g., Gao

et al., 2020; Kawashima & Ikoma, 2019; Morley et al., 2015), is not always needed to produce substantial amounts of haze (Fleury et al., 2019; He et al., 2018a; He et al., 2020a; He et al., 2020b; Hörst et al., 2018a) and that exoplanet hazes likely contain more than just hydrocarbons or by-products of methane photolysis (Reed et al., 2020; Vuitton et al., 2021). While methane may be an intermediary gas product in some of the experiments that use CO and CO_2 as the primarily carbon reservoir, as in Fleury et al. (2019), gas phase results show that it is not part of the chemical pathway in all cases, which instead seem more dependent on CO or CO_2 photolysis (He et al., 2019; He et al., 2020b). Additionally, photochemical models are typically limited to hydrocarbon species containing up to only five carbon atoms (Arney et al., 2017; Zahnle et al., 2016) or even fewer (Kawashima & Ikoma, 2019), but laboratory work focusing on Titan hazes shows that higher order reactions must be considered to realistically capture aerosol growth (Berry et al., 2019). Taken as a whole, laboratory results have clearly shown that the formation of haze in exoplanet atmospheres is not nearly as simple as that assumed in previous and current models (Gao et al., 2020). Given the vast phase space in temperature and composition that exoplanets likely occupy, a correspondingly complex array of haze species and properties should be inferred.

These results may complicate the idea that a transition exists from silicate clouds to hydrocarbon hazes in light of the possible increase of CH_4 below 950 K (Crossfield & Kreidberg, 2017; Gao et al., 2020). However, both the hot Jupiter results (Fleury et al., 2019) and the mini-Neptune/super-Earth results (He et al., 2018b) tentatively suggest that increased temperatures result in refractory haze particles, which could be consistent with hydrocarbon "soots" that are also sometimes used in exoplanet modeling studies (Gao et al., 2020; Lavvas & Koskinen, 2017; Morley et al., 2013). Many more experiments must be performed to fully validate this hypothesis in conjunction with observations to test the proposed hydrocarbon haze to silicate cloud

transition.

Gavilan et al. (2017) and Gavilan et al. (2018) conducted spectroscopy and ellipsometry of solid material produced from essentially Titan-like atmospheres at 300 K, with the addition of CO_2. They found that the aerosols they made were composed of complex organics, with prominent amide, hydroxyl, and carbonyl groups. In addition, the increased oxidation of the hazes were found to strongly increase their absorptivity in the UV and the mid-IR, particularly between 0.13 and 0.3 μm and 6 and 10 μm, as well as blueshift the absorption edge from the visible to the UV, consistent with an early Earth experiment of similar composition (Hasenkopf et al., 2010). In contrast, another similar composition early Earth-focused laboratory study, but which also contained molecular oxygen, found no UV absorption from oxidized hazes, though their experimental set-up limited their results to discrete wavelength measurements at 405 and 450 nm (Ugelow et al., 2018). These works constitute the only measurements of spectra or refractive indices of exoplanet haze analogs thus far and likely represent only a tiny fraction of the potential diversity of haze optical properties. Solar system studies have shown that gas composition, pressure, temperature, and energy source all impact the spectral response of the resulting haze particles (Brassé et al., 2015; Imanaka et al., 2004).

Measuring the optical properties of exoplanet aerosol materials allows for a direct link to observations and models of exoplanet atmospheres. While refractive indices of a variety of cloud compositions exist (Wakeford & Sing, 2015); see Figure 1.12, these measurements are not necessarily representative of exoplanet atmospheric conditions since most were performed at temperatures and pressures easier to replicate in Earth-based laboratories. Meanwhile, the most frequently used (e.g., Gao et al., 2020; Kawashima & Ikoma, 2019; Kitzmann & Heng, 2018; Morley et al., 2015; Ohno & Kawashima, 2020; Wakeford & Sing, 2015) set of haze refractive indices in exoplanet investigations have come from the work of Khare et al. (1984), who measured the

optical properties of Titan tholins from the X-ray to mid-IR. Given the diversity in visible color seen in Figure 1.11, this assumption for the refractive of indices of exoplanet hazes is likely quite simply incorrect, but without wide wavelength coverage of more relevant exoplanet-like hazes[23], the reliance on Khare et al. (1984) will likely continue.

The particle size distribution of aerosols offer a glimpse of the microphysical processes involved in aerosol formation and growth. Size distributions measured by He et al. (2018a), He et al. (2018b), He et al. (2020b) for the temperate, high metallicity mini-Neptune and super-Earth atmospheres ranged between 20 and 200 nm for the temperatures, initial gas mixtures, and energy sources considered (Figure 1.13), which would be able to produce spectral slopes in optical and near-infrared exoplanet transmission spectra, as further discussed in Chapter 2. Size distributions were wider for experiments conducted with UV as the energy source than for those conducted with plasma, but the plasma experiments generated more particles. This variance in particle sizes likely results from the difference in energy densities imparted by the UV versus the plasma discharge, but extrapolation to meaningful proxies for diverse stellar types is unclear (see discussion in Chapter 3). High temperatures produced narrower size distributions than cooler temperatures, but the cooler temperatures bore the largest particles. Higher metallicity atmospheres produce both more and larger particles, suggesting that the increased chemical complexity of the atmosphere is able to generate increasingly large, complex molecules. This is further displayed with the addition of sulfur in the form of H_2S to the initial gas mixture, which resulted not only in increased particle production (He et al., 2020a), but also in larger particle effective densities (Reed et al., 2020). Microscopy of the particles showed that not all of them are spherical, and that some particles clump into more aggregate structures, while some form linear chains. Though this is qualitatively consistent with modeling

[23]just you wait

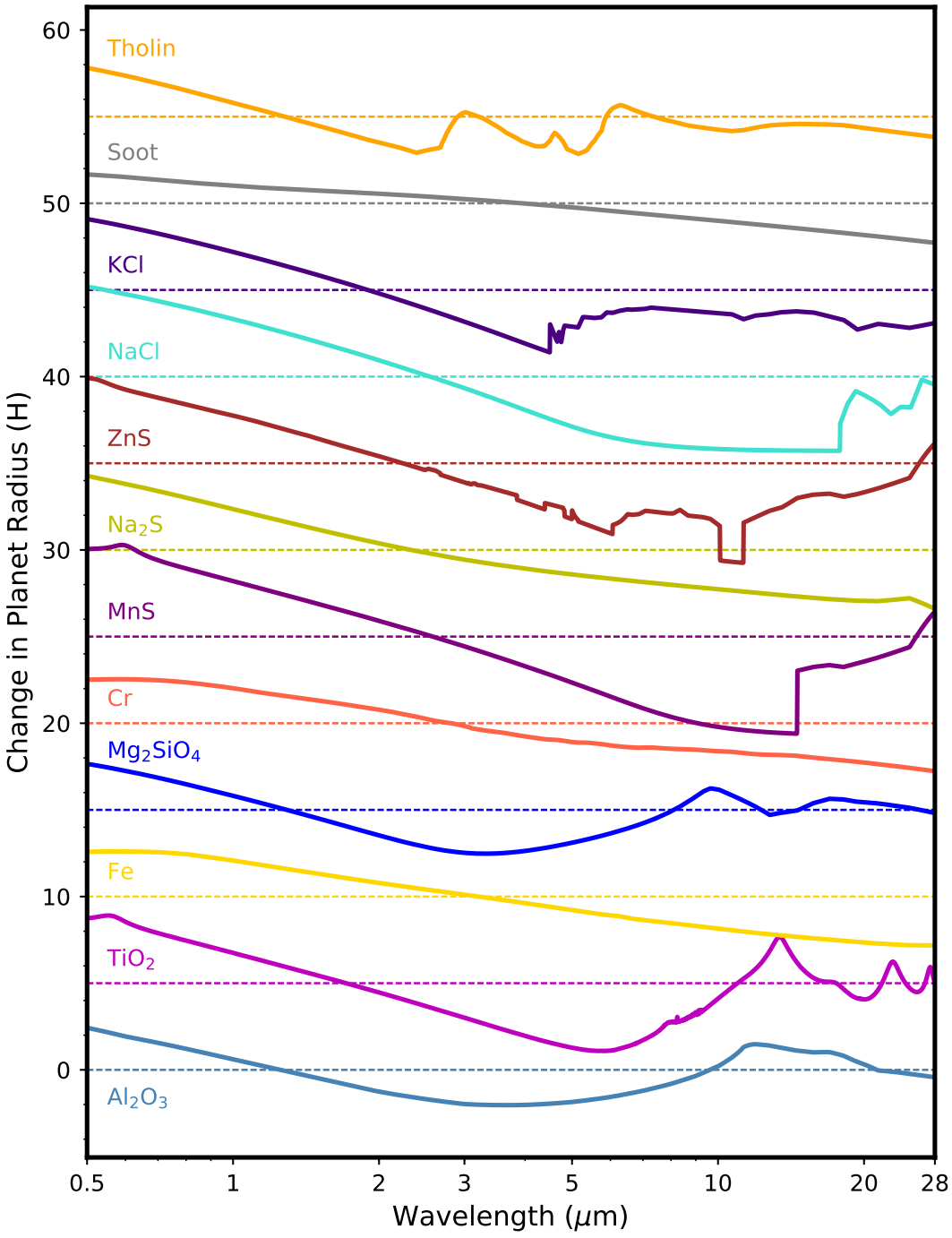

Figure 1.12. The scattering behavior of various proposed exoplanet aerosols, including the Titan-like tholin of Khare et al. (1984), as a function of the spectral features normalized by atmospheric scale height. Adapted from Gao et al. (2021)

.

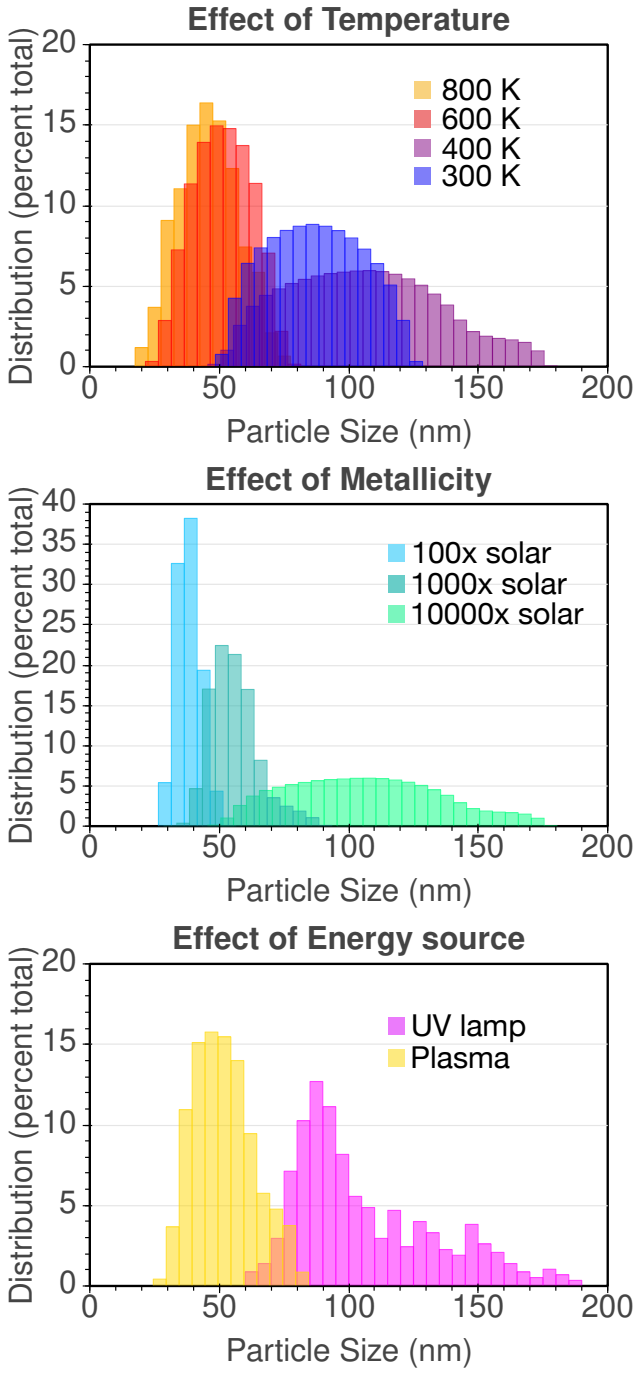

Figure 1.13. Summary of particle size distributions from the laboratory haze experiments of He et al. (2018a), He et al. (2018b), He et al. (2020a) for 300–800 K (top), 100×–10000× solar metallicity (middle) atmospheres bombarded by UV photons and plasma discharges (bottom). Adapted from Gao et al. (2021).

studies that consider aggregate particles (Adams et al., 2019; Arney et al., 2017; Ohno & Kawashima, 2020), the specific growth mechanisms of exoplanet hazes made in the laboratory remains highly uncertain past their initial formation. It should also be noted that these laboratory hazes were generated at pressures of a few mbar, and so the pressure-dependence of particle size is uncertain for exoplanets, though Titan studies show the composition and spectral response does change as a function of pressure (Imanaka et al., 2004). Moreover, the experiments do not fully capture the dynamics of haze particles in the atmosphere. Atmospheric dynamics can cause particles to move through the atmosphere, collide, coagulate, and grow, whereupon they may sediment out of the atmosphere or be upwardly mixed[24].

1.7 This Work

Evidence for planetary aerosols abounds, yet the possibly unique compositions of these aerosols and the energetic regimes in which they are formed remains an outstanding and open question even as new planet candidates are discovered with *TESS* and as new missions to worlds within the Solar System are debated. A few questions I seek to answer in this dissertation include:

- What are the chemical and physical properties of clouds and hazes formed in exoplanets and Solar System worlds?

- How will our knowledge of analogue hazes generated in the laboratory, and their coupling to clouds, aid in observational predictions made for Hubble, JWST, and future observatories and planetary missions?

- What implications do these clouds and hazes have for the habitability of these worlds?

[24] but that's a thesis for another day

In light of the above context, this dissertation therefore makes the first attempts to link exoplanet laboratory haze information to atmospheric models; this is the subject of Chapter 2, which is published in *The Astronomical Journal* as Moran et al. (2018). Next, I investigate in Chapter 3 the chemical composition of the first laboratory hazes produced for super-Earth and mini-Neptune exoplanets, which is published as Moran et al. (2020) in the *Planetary Science Journal*. Chapter 4 has been submitted to the *Journal of Geophysical Research – Planets* and concerns the detailed chemistry and spectra of laboratory hazes made under Triton-like conditions.

Chapter 2

Limits on Clouds and Hazes for the TRAPPIST-1 Planets

"A philosopher once asked, 'Are we human because we gaze at the stars, or do we gaze at them because we are human?' Pointless, really... 'Do the stars gaze back?' Now, that's a question."

– Neil Gaiman, *Stardust*

2.1 Introduction

[1]Aerosols, including clouds and hazes, in the atmospheres of exoplanets are currently the subject of intense scrutiny. These aerosols can hinder our ability to study the presence and composition of exo-atmospheres, and their presence is often invoked to explain a lack of large spectral features in transmission spectroscopy studies (e.g., Dragomir et al., 2015; Knutson et al., 2014a; Knutson et al., 2014b; Kreidberg et al., 2014a; Sing et al., 2016). Yet, much remains uncertain as to the likelihood of aerosol formation and physical properties in unexplored radiation regimes, such as those of M-dwarf systems like the TRAPPIST-1 planets. Here, we connect *Hubble Space Telescope (HST)* observations to a laboratory-based study of exoplanetary haze properties to investigate the likelihood of aerosols in hydrogen-rich atmospheres for

[1]This chapter is published in as Moran, Hörst, Batalha, Lewis, and Wakeford (2018), "Limits on Clouds and Hazes for the TRAPPIST-1 Planets," *the Astronomical Journal*, 156 (6), [252], doi: 10.3847/1538-3881/aae83a

the TRAPPIST-1 system.

The TRAPPIST-1 system (Gillon et al., 2017) is the first known multi-planet system of Earth-sized worlds. Additionally, three to four of its currently known planets are in the classically defined habitable zone, and all seven currently known are amenable to observational transmission spectroscopy studies. Here and throughout this work, we refer to the "classical" habitable zone, defined as the circumstellar region where liquid water can persist on a planet's surface given a substantial planetary atmosphere (Kasting et al., 1993). As such, TRAPPIST-1 is a powerful natural system for insights into the formation and evolution of planetary atmospheres in a system outside our own. Furthermore, the *Transiting Exoplanet Survey Satellite (TESS)*, launched in April 2018, is expected to find hundreds of terrestrial planets around M-dwarf stars in the nearby galactic neighborhood (Sullivan et al., 2015). These new worlds will have their own unique radiation regimes and will require further study to understand their aerosol content and the effects of any aerosols on future observations.

Previous studies of the TRAPPIST-1 planets have investigated their orbital evolutionary histories (Luger et al., 2017; Quarles et al., 2017; Tamayo et al., 2017; Unterborn et al., 2018b). These planets have long-term stable orbits, which provides adequate time for substantial evolution of the planetary atmospheres (Dong et al., 2018). Despite the high UV-flux of the host star (O'Malley-James & Kaltenegger, 2017; Wheatley et al., 2017) as well as frequent flaring events (Vida & Roettenbacher, 2018), the planets of the TRAPPIST-1 system still may have large amounts of water (Bolmont et al., 2017; Bourrier et al., 2017). This has motivated multiple investigations of the planets' habitability through the presence of surface liquid water and biomarkers (Alberti et al., 2017; Barstow & Irwin, 2016; Turbet et al., 2018; Wolf, 2017). Studies regarding the interior structure (Kislyakova et al., 2017; Suissa & Kipping, 2018) and bulk densities (Grimm et al., 2018) of the TRAPPIST-1 planets also suggest terrestrial rather than gaseous worlds.

Observations from *HST* have determined that TRAPPIST-1 d, e, and f have muted transmission spectra with features in the <500 ppm range, rather than the large features (∼1000 ppm) expected for extended, clear hydrogen-rich atmospheres (de Wit et al., 2018). "Hydrogen-rich", in this case and throughout our analysis, refers to H_2-He envelopes greater than 0.01% of the total planet masses given their radii. de Wit et al. (2018) ruled out clear hydrogen-rich atmospheres for TRAPPIST-1 d, e, and f to high confidence. Later, the TRAPPIST-1 planetary mass measurements were updated (Grimm et al., 2018). The scale height of the atmosphere, given by $H = \frac{kT}{\mu g}$ where k is the Boltzmann constant, T is temperature, μ is the mean molecular weight of the atmosphere, and g is the gravity, is dependent on planetary mass. The predicted atmospheric scale heights for these planets have thus changed in light of these new mass estimates. Therefore, the initial findings of de Wit et al. (2018), in which clear hydrogen-rich atmospheres were ruled out, must be revisited. We do so as part of our analysis for this study. Any further mass refinements will have an effect on these results, which we explore in more detail in §4.

Clouds and/or hazes in planetary atmospheres can obscure and mute the larger spectral features indicative of clear hydrogen-rich atmospheres. There is ample evidence for the presence of clouds and hazes in the atmospheres of planets across all masses, from hot Jupiters (e.g., Sing et al., 2016) to exo-Neptunes (e.g., Knutson et al., 2014b; Lothringer et al., 2018) to super-Earths (e.g., Kreidberg et al., 2014a). Hazes in these atmospheres are of particular astrobiological interest. Hazes can substantially impact the planetary surface temperature as well as provide a source of UV absorption to protect the planetary surface (e.g., Arney et al., 2017). TRAPPIST-1 A has high flux in the UV and X-ray (Wheatley et al., 2017), as is typical of late M-dwarfs (France et al., 2013). Protection from the high flux of the host star would likely be paramount for any possible life to persist. Furthermore, hazes themselves are thought to be important for the formation of prebiotic molecules (e.g, Hörst et al., 2018b; Hörst

et al., 2012; Rimmer et al., 2018).

The formation mechanisms and physical likelihoods of clouds and hazes in the atmospheres of exoplanets, and their subsequent effect on observations, remain largely unknown. Nearly all previous studies of haze and clouds in exoplanet atmospheres have depended upon the particle sizes and compositions of Solar System photochemical hazes (e.g., Howe & Burrows, 2012; Lincowski et al., 2018; Miller-Ricci Kempton et al., 2012; Morley et al., 2013; Morley et al., 2015; Rackham et al., 2017) rather than those in exoplanet atmospheres, as no direct measurements of these aerosols are currently possible. From these Solar System-like hazes, previous studies then assume these properties *a priori* and provide predictions for the types of transmission and emission spectra expected.

Here, we take the opposite approach, by making no direct assumptions about the cloud or haze species contributing to these transmission spectra. Instead, we calculate from the recent *HST* (de Wit et al., 2018) observations upper limits on possible cloud and hazes, remaining agnostic about their origin. We then compare these values to recent experimental work investigating exoplanet haze properties for the first time in the laboratory. These exoplanet experiments studied haze formation under a range of planetary temperatures and atmospheric compositions, including under hydrogen-rich, water-rich, and carbon dioxide-rich cases (He et al., 2018a; He et al., 2018b; Hörst et al., 2018a). These experiments are thus applicable to expected scenarios for the TRAPPIST-1 planets near and within the classical habitable zone. As such, our investigation represents a new approach to characterizing the TRAPPIST-1 planets.

In §2, we describe our methodology for modeling spectra informed by the laboratory results; in §3, we present our results; in §4, we discuss and contextualize the results we have obtained; and in §5 we summarize our findings with concluding remarks.

2.2 Methods

We aim to determine lower limits on the cloud top pressures and upper limits on the strength of haze scattering in the outer TRAPPIST-1 planets d, e, f, and g. To do so, we use *CaltecH Inverse ModEling and Retrieval Algorithms* (or `CHIMERA`) (Line et al., 2013b) to generate model transmission spectra to compare to the *HST* observations of these atmospheres. Table 2.I shows the TRAPPIST-1 planetary parameters explored here, with the measurements we used in our models. We begin by first noting an important distinction between our definitions of a cloud versus a haze, as these terms are often used interchangeably when, at least in our analysis, we use them to mean very specific physical phenomena. Hazes refer to the solid, suspended particles that are the result of photochemical reactions in the atmosphere. Clouds, on the other hand, are either solid or liquid particles that are the result of condensation processes due to temperature and pressure conditions of the atmosphere. Together, these two sets of suspended particles are encompassed by the generic term "aerosols".

We investigate three different effects clouds and hazes can have on an atmosphere. First, for each planet, we investigate the effect of adding haze into our spectral models. We fix the composition of a cloud-free model while varying the magnitude of Rayleigh-scattering haze. We increase the strength of the haze until the model attains a statistically significant agreement to the *HST* data, using a cutoff threshold of reduced-χ^2 of 1.16 (or 1σ, based on the 10 *HST* data points) and then again until we reach a reduced χ^2 of 2.8 (3σ). If we cannot reach these cutoffs, we report the highest confidence value we are able to obtain, with all of our results, in Table 2.II.

Second, we examine the effect of atmospheric composition in a cloudy atmosphere. We fix the strength of haze scattering to zero and keep the cloud top pressure at 0.1 bar, the expected pressure of the tropopause (Robinson & Catling, 2014), while varying the amount of water in the atmosphere. We increase the water mixing ratio until

our model reaches the 1σ and 3σ uncertainty bounds of the *HST* data. Third, we fix the atmospheric composition and vary the cloud-top pressure, effectively moving the cloud layer in altitude until we again reach the 1σ and 3σ thresholds. The simplicity of this method is motivated by the low precision of the de Wit et al. (2018) data. We describe each of these methods in more detail in the following subsects.

2.2.1 Modeling Haze Opacity with Laboratory Measurements

Different methods exist to account for the effect of hazes on transmission spectra in exoplanet atmospheres. These techniques range in complexity from including the output of a full set of haze species' opacity coupled to photochemical models (e.g., Miller-Ricci Kempton et al., 2012; Morley et al., 2013) to a more simplistic treatment wherein the haze scattering is parameterized by a power law (e.g., Line et al., 2014; Line et al., 2013b; Robinson & Catling, 2014; Robinson & Catling, 2012; Sing et al., 2016). This simpler method is often employed where data are not sufficiently precise to merit more complex treatment.

In light of the large uncertainties associated with the *HST* TRAPPIST-1 observations (de Wit et al., 2018), we use the parameterization for the scattering cross section, σ, derived in Lecavelier Des Etangs et al. (2008):

$$\sigma = \sigma_0(\lambda/\lambda_0)^\alpha \tag{2.1}$$

where σ_0 is the reference scattering cross section, λ_0 is a reference wavelength, λ is the wavelength of radiation, and α is the power law slope of scattering. The Rayleigh approximation, in which α = -4, applies when the diameter of particle $d_p << \lambda$. The exoplanet haze analogues from the laboratory range in particle size d_p from 25 nm to 180 nm (He et al., 2018a; He et al., 2018b). For the wavelengths covered by the *HST*/WFC3 observations, from $\lambda = 1.1$ μm to 1.7 μm, this allows us to treat these exoplanet haze analogues as Rayleigh scatterers in our model. The scaling factor of

the haze cross section σ_0 can be approximated by

$$\sigma_0 = \frac{\tau_0}{n_0 H} \tag{2.2}$$

where τ_0 is the optical depth at a reference altitude, n_0 is the number density of the scatterer at the reference altitude, and H is the scale height of the atmosphere. We compute upper limits on σ_0 based on the *HST* observations and then compare these results to the laboratory results of Hörst et al. (2018a) to determine whether our computed upper limits are physically plausible.

There is no direct physically motivated formulation to turn the exoplanet haze production efficiencies from the laboratory (Hörst et al., 2018a) to a theoretical scattering cross section. However, laboratory results from Hörst et al. (2018a) show maximum production rates for 300 K to 600 K exoplanetary atmospheres similar to the production rate of Titan experiments with the same experimental set-up. Therefore, we are able to use Titan as a benchmark because its haze formation is well-studied in the laboratory (e.g., He et al., 2017) as well as directly observed through remote sensing.

To approximate the connection from laboratory production rates to Eqn. 2.1, we calculate σ_0 as defined in Eqn. 2.2 from the combined results of Tomasko et al. (2008) and Robinson et al. (2014). Tomasko et al. (2008) reports the measured haze particle number density as a function of altitude on Titan, and Robinson et al. (2014) used the haze parametrization of Lecavelier Des Etangs et al. (2008) to fit the slope of Titan solar occultation observations, in effect treating Titan as an exoplanet in transit. Tomasko et al. (2008) and Robinson et al. (2014) suggest a scattering cross section for Titan's haze of $\sigma_0 \sim 10^{-7}$ cm^2. For reference, Earth's scattering cross section is on the order of $\sim 10^{-27}$ cm^2. The haze production rates for the exoplanet experiments were not higher than for similar Titan experiments (Hörst et al., 2018a). Therefore, we assume that this scaled haze scattering cross section 10^{-7} cm^2 is a reasonable physical

upper limit for haze scattering in the TRAPPIST-1 atmospheres.

We reiterate the important caveat to our methodology described here: the production efficiency measured in the laboratory does not directly correspond to the cross sectional strength of the haze observed in a planetary atmosphere. The laboratory cannot capture processes such as atmospheric escape and rainout, which would both work to decrease the column density and decrease the cross sectional scattering strength. Thus our assumption of the production efficiency being representative of the column density of the haze particles is an approximation. For our purposes of attempting to estimate the haze content of the TRAPPIST-1 planets, our approximation is justified by the large uncertainties already inherent to the *HST* observations from de Wit et al. (2018), as well as guided by our overall goal of obtaining an upper limit rather than an exact constraint of the atmospheric scattering due to haze.

2.2.2 Modeling Cloud Opacity

There are many techniques to account for the effects of clouds on transmission spectra. These techniques exist along a continuum of complexity. These range from full 3-D dynamically-radiatively-convectively driven cloud microphysics models (e.g., Lee et al., 2015), to models which globally average the balance between turbulent mixing and sedimentation of condensates (e.g., Ackerman & Marley, 2001), to simply modeling a grey opacity source (e.g., Batalha & Line, 2017; Line et al., 2013b). Here, we choose to use the method of Batalha et al. (2018), where a grey absorbing cloud is set at a specific pressure, below which the transmittance is zero. This allows us to remain agnostic about the properties of the cloud being formed in each case, and provides a lower limit on where an optically thick, global cloud layer would have to exist to match the *HST* observations. This method has been used in observations of hot Jupiters (e.g., Sing et al., 2016), warm Neptunes (e.g., Kreidberg et al., 2014a; Wakeford et al., 2017), and studies of the TRAPPIST-1 system (e.g., Batalha et al., 2018; Morley

et al., 2017b).

To provide additional context for our cloudy cases, we also run models wherein we place this opaque cloud at the nominal tropopause of 0.1 bar. This follows the analysis of Robinson and Catling (2014), which observes that all Solar System planetary bodies have a tropopause at 0.1 bar, where thick clouds are observed to form. In our models with tropospheric clouds, we examine the effect of increasing the metallicity of the atmospheres by varying the water mixing ratio. Multiple studies have suggested that the outer TRAPPIST-1 planets in the classical habitable zone, due to their likely origin further out in the protostellar disk before inward migration (Quarles et al., 2017; Unterborn et al., 2018b), are still able to harbor multiple Earth ocean's worth of water despite having lost huge amounts of water over their evolutionary histories (Bolmont et al., 2017; Bourrier et al., 2017; Dong et al., 2018). Recent revisions of mass estimates for the planets (Grimm et al., 2018) allows a large water reservoir to remain a reasonable assumption (Unterborn et al., 2018a). This motivates our approach to using water as our proxy for heavy atmospheric enrichment. We also focus on water because of the significant water feature at 1.4 μm centered in the *HST*/WFC3 bandpass. Additionally the equilibrium temperatures of the outer TRAPPIST-1 planets d, e, f, and g, ranging from about 300 K to 200 K, include water's triple point. Water could then contribute to atmospheric dynamics on the TRAPPIST-1 planets as it does on Earth through cloud condensation and rainout processes (e.g., Turbet et al., 2018). We start from the solar water mixing ratio of 7.8 x 10^{-4} (with a solar C/O ratio of 0.5) (Lodders, 2003), and increase this value until reaching our statistical thresholds of 1σ and 3σ.

Finally, for clouds we explore the degeneracy between cloud top pressure and metallicity by running a full grid of forward models in fixed parameter combinations. We examine a range of metallicities from 1× to 1000× solar (in fifteen logarithmic steps), as well as a range of cloud top pressures (in ten steps) from a clear atmosphere

(i.e., where molecular opacity becomes optically thick well before the cloud deck) to a cloud deck at 1 μbar. Our grid thus includes a total of 150 distinct models each for TRAPPIST-1 d, e, f, and g.

2.2.3 Modeling the Transmission Spectra

We use a version of the atmospheric modeling code `CHIMERA` (Line et al., 2013a; Line et al., 2014; Line et al., 2013b), a radiative transfer code that uses the correlated-k distribution technique. `CHIMERA` has been used to model hot Jupiters (Kreidberg et al., 2014b), sub-Neptunes (Kreidberg et al., 2014a) and recently the TRAPPIST-1 system (Batalha et al., 2018). Given molecular opacities, planetary mass, radius, temperature, atmospheric mixing ratios, cloud top pressure level, and haze cross section (σ), we produce transmission spectra at R = 100, consistent with the *HST*/WFC3 measurements.

For our temperature-pressure profiles, we use the parameterized 1-D, 5 parameter profile of Guillot (2010). We include molecular opacities from to H_2/He CIA, CH_4, H_2O, CO_2, and N_2 (Freedman et al., 2014; Freedman et al., 2008), informed by the dominant gases in the atmospheres of Solar System worlds as well as previous TRAPPIST-1 atmospheric studies (Batalha et al., 2018; Morley et al., 2017b). For our atmospheric mixing ratios, we take two separate approaches: one composition for hazy atmospheres and a separate set of compositions for cloudy atmospheres. Both of our approaches involve setting mixing ratios rather than exploring a fully self-consistent calculation of gases in chemical equilibrium. The TRAPPIST-1 atmospheres are likely not in chemical equilibrium (Bourrier et al., 2017; Dong et al., 2018). Additionally, in our models with photochemical haze formation, we inherently assume that this is not the case. We assign mixing ratios in order to determine upper limits on aerosol content rather than providing constraints for any physical atmospheric parameters.

For our hazy atmospheres, we use H_2/He background gas atmospheres with 1%

mixing ratios of CH_4, H_2O, CO_2, and N_2, giving a mean molecular weight μ of 3.02. This composition is motivated by two factors. First, nitrogen, methane, water, and other carbon-bearing species have all been shown to play important roles in haze production in laboratory settings (e.g., Hörst & Tolbert, 2014; Imanaka & Smith, 2010; Trainer et al., 2012; Trainer et al., 2004). Second, these constituent gases were used in the relevant exoplanet laboratory haze experiments (He et al., 2018a; He et al., 2018b; Hörst et al., 2018a).

For our cloudy atmospheres, we consider atmospheres of H_2/He and H_2O since we are comparing our results to the *HST*/WFC3 G141 bandpass, where water has a prominent molecular feature. Therefore we use the water mixing ratio as a proxy for varying the scale height due to increasing metallicity (where metallicity refers to the overall heavy-element abundance). We begin from a H_2/He atmosphere with a solar H_2O mixing ratio with a mean molecular weight μ of 2.32 and then scale upward to higher metallicities by increasing the water mixing ratio.

Planet	Mass ($\oplus$)	Radius ($\oplus$)	T_{eq} (K)
d	0.297	0.784	288.0
e	0.772	0.910	251.3
f	0.934	1.046	219.0
g	1.148	1.154	198.6

Table 2.I. TRAPPIST-1 planet parameters via Grimm et al. (2018) used in our model atmospheres.

2.3 Results

Photochemical hazes are not expected to persist in temperate hydrogen-rich atmospheres from theory (Hu & Seager, 2014; Miller-Ricci Kempton et al., 2012; Morley et al., 2015). Laboratory measurements (He et al., 2018b; Hörst et al., 2018a) suggest inefficient photochemical haze production for hydrogen-rich background gas mixtures. Our results in Figure 2.1 show the model outputs for hydrogen-rich atmospheres

containing 1% volatiles with haze amplitudes to the 1σ and 3σ confidence levels for *HST* data of TRAPPIST-1 d, e, and f. Clear hydrogen-rich atmospheres with 1% volatiles as well as solar composition atmospheres are also shown for planets d, e, f, and g. Additionally, we show in Figure 2.2 our model outputs to 1σ and 3σ levels for a global cloud deck at the nominal tropopause with high metallicity atmospheres as well as for a global cloud deck with a solar composition atmosphere. Finally, we compare the results of increasing metallicity to increasing cloud top pressure in Figure 2.3. We show that aerosols, either as photochemical haze or as an opaque equilibrium cloud layer, are likely unable to mute spectral features to within the observational uncertainties from de Wit et al. (2018) for all but planet g, if we consider the laboratory-supported haze production rates. A summary of our results given the model conditions and the statistical significance of the models is found in Table 2.II.

2.3.1 Haze

Adding a global layer of Rayleigh-scattering haze weakens spectral features short of 1.7 microns, as seen in our transmission spectra models in Figure 2.1. We increased the strength of the haze scattering cross section while maintaining a Rayleigh scattering slope of λ^{-4} as described in §2.2. We determined that to 1σ for TRAPPIST-1 d, e, and f, we can rule out models with large haze scattering cross sections. However, to 3σ, our model outputs with updated mass constraints cannot exclude purely haze-free solar composition atmospheres except for planet d.

For TRAPPIST-1 d, a clear solar atmosphere is excluded to $>20\sigma$, while a clear hydrogen-rich atmosphere with 1% water, carbon dioxide, nitrogen, and methane is excluded to $>15\sigma$. We are able to exclude these cases for TRAPPIST-1 d to such high certainty because of the planet's low gravity and (relatively) high temperature. At TRAPPIST-1 d's equilibrium temperature of 288 K, mass of 0.297 $M_\oplus$, radius of 0.784 $R_\oplus$, assuming a solar composition atmosphere with μ of 2.32, we obtain a

Planet	Haze Scattering Cross Section (cm^2)	
	1σ	3σ
d	1×10^{-19}	6×10^{-20}
e	3×10^{-23}	9×10^{-25}
f	6×10^{-23}	3×10^{-25} (2.5σ)
g	$< 1\sigma$	$< 1\sigma$

Planet	Cloud Top Pressure (bar)	
	1σ	3σ
d	8×10^{-7}	2×10^{-6}
e	2×10^{-2}	1×10^{-1} (2σ)
f	1.26×10^{-2}	clear (2σ)
g	$< 1\sigma$	$< 1\sigma$

Planet	Metallicity ($\times$solar)	
	1σ	3σ
d	500	300
e	500	100
f	630	60
g	$< 1\sigma$	$< 1\sigma$

Table 2.II. Summary of upper and lower limits found from model outputs for our test cases with statistical certainties to *HST* data. Our haze scattering cross sections represent the scattering strength needed to reach 1σ and 3σ agreement to the *HST* data in hydrogen/helium atmospheres with 1% H_2O, CO_2, CH_4, and N_2 mixing ratios. Cloud top pressures given are the lower boundary of pressure levels required in each atmosphere with a solar composition to agree with the *HST* data to 1σ and 3σ. The metallicity given is the lower limit of the water mixing ratio, with a cloud at 0.1 bar, needed to agree with the *HST* observations to 1σ and 3σ. For planet g, the observational uncertainty is such that we are unable to generate any models that can be confidently excluded from agreement with the *HST* data.

scale height of 216 km. This is likely unphysical for such a small planet; for reference, Earth and Venus have scale heights of ~8.5 km and 16 km, respectively. To 3σ, we exclude haze scattering cross sections of less than 6×10^{-20} cm^2 for TRAPPIST-1 d; to 1σ we can increase the haze cross section up to 1×10^{-19} cm^2. This haze scattering cross section for TRAPPIST-1 d suppresses the molecular features of the spectrum to the point where only the small scattering slope remains to be observed. For reference, our computed cross sections for TRAPPIST-1 d to 1σ and 3σ are both on the order of 10^7 times that of the scattering of Earth's atmosphere.

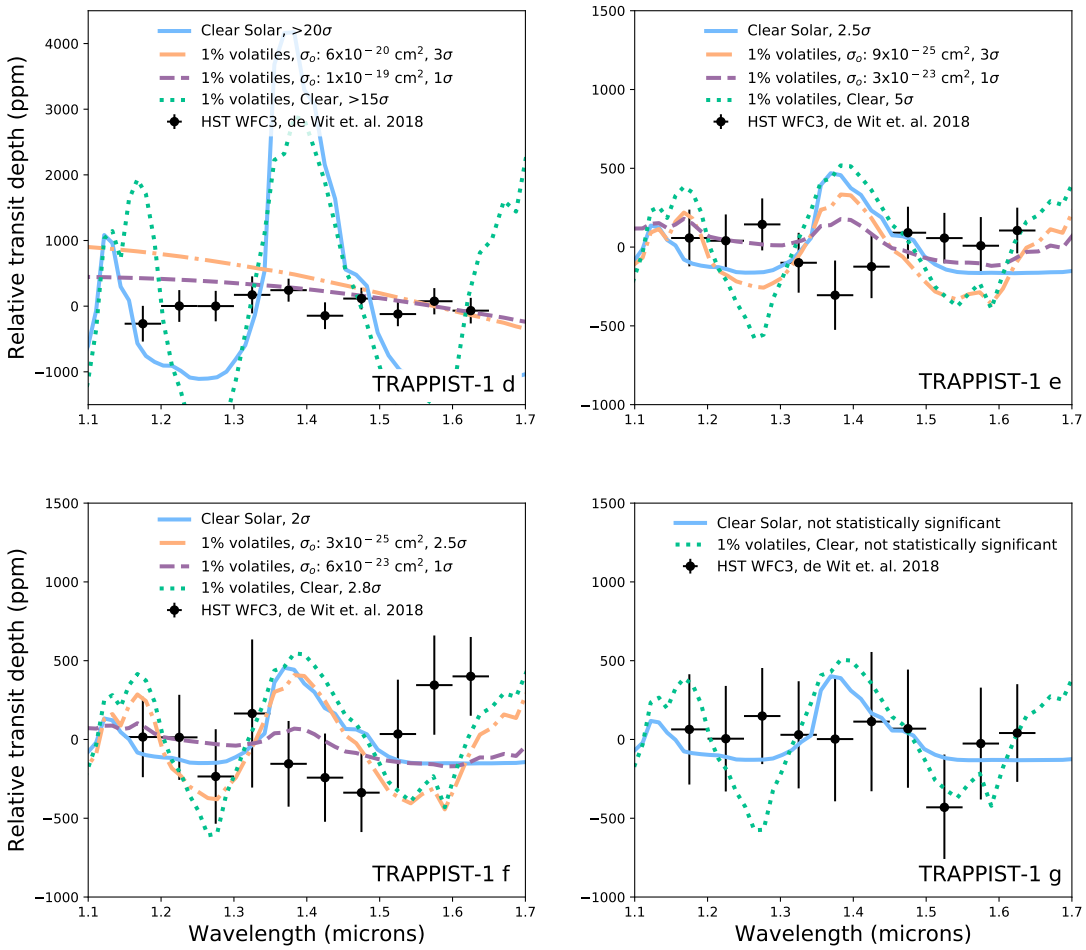

Figure 2.1. Black circles and error bars indicate the previous *HST*/WFC3 observations (de Wit et al., 2018) for TRAPPIST-1 planets d, e, f, and g. The blue solid lines indicate our baseline aerosol-free solar composition case. The rest are models of a hydrogen-rich atmosphere containing Rayleigh scattering haze, with mixing ratios for water, carbon dioxide, nitrogen, and methane at 1%. Green dotted lines indicate a zero magnitude haze scattering cross section; purple dashed lines indicate that the haze cross section was increased to give 1σ agreement with the *HST* data; orange dash-dot lines display haze cross sections increased to give 3σ agreement with the *HST* data. Only planet d results in the clear exclusion of a haze-free atmosphere.

For TRAPPIST-1 e, we can only exclude a clear solar atmosphere to 2.5σ, in contrast to the result of de Wit et al. (2018) which used previous mass estimates in their analysis to exclude such a case to high confidence ($> 6\sigma$). A clear hydrogen-rich atmosphere with 1% volatiles, however, is excluded with 5σ certainty. We can rule out haze scattering cross sections of less than 9×10^{-25} cm^2 to 3σ and 3×10^{-23} cm^2 to

1σ. These values are $\sim$ 450$\times$ and 14000$\times$ Earth's mean atmospheric scattering.

For TRAPPIST-1 f, a clear solar atmosphere, a 1% volatiles atmosphere, or an atmosphere with a 3×10^{-25} cm^2 haze scattering cross section are unable to provide a solid 3σ exclusion by the *HST* data, with confidence values of 2σ, 2.8σ, and 2.5σ respectively. For the hazy model, we maximize our confidence value at this haze scattering cross section of 3×10^{-25} cm^2 (125$\times$ Earth scattering). For our 1σ cutoff, we are able to impose a maximum value of 6×10^{-23} cm^2 (28000$\times$ Earth scattering) for the haze scattering cross section.

For TRAPPIST-1 g, the *HST* observations are not sufficiently precise to exclude a clear 1% volatile or solar composition atmosphere, as in de Wit et al. (2018). As such, our hazy models do not provide any meaningful additional limits on the TRAPPIST-1 g atmosphere and will await future observations of higher precision.

2.3.2 Clouds

Our cloudy atmosphere model results are displayed in Figure 2.2. We are able to rule out a clear solar composition atmosphere for TRAPPIST-1 d. However, such clear atmospheres cannot be ruled out to high confidence for planets e, f, and g (the statistical significance of these cases are 2.5σ, 2σ, and $< 1\sigma$, respectively). This result for planets e and f is in contrast to de Wit et al. (2018), whose analysis depended on previous planet mass estimates.

2.3.2.1 Increasing the Water Mixing Ratio with Tropospheric Clouds

With a grey cloud at 0.1 bar (the tropopause of Solar System bodies, following Robinson and Catling (2014)), the mean molecular weight must be supersolar in order to statistically match the *HST* observations. This is shown in Figure 2.2. For TRAPPIST-1 d and e, the model with a cloud deck at the tropopause requires an H_2O mixing ratio of 39%, or $\sim$500$\times$ the solar ratio, to agree with the *HST* observational

error bars to 1σ. To 3σ, we calculate a water mixing ratio of 24%, or a $\sim$300$\times$ solar atmosphere for TRAPPIST-1 d. For TRAPPIST-1 e, the tropospheric cloud layer necessitates a model with an 8% water mixing ratio, or $\sim$100$\times$ solar, to 3σ confidence. To produce a model with a cloudy tropopause, consistent at 1σ with TRAPPIST-1 f observations, entails a 49% water mixing ratio ($\sim$630$\times$ that of solar). At 3σ confidence, however, only a 4.5% water mixing ratio (60$\times$ solar) is needed. As in our hazy model results, adding clouds to the tropopause of a hydrogen-rich version of planet g offers no better statistical certainty than a clear hydrogen-rich atmosphere.

2.3.2.2 Moving Clouds in Pressure Space

If instead the cloud layer is allowed to move in pressure space while keeping the H_2O ratio steady at 0.08% (a 1$\times$ solar ratio), we find that high altitude clouds ($< 12 mbar$) are needed in the model for a 1σ exclusion of the data except for planet g, where again no statistically significant model can be found with the current observational uncertainties. For TRAPPIST-1 d, e, and f, these clouds are at 0.8 μbar, 20 mbar, and 12.6 mbar, respectively. These pressures in Earth's atmosphere are comparable to that of the thermosphere (0.8 μbar) and stratosphere (20 and 12.6 mbar). Under our more conservative 3σ cutoff, we rule out clouds below 2 μbar for TRAPPIST-1 d, again placing an opaque cloud deck in what would be the thermosphere on Earth. For TRAPPIST-1 e, we can only rule out clouds below the level of Earth's tropopause (0.1 bar) to 2σ in a solar composition atmosphere while for f we cannot rule out a clear solar atmosphere beyond 2σ.

2.3.2.3 The Intersection of Cloud Top Pressure and Atmospheric Metallicity

There is a known degeneracy between cloud top pressure and metallicity, which both act to mute spectral features (Batalha et al., 2017; Kempton et al., 2017). Here we explore both cloud top pressure level and metallicity, using the water mixing ratio

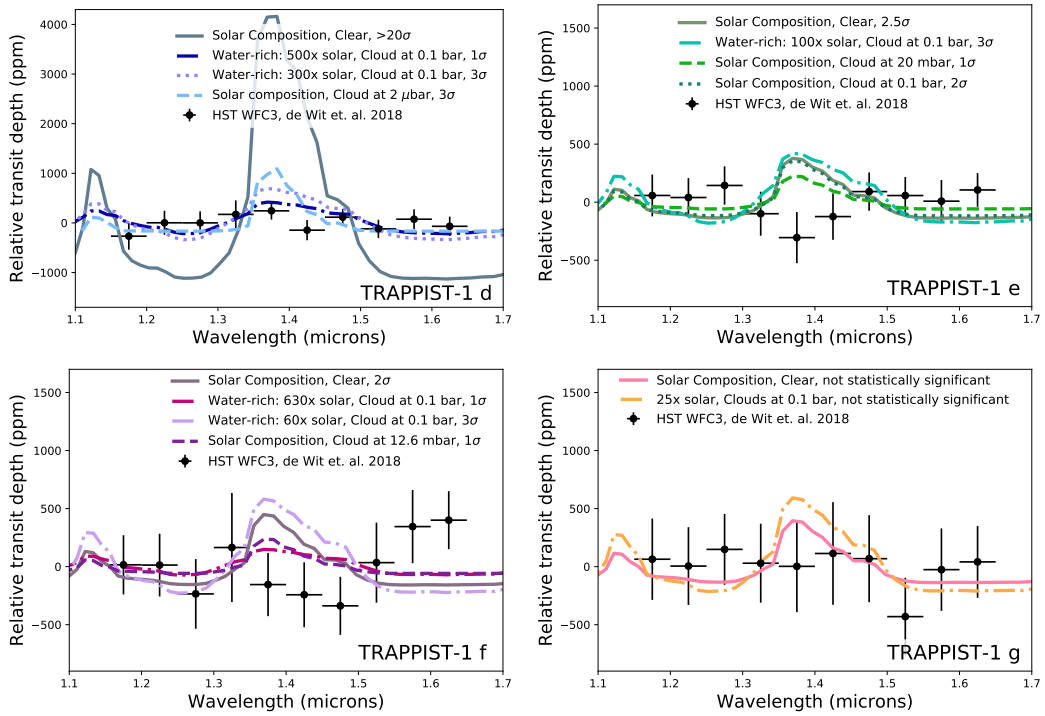

Figure 2.2. Black circles and error bars are from the *HST* observations (de Wit et al., 2018) in all plots. Solid lines are model output atmospheres of solar composition with no clouds, dashed lines are for solar composition atmospheres with a cloud at high altitude, dash-dot lines are model outputs for metallicity-enhanced atmospheres with a cloud layer at the tropopause. All cases are labeled with statistical significance. We have chosen, in cases where multiple cases are statistically significant to the same confidence level, to show the higher metallicity value. Metal-rich atmospheres offer 1σ agreement to the data for planets d, e, and f. High altitude clouds are required with planet d observations to both 1σ and 3σ, but high clouds are only needed for planets e and f within the 1σ uncertainty bound.

as a metallicity proxy (e.g. Batalha et al., 2017). We map the statistical significance from our previous analysis onto this parameter space. Figure 2.3 shows our results for these combined parameters. We define line strength as the difference between the maximum peak and minimum of the continuum of the transmission spectrum between 1.1 μm and 1.7 μm. The line strength peak observable in the cloud contours results from the water feature at 1.4 μm. As the water content of the atmosphere increases, this water feature gets stronger and creates a spectral feature of larger amplitude. At the same time, increasing the water mixing ratio increases the mean molecular weight μ. As scale height is an inverse function of mean molecular weight, adding more water decreases the scale height and thus weakens the line strength observed in transmission. A competition thus develops between scale height and the height of the individual water feature as water content increases, which manifests as the turnover observed in our contour plots.

We can rule out distinct combinations of both metallicity and cloud top pressure for TRAPPIST-1 d, e, and f. For TRAPPIST-1 d, we can exclude clouds at 1μbar up to 20$\times$ solar metallicity, and a clear atmosphere up to around 400$\times$ solar. For TRAPPIST-1 e, we can exclude "tropospheric" clouds at 0.1 bar between 4$\times$ solar and 100$\times$ solar, while for TRAPPIST-1 f we exclude clouds at 0.1 bar between 8$\times$ solar and 60$\times$ solar. Again, as the precision of observational data for TRAPPIST-1 g is relatively poor, we are unable to make any significant diagnostics across either metallicity or cloud pressure space. Additionally, we show the level of precision needed to distinguish between various high metallicity atmospheres with clouds for all planets, regardless of the current *HST* observations. For example, we show for TRAPPIST-1 d that the difference between a clear atmosphere and a cloud deck at the tropopause will not be observable even with 1 ppm precision. For TRAPPIST-1 e and f, we will be able to distinguish between a cloudy tropopause and a completely clear atmosphere at approximately 20 ppm precision.

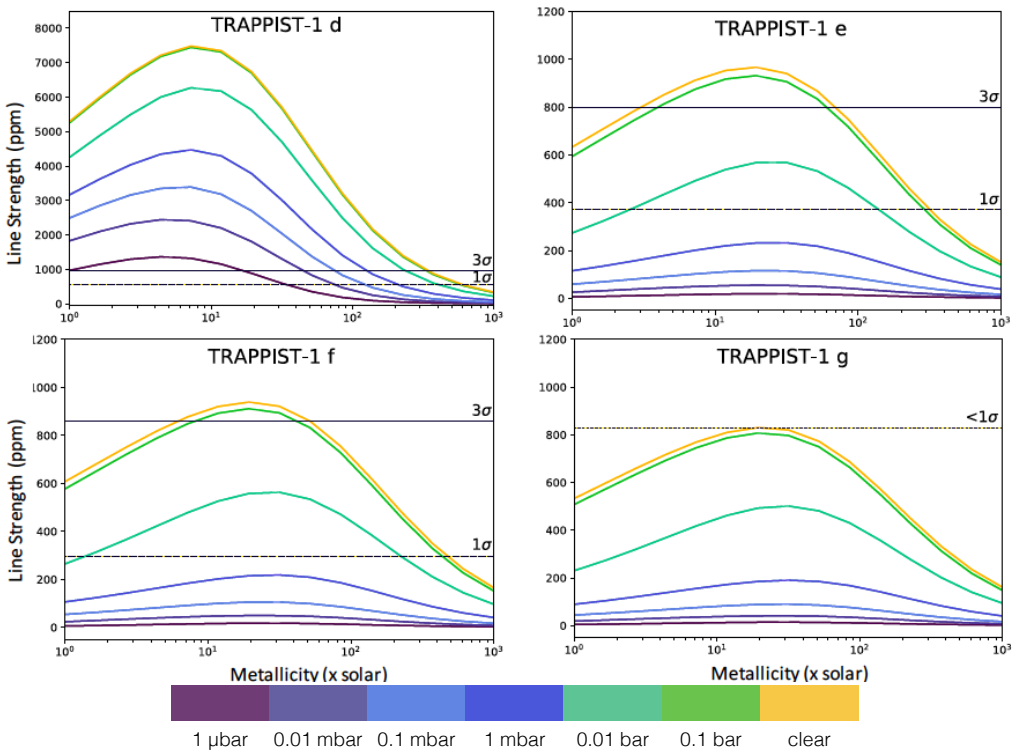

Figure 2.3. All plots show line strength as a function of metallicity for TRAPPIST-1 d, e, f and g (labeled). We define line strength as the difference between the maximum peak and minimum continuum of the transmission spectrum between 1.1 μm and 1.7 μm. Each curve shows cloud-top pressures according to the color bar. 1σ and 3σ lines show the uncertainty bounds of the model to the *HST* observations of de Wit et al. (2018). For planet g, we plot the highest reduced-χ^2 we were able to obtain as the line labeled $<1\sigma$. Note that planet d has a larger range of line strengths, due to its higher temperature and lower density coupling to give it a significantly larger scale height.

2.4 Discussion

2.4.1 Stellar Contamination in the Transmission Spectra

Our results are predicated on the observations of de Wit et al. (2018). Rackham et al. (2018) recently called into question the fidelity of these *HST* measurements because of the effects of unaccounted-for stellar contamination. Spots and faculae in the photosphere of M-dwarf host stars, such as TRAPPIST-1 A, may contribute to stellar contamination in the planetary spectra, which Rackham et al. (2018) refer to as the "transit light source effect". Specifically, this effect impacts the near-IR

HST/WFC3 bandpass to which we compare our models. To address this question of stellar contamination, Zhang et al. (2018) reanalyze the *HST*/WFC3 data previously published by de Wit et al. (2018). They use a different data reduction strategy in an attempt to minimize systematics, and ultimately find transit depths consistent with those of de Wit et al. (2018) within error bars. However, they also model the "transit light source effect" and determine that these data are fully consistent with stellar contamination in the transmission spectrum.

With this possibility of stellar contamination in the TRAPPIST-1 spectra (Zhang et al., 2018), Rackham et al. (2018) suggest that any molecular features in the region of interest (as here, from 1.1 to 1.7 μm) would be impacted up to 77 ppm. However, for the *HST*/WFC3 data presented in de Wit et al. (2018), the uncertainty due to signal and potentially unaccounted-for instrument systematics are actually larger than this across the entire wavelength band, with a minimum error twice that ($\sim$145 ppm). Only for higher precision transit observations, such as with the *James Webb Space Telescope (JWST)* with a noise floor of 30 ppm (Batalha et al., 2018), is stellar contamination likely to impact planetary spectra and molecular feature identification. Still, in light of these complexities, our analysis, as described in §2, does not attempt to *fit* our model to the *HST* data. Instead, in order to calculate conservative limits of the metallicity, cloud top pressure, and haze scattering cross sections of the TRAPPIST-1 planets d, e, f, and g, we only report agreement of our models within the *HST* uncertainty bounds. Our analysis presented here is therefore minimally affected by spots or faculae in the stellar spectrum. Our results do not depend on a true fitting of the transit spectra and further efforts to characterize any stellar contamination present would likely only reduce the uncertainties inherent to the *HST* data and improve our results.

2.4.2 Effect of Temperature-Pressure Profiles and Planetary Mass on Scale Heights

We use water as a proxy for increased metallicity in our model atmospheres (see §2). We find that for TRAPPIST-1 d, e, and f, 500× to 600× solar metallicities are within the bounds of the *HST* uncertainties to 1σ if a tropospheric cloud layer is included in the model. These results imply large (> 6) mean molecular weights, μ, which work to reduce the scale height of the atmosphere, given by $H = \frac{kT}{\mu g}$. However, the effect of temperature T on scale height is dependent on our assumed T-P profiles, where we use the parameterized 1-D, 5 parameter profile of Guillot (2010). Our T-P profiles are in agreement with those explored in Morley et al. (2017b) and Batalha et al. (2018); however the true temperature structures of the TRAPPIST-1 planets are highly unconstrained. If the true temperatures were warmer, our upper limits for metallicity would have to be larger to compensate for this increase in temperature. Alternatively, our models would have to include higher altitude clouds or more strongly scattering haze particles. Quantitatively, any 50 K difference in our models changes our upper limit of metallicity by ∼2-2.5 dex (e.g., from 500 to 700×solar) for planet d and 1 dex for planets e and f. Our cloud top pressure changes by 1 mbar for planet d, 10 mbar for planet e, and 6 mbar for planet f with a 50 K change in temperature. Finally, our haze scattering cross sections change by no more than 9×10^{-27} cm^2 for all planets with any 50 K temperature adjustment. This 50 K change is within the range of albedo explored by Morley et al. (2017b). Because we only consider transmission spectra, as opposed to highly temperature-dependent emission spectra, our results are relatively unchanged by our choice of T-P profile parameterization. With our current T-P parameterization, our results provide a conservative limit to the metallicity and/or aerosol content of the TRAPPIST-1 planet atmospheres.

Like temperature, the mass of the planet is linearly related to the scale height. The masses of the planets in the TRAPPIST-1 system have undergone several refinements

with additional TTV measurements, as reported in Grimm et al. (2018). These mass updates changed the mass estimates by 10% to 25%, and correspondingly affect the computed scale heights for our model atmospheres by the same amount. This allows us to show that the solar composition atmospheres which de Wit et al. (2018) exclude for TRAPPIST-1 e and f cannot be discounted. Any further mass refinements will thus affect the atmospheric scale heights and could substantially change the atmospheric metallicity and aerosol contents we find in this work. For example, if the planetary mass of TRAPPIST-1 e were to decrease by 15%, we could exclude a hydrogen-rich atmosphere to 3σ. If TRAPPIST-1 d were to increase in mass by 25%, our exclusion of a hydrogen atmosphere would fall from $>20\sigma$ to only $>7\sigma$. These examples demonstrate the extreme importance of having high-precision, high-fidelity mass measurements for these small planets, as determining the nature of their atmospheres is highly dependent on this information.

2.4.3 Aerosol Mass Loading

For our cloudy models, our findings suggest a solid layer of high altitude clouds for TRAPPIST-1 d, e, and f as an upper limit within 1σ. The lower boundary of the cloud layers are, at minimum, at 0.8 μbar, 20 mbar, and 12.6 mbar respectively for each planet, consistent with pressures in the thermosphere (0.8 μbar) and stratosphere (20 and 12.6 mbar) on Earth. However, our treatment of the cloud opacity does not attempt to self-consistently model the cloud formation. In a real atmosphere, there is likely not enough material for solid, grey clouds to form at the altitudes of our lower limits – stratospheric clouds and higher are optically thin on Earth due to the low number density of molecules available at these millibar pressures (Seinfeld & Pandis, 1998). A solid grey cloud at the 0.01 bar level is the most pessimistic case considered in Batalha et al. (2018), for example. However, Kopparapu et al. (2017) suggest that for slowly or synchronously rotating planets, thick convective clouds may be more

easily able to form and persist at higher altitudes. Despite this, for TRAPPIST-1 d, even at 3σ, an opaque cloud no lower than 2 μbar is required by our model. This pressure can be safely ruled out even in the most generous of cloud formation models, implying that clouds are not the source of the observed muted transmission features for planet d. At 3σ only TRAPPIST-1 e allows a cloud at 0.01 bar, but e has a density of 1.024 $\rho_\oplus$ (Grimm et al., 2018), which is consistent with a volatile-rich rather than extended hydrogen-rich atmosphere Lopez and Fortney, 2014; Rogers, 2015.

If we turn to haze scattering as an aerosol source, we find haze scattering cross sections 10^2 to 10^7 times that of Earth's atmospheric scattering are needed to be within the uncertainty of the *HST* observations for planets TRAPPIST-1 d, e, and f. However, laboratory results show that hydrogen-rich atmospheres are not very efficient at making haze (He et al., 2018a; Hörst et al., 2018a), and all of our model atmospheres considered here are heavily hydrogen-rich with minor volatile contents. For Titan, the haze scattering cross section is $\sim 10^{-7}$ cm^2, as described in §2.1. Laboratory results for Titan's haze production rate are the same order of magnitude for the most efficient exoplanet haze production rates (Hörst et al., 2018a), suggesting that any haze scattering cross sections substantially greater than Titan's are unphysical. However, the most haze-productive laboratory atmospheres were run at temperatures of 400 K (the equilibrium temperature of TRAPPIST-1 b rather than those of the outer planets d, e, f, and g considered here). Furthermore, these highly productive laboratory experiments contained more metal-rich atmospheric compositions (1000× solar) than our models (∼100× solar). For the laboratory atmospheres comparable to TRAPPIST-1 d conditions considered here (300 K, ∼100× solar), the haze production rate is three orders of magnitude lower. Again, there is no direct way to translate laboratory-measured haze production rates to haze mass loading in a planetary atmosphere. Still, it is likely that the less productive laboratory cases also represent less hazy worlds. Our results only conclusively rule out haze scattering cross sections well under that of

Titan-like conditions, but the disconnect between the laboratory conditions and our models means that more precise constraints remain elusive.

Lincowski et al. (2018) used a coupled photochemical, climate, and radiative transfer model to consider the effects of Earth- and Venus-like aerosols such as water and sulfuric acid clouds as well as the photochemical products of these and other molecules within the TRAPPIST-1 planets, for oxygen-rich and carbon dioxide-rich atmospheres. They found aerosol scattering cross sections up to 10^3 times that of Earth's ozone, which is consistent with our result for the upper limit of the haze scattering cross section suggested by the laboratory exoplanet haze samples. Within the current *HST* observational uncertainty, we cannot make statistically significant determinations regarding the likelihood of such hazy metal-rich atmospheres based on observations. Our findings thus represent an upper limit to haze in hydrogen-rich models of the TRAPPIST-1 outer planet atmospheres. The laboratory measurements of Hörst et al. (2018a) and He et al. (2018a), He et al. (2018b), as well as the modeling work of Lincowski et al. (2018), help to inform whether our results are physically realistic. More observations to better precision of the TRAPPIST-1 planets (as are currently planned with *JWST* GTO Cycle 1) will be required to make further predictions as to the haze content of these worlds. Figure 2.3 shows the precision required to rule out aerosols in heavy mean molecular weight atmospheres. For TRAPPIST-1 e and f, the worst-case scenario of 1000× solar with low clouds requires a precision of approximately 20 ppm, which is beyond the expected 30 ppm noise floor for *JWST* (Batalha et al., 2018). However, for more optimistic scenarios, 50 to 100 ppm would be enough to differentiate between various cloud cases for metallicities on the order of 100× solar.

2.4.4 Complexity of Combined Parameters

In Figure 2.3, we show the intersection of cloud top pressure levels with increasing metallicity and how this changes the observed strength of the transmission spectra. These results demonstrate the important likelihood that a combination of factors is at play in the small (< 500 ppm) features of the TRAPPIST-1 spectra. If indeed these atmospheres are not mainly primordial hydrogen, but secondary and composed of higher metallicity species, we may begin to speculate as to the types of clouds present in these atmospheres and on the ability of these cloud species to form thick, grey absorbing clouds. Schaefer et al. (2012) suggests that H_2O and CO_2 are the likeliest components of secondary atmospheres of Earth-like planets, and therefore these cloud species merit further investigation (Marley et al., 2013).

2.4.5 Aerosol Particle Properties

While we include in our models the effects of Rayleigh scattering haze, this does not capture the complexity of the full distribution of particles that may exist in the TRAPPIST-1 planet atmospheres. The laboratory results upon which we base our models show that very small particles are produced and are readily treatable by the Rayleigh approximation at *HST*/WFC3 wavelengths. However, it is possible that in a real planetary atmosphere, haze particle aggregates would form and grow large enough that their effect on radiative transfer would lie in the Mie regime (where the particle diameter $d_p \sim \lambda$) and require full treatment with Mie theory to capture (e.g., Kitzmann & Heng, 2018; Wakeford & Sing, 2015).

Additionally, the optical properties of particles must still be accounted for even if particles are small. In fact, the laboratory results of He et al. (2018b) show that the exoplanet haze particles have varying colors in the visible, which may suggest that their scattering and absorption properties in the near-IR wavelengths considered here may not be a simple matter of inducing a Rayleigh scattering slope. This question

awaits further laboratory measurements to characterize the optical properties of these haze analogues, which can then be more rigorously implemented into our models.

2.4.6 Future Observations

While the current *HST* observations have considerable limitations that prevent robust, specific predictions of the atmospheric properties of such small planets as found in the TRAPPIST-1 system, the *James Webb Space Telescope (JWST)* will have both the resolution and wavelength coverage to greatly enhance our ability to measure their atmospheres (Batalha et al., 2018). The effects of differing atmospheric compositions as well as the effects of any aerosols should be observable for several of the TRAPPIST-1 planets in only a few orbits (Morley et al., 2017b). Furthermore, upcoming *HST* observations of TRAPPIST-1 g (GO Proposal 15304, PI J. de Wit) may offer additional precision on its atmosphere. Planet h's atmosphere has not yet been observed in transit, though these observations are also upcoming (GO Proposal 15304, PI J. de Wit), and would naturally provide additional information as to the nature of this system. Finally, our results show that, in light of updated mass measurements, the previous *HST* observations do not rule out hydrogen-rich atmospheres for either planet e or f, as found by de Wit et al. (2018). This motivates new observations with higher precision, such as *JWST* can achieve, to provide better constraints on these atmospheres.

2.5 Conclusion

We have performed a modeling analysis supported by recent laboratory measurements to explore the nature of the outer TRAPPIST-1 planetary atmospheres. We find that, using laboratory-based and Solar System constraints for haze formation, there are upper limits on haze scattering cross sections in a hydrogen atmosphere to high statistical certainty with the *HST* data. These haze scattering cross sections range

from a minimum of 9×10^{-25} cm^2 for planet e to a maximum of 1×10^{-19} cm^2 for planet d. We found a minimum and maximum metallicity for a case with a 0.1 bar grey opacity source. Using water as a proxy for metallicity, we find that planets d, e, and f allow, at maximum, hydrogen-to-water mixing ratios of 500 to 630× solar, respectively. For our cloudier cases, we find that a high altitude cloud deck (12 mbar or lower in pressure) is needed to generate a model within the current precision of the *HST* data for planets d and e with solar composition. It is likely unphysical that such clouds could form and persist in the TRAPPIST-1 d and e atmospheres. The possibility of enhanced atmospheric metallicity has also been posed by previous studies about the water content of the TRAPPIST-1 system. Some of our results differ considerably from those of the original *HST* analysis; this difference ensues from additional mass constraints of the TRAPPIST-1 planets. High-precision mass measurements are of utmost importance to constrain the atmospheres of small terrestrial planets, and any further improvements on mass will allow better estimates of both atmospheric composition and aerosol content.

Our results further support secondary, post-primordial atmospheres for the TRAPPIST-1 planets d, e, and f, which could include substantial amounts of aerosols. Here we seek only to provide limits on the possible metallicity, cloud top pressure, and haze scattering cross sections of these atmospheres in light of the recent *HST* campaign. While our results suggest that the outer worlds d, e, and f of the TRAPPIST-1 system could have volatile-rich secondary atmospheres, determining the aerosol content of such volatile-rich atmospheres requires greater precision than the current set of *HST* data can provide. We show that at least 20 ppm precision will be needed to discern between cloudy versus clear cases in high metallicity atmospheres. Further investigations into the habitability of these worlds must include full consideration of atmospheric composition and aerosol content. In light of these possibilities, the TRAPPIST-1 planets should be of high priority for further examination with both

current and future observatories.

Chapter 3

Chemistry of Temperate Super-Earth and Mini-Neptune Atmospheric Hazes from Laboratory Experiments

"Knowledge is invariably a matter of degree: you cannot put your finger upon even the simplest datum and say 'this we know'."

— T.S. Eliot, *Knowledge and Experience in the Philosophy of F.H. Bradley*

3.1 Introduction

[1]Exoplanets, those planets outside our own solar system, can now be counted in the thousands thanks to past and ongoing surveys, e.g., *Kepler* (Borucki et al., 2010) and the *Transiting Exoplanet Survey Satellite (TESS)* (Ricker et al., 2014). Follow-up observations of the most promising planetary targets with the *Hubble Space Telescope*, *Spitzer Space Telescope*, and ground-based facilities have thus far shown a wide range of atmospheric conditions. Many of these planets host atmospheres that have muted transmission spectra (Wakeford et al., 2019b), indicative of significant and as of yet unidentified opacity sources in their atmospheres. Either condensate clouds or

[1]This chapter is published as Moran, Hörst, Vuitton, He, Lewis, Flandinet, Moses, North, Orthous-Daunay, Sebree, Wolters, Kempton, Marley, Morley, and Valenti (2020), "Chemistry of Temperate Super-Earth and Mini-Neptune Atmospheric Hazes from Laboratory Experiments," *the Planetary Science Journal*, 1 (17). doi: 10.3847/PSJ/ab8eae

photochemical hazes in these atmospheres, or some combination thereof, are compelling candidates to explain the observed spectra (Dragomir et al., 2015; Knutson et al., 2014b; Kreidberg et al., 2014a; Sing et al., 2016). As clouds and/or hazes are observed in our solar system on every world with a substantial atmosphere, the presence of such aerosols on extrasolar worlds comes as no surprise. Yet, the possibly unique compositions of these aerosols and the energetic regimes in which they are formed remain outstanding questions.

Photochemical hazes in particular can impact planetary atmospheric temperature structure (e.g., Zhang et al., 2017), the chemical inventory of the atmosphere and surface (e.g., Grundy et al., 2018), and ultimately the habitability of worlds near and far (e.g., Hörst et al., 2012; Trainer et al., 2006). The composition of photochemical hazes will impact their spectroscopic properties, and thus their ability to absorb radiation across the electromagnetic spectrum. Haze opacity affects general energy transport and atmospheric dynamics (Helling, 2019; Marley et al., 2013), can shield the planetary surface from harmful radiation (Arney et al., 2017), and affects telescope observations of exoplanets in both transmission and emission (e.g., Morley et al., 2017a) and reflected light (e.g., Gao et al., 2017b).

Titan, the largest moon of Saturn, is the best-studied hazy world of our solar system and provides critical context for the study of hazes on other worlds. However, *in-situ* measurements of distant solar system worlds, such as Titan, remain challenging. Therefore, a long history of laboratory experiments has shed light on the formation, physical properties, and chemical structures of potential hazes in the atmospheres of solar system planets (Cable et al., 2012). These experiments have provided insights into the chemical pathways to haze formation in Titan's atmosphere (e.g., Bonnet et al., 2013; Gautier et al., 2014; Gautier et al., 2016; Hörst et al., 2018c; Vuitton et al., 2010), and revealed that photochemical processes can produce amino acids and nucleobases suggestive of prebiotic chemistry (Hörst et al., 2012). This legacy

of laboratory work has contributed greatly to our understanding of Titan's overall atmospheric chemistry and climate (see, e.g., Hörst 2017).

The haze analogues formed in these solar system experiments – so-called "tholins" – have thus far been the product mainly of methane, nitrogen, and carbon monoxide gas mixtures that represent the atmosphere of Titan or conditions on the early Earth (e.g., Hörst et al., 2018b). Additionally, models of exoplanet photochemistry have also primarily focused on "hydrocarbon" hazes similar to that of Titan (e.g., Howe & Burrows, 2012; Kawashima & Ikoma, 2019; Miller-Ricci Kempton et al., 2012; Morley et al., 2013; Morley et al., 2015), if only because these are the chemical pathways for which there are data. Experiments exploring the wide range of possible atmospheric conditions found in exoplanet atmospheres remain mostly untapped. The few that have been performed have focused either on optical properties of essentially Titan-like atmospheres with increased oxidation to mimic early Earth-like exoplanets (Gavilan et al., 2017; Gavilan et al., 2018) or gas phase chemistry of hot Jupiter-like atmospheres with temperatures in excess of 1000 K and with H_2/CO-dominated gas mixtures (Fleury et al., 2019).

This work presents the first solid phase chemical composition measurements from a series of experiments designed to explore the wide range of possible atmospheric compositions for sub-Neptune planets. Current exoplanet population statistics suggest a dichotomy between planets 1.75-3.0 $R_\oplus$ and planets 1.1-1.75 $R_\oplus$ (Fulton & Petigura, 2018; Fulton et al., 2017; Hardegree-Ullman et al., 2020), which have been termed "super-Earths" and "mini-Neptunes," respectively. Theories of planetary formation and evolution have suggested that these could be two distinct planet classes that differ due to the presence or absence of a substantial hydrogen-helium envelope, which is then eroded by subsequent stellar photoevaporation (Cloutier & Menou, 2019; Lehmer & Catling, 2017; Lopez & Fortney, 2014; Owen & Wu, 2016). Another model, core-powered mass loss, suggests that these planets form with hydrogen-poor

atmospheres (Gupta & Schlichting, 2019), and can also explain the radius gap between mini-Neptunes and super-Earths as the result of late-stage planet-disk interactions. Current population statistics do not favor one model over the other (Loyd et al., 2020), and it is unclear whether these are in fact two separate outcomes of planet formation or if they are a single planet population sculpted by atmospheric evolution through time (Leconte et al., 2015).

Moreover, observational data to determine the atmospheric compositions of these planets is also extremely sparse. Only two observational constraints at the mini-Neptune end of this planet distribution currently exist, and have confirmed hydrogen-rich atmospheres for two planets, K2-18 b (Benneke et al., 2019b; Tsiaras et al., 2019) and GJ 3470 b (Benneke et al., 2019a). On the super-Earth end of the planet distribution, while H_2-rich atmospheres have been ruled out for a number of planets (e.g., Demory et al., 2016; Kreidberg et al., 2019), no definitive atmospheric composition constraints are possible with current instruments. Compositional constraints of heavier mean molecular weight atmospheres will require the higher-precision capabilities of future observatories like the *James Webb Space Telescope*, the *ARIEL Space Telescope*, or Extremely Large Telescopes on the ground. Therefore, the experiments described here have had to rely on atmospheric modeling approaches to determine the likely kind of atmospheres to consider for super-Earths and mini-Neptunes. These theoretical modeling studies have shown that these atmospheres could range from secondary "terrestrial" compositions due to outgassing to primordial H_2-dominated compositions (Elkins-Tanton & Seager, 2008; Fortney et al., 2013; Hu & Seager, 2014; Moses et al., 2013; Schaefer et al., 2012).

Previous measurements resulting from these super-Earth to mini-Neptune experiments have reported production rates for a range of composition, temperature, and energy sources (He et al., 2018a; Hörst et al., 2018a), the color and size of haze particles (He et al., 2018b), and the gas phase chemistry occurring during the experi-

ments (He et al., 2019). Here, we explore the effect of temperature, composition, and energy source on the chemistry of the resulting solid haze particles across the range of experimental conditions.

3.2 Methods

We produced analogue haze particles in an atmospheric chamber under theoretical super-Earth and mini-Neptune conditions. We then collected the solid sample produced in this experiment and performed very high resolution mass spectrometry with a Thermo Fisher Scientific LTQ-Orbitrap XL mass spectrometer. We also performed elemental combustion analysis to provide a starting point for the compositional study in order to identify specific molecules. Once measurements were taken, we used custom IDL software, *idmol*, to analyze the data and make molecular identifications. A detailed summary of each step in our procedure follows.

3.2.1 Laboratory Haze Sample Production

We produced laboratory exoplanet haze analogues in the PHAZER chamber (He et al., 2017) at Johns Hopkins University, a set-up that allows us to simulate particle production over a variety of atmospheric conditions. A schematic of the PHAZER chamber and supporting equipment is provided below as Figure 4.1.

The conditions explored for this particular experiment target a broad range of possible super-Earth and mini-Neptune atmospheric conditions, including three different temperatures (300 K, 400 K, and 600 K) and two kinds of energy sources: a Lyman-α UV lamp, which is a proxy for the UV flux from a stellar host; and an AC cold plasma discharge. The AC cold plasma glow discharge does not directly replicate a specific atmospheric process, but it is a useful proxy for the energetic environments of planetary upper atmospheres in which dissociation of more stable molecular bonds occurs (Cable et al., 2012).

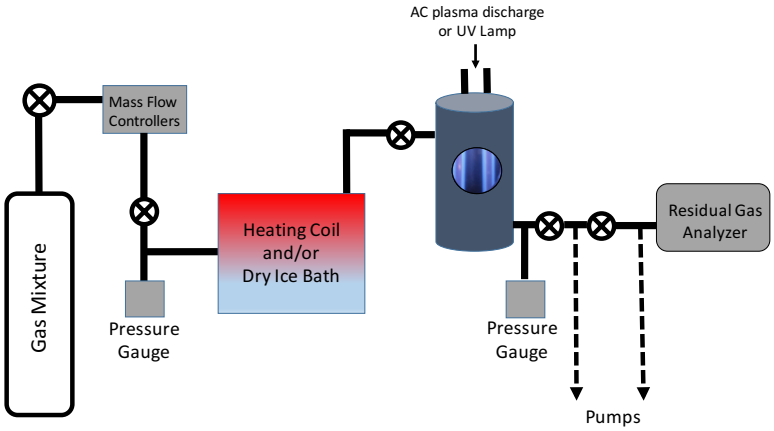

Figure 3.1. Generalized schematic of PHAZER chamber experimental apparatus used to produce the exoplanet haze analogues. Specific gas mixtures, temperature, and energy source differs between experimental conditions.

Within each temperature bin, we simulated three compositional regimes: 100×, 1000×, and 10000× metallicity atmospheres. Metallicity is the enhancement factor for all elements other than hydrogen and helium, relative to composition of the solar atmosphere. Broadly, our experimental conditions simulated hydrogen-rich, water-rich, and carbon-dioxide rich atmospheres at the three temperatures. These compositional breakdowns were determined through equilibrium chemistry calculations (Moses et al., 2013) for each temperature at 1 mbar in atmospheric pressure. Chemical equilibrium is a good first-order approximation of the dominant available constituents in a planetary atmosphere. Various modeling approaches (Hu & Seager, 2014; Moses et al., 2013) have suggested a range of possible gas mixtures resulting from chemical equilibrium. These cases can range from H_2-rich atmospheres, likely more representative of a primordial atmosphere that accreted directly from the proto-planetary disk, to outgassed atmospheres dominated by water or carbon dioxide. Without a statistically significant sample of observational constraints to work from, our gas mixtures are by necessity determined from theoretical modeling outputs. Our experimental conditions therefore sample a range of potential theoretical atmospheric outcomes thought to be common

for super-Earths and mini-Neptunes. We derive the mixing ratios from equilibrium chemistry calculations based on the Chemical Equilibrium and Applications code (CEA, Gordon and McBride 1996) and cap the constituent gases present at 1% or greater to provide a reasonable amount of experimental complexity. More details about the reasoning behind our initial gas mixtures can be found in He et al. (2018a) and He et al. (2018b), Hörst et al. (2018a).

Table 3.I lists initial gas mixing ratios for all nine experimental conditions. Each experiment was run with gases flowing continuously for 72 hours to produce ample solid sample and to provide comparison to previous Titan experimental production rates (Hörst et al., 2018a). Each experiment was performed at 1 mbar in pressure, where haze formation occurs in Titan's atmosphere (Cable et al., 2012; Hörst, 2017) and where we perform Titan tholin experiments for comparison. The experimental chamber was then moved to a dry (< 0.1 ppm H_2O), oxygen-free (< 0.1 ppm O_2) N_2 glove box (Inert Technology Inc., I-lab 2GB). Within the glove box, solid sample produced was collected from the chamber walls (in the case of high production) and from mica or glass discs placed at the bottom of the chamber during the experiment (in the case of low sample production). In the dry, oxygen-free glove box, samples were then transferred to plastic vials or cases, which were then sealed with parafilm and covered with aluminium foil for storage. The use of the glove box prevented alteration of the samples by ambient Earth atmospheric conditions or light sources. Additional details about the sample production can also be found in He et al. (2019) and He et al. (2018a), He et al. (2018b), Hörst et al. (2018a).

3.2.2 Orbitrap Mass Spectrometry Measurements

Each sample was prepared immediately prior to performing measurements, in order to minimize contamination by ambient atmosphere. If enough solid sample was produced, we dissolved each sample in CH_3OH (methanol) at 1 mg/mL. If the PHAZER chamber

	Metallicity		
Temperature	100×	1000×	10000×
600 K	72.0% H_2	42.0% H_2	66.0% CO_2
	6.3% H_2O	20.0% CO_2	12.0% N_2
	3.4% CH_4	16.0% H_2O	8.6% H_2
	18.3% He	5.1% N_2	5.9% H_2O
		1.9% CO	3.4% CO
		1.7% CH_4	4.1% He
		13.3% He	
400 K	70.0% H_2	56.0% H_2O	67.0% CO_2
	8.3% H_2O	11.0% CH_4	15.0% H_2O
	4.5% CH_4	10.0% CO_2	13.0% N_2
	17.2% He	6.4% N_2	5.0% He
		1.9% H_2	
		14.7% He	
300 K	68.6% H_2	66.0% H_2O	67.3% CO_2
	8.4% H_2O	6.6% CH_4	15.6% H_2O
	4.5% CH_4	6.5% N_2	13.0% N_2
	1.2% NH_3	4.9% CO_2	4.1% He
	17.3% He	16.0% He	
PHAZER Titan "tholin"	95.0% N_2		
	5.0% CH_4		

Table 3.I. Initial gas mixtures used in each exoplanet experiment, determined by equilibrium chemistry calculations at the specified pressure and composition relative to the Sun (Moses et al., 2013). Metallicities of 100×, 1000×, and 10000× solar generally correspond to H_2-rich, H_2O-rich, and CO_2-rich atmospheres. PHAZER Titan gas mixture also shown.

produced only a thin film, we collected the film from the mica or glass disc by soaking the disc in 1 mL of CH_3OH for a minimum of 3 hours before collecting the resulting CH_3OH-sample mixture and transferring it into a vial. Samples then underwent sonification (1 hr) and centrifugation (5 minutes, 10000 rpm) before an additional dilution at 1 mg/mL in CH_3OH. The soluble fraction of the sample was then injected into a Thermo Fisher Scientific LTQ-Orbitrap XL mass spectrometer (Hu et al., 2005; Perry et al., 2008) with electrospray ionization (ESI) (IPAG, Grenoble, France). The Orbitrap provides high resolution mass spectrometry, with resolving power better than 10^5 between 200 m/z and 400 m/z and exact mass determination accuracy of ±2ppm. "Blank" solutions from either a blank sample vial or disc and CH_3OH, but no sample,

were also injected and measured in the Orbitrap to account for any possible background contamination in the measurements (see Figure 3.4). Mass calibration using Thermo Fisher Scientific caffeine, MRFA peptide, and Ultramark solution was performed prior to measurements each day. Measurements were taken in three mass-to-charge (m/z) range bins, from 50 - 300 m/z, 150 - 450 m/z, and 400 - 1000 m/z. Overlap between bins ensures that signal at the edges of mass bins is properly accounted for. Instrument settings in each mass range were adjusted to ensure the best signal: the tube lens was set to 50 V, 70 V, and 90 V, respectively. We obtained 128 microscans at a flow rate of 3 μL/min with 4 scans per mass bin. We obtained measurements in both positive and negative ion polarities, as the resulting ions have displayed different molecular formulas for previous studies and thus allow a more complete view of the whole sample (Bonnet et al., 2013; Hörst, 2011). Samples in solution were stored in the refrigerator when not in use.

As some samples were insoluble in CH_3OH, additional solvents were also used in combination with CH_3OH, including toluene (C_7H_8), dichloromethane (CH_2Cl_2), and hexane (C_6H_{14}). Figure 3.3 shows which haze analogues were dissolved in which solvents. See Section 3.4.1 for further discussion about the solubility of the haze samples. These additional solvents were combined in approximately 1:1 solutions with methanol. Data acquisition and preliminary processing were performed with Thermo Fisher Scientific Xcalibur software provided by the manufacturer.

3.2.3 Combustion Analysis

Elemental combustion analysis was performed with a Thermo Scientific Flash 2000 Elemental Analyzer (Department of Chemistry and Biochemistry, University of Northern Iowa, IA, USA) on the two haze analogues that produced the most sample volume, the 400 K and 300 K at 1000× solar metallicity under the plasma source. We placed 1 to 2 mg of each sample in the analyzer for combustion analysis. The resulting elemental

percentages of C, H, and N are directly measured and the percentage of O is then determined by mass subtraction. These elemental ratios are presented in Table 3.II for the plasma products and Table 3.III for the UV products. PHAZER standard "Titan tholin" composition (produced from a 5% CH_4 in N_2 gas mixture) is provided as a point of comparison. Figure 3.2 shows this information in graphic form.

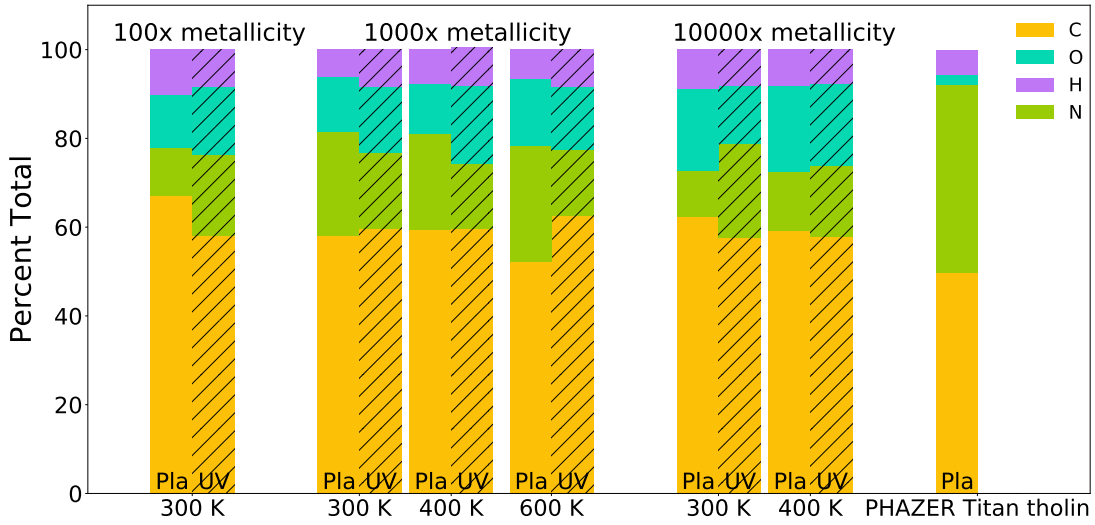

Figure 3.2. Results of elemental analysis performed with assignments based on Orbitrap MS measurements and *idmol* analysis. "Pla" and "UV" labels denote whether the sample was produced via AC plasma or the UV lamp energy source. These values are compared to PHAZER standard Titan tholin sample, with elemental ratios determined by combustion analysis. All exoplanet experimental samples have dramatically more oxygen than the Titan sample, presumably due to enhanced oxygen in the initial gas mixtures, suggesting that oxygen is readily incorporated into the solid. These measurements are subject to significant uncertainties as discussed in Section 3.2.4 and reported in Tables 3.II and 3.III.

3.2.4 Data Analysis

Only samples which showed substantial solubility (see Section 3.4.1) were subjected to detailed data analysis, i.e., the green shaded boxes in Figure 3.3. We accounted for solubility and potential contamination in two ways. We compared the mass spectrum of a blank taken directly prior to the sample with the mass spectrum of the sample. The intensity of the signal in the mass spectrum was used as a first pass diagnostic; however, the Orbitrap instrument always tries to maximize the number of

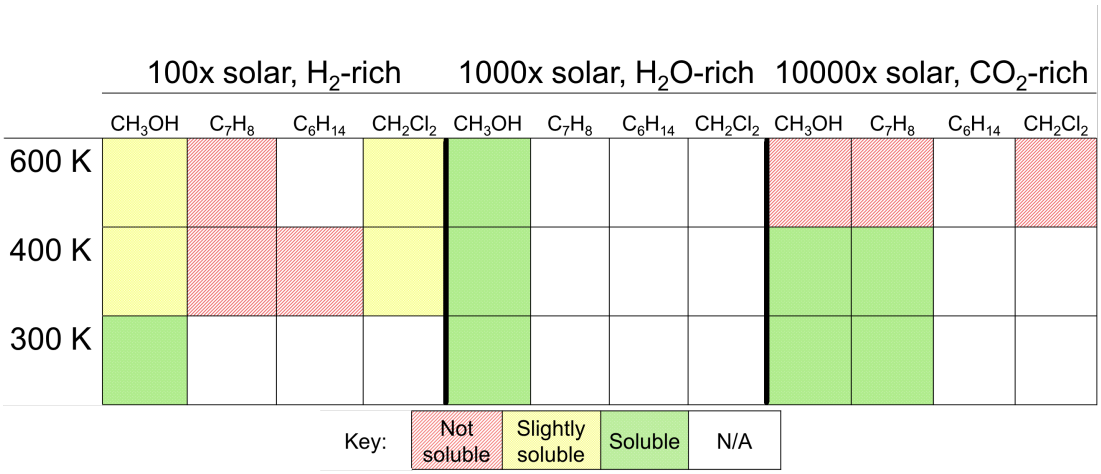

Figure 3.3. Results of testing various solvents to dissolve the exoplanet haze analogue solid products for use in the Orbitrap. All samples here were produced by plasma discharge, as the amount of UV-produced samples tend to be small and qualitative solubility observations are not possible. Red hatched squares indicate complete lack of solubility, yellow checkered squares indicate that solids partially dissolved, and green shaded squares indicate substantial solubility. The solvents were tested in subsequent order left-to-right, stopping if a solvent dissolved the sample. The solvents tested were methanol (CH_3OH), followed by a toluene-methanol (C_7H_8 - CH_3OH) solution, followed finally by a hexane-methanol (C_6H_{14} - CH_3OH) and/or a dichloromethane-methanol (CH_2Cl_2 - CH_3OH) solution.

ions accumulated and therefore intensities alone are not sufficient to determine signal (Hu et al., 2005). The next comparison was the structure of the mass spectrum itself. Repeating mass peak groupings are clearly observed in cases of true sample signal as compared to the blank, as shown in Figure 3.4.

These data contain many hundreds to thousands of peaks, making manual identification impractical. As such, data were analyzed with custom IDL/FORTRAN software, called *idmol* (Hörst, 2011), which quickly assigns molecular peaks. First, *idmol* calculates all possible molecules from the mass spectrum and then narrows down the options based on user input parameters such as the maximum number of oxygen molecules, the mass tolerance, and the nitrogen-to-carbon ratio. The program then eliminates peaks that are below the noise level or due to Fourier ringing in the most intense peaks (Hörst, 2011). *Idmol* uses the nitrogen rule (i.e., that compounds

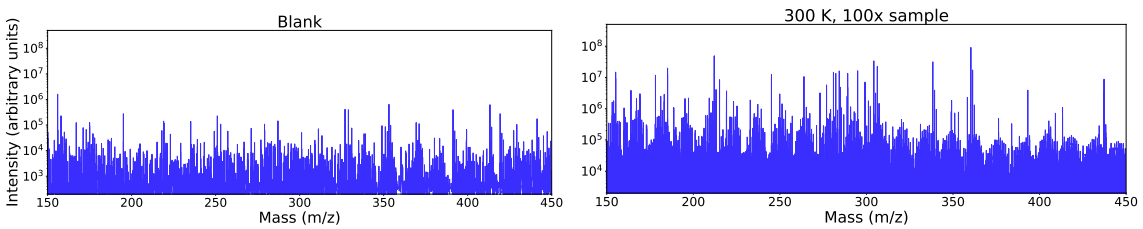

Figure 3.4. Mass spectrum of a blank (left). Mass spectrum of a soluble sample (right). The blank spectrum intensity is typically lower and no clear structure exists as compared to the mass spectrum of the sample. The insoluble samples have mass spectra that appear more similar to blank (left) than to the samples that were soluble (right). We also compared assigned peaks in the sample against the blank to ensure no potential contamination was unaccounted for.

with an even nominal mass have an even number of nitrogen atoms and vice versa for compounds with odd nominal masses) to make assignments for lower mass peaks and then assigns likely higher mass peaks based upon its previous lower mass assignments. Assigned molecules are then compared against a database of known molecular formulas for prebiotic material, including amino acids, nucleobases, and simple sugars taken from the literature (e.g., Cooper et al., 2018; Lu & Freeland, 2006). Once formula assignments were made by *idmol*, we checked each assigned peak in the sample against the corresponding blank to ensure any potential contamination was accounted for in the sample. No assigned peaks listed in Tables 3.IV, 3.V, 3.VI, 3.VII, 3.VIII, or 3.IX appeared in the corresponding blank data.

Additionally, final molecular assignments from *idmol* were compared to the elemental ratios from combustion analysis, as confirmation of accurate molecular identification. Elemental ratios were determined by calculating the intensity weighted average composition based on the assignments made by *idmol*. Previous work (Hörst, 2011) shows that oxygen-containing molecules tend to have lower intensities as measured by Orbitrap, and that boosting the lowest 10% intensities by a factor 10 brings elemental analysis results from Orbitrap and combustion analysis into reasonable agreement; therefore, we have performed this same correction here. Tables 3.II and 3.III and Figure 3.2 present results averaged over positive and negative ions. Previous analysis

of Titan haze analogues demonstrates that averaging over positive and negative ion modes is necessary to obtain accurate bulk sample composition (Hörst, 2011). Certain species are more likely to be either negatively ionized or positively ionized within the mass spectrometer, requiring measurement in both modes to describe the bulk sample. Error is reported as the standard deviation of the calculated ratios of all mass ranges for both positive and negative ions. Differing ionization efficiencies between molecules and the fact that the samples are not completely soluble will affect the Orbitrap results. Thus the intensity-weighted elemental analysis reported here has significant uncertainties associated with it, which the errors reported in Tables 3.II and 3.III reflect. The elemental ratios reported here should therefore be interpreted as general trends in the bulk sample composition rather than a strict adherence to the specific values reported.

3.3 Results

We observe broad trends in haze chemical properties for different metallicities and temperatures, driven in part by the impact of the initial gas mixture. Further experiments isolating only temperature or only the initial gas mixtures would provide additional insight as to the particular formation conditions of each solid compound. For this work, we focus on the broad trends observed and prebiotic molecular formulas detected in each experiment.

We observe regular spacings of peak groups within each metallicity case, observing spacings of 13.5 u for the 300 K, 100× (hydrogen-rich gas mixture) hazes, between 13 and 14 u for the 1000× (water-rich gas mixture) hazes at all three temperatures, and between 10-14 u for the 10000× (carbon dioxide-rich gas mixtures) hazes at 300 and 400 K. These groupings likely correspond to chemical families in the solid products. Figures 3.5, 3.6, and 3.7 show the mass spectrum for each sample for both positive and negative ions, as well for both plasma discharge- and UV-produced samples.

Additionally, we detect hundreds to thousands of different stoichiometries in each particular haze analogue, indicating very complex mixtures. Each individual stoichiometry represents a possible molecule. Tables 3.IV, 3.V, 3.VI, 3.VII, 3.VIII, and 3.IX report those with the molecular formulas for amino acids (both biological and non-proteinogenic), nucleotide bases, and sugars and their derivatives for each metallicity case.

3.3.1 Hydrogen-rich Atmospheres Results

For the hydrogen-rich (100× metallicity) initial gas mixtures, only the 300 K condition produced particles that were adequately soluble for further analysis within the Orbitrap. We observe repeating mass peak group spacings of 13.5 u in both the positive and negative ions of the data, likely corresponding to additions of repeated chemical groups combining in specific ratios, as has been seen previously in studies of Titan "tholin" (Hörst, 2011). In this set of gas mixtures, only the 300 K case contained NH_3, which suggests that ammonia, despite only being present at the ∼1% level in the gas phase, plays a key role in the resulting chemical incorporation of solid particles. NH_3 is highly susceptible to photolysis, as demonstrated in the models of Miller-Ricci Kempton et al. (2012).

Figure 3.5 shows mass spectra for all temperature cases. The 400 K and 600 K samples yielded noisy spectra with little to no structure. Both positive and negative mode data are superimposed upon each other, showing the spectral intensity for negative ions is systematically lower than the intensity for positive ions, as is typical for the Orbitrap instrument and results from differences in ionization efficiencies between positive and negative modes and instrument systematics (Hu et al., 2005; Perry et al., 2008). The 300 K plot shows intensities offset by a factor 10 so that the clearly structured stair-step pattern in the mass spectra of the positive and negative mode is more visible.

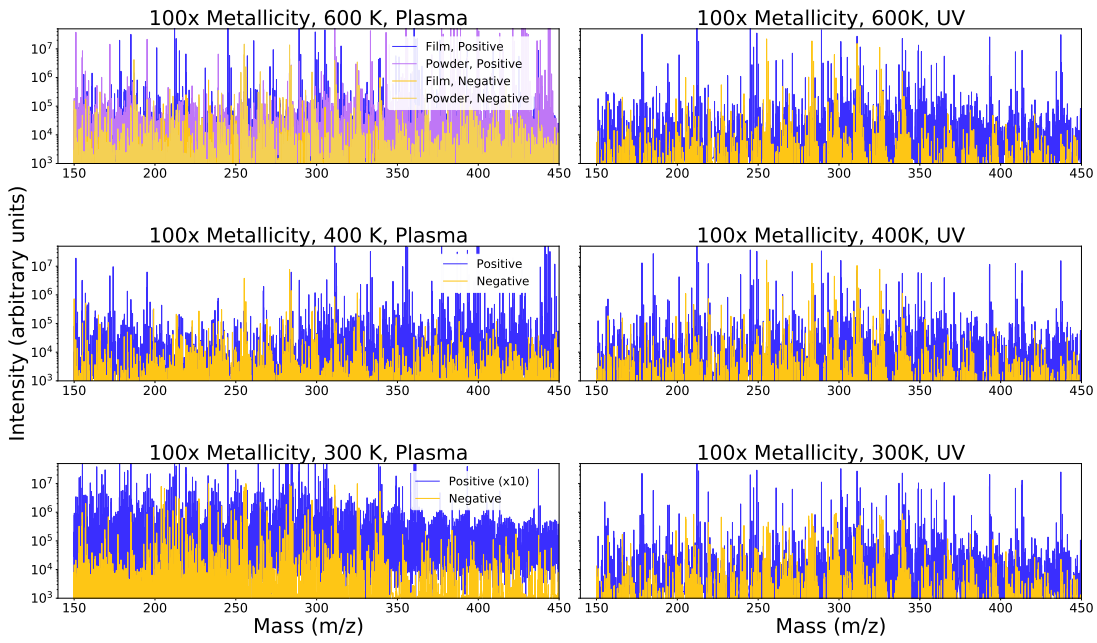

Figure 3.5. Mass spectra from 150 to 450 m/z for all 100x metallicity plasma and UV samples, all dissolved in methanol. The 300 K plasma discharge case shows clear signs of structure, while the two higher temperature samples are noisy and were not subjected to further analysis. The 300 K plasma sample intensities were offset by a factor 10 to clearly show the stair-step structure of the mass spectra. UV sample spectra are less structured, likely due to lower sample concentrations.

For our molecular detections, we report in Table 3.IV only the molecular formulas for amino acids, nucleotide bases, and sugars. The 300 K 100× sample showed the presence of $C_3H_6O_3$, which is the formula for glyceraldehyde. This is the first known atmospheric experiment in the absence of liquid water, to our knowledge, to detect the molecular formula of a simple sugar from the solid products (for further context and discussion, see Section 3.4.2). Additionally, we detected the formulas for adenine, glutamic acid, and histidine, which are a nucleobase and proteinogenic amino acids respectively, from the 300 K hydrogen-rich gas mixture. All play vital roles in Earth-based metabolisms. We explore the implications of this further in Section 3.4.2.

3.3.2 Water-rich Atmospheres Results

For the water-rich (1000× metallicity) initial gas mixtures, all samples produced highly structured mass spectra, indicating that the samples are composed of highly complex molecular compounds, as well as that they were soluble in methanol. We observe repeating mass peak groupings of between 13 and 14 u in both the positive and negative ions of the data, again pointing to repeating distinct chemical groups. Mass spectra for all conditions are found in Figure 3.6. The water-rich cases yielded the largest number of molecules with prebiotic roles, so we provide a separate table for each temperature. Tables 3.V and 3.VI present results for 600 K, Table 3.VII presents results for 400 K, and Table 3.VIII presents results for 300 K.

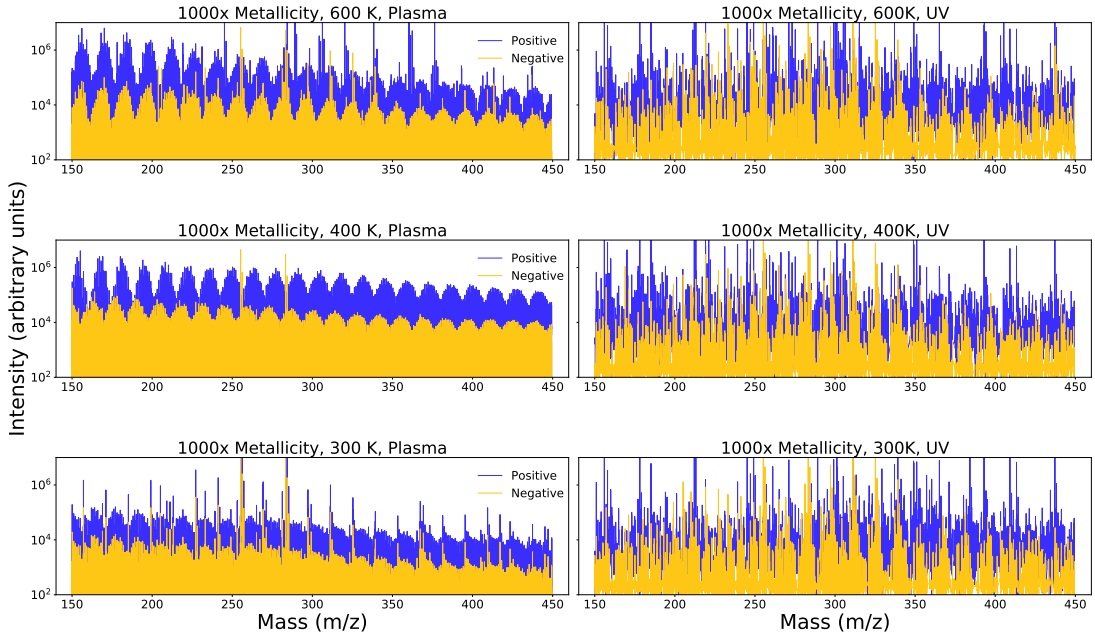

Figure 3.6. Mass spectra from 150 to 450 m/z for all 1000× metallicity plasma and UV samples, dissolved in methanol. While all are highly structured, the 300 K case of the plasma products displays a unique shape that indicates its distinctive chemistry as compared to the hotter two samples. UV sample mass spectra are all less structured, likely due to lower sample concentrations.

The 600 K and 400 K samples have similarly shaped peak groupings separated by 13 to 14 amu (averaging to 13.5 u). The 300 K sample has a different peak group

shape with consistent spacing of 14 u. The water-rich cases can be differentiated by certain unique constituents: only the 600 K case contained CO and only the 300 K gas did not contain H_2. Additional experiments isolating changes in temperature or gas mixture could help identify the source of the 300 K sample's unique mass spectrum shape.

We detected a multitude of formulas for amino acids, both biological and non-proteinogenic, in each set of solid particles produced from the water-rich gas mixtures, for both positive and negative ions. We detected nucleotide base formulas in the water-rich samples from each set of temperatures – all three contain the formula for guanine, while the 300 K condition additionally contains the formula for adenine. The 600 K and 300 K samples have the formula for thymine glycol, a derivative of the nucleotide base thymine. Finally, we detected the formula for the sugar acid gluconic acid in the 600 K sample and the formula for glyceraldehyde, the simplest monosaccharide, in the 300 K water-rich sample.

3.3.3 Carbon Dioxide-rich Atmospheres Results

For the carbon dioxide-rich (10000× solar metallicity) inital gas mixtures, only the two lower temperature samples produced structured mass spectra, indicating soluble complex molecular compounds in the solid products. We observe repeating mass peak groups, though far less regular than that of the lower metallicity cases, of 10 u to 14 u in both the positive and negative ions of the data. The less regular mass peak groupings likely result from a weaker overall signal from these samples. Figure 3.7 shows mass spectra, while Table 3.IX lists molecular formulas.

Carbon dioxide-rich cases produced very small amounts of sample, relative to the water-rich cases, and analysis was feasible for only two cases (300 K and 400 K). Nevertheless, in both samples we still find a number of prebiotic molecular formulas, including those for both derivatives of biological amino acids as well as

non-proteinogenic amino acids. Notably, both soluble 10000× metallicity samples contain the formula for sugar alcohol glucitol, while the 300 K sample also contains the formula for glucose, the most common monosaccharide on Earth.

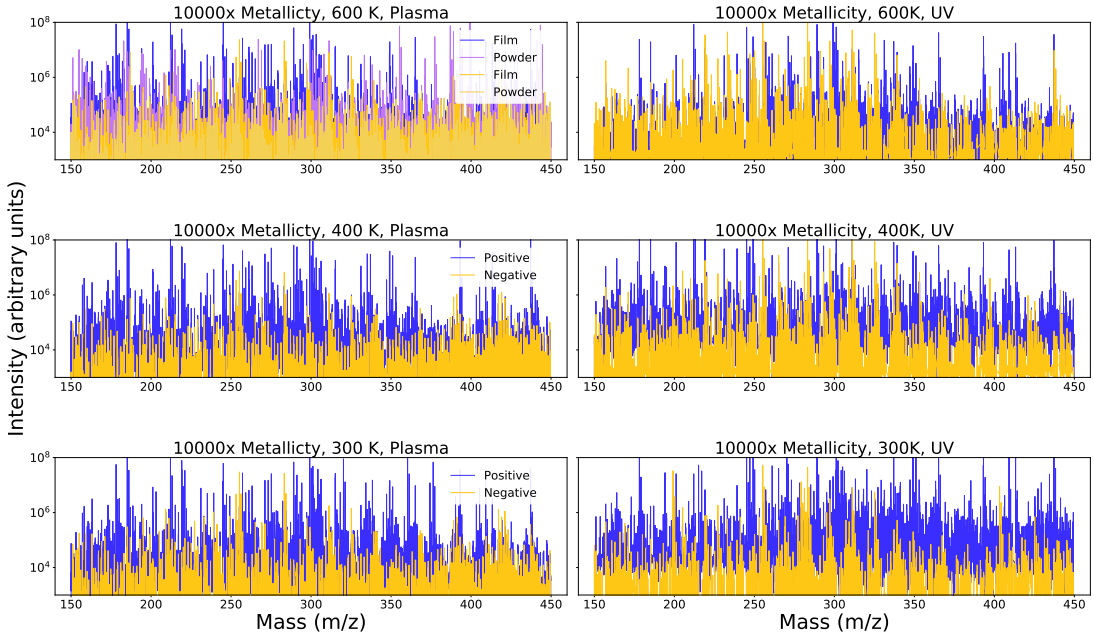

Figure 3.7. Mass spectra from 150 to 450 m/z for all 10000× metallicity plasma and UV produced samples, dissolved in methanol. Both the 300 K and 400 K samples were determined to be soluble based on their mass spectra.

3.4 Discussion

3.4.1 Solubility of Exoplanet Haze Analogues

As shown in Figure 3.3, the exoplanet haze analogues produced in the laboratory with the plasma energy source exhibited diverse solubility behavior. Quantitative measurements of solubility were outside the scope of this study. Additionally, there are various inconsistencies in the literature about protocols used to determine solubility of the complex mixtures often referred to as "tholin" (for discussion see e.g., Carrasco et al., 2009; He & Smith, 2014). Instead our solubility metric was qualitative, determined both by visual inspection of the sample within the solvent as well as visual inspection of the resulting mass spectral data (which can be affected by other chemical properties).

During visual inspection of a sample in a solvent, we noted any color change and any visible decrease in the amount of solid. We also visually compared the mass spectrum for each sample in solution with corresponding results for a control blank solvent (see Figure 3.4). From these post-measurement observations, we made a determination about the fidelity of the signal, and thus whether any sample had dissolved in the solvent. As the UV energy source produces significantly less sample (He et al., 2018a), solubility observations of the kind performed here were not possible.

As discussed in detail below, the lower temperature plasma samples always appeared soluble while the higher temperature samples were more likely to resist dissolving in a particular solvent. The hydrogen-dominant (100× solar metallicity) initial gas mixtures yielded methanol-insoluble solid haze particles except for the 300 K condition, which notably includes trace amounts of NH_3, ammonia. For the water-rich (1000× metallicity) cases, all solid samples appeared soluble in methanol, the first choice solvent for measurements. This solubility behavior is similar to Titan-like "tholin" haze analogues that result from nitrogen gas mixtures with trace amounts of methane and carbon monoxide (Carrasco et al., 2009), which often demonstrate significant solubility in methanol. Finally, the two lower temperature cases for the CO_2-dominant (10000× metallicity) gas mixtures were somewhat soluble in methanol, while the highest temperature 600 K condition yielded highly insoluble solid products.

Both polar solvents and polar-nonpolar mixtures were tested. Samples were only soluble in the pure polar solvents. From previous measurements of the particle structure (He et al., 2018b), long chains of particles were observed for the water-rich (1000×) 300 K and 400 K solid products. This structure suggests that the compounds themselves are polar, and thus their high solubility in the polar solvent of methanol is consistent with the general chemical rule "like dissolves like". The other polar solvent, dichloromethane, was also effective at dissolving the solid haze analogue samples. Titan "tholin" also exhibits highly polar solubility (see e.g., Carrasco et al., 2009), marking an

additional similarity in the broad chemical behavior of our exoplanet "tholin". While the 1000× metallicity exoplanet analogues share some physical characteristics with Titan haze analogues, elemental analysis (see Table 3.II) shows they are chemically distinguishable.

While earlier works suggested that the soluble fraction of "tholin" from Titan and similar planetary atmospheric experiments were representative of the sample as a whole (Carrasco et al., 2009), more recent studies found that the soluble and insoluble fractions may be chemically distinct (Maillard et al., 2018; Somogyi et al., 2016). This suggests that in addition to the limitations of our study regarding the solubility of our samples, the data we do have may not reveal the full chemical complexity of our exoplanet haze analogues. Future work on the chemistry of exoplanetary hazes should consider additional measurements that are not solubility dependent. For example, laser desorption/ionization (LDI) mass spectrometry measurements do not require soluble sample and have successfully identified insoluble macromolecules in Martian meteorite samples (Somogyi et al., 2016).

In addition to practical experimental considerations, the solubility of planetary haze analogues has further implications for planetary atmospheres themselves. For example, haze particles are known to act as cloud condensation nuclei (CCN) in many atmospheres, such as the organic haze for ethane/methane clouds on Titan (Hörst, 2017), meteoritic smoke particles for water ice clouds on Mars (Hartwick et al., 2019), and sand storms and seaspray for low lying clouds on Earth (Helling, 2019). Solids that are soluble in the atmospheric condensates of a world (such as salt in seaspray in water vapor on Earth) promote cloud formation and enable the creation of significant cloud belts. These condensation seeds facilitate cloud formation by reducing the level of saturation required for cloud materials to condense (Helling, 2019). The production of polar soluble solid haze particles high in the atmosphere, as analogous to the experiments considered here, may suggest that polar condensible

atmospheric constituents may more easily form clouds in exoplanet environments similar to our experimental atmospheres. For example, the hazes produced in our laboratory simulations might promote water cloud formation in cool enough atmospheres, which would be particularly relevant to our 300 K temperature regime across all metallicity conditions. Both the composition of the insoluble experimental hazes and their effectiveness as cloud seed particles are avenues for future study.

3.4.2 Prebiotic Material in Exoplanet Haze Analogues

Some of the first investigations of prebiotic chemistry assumed that synthesis required liquid water to occur (Miller, 1953; Miller & Urey, 1959). However, aerosols have long since been recognized as a source of prebiotic material, including amino acids, nucleobases, sugars, purines, and pyrimidines on the early Earth (e.g., Dobson et al., 2000). Mass spectrometry has been used in a variety of exobiology focused investigations from meterorites to Mars to Titan (e.g., Callahan et al., 2011; Neish et al., 2010; Sarker et al., 2003; Somogyi et al., 2016; Vuitton et al., 2014, and references therein), and its use has successfully enabled identification of amino acids and nucleobases in the products of Titan atmosphere simulation experiments (Hörst et al., 2012; Sebree et al., 2018), as well as both amino acids and sugars in meteorite samples suggested to have seeded the early Earth (Cooper et al., 2001).

Here, we have identified molecular formulas for eight biological amino acids (tyrosine, tryptophan, histidine, pyrrolysine, lysine, arginine, glutamine, glutamic acid) as well as dozens of their derivatives and two nucleobase formulas (guanine and adenine) as well as the formula for a derivative (thymine glycol deriving from thymine). We also detect, for the first time in the products of an atmospheric experiment that did not contain liquid water, the molecular formulas for simple sugar molecules and sugar derivatives (collectively called polyols): glyceraldehyde, gluconic acid, sucrose, glucitol, and glucose.

Previous laboratory simulations of UV-radiated precometary ice analogues (de Marcellus et al., 2015; Meinert et al., 2016; Nuevo et al., 2018) and laboratory simulations of high velocity impacts (e.g., Civis et al., 2016; Ferus et al., 2019) have detected numerous saccharides including ribose and deoxyribose, bolstering the theory that prebiotic planetary chemistry relies on external delivery via cometary, meteoritic, or interplanetary dust sources. Moreover, analysis of extraterrestrial sources such as the Murchison and Murray meteorites also shows the presence of both simple sugars, sugar alcohols, and sugar acids (Cooper et al., 2001; Cooper et al., 2018). Even more recently, bioessential sugars such as ribose and other pentoses have also been found in Murchison and NWA 801 meteorite samples (Furukawa et al., 2019). Other probes of external delivery sources farther afield than the local solar system neighborhood also exist. The simplest sugar-related molecule, glycolaldehyde, has been detected in interstellar molecular clouds (Hollis et al., 2000), and amines and amides have been detected throughout the interstellar medium (Kwok, 2016). In addition, the well-studied formose reaction, in which formaldehyde reacts to form a multitude of sugar molecules, has been studied both for interstellar synthesis of sugars in the gas phase (Jalbout et al., 2007) as well as extensively in aqueous solutions mimicking hydrothermal vents deep in the prehistoric Earth's ocean (Kopetzki & Antonietti, 2011) and under more temperate alkaline liquid water conditions (Pestunova et al., 2005).

Our results suggest that, given the right mixture of gases, a planetary atmosphere alone could photochemically generate not only amino acids and nucleobases, but even simple sugars. While not discounting external delivery of prebiotic materials, this result underscores the idea that at least preliminary abiogenesis can occur both in interstellar space and via external delivery as well as *in situ* in the atmospheres of planets themselves. The yields of any such prebiotic materials made in planetary atmospheres would require careful consideration, however (e.g., Harman et al., 2013),

and further reactions to generate more complex sugars and eventually biomolecules still would likely require liquid water and remain challenging (Schwartz, 2007).

Our 300 K, 100× metallicity simulated atmosphere, which is primarily hydrogen with lesser amounts of water and methane and trace amounts of ammonia, produced the formula for the simplest monosaccharide, glyceraldehyde ($C_3H_6O_3$). This atmosphere, with its high H_2 content, is likely most analogous to that of a mini-Neptune. The heavier metallicity experimental atmospheres (likely more analogous to super-Earth atmospheres) containing larger amounts of water, carbon dioxide, and methane were additionally able to produce more complex sugar molecular formulas such as glucose, sucrose, glucitol, and gluconic acid. Notably, these molecular formulas all occur across our range of temperatures from 600 K to 300 K.

We advise a note of caution in all our reported molecular detections. We detect only the formulas for all of the molecules in Tables 3.IV, 3.V, 3.VI, 3.VII, 3.VIII, and 3.IX. Our instrumental set-up alone cannot confirm molecular structure. High resolution mass spectrometry, as performed here, gives very precise molecular mass measurements. However, with complex mixtures of the kind examined here, many possible molecular combinations exist and overlap. Identifications that rely on mass only for such complex mixtures are therefore highly degenerate. Verification of the prebiotic molecules discussed here will involve follow-up measurements with other techniques that can infer and isolate molecular structure, such as high performance liquid chromatography (HPLC).

3.4.3 Chemical Pathways to Haze Formation

Gas phase results from these laboratory experiments have already been published (He et al., 2019), and allow us to hypothesize some chemical pathways for the formation of the solid hazes discussed here. Our gas phase study found that abiotic production of

oxygen, organics, and prebiotic molecules occurs readily in these mini-Neptune to super-Earth analogue atmospheres, suggesting that even the co-presence of such molecules ought not to be taken as a biosignature. The results presented here about the ability of such atmospheres to form sugars, amino acids, and nucleobases shows that while the presence of such "false positive" biosignature gases should be treated with skepticism, they also allow for the formation of a rich prebiotic inventory. The remaining steps from prebiotic chemistry to biology remains an open question. Observers in future exoplanet studies must balance biosignature searches with the knowledge that while abiotic production must always first be ruled out, the coexistence of such gases may also indicate that prebiotic chemistry has progressed significantly in the atmosphere and could further develop on any putative surface.

For the conditions in which we detected the formula for glyceraldehyde (the 300 K 100× and 1000× experiments), the gas phase results showed increased production of hydrogen cyanide (HCN) and formaldehyde (HCHO) (He et al., 2019), both known to participate in the generation of sugars (Cleaves, 2008; Schwartz et al., 1984). The production of the variety of amino groups in the solid phase is also unsurprising given the number of organic precursors observed in the gas phase.

Between different atmospheres, we observe that the solid haze analogues appear to incorporate certain molecules more readily than others. In Figure 4.6, we show Van Krevelen diagrams, which are widely used in the petroleonomics field and have since been used for Titan atmospheric haze studies (e.g., Hörst, 2011). These diagrams help visualize classes of compounds, as these have characteristic elemental ratios, resulting in clustering of similar compounds in specific locations on a Van Krevelen diagram (Kim et al., 2003). We show two forms of this diagram. The first (top row of Figure 4.6) compares H/C to N/O, which shows that distinct nitrogen-to-oxygen ratios form in all of our samples. The second (bottom row of Figure 4.6) shows H/C vs O/C. We follow the ratio bounds of Ruf et al. (2018) to map where carboxylic acids (fatty acids),

unsaturated hydrocarbons, aromatic hydrocarbons, amino-acid-like compounds, and carbohydrates/sugars fall in this H/C vs O/C phase space. Distinct diagonal, vertical, and horizontal lines are visible in this phase space as well. Such lines form along characteristic H/C and O/C ratios, which are characteristic of particular reaction pathways, such as methylation or demethylation, oxidation or reduction, etc. (Kim et al., 2003).

Interestingly, in the 1000× experiments, in the initial gas mixtures oxygen increases with decreasing temperature, but the opposite is seen in the elemental analysis of the solid haze products. From the least oxygen-rich and most carbon-rich gas mixture (the 600 K case), we see the strongest incorporation of oxygen into the solid, while with the least carbon-rich and most oxygen-rich gas mixture (the 300 K case), we see the least oxygen. This is clearly observed in the middle panel of the bottom row of Figure 4.6, which is in part why we are able to identify so many amino-acid-like formulas in this sample. Previous experiments on haze formation found that the increasing presence of carbon monoxide promotes aerosol production (Hörst & Tolbert, 2014), which the authors speculate could occur by shifting the oxygen incorporation more readily into the solid phase. Notably, the 1000× experiment showing the largest oxygen solid content (the 600 K case) is the only initial gas mixture to contain carbon monoxide, which is consistent with this interpretation by Hörst and Tolbert (2014). This further suggests that not only does the initial gas mixture matter in terms of the elemental species present, but the molecular carriers of these species matters greatly as well because these molecular carriers determine which elements are able to participate effectively in haze formation.

Furthermore, the role of nitrogen in haze formation is clearly very important, yet poorly understood (e.g., Hörst et al., 2018c; Imanaka & Smith, 2007; Trainer et al., 2012). Our only 100× experiment to produce soluble haze products is also the only 100× experiment that contained a nitrogen-bearing molecule in the initial

gas mixture, NH_3. With the UV energy source, this nitrogen-containing gas mixture also had the highest production rate of the 100× conditions and the second highest production rate of any condition (He et al., 2018a). This 300 K, 100× experiment produced the formulas for a nucleotide base, a monosaccharide, and both biological and non-proteinogenic amino acids, underscoring the dramatic role nitrogen can play in haze formation. Its ability to change the solubility of the hazes produced may have additional implications for its role in the chemistry of the system as well.

In comparison to previous Titan work, all our haze samples across metallicities and temperatures have far more oxygen, as shown in Figure 3.2. Although some of the physical characteristics of the haze products are similar, i.e., production rate (Hörst et al., 2018a), color and particle size (He et al., 2018b), and solubility (this work), our elemental analysis demonstrates robustly that these haze analogues are quite distinct chemically. Therefore, modeling efforts that use so-called "hydrocarbon" haze as a proxy in exoplanet studies must practice due caution as the optical properties and spectroscopic impact of true exoplanet hazes, at least for a wide range of super-Earths and mini-Neptunes, will likely also be different than that of hydrocarbon hazes. Furthermore, aside from incorrect observational interpretations from exoplanet transmission, emission, or reflectance spectroscopy, the chemical interpretations of such worlds will also be misconstrued if hydrocarbon haze proxies are used. Finally, such photochemical modeling efforts typically only include up to C_6 species due to computational complexity and expense as well as a lack of required information such as reaction rates and photolysis cross sections (Vuitton et al., 2019). However, recent work exploring Titan-like hazes shows that heavy molecular weight compounds ($\geqslant C_8$) are needed to fully explain aerosol formation and growth for Titan's haze (Berry et al., 2019). Considering the significant addition of oxygen in the exoplanet simulations performed here, inclusion of heavy molecular weight compounds is likely paramount to properly capturing exoplanet hazes through photochemical modeling.

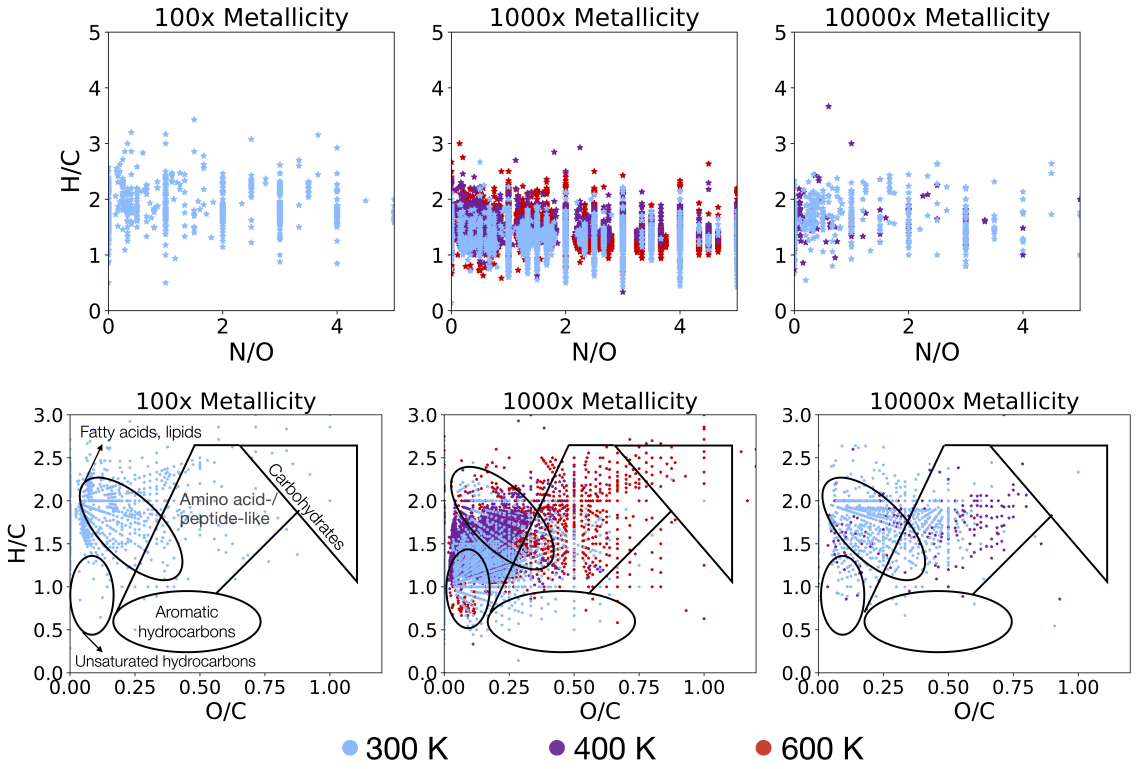

Figure 3.8. Van Krevelen diagrams of each measured set of samples, showing the hydrogen-to-carbon vs nitrogen-to-oxygen ratios (top row) and hydrogen-to-carbon vs oxygen-to-carbon ratios (bottom row) in each set of solid haze analogue material. Red symbols correspond to the 600 K samples, purple to 400 K samples, and blue to 300 K samples. The labels of compound regions on the lower 100× plot apply to the entire lower row.

3.4.4 Influence of Different Energy Sources on Haze Formation and Composition

Our results show general broad agreement within error between the elemental composition of hazes produced with the AC plasma and the FUV lamp. As noted previously, the AC plasma is not directly mimicking any specific process, but is instead a proxy for highly energetic upper planetary atmospheres. This suggests that the overall elemental composition of atmospheric hazes may not be as strongly affected by the source of energy imparted onto the atmosphere. However, the specific molecular identifications we are able to make does vary greatly between the two energy sources. As the energy density of the UV lamp is lower than that of the plasma (He et al., 2019),

the plasma source typically produces both more and larger solid particles (He et al., 2018a; He et al., 2018b). This may contribute to our seeing many more molecules in the mass spectral data of the plasma produced particles, as well as our ability to make molecular identifications. Additionally, because there is less sample to dissolve in the solvent, the concentration of the UV produced haze analogues injected into the mass spectrometer is typically lower than that of the plasma. These results are consistent with a study of Titan-like aerosols, in which the use of UV-photolysis as the energy source also generated fewer MS/MS detected prebiotic molecules than did plasma-produced aerosols (Sebree et al., 2018). Because the UV light source imparts less energy into the system, longer experimental steady states (beyond what is practical for the laboratory) would likely be required to generate more complex molecules. In a real planetary atmosphere, such timescales of UV photon bombardment may be less of an issue. However, the gases in the atmosphere will still require sufficiently energetic UV fluxes to dissociate their bonds to produce photochemical aerosols of any complexity.

These results may have implications for the ability of various stellar types of stars to induce complex photochemistry on their hosted planets. Recent modeling of quiescent M-dwarfs with less intense UV fluxes has shown that reaction rates for prebiotic chemistry on planets around M-dwarfs should be slower and that prebiotic pathways may in some cases be unable to proceed at all (Ranjan et al., 2017). Additional studies comparing the reaction rates of known pyrimidine synthesis in the presence and absence of UV light reiterates this result for M-dwarf planets, though they also consider whether the more frequent powerful flaring events on M-dwarfs may be enough to overcome this lack of quiescent UV flux during most of the stellar lifetime (Rimmer et al., 2018).

Another complication is that currently, we have relatively few measurements of planet host spectra in the UV. While these data gaps can be overcome with modeling

approaches (e.g., Peacock et al., 2019) and additional observational campaigns (e.g., Youngblood et al., 2017), translating these UV fluxes into proxies usable in the laboratory remains challenging. Any close-in exoplanet would likely be subject to charged particles traveling along stellar magnetosphere lines or bombardment by cosmic rays. These high energy particles could induce prolific chemistry in a planetary atmosphere. However, constraining the rates and magnitudes of such energetic particles deposited into the atmosphere is also outside the ability of current observations, and thus quantifying this energy flux for use in laboratory simulations is also difficult.

3.4.5 Prospects for the Observability of Exoplanet Haze Chemistry

As shown in this work, we expect a broad range of hazes over the diverse phase space of exoplanet atmospheres. While the chemistry described here is intriguing for exoplanet studies, there is currently a disconnect between laboratory production of these haze analogues and detection of these materials in exoplanet observations. Future measurements to obtain the optical properties of these hazes will provide observers with spectral features to search for with future spectroscopic observatories such as the *James Webb Space Telescope (JWST)*, the *ARIEL Space Telescope*, or the *Wide Field Infrared Survey Telescope (WFIRST)* beyond merely the muting of spectral features as observed thus far (e.g., Kreidberg et al., 2014a). Moreover, such optical property measurements would provide an additional layer of confirmation as to the presence of various chemical bonds in the haze particles and would thus provide additional evidence for our compositional measurements performed here.

The ubiquity of planetary hazes will impact both transiting exoplanet studies as well as future direct imaging missions to obtain spectra of exoplanet atmospheres in reflected light. Our experiments show substantial differences in haze production (He et al., 2018a; Hörst et al., 2018a), likely leading to impacts for observations across

a diverse range of atmospheres. However, observations of the atmospheres of mini-Neptunes and super-Earths to obtain their gas composition across wide wavelength ranges that probe different pressures in the atmosphere may also help reveal whether any substantial photochemistry is occurring on the planet. As we now have both gas phase chemistry (He et al., 2019) and solid phase chemistry constraints (this work) for photochemistry of a subset of these atmospheres, we may begin to infer the presence or absence of these processes from observations.

Observations of mini-Neptune atmospheres have just begun to produce compositional constraints. For example, a recent study of GJ 3470 b found a hydrogen-dominated atmosphere with depleted water, ammonia, and methane gas and Mie scattering aerosols (Benneke et al., 2019a), reminiscent of the gas phase chemistry of our 300 K, 100× metallicity experiment (He et al., 2019), though this planet has a much higher equilibrium temperature of nearly 700 K. Another cooler (∼300 K) mini-Neptune, K2-18 b, was recently shown to have significant water and possible water clouds in its atmosphere (Benneke et al., 2019b; Tsiaras et al., 2019), showing the diversity of mini-Neptune atmospheres.

This diversity may result from temperature differences between the planets resulting in differing atmospheric chemistry, as shown is likely from our laboratory experiments. When optical properties of the hazes discussed here are obtained, these exoplanets would make fascinating targets for future observatories. With observations of both individual planets as case studies and of larger planetary trends in temperature and atmospheric composition, we can explore whether any of the hazes we find experimentally are truly present in existent exoplanetary atmospheres and thus further investigate the prevalence of various chemical pathways.

3.5 Conclusion

We have conducted very high resolution Orbitrap mass spectrometry measurements of the solid haze products resulting from a suite of laboratory experiments from the PHAZER chamber, exploring temperate exoplanet atmospheres over a range of initial gas chemistries. We find that these haze products show varying solubility behavior, with all solids being at least partially soluble in polar solvents, suggesting that these hazes may make for effective cloud condensation nuclei in exoplanetary atmospheres with polar condensible material. Additionally, we find that all haze products have very large oxygen contents in the solid products, showing a marked difference in elemental composition to previous Titan atmospheric work. Finally, we detect a number of prebiotic molecular formulas, including those for biological and non-proteinogenic amino acids, for two nucleotide bases, and for the first time from an atmospheric experiment without liquid water, formulas for simple sugars.

This work demonstrates the power of laboratory experiments in understanding the complex chemistry at work in exoplanet atmospheres, both at large general scales as well as at for detailed single compound detections. Future follow up work is required to confirm the presence of our prebiotic molecular formula detections, as well as to understand the ability of haze particles to act as cloud condensation nuclei in such atmospheres. Connecting the chemical information gathered here to a telescopic observable will be highly important to make the most of these results and their implications for distant worlds.

Sample	Carbon wt%	Hydrogen wt%	Nitrogen wt%	Oxygen wt%	C/O ratio	C/N ratio
via Orbitrap MS	Plasma	Plasma	Plasma	Plasma	Plasma	Plasma
600 K, 100×	-	-	-	-	-	-
400 K, 100×	-	-	-	-	-	-
300 K, 100×	67.0±5.2%	10.3±1.0%	10.8±6.6%	11.9±6.6%	5.6±3.2	6.2±3.8
600 K, 1000×	52.2±2.6%	6.6±1.7%	26.0±11.0%	15.3±8.0%	3.4±1.8	2.0±0.9
400 K, 1000×	59.4±4.5%	7.7±1.1%	21.6±2.5%	11.3±3.9%	5.3±1.9	2.7±0.4
300 K, 1000×	58.1±1.3%	6.1±0.4%	23.5±2.1%	12.4±2.4%	4.7±0.9	2.5±0.2
600 K, 10000×	-	-	-	-	-	-
400 K, 10000×	59.2±4.2%	8.2±1.2%	13.2±17.0%	19.5±11.6%	3.0±1.8	4.5±5.8
300 K, 10000×	62.3±5.1%	8.8±1.1%	10.3±13.2%	18.7±6.9%	3.3±1.3	6.1±7.8
via Combustion						
400 K, 1000×	56±2.5%	6.1±0.2%	21.1±0.5%	17±3.2%	3.3±0.6	2.7±0.6
300 K, 1000×	51±1.2%	6.1±0.1%	27.1±0.7%	15±2.0%	3.4±0.5	1.9±0.5
PHAZER Titan "tholin"	49.6±0.5%	5.6±0.5%	42.5±0.5%	2.2±0.5%	22.5±0.5	1.2±0.5

Table 3.II. For samples produced by plasma discharge, elemental ratios and associated carbon-to-oxygen and carbon-to-nitrogen ratios. Some plasma samples were not soluble and thus were not subjected to further analysis; these rows are left empty in the table. Errors from the Orbitrap are the standard deviation of all mass ranges for both positive and negative ions for each sample. Errors reported for combustion analysis are the standard deviations of 3 runs for the 400 K sample and 4 runs for the 300 K sample. Similar results from the combustion analysis confirm that the *idmol* molecular assignments based on LTQ Orbitrap measurements are accurate. Standard PHAZER Titan "tholin" elemental analysis provide a point of comparison.

Sample	Carbon wt%	Hydrogen wt%	Nitrogen wt%	Oxygen wt%	C/O ratio	C/N ratio
via Orbitrap MS	UV	UV	UV	UV	UV	UV
600 K, 100×	–	–	–	–	–	–
400 K, 100×	–	–	–	–	–	–
300 K, 100×	58.1±7.3%	8.2±1.1%	18.3±5.6%	15.4±5.1%	3.8±1.3	3.2±1.1
600 K, 1000×	62.7±7.2%	8.5±1.2%	14.8±12.7%	14.1±4.4%	4.4±1.5	4.3±3.7
400 K, 1000×	59.8±5.4%	8.5±1.5%	14.5±11.0%	17.7±3.3%	3.4±0.7	4.1±3.2
300 K, 1000×	59.8±6.5%	8.3±1.1%	17.1±7.2%	14.8±4.8%	4.1±1.4	3.5±1.5
600 K, 10000×	–	–	–	–	–	–
400 K, 10000×	57.9±7.4%	7.7±0.8%	16.0±10.8%	18.4±8.5%	3.1±1.5	3.6±2.5
300 K, 10000×	57.7±9.0%	8.1±1.1%	21.2±8.3%	13.0±6.9%	4.4±2.5	2.7±1.1

Table 3.III. For samples produced by UV illumination, elemental ratios and associated carbon-to-oxygen and carbon-to-nitrogen ratios. Errors reported are the standard deviation of all mass ranges and both polarities for each sample. Some plasma products were insoluble and unable to provide adequate signal for measurement and analysis. The corresponding UV samples also had very poor signal and attempts at analysis were inconclusive. Compositional differences between the samples produced by different energy sources exist, but mostly fall within error.

			100× Results	
			600 K *material insoluble*	
			400 K *material insoluble*	
			300 K	
Mass (m/z) ±Δppm	*Detection*	*Formula*	*Potential Molecule*	*Relevance*
90.0317 ±2.4	-	$C_3O_3H_6$	glyceraldehyde	monosaccharide
129.0426 ±0.9	-	$C_5NO_3H_7$	pyroglutamic acid	non-proteinogenic amino acid
135.0545 ±2.1	-	$C_5N_5H_5$	adenine	nucleotide base
147.0532 ±1.5	-	$C_5NO_4H_9$	glutamic acid	biological amino acid
155.0695 ±2.3	-	$C_6N_3O_2H_9$	histidine	biological amino acid
159.0895 ±0.8	-	$C_7NO_3H_{13}$	L-valine, N-acetyl	non-proteinogenic amino acid
211.0845 ±1.3	p	$C_{10}NO_4H_{13}$	tyrosine, 3-methoxy	non-proteinogenic amino acid
219.0743 ±1.8	p	$C_8NO_6H_{13}$	*O*-Succinylhomoserine	non-proteinogenic amino acid
246.1216 ±1.2	+/p	$C_{10}N_2O_5H_{18}$	Boc-L-glutamine	non-proteinogenic amino acid

Table 3.IV. Molecular formulas detected from each 100× metallicity experiment. Detection column indicates energy source and detection polarity. Plasma (+: positive ion, -: negative ion) and UV (p: positive ion, n: negative ion). We report the smaller Δppm between measured m/z and exact m/z when a detection was made in more than one instrument mode.

		1000×, 600 K Results		
Mass (m/z) ±Δppm	*Detection*	*Formula*	*Potential Molecule*	*Relevance*
102.0429 ±1.7	+	$C_3N_2O_2H_6$	cycloserine	non-proteinogenic amino acid
103.0633 ±1.7	+	$C_4NO_2H_9$	N,N-Dimethylglycine	amino acid derivative
114.0429 ±1.4	+	$C_4N_2O_2H_6$	β-cyanoalanine	non-proteinogenic amino acid
132.0899 ±1.0	+	$C_5N_2O_2H_{12}$	ornithine	non-proteinogenic amino acid
146.0691 ±2.4	+	$C_5N_2O_3H_{10}$	glutamine	biological amino acid
146.1055 ±2.3	+	$C_6N_2O_2H_{14}$	lysine	biological amino acid
151.0494 ±2.7	-	$C_5N_5OH_5$	guanine	nucleotide base
153.0426 ±2.6	-	$C_7NO_3H_7$	*p*-Aminosalicyclic acid	aminobenzoic acid
153.0790 ±0.4	+/-	$C_8NO_2H_{11}$	dopamine	non-proteinogenic amino acid
155.0695 ±0.02	+/-	$C_6N_3O_2H_9$	histidine	biological amino acid
156.0647 ±0.3	+/-	$C_5N_4O_2H_8$	1,2,4-Triazole-3-alanine	non-proteinogenic amino acid
157.0375 ±3.0	-	$C_6NO_4H_7$	aminohexa-dienedioic acid	non-proteinogenic amino acid
157.0739 ±0.4	+/-	$C_7NO_3H_{11}$	furanomycin	non-proteinogenic amino acid
157.1103 ±0.6	+	$C_8NO_2H_{15}$	cyclohexylglycine	non-proteinogenic amino acid
158.0328 ±2.7	-	$C_5N_2O_4H_6$	dihydroorotic acid	pyrimidinemonocarboxylic acid
159.0895 ±3.5	-	$C_7NO_3H_{13}$	L-valine, N-acetyl	non-proteinogenic amino acid
159.1259 ±0.2	+	$C_8NO_2H_{17}$	octanoic acid, 8-amino-	non-proteinogenic amino acid
160.0484 ±3.4	-	$C_5N_2O_4H_8$	thymine glycol	nucleotide base derivative
160.1212 ±0.4	+	$C_7N_2O_2H_{16}$	L-Lysine, N^6-methyl-	non-proteinogenic amino acid
161.0688 ±1.9	-	$C_6NO_4H_{11}$	2-Aminohexanedioic acid	non-proteinogenic amino acid
167.0695 ±0.02	+/-	$C_7N_3O_2H_9$	β-Pyrazinyl-L-alanine	non-proteinogenic amino acid
169.0851 ±0.13	+/-	$C_7N_3O_2H_{11}$	3-Methylhistidine	non-proteinogenic amino acid
171.0644 ±1.0	+/-	$C_6N_3O_3H_9$	β-hydroxyhistidine	non-proteinogenic amino acid
171.1259 ±0.2	+	$C_9NO_2H_{17}$	cyclohexylalanine	non-proteinogenic amino acid
172.0960 ±1.0	+/-	$C_6N_4O_2H_{12}$	enduacididine	non-proteinogenic amino acid
173.0437 ±2.9	-	$C_5N_3O_4H_7$	azaserine	non-proteinogenic amino acid
174.1004 ±1.3	+/-	$C_7N_2O_3H_{14}$	formyllysine	non-proteinogenic amino acid
174.1117 ±0.8	+	$C_6N_4O_2H_{14}$	arginine	biological amino acid
175.0845 ±2.7	-	$C_7NO_4H_{13}$	spermidic acid	non-proteinogenic amino acid
175.0957 ±0.9	+/-	$C_6N_3O_3H_{13}$	citrulline	non-proteinogenic amino acid
181.0739 ±2.5	-	$C_9NO_3H_{11}$	tyrosine	biological amino acid
182.0804 ±1.5	+/-	$C_7N_4O_2H_{10}$	lathyrine	non-proteinogenic amino acid
188.1161 ±0.8	+/-	$C_8N_2O_3H_{16}$	leucine, glycyl-	non-proteinogenic amino acid
188.1273 ±1.1	+	$C_7N_4O_2H_{16}$	homoarginine	non-proteinogenic amino acid
195.0895 ±3.4	-/n	$C_{10}NO_3H_{13}$	tyrosine, O-methyl	non-proteinogenic amino acid
196.0484 ±3.2	-	$C_8N_2O_4H_8$	phenylglycine, m-nitro	non-proteinogenic amino acid
196.0848 ±2.6	-	$C_9N_2O_3H_{12}$	pyridinylmethylserine	non-proteinogenic amino acid
196.0583 ±2.2	+	$C_6O_7H_{12}$	gluconic acid	sugar acid
199.0845 ±3.1	-	$C_9NO_4H_{13}$	anticapsin	non-proteinogenic amino acid

Table 3.V. Molecular formulas detected from the 600 K, 1000× metallicity experiment. Detection column indicates energy source and detection polarity. Plasma (+: positive ion, -: negative ion) and UV (p: positive ion, n: negative ion). We report the smaller Δppm between measured m/z and exact m/z when a detection was made in more than one instrument mode.

1000×, 600 K Results				
Mass (m/z) $\pm\Delta ppm$	*Detection*	*Formula*	*Potential Molecule*	*Relevance*
205.0851 ±3.0	-	$C_{10}N_3O_2H_{11}$	tryptazan	non-proteinogenic amino acid
206.0804 ±3.5	-	$C_9N_4O_2H_{10}$	benzotriazolylalanine	non-proteinogenic amino acid
208.0848 ±2.8	-	$C_{10}N_2O_3H_{12}$	phenylasparagine	non-proteinogenic amino acid
210.0641 ±2.8	-	$C_9N_2O_4H_{10}$	p-Nitrophenylalanine	non-proteinogenic amino acid
211.0845 ±3.6	-	$C_{10}NO_4H_{13}$	tyrosine, 3-methoxy	non-proteinogenic amino acid
224.0797 ±3.2	-	$C_{10}N_2O_4H_{12}$	3-hydroxykynurenine	amino acid metabolite
226.1066 ±3.1	-	$C_9N_4O_3H_{14}$	alanylhistidine	amino acid metabolite
246.1328 ±1.8	+/-	$C_9N_4O_4H_{18}$	octopine	amino acid derivative
255.1583 ±1.1	+/-	$C_{12}N_3O_3H_{21}$	pyrrolysine	biological amino acid
267.1219 ±3.0	-	$C_{12}N_3O_4H_{17}$	agaritine	non-proteinogenic amino acid
270.0964 ±3.1	-	$C_{10}N_4O_5H_{14}$	histidine, β-aspartyl	non-proteinogenic amino acid
342.1162 ±1.3	n	$C_{12}O_{11}H_{22}$	sucrose	disaccharide
465.3090 ±1.2	+	$C_{26}NO_6H_{43}$	glycocholic acid	bile acid

Table 3.VI. Molecular formulas detected (continued) from the 600 K, 1000× metallicity experiment. Detection column indicates energy source and detection polarity. Plasma (+: positive ion, -: negative ion) and UV (p: positive ion, n: negative ion). We report the smaller Δppm between measured m/z and exact m/z when a detection was made in more than one instrument mode.

		1000×, 400 K Results		
Mass (m/z) ±Δppm	*Detection*	*Formula*	*Potential Molecule*	*Relevance*
151.0494 ±3.9	-	$C_5N_5OH_5$	guanine	nucleotide base
151.0633 ±3.6	-	$C_8NO_2H_9$	2-Phenylglycine	non-proteinogenic amino acid
153.0426 ±1.7	-/n	$C_7NO_3H_7$	*p*-Aminosalicyclic acid	aminobenzoic acid
153.0790 ±4.3	-	$C_8NO_2H_{11}$	dopamine	non-proteinogenic amino acid
155.0695 ±4.4	-	$C_6N_3O_2H_9$	histidine	biological amino acid
156.0647 ±4.0	-	$C_5N_4O_2H_8$	1,2,4-Triazole-3-alanine	non-proteinogenic amino acid
157.0739 ±3.4	-	$C_7NO_3H_{11}$	furanomycin	non-proteinogenic amino acid
159.0895 ±3.5	-	$C_7NO_3H_{13}$	L-valine, N-acetyl	non-proteinogenic amino acid
165.0790 ±3.5	-	$C_9NO_2H_{11}$	phenylalanine	non-proteinogenic amino acid
167.0695 ±4.1	-	$C_7N_3O_2H_9$	β-Pyrazinyl-L-alanine	non-proteinogenic amino acid
169.0851 ±0.1	+/-	$C_7N_3O_2H_{11}$	3-Methylhistidine	non-proteinogenic amino acid
171.0644 ±3.7	-	$C_6N_3O_3H_9$	β-hydroxyhistidine	non-proteinogenic amino acid
176.0586 ±3.7	-	$C_9N_2O_2H_8$	phenylglycine, m-cyano	non-proteinogenic amino acid
179.0946 ±4.5	-	$C_{10}NO_2H_{13}$	homophenylalanine	non-proteinogenic amino acid
181.0739 ±3.7	-	$C_9NO_3H_{11}$	tyrosine	biological amino acid
182.0804 ±3.5	-	$C_7N_4O_2H_{10}$	lathyrine	non-proteinogenic amino acid
193.0739 ±4.2	-	$C_{10}NO_3H_{11}$	phenylglycine, m-acetyl	non-proteinogenic amino acid
195.0895 ±3.4	-/n	$C_{10}NO_3H_{13}$	tyrosine, O-methyl	non-proteinogenic amino acid
196.0848 ±3.9	-	$C_9N_2O_3H_{12}$	pyridinylmethylserine	non-proteinogenic amino acid
204.0899 ±4.3	-	$C_{11}N_2O_2H_{12}$	tryptophan	biological amino acid
205.0851 ±4.4	-	$C_{10}N_3O_2H_{11}$	tryptazan	non-proteinogenic amino acid
206.0804 ±3.5	-	$C_9N_4O_2H_{10}$	benzotriazolylalanine	non-proteinogenic amino acid
208.0848 ±4.2	-	$C_{10}N_2O_3H_{12}$	phenylasparagine	non-proteinogenic amino acid
210.0651 ±4.2	-	$C_9N_2O_4H_{10}$	*p*-Nitrophenylalanine	non-proteinogenic amino acid
220.0848 ±3.8	-	$C_{11}N_2O_3H_{12}$	5-Hydroxytryptophan	biological amino acid derivative
224.0797 ±4.7	-	$C_{10}N_2O_4H_{12}$	3-hydroxykynurenine	biological amino acid metabolite
226.1066 ±4.5	-	$C_9N_4O_3H_{14}$	alanylhistidine	biological amino acid metabolite
236.0797 ±3.8	-	$C_{11}N_2O_4H_{12}$	N-formylkynurenine	non-proteinogenic amino acid
246.1004 ±4.0	-	$C_{13}N_2O_3H_{14}$	acetyltryptophan	biological amino acid derivative
246.1216 ±3.8	-	$C_{10}N_2O_5H_{18}$	Boc-L-glutamine	non-proteinogenic amino acid
246.1328 ±3.8	-	$C_9N_4O_4H_{18}$	octopine	biological amino acid derivative
255.1583 ±0.1	+/-	$C_{12}N_3O_3H_{21}$	pyrrolysine	biological amino acid
267.1219 ±3.0	-	$C_{12}N_3O_4H_{17}$	agaritine	non-proteinogenic amino acid
276.1321 ±2.4	-	$C_{11}N_2O_6H_{20}$	saccharopine	biological amino acid derivative
342.1162 ±1.3	n	$C_{12}O_{11}H_{22}$	sucrose	disaccharide
449.3141 ±0.1	+/-	$C_{26}NO_5H_{43}$	glycodeoxycholic acid	bile acid
465.3090 ±1.3	+	$C_{26}NO_6H_{43}$	glycocholic acid	bile acid

Table 3.VII. Molecular formulas detected from the 400 K, 1000× metallicity experiment. Detection column indicates energy source and detection polarity. Plasma (+: positive ion, -: negative ion) and UV (p: positive ion, n: negative ion). We report the smaller Δppm between measured m/z and exact m/z when a detection was made in more than one instrument mode.

1000×, 300 K Results				
Mass (m/z) ±Δppm	*Detection*	*Formula*	*Potential Molecule*	*Relevance*
90.0317 ±4.5	-	$C_3O_3H_6$	glyceraldehyde	monosaccharide
135.0545 ±5.8	-	$C_5N_5H_5$	adenine	nucleotide base
137.0477 ±5.9	-	$C_7NO_2H_7$	homarine	non-proteinogenic amino acid
141.0426 ±4.9	-	$C_6NO_3H_7$	aminomuconic semialdehyde	biological amino acid metabolite
151.0494 ±4.9	+/-	$C_5N_5OH_5$	guanine	nucleotide base
151.0633 ±4.7	-	$C_8NO_2H_9$	2-Phenylglycine	non-proteinogenic amino acid
153.0426 ±5.9	-	$C_7NO_3H_7$	*p*-Aminosalicyclic acid	aminobenzoic acid
153.0790 ±5.4	-	$C_8NO_2H_{11}$	dopamine	non-proteinogenic amio acid
155.0695 ±4.4	-	$C_6N_3O_2H_9$	histidine	biological amino acid
156.0647 ±5.1	-	$C_5N_4O_2H_8$	1,2,4-Triazole-3-alanine	non-proteinogenic amio acid
157.0739 ±4.6	-	$C_7NO_3H_{11}$	furanomycin	non-proteinogenic amio acid
160.0484 ±4.6	-	$C_5N_2O_4H_8$	thymine glycol	nucleotide base derivative
165.0790 ±4.7	-	$C_9NO_2H_{11}$	phenylalanine	non-proteinogenic amio acid
167.0695 ±5.4	+/-	$C_7N_3O_2H_9$	β-Pyrazinyl-L-alanine	non-proteinogenic amio acid
169.0851 ±4.6	+/-	$C_7N_3O_2H_{11}$	3-Methylhistidine	non-proteinogenic amio acid
171.0644 ±3.7	+/-	$C_6N_3O_3H_9$	β-hydroxyhistidine	non-proteinogenic amio acid
176.0586 ±3.7	+/-	$C_9N_2O_2H_8$	phenylglycine, m-cyano	non-proteinogenic amio acid
179.0946 ±4.5	-	$C_{10}NO_2H_{13}$	homophenylalanine	non-proteinogenic amio acid
181.0739 ±3.7	+/-	$C_9NO_3H_{11}$	tyrosine	biological amino acid
182.0804 ±3.5	+/-	$C_7N_4O_2H_{10}$	lathyrine	non-proteinogenic amio acid
193.0739 ±9.1	+	$C_{10}NO_3H_{11}$	phenylglycine, m-acetyl	non-proteinogenic amio acid
195.0895 ±3.4	+/-	$C_{10}NO_3H_{13}$	tyrosine, O-methyl	non-proteinogenic amio acid
196.0484 ±8.4	+	$C_8N_2O_4H_8$	phenylglycine, m-nitro	non-proteinogenic amio acid
196.0848 ±2.6	+/-	$C_9N_2O_3H_{12}$	pyridinylmethylserine	non-proteinogenic amio acid
204.0899 ±3.0	+/-	$C_{11}N_2O_2H_{12}$	tryptophan	biological amino acid
205.0851 ±4.4	+/-	$C_{10}N_3O_2H_{11}$	tryptazan	non-proteinogenic amino acid
206.0804 ±3.5	+/-	$C_9N_4O_2H_{10}$	benzotriazolylalanine	non-proteinogenic amino acid
208.0848 ±1.5	+/-	$C_{10}N_2O_3H_{12}$	phenylasparagine	non-proteinogenic amino acid
210.0641 ±7.7	+	$C_9N_2O_4H_{10}$	*p*-Nitrophenylalanine	non-proteinogenic amino acid
211.0845 ±0.1	p	$C_{10}NO_4H_{13}$	tyrosine, 3-methoxy	non-proteinogenic amino acid
220.0848 ±8.9	+/-	$C_{11}N_2O_3H_{12}$	5-Hydroxytryptophan	biological amino acid derivative
224.0797 ±8.3	+	$C_{10}N_2O_4H_{12}$	3-hydroxykynurenine	biological amino acid metabolite
226.1066 ±1.7	+/-	$C_9N_4O_3H_{14}$	alanylhistidine	biological amino acid metabolite
246.1004 ±8.1	+	$C_{13}N_2O_3H_{14}$	acetyltryptophan	biological amino acid derivative
246.1216 ±1.2	p	$C_{10}N_2O_5H_{18}$	Boc-L-glutamine	non-proteinogenic amino acid
267.1219 ±6.0	+/-	$C_{12}N_3O_4H_{17}$	agaritine	non-proteinogenic amino acid
276.1321 ±4.0	-	$C_{11}N_2O_6H_{20}$	saccharopine	biological amino acid derivative

Table 3.VIII. Molecular formulas detected from the 300 K, 1000× metallicity experiment. Detection column indicates energy source and detection polarity. Plasma (+: positive ion, -: negative ion) and UV (p: positive ion, n: negative ion). We report the smaller Δppm between measured m/z and exact m/z when a detection was made in more than one instrument mode.

10000× Results				
600 K *material insoluble*				
400 K				
Mass (m/z) ±Δppm	*Detection*	*Formula*	*Potential Molecule*	*Relevance*
182.0790 ±0.1	-/n	$C_6O_6H_{14}$	glucitol	sugar alcohol
192.1110 ±1.7	p	$C_7N_2O_4H_{16}$	orthinine acetate	non-proteinogenic amino acid
195.0895 ±0.1	-	$C_{10}NO_3H_{13}$	tyrosine, O-methyl	non-proteinogenic amino acid
211.0845 ±0.1	p	$C_{10}NO_4H_{13}$	tyrosine, 3-methoxy	non-proteinogenic amino acid
246.1216 ±1.2	p	$C_{10}N_2O_5H_{18}$	Boc-L-glutamine	non-proteinogenic amino acid
246.1328 ±1.2	p	$C_9N_4O_4H_{18}$	octopine	biological amino acid derivative
267.1219 ±1.1	p	$C_{12}N_3O_4H_{17}$	agaritine	non-proteinogenic amino acid
276.1321 ±1.1	p	$C_{11}N_2O_6H_{20}$	saccharopine	biological amino acid derivative
300 K				
Mass (m/z) ±Δppm	*Detection*	*Formula*	*Potential Molecule*	*Relevance*
180.0634 ±0.7	n	$C_6O_6H_{12}$	glucose	monosaccharide
182.0790 ±0.2	+/-	$C_6O_6H_{14}$	glucitol	sugar alcohol
192.1110 ±1.7	p	$C_7N_2O_4H_{16}$	orthinine acetate	non-proteinogenic amino acid
195.0895 ±0.1	-	$C_{10}NO_3H_{13}$	tyrosine, O-methyl	non-proteinogenic amino acid
246.1328 ±0.3	p	$C_9N_4O_4H_{18}$	octopine	biological amino acid derivative
276.1321 ±1.1	p	$C_{11}N_2O_6H_{20}$	saccharopine	biological amino acid derivative

Table 3.IX. Molecular formulas detected from the 10000× metallicity experiments. Detection column indicates energy source and detection polarity. Plasma (+: positive ion, -: negative ion) and UV (p: positive ion, n: negative ion). We report the smaller Δppm between measured m/z and exact m/z when a detection was made in more than one instrument mode.

Chapter 4

Triton Haze Analogues: the Role of Carbon Monoxide in Haze Formation

"So the universe is not quite as you thought it was. You'd better rearrange your beliefs, then. Because you certainly can't rearrange the universe."

— Isaac Asimov, *Nightfall*

4.1 Introduction

[1]Triton, as Neptune's largest moon, is unique among the ice giant moons because of its thin nitrogen atmosphere and its status as a captured Kuiper Belt Object (KBO) (Agnor & Hamilton, 2006; McKinnon, 1984). Also considered a candidate ocean world, Triton thus is a natural comparison to two other worlds, Titan and Pluto, which also have nitrogen-rich atmospheres with trace amounts of carbon monoxide and methane, though the absolute mixing ratios differ between the three. Rich photochemistry has been observed both on Titan and Pluto from dedicated spacecraft observations by the Cassini-Huygens mission to the Saturn system and the New Horizons flyby of Pluto. Dramatic haze layers are seen in the atmospheres of both worlds from these two

[1]This chapter has been submitted to *The Journal of Geophysical Research – Planets* as Moran, Hörst, He, Radke, Sebree, Izenberg, Vuitton, Flandinet, Orthous-Daunay, Wolters, "Triton Haze Analogues: the Role of Carbon Monoxide in Haze Formation" for publication therein.

missions (Porco et al., 2005; Stern et al., 2015). Voyager 2 observations also suggest that Triton has a haze layer and potentially nitrogen ice clouds (Herbert & Sandel, 1991; Rages & Pollack, 1992; Strobel & Summers, 1995; Yelle et al., 1995), though the haze properties, especially as compared to that of Titan and Pluto, remain poorly characterized due to Voyager 2 phase angle and detection limit constraints (Pollack et al., 1990).

Triton's atmosphere, due to its extremely cold surface temperature of 38 K (Conrath et al., 1989), is in vapor pressure equilibrium with its surface ices, making atmosphere-surface interactions active and strongly seasonally dependent (Cruikshank et al., 1993; Hansen & Paige, 1992). Similar activity is observed for Pluto (Lewis et al., 2020), where seasonal sublimation appears to drive winds (Telfer et al., 2018). Measurements of Triton's atmospheric pressure at the surface range from 14±1 μbar in 1989 from Voyager 2 radio science (Tyler et al., 1989) to 19±1.8 μbar from stellar occultations in 1995 and 1997 (Elliot et al., 1998; Olkin et al., 1997), suggestive of seasonal sublimation and deposition. Nitrogen dominates the atmosphere, and vertical profiles of the N_2 (Krasnopolsky et al., 1993) and CH_4 content, which decreases with altitude (Herbert & Sandel, 1991), have been known since Voyager 2. From the surface at 38 K, the upper atmosphere reaches temperatures of approximately 90 K (Strobel & Zhu, 2017). With the Very Large Telescope of the European Southern Observatory, Lellouch et al. (2010) was able to measure the amount of CO in the atmosphere, where only upper limits were achieved by Voyager 2. Lellouch et al. (2010) found a partial pressure of 24±3 nbar for CO, but did not measure a surface pressure at the time of observations.

Triton's young ($\leqslant$ 10 Ma) surface (Schenk & Zahnle, 2007; Stern & McKinnon, 2000) requires geological activity suggestive of significant internal heating, potentially provided by obliquity tides (Nimmo & Spencer, 2015), which could maintain a sub-surface liquid ocean. Plumes/geysers on Triton, observed by Voyager 2, also suggest seasonally driven winds and/or subsurface activity (Hammond et al., 2018; Hansen

et al., 1990). Organic material generated by photochemistry in the atmosphere could then interact with this potential subsurface ocean, or even the plume outflow material itself, furthering prebiotic chemical reactions, as may also occur on Titan (Neish et al., 2010).

In Titan's atmosphere, the dissociation of N_2, CH_4, and other minor species that initiate haze formation is primarily driven by solar UV radiation (Vuitton et al., 2019), while galactic cosmic ray impacts can also initiate ionization reactions to a lesser degree (Gronoff et al., 2009; Gronoff et al., 2011). Magnetospheric ions from Saturn on the order of up to 1 keV with flux 10^{-6} cm^{-2} s^{-2} have been detected at Titan (Hartle et al., 2006) and are a minor driver of atmospheric chemistry on the moon. However, at Triton, Neptune's magnetospheric particles interact with Triton's ionosphere with energies an order of magnitude higher (Krimigis et al., 1989; Stone et al., 1989; Thompson et al., 1989) and thus may play an increased role in atmospheric chemistry, though solar EUV photons likely still dominate (Lyons et al., 1992). The flux of solar photons naturally decreases with distance from the Sun from Titan to Triton to Pluto, from $\sim$15 W m^{-2} to $\sim$1.5 W m^{-2} to $\sim$0.9 W m^{-2}. Determining how far organic atmospheric chemistry has proceeded on Triton as a result of haze formation processes, and how this compares to Pluto and Titan, is thus of high interest given the similarities in bulk composition yet major differences in energy distribution between the three planetary bodies.

In situ missions to the outer solar system to characterize atmospheric chemistry are both few and far between, and often only reveal far more complexity than previously assumed, as in the case of both Titan and Pluto. Additionally, the theorized haze layer of the Early Earth is also impossible to study *in situ* in the present day. Moreover, because of the unique and highly complex chemistry occurring in these haze layers, theoretical models often cannot fully capture haze formation from initial gases to complex haze molecules due to both a lack of chemical kinetics of the relevant chemical

reactions as well as computational expense (Berry et al., 2019; Vuitton et al., 2019). As such, laboratory synthesis of atmospheric hazes has been performed to generate and study analogue particles to those potentially made in planetary atmospheres, including those for Titan (e.g., Imanaka et al., 2004; Khare et al., 1984; Vuitton et al., 2010), the Early Earth (e.g., Hasenkopf et al., 2010; Hörst et al., 2018b; Trainer et al., 2006), and even exoplanets (e.g., Gavilan et al., 2018; Hörst et al., 2018a). These experiments have revealed a wealth of information about haze formation and properties, including their effect on spectra (Brassé et al., 2015), the production of prebiotic molecules (Hörst et al., 2012; Sebree et al., 2018), and potential chemical pathways to haze formation (Gautier et al., 2014; Gautier et al., 2016).

Previous atmospheric haze formation experiments also exist for Triton specifically (McDonald et al., 1994; Thompson et al., 1989), but these past experiments included only nitrogen and methane in their starting gas mixtures. Thanks to more recent ground-based observations (Lellouch et al., 2010), we now know that CO is in fact the second most abundant molecule in Triton's N_2 atmosphere, unlike the Plutonian and Titanian atmospheres where CH_4 is found in higher mixing ratios than CO (Krasnopolsky, 2012). Some experiments have included CO in Titan-like mixtures (Bernard et al., 2003; Coll et al., 2003; Tran et al., 2008), suggesting oxygenated molecules play a role in the gas phase chemistry. More recent laboratory experiments have shown that an initial inventory of gas phase CO also substantially affects resulting tholin particles (He et al., 2017; Hörst & Tolbert, 2014). CO was included in recent atmospheric experiments of a Pluto-like atmosphere (Jovanović et al., 2020), with substantial impact on the tholin produced. However, this Pluto experiment, as well as the previous Triton experiments, were performed at room temperature, though temperature should also influence the chemistry occurring in the atmosphere. Moreover, the published spectra and chemical measurements from every N_2-CH_4-CO experiment to date has been performed with mixing ratios where $CH_4 \geqslant CO$, as

is more representative of Titan and Pluto rather than Triton. The only published experiments performed with CO > CH_4 only examined the particle density and size of the resulting solid (Hörst & Tolbert, 2014), not its chemistry. Therefore, in this study, we perform a new set of atmospheric chamber experiments for a Triton-like atmosphere – including this second most abundant molecule of CO at a higher percentage than CH_4 and at Triton-like temperatures – to examine the chemical and physical properties of hazes that may influence Triton's atmosphere and climate, surface, and planetary evolution.

4.2 Methods

First, we generated Triton haze analogue particles within the PHAZER (Planetary HAZE Research) chamber (He et al., 2017) under Triton-relevant temperatures and pressures with an AC cold plasma discharge as the energy source. We subjected the resulting solid particles to combustion analysis to obtain the elemental ratios of C, H, O, and N that make up the particles. Next, we performed a more in-depth analysis of the chemical composition of the solids produced in the PHAZER chamber by utilizing very high resolution Thermo Fisher Scientific LTQ-Orbitrap XL mass spectrometry. Once mass spectrometer measurements were complete, we employed custom software called *idmol* (Hörst, 2011) to make molecular identifications and perform data analysis from the mass spectrometry data. Finally, we obtained the transmittance and reflectance of the Triton haze analogues by measuring thin films of the particles with a Bruker Vertex 70V Fourier Transform Infrared Spectrometer.

4.2.1 Triton Haze Analogue Production

With the PHAZER chamber and accompanying apparatus (JHU, Baltimore, MD), we produced Triton haze analogue particles. We continuously flowed a gas mixture of 0.5% CO (Airgas) and 0.2% CH_4 (Airgas) in N_2 (Airgas) for 72 hours, as is standard

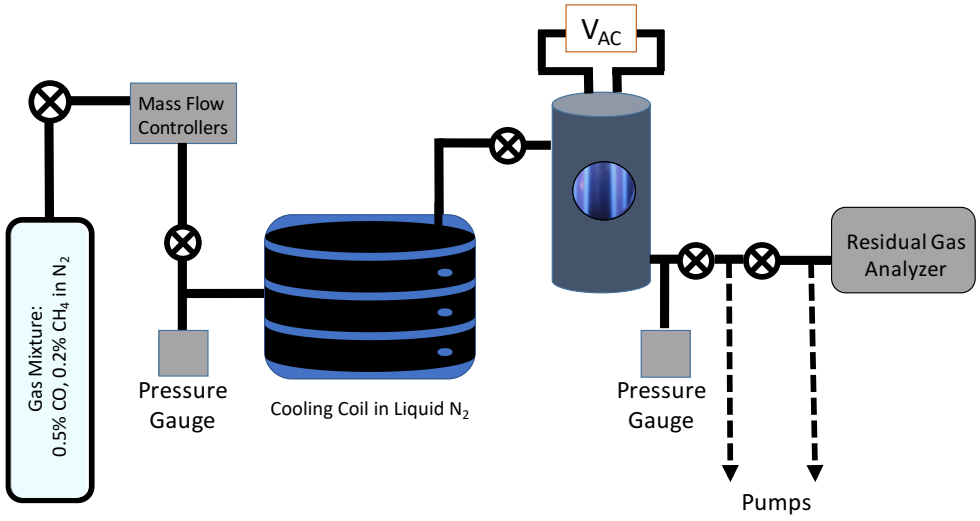

Figure 4.1. Schematic of the PHAZER chamber set-up at Johns Hopkins University. The 0.5% CO, 0.2% CH_4 in N_2 gas mix is flowed through the cooling coil submerged in the liquid N_2 bath before flowing into the reaction chamber. The mass flow controllers are set at 10 sscm so that the pressure in the chamber is 1 mbar. The gas mixture is then exposed to the AC glow discharge, and analogue haze chemistry proceeds.

PHAZER protocol (He et al., 2017) for the generation of substantial macroscopic sample. To calculate these mixing ratios, we use the partial pressure of CO determined by Lellouch et al. (2010), 24 nbar within a factor 3. We multiply the upper limit of this partial pressure times the surface pressure determined by Voyager 2, 14 μbar, to obtain 0.5% CO in our mixture. Lellouch et al. (2010) reports the surface partial pressure ratio CO/CH_4 to be $\sim$2.5, resulting in our CH_4 mixing ratio 0f 0.2%. The gas mixture first is flowed through the cooling coil immersed in a liquid 77 K N_2 bath, and then into the reaction chamber so that gases in the chamber are approximately 90 K (He et al., 2017), following the best fit upper atmospheric temperature determined by Strobel and Zhu (2017). An AC cold plasma glow discharge then provides an energy density of order 170 W m^{-2} into the system (He et al., 2019), which corresponds to approximately 340 days of solar irradiation at Triton. The plasma source is energetic enough to dissociate even extremely stable molecules, such as N_2 and CO (Cable et al., 2012).

This cold plasma does not directly replicate any single energetic atmospheric process, photochemical or otherwise. Instead it provides a method by which to approximate the energetics of upper atmospheres. For Triton's upper atmosphere, such energy distributions may derive from a combination of sources such as incident UV solar photons, cosmic ray bombardment, or charged particles from the magnetic field of Neptune.

The gases were flowed at 10 sscm so that the pressure within the chamber was maintained at 1 mbar, which is higher than any pressure in Triton's atmosphere, which at highest is estimated to be 40 μbar (Lellouch et al., 2010). Maintaining the experimental chamber at 1 mbar pressure reduces reaction times, allowing for completion of experimental runs within a reasonable timeframe. Additionally, this pressure is dictated by the mean free path within the size of the reaction chamber. Furthermore, many other haze formation experiments are run at this pressure (e.g., He et al., 2017; Jovanović et al., 2020; Khare et al., 1984), which allows for comparison of the chemical and physical properties of the resulting tholins as a function only of gas species and temperature without the additional variable of pressure, which previous work has shown to affect the tholin composition and spectra (Imanaka et al., 2004).

As ionization and dissociation of the inital N_2, CO, and CH_4 gas molecules proceeds, these ions and radicals react to make new molecules, and some combination of initial and newly created molecules generate longer and longer molecular chains. Eventually, some such molecules become macroscopic solids and deposit out in the form of orange-brown powder on the chamber walls, floor, and quartz disks placed at the bottom of the chamber. After 72 hours, the gas flow is turned off and remains under vacuum for 48 hours to allow volatile dissipation. The chamber is then moved into a dry (< 0.1 ppm H_2O), oxygen-free (< 0.1 ppm O_2) N_2 glove box (Inert Technology Inc., I-lab 2GB) where solid sample is collected and stored, insulated from ambient atmosphere and light sources.

4.2.2 Combustion Analysis

We employed elemental combustion analysis with a Thermo Scientific Flash 2000 Elemental Analyzer (Department of Chemistry and Biochemistry, University of Northern Iowa, IA, USA) of the Triton haze analogues produced in the PHAZER chamber. We placed 1 mg of particles in the analyzer to directly measure percentages of C, H, and N. We then perform mass subtraction to calculate the percentage of O. Figure 4.3 shows the resulting elemental ratios from combustion analysis in the fourth column.

4.2.3 Fourier Transform Infrared Spectroscopy

Using a Bruker Vertex 70V Fourier Transform Infrared Spectrometer (JHU, Baltimore, MD), we measured the transmission and reflectance of thin films of Triton haze analogue deposited on quartz substrates from 0.4 to 5 microns. From 0.4 to 1.1 microns, we use a Si-diode detector while from 0.83 microns to 5 microns, we employ a DLaTGS detector. Overlap between detectors allows for calibration between the wavelength ranges. The spectrometer is fitted with a quartz beamsplitter, and uses a near-IR source of a tungsten-halogen lamp. A silicon carbide globar provides the mid-IR source. When performing measurements, we vent the optical bench to $\leqslant 1$ hPa. All measurements were performed at room temperature, monitored and held stable at 294 K. We first take transmission and reflectance measurements of a blank quartz disc to provide a baseline correction before measuring the Triton sample deposited on the quartz substrate. We use a source aperture size of 2 mm and average over 250 scans for each measurement. With the instrument settings as configured, our measurements have a resolution of 5 cm^{-1}. Interference fringes are observed in the optical to near-IR range (0.4 micron to 3.5 micron), and we perform a correction for this fringing following the moving average method of Neri et al. (1987), as in He et al.

(2021). This correction is given as

$$F(x_n) = \frac{1}{4}(2G(x_n) + G(x_{n+m}) + G(x_{n-m})) \tag{4.1}$$

where $F(x_n)$ is the fringe-removed spectrum, $G(x_n)$ is the original spectrum, and 2m is the number of integer points in d, the average fringe spacing. We find m to be 565 for our transmission and reflectance spectra.

Once fringe removal is complete, we then compare the spectral features observed in the Triton tholin to both previous results of relevant planetary haze analogues as well as to general spectral databases in order to identify chemical bonds and functional groups.

4.2.4 Orbitrap Mass Spectrometry

To investigate the detailed chemical composition of the Triton haze analogue sample, we employed very high resolution mass spectrometry with a Thermo Fisher Scientific LTQ-Orbitrap XL mass spectrometer with an Ion Max electrospray ionization source (ESI) (IPAG, Grenoble, FR), which has resolving power ($M/\Delta m$) of at least 10^5 up to 400 m/z and an exact mass accuracy of ± 2 ppm. Prior to sample measurement, we performed mass calibration between 200 and 2000 m/z with Thermo Fisher Scientific Calmix (caffeine, MRFA peptide, and Ultramark 1621 for positive mode and sodium dodecyl sulfate, sodium taurocholate, and Ultramark 1621 in negative mode) solution. We also measured a blank solution from 150-1000 m/z of pure CH_3OH with the Orbitrap to account for and remove any potential contamination in sample signal from the mass calibration solution, ambient conditions, or the sample vial. To prepare the sample, we dissolved the Triton haze analogue in CH_3OH (methanol) at a concentration of 1 mg/mL. We then subjected the dissolved sample to sonification for 1 hour, followed by centrifugation at 10,000 rpm for 10 minutes. The soluble fraction of the Triton sample was then diluted again in CH_3OH at 1 mg/mL. We injected the diluted soluble

fraction into the Orbitrap with electrospray ionization (ESI) and obtained overlapping mass-to-charge (m/z) bin measurements of 50-300 m/z, 150-450 m/z, and 400-1000 m/z. The tube lens voltage was set to 50 V, 70 V, and 90 V respectively, with source voltages of 3.5 kV (positive) and 3.8 kV (negative). For each mass-to-charge bin, our measurements averaged together four scans of 128 microscans, with the injection of sample set at a flow rate of 3 μL minute^{-1}, to maximize signal and reduce noise (Wolters et al., 2020). Initial measurements were taken in positive ion mode. The instrument polarization was then switched to negative ion mode and allowed to re-equilibrate for 90 minutes. With the instrument in standby, the capillaries were flushed with 10 μL of CH_3OH and then the direct injection polyetheretherketone (PEEK) capillary replaced. The instrument was then mass calibrated again and another blank solution was taken in negative polarity before the Triton sample was measured in negative ion mode with the same instrument settings as above.

4.2.5 Data Analysis of Orbitrap MS with `idmol`

After data acquisition and preliminary inspection with Thermo Fisher Scientific XCalibur software, we use custom IDL/Fortran software called *idmol* (Hörst, 2011) to extract and analyze the mass spectral data. First, we compare the mass spectra of blank solution to that of the Triton analogue and remove contaminant peaks with intensities greater than 2×10^5 in the Triton spectra. More recent work suggests that this method of blank subtraction can remove useful signal due to the behavior of the automatic gain control (AGC) of the Orbitrap (see Wolters et al., forthcoming), but in this case we do not remove many peaks and therefore expect minimal impact on our results. Next, we use *idmol* to assign molecular peaks, where the program calculates all potential molecular combinations and then uses a series of decision trees based on user inputs regarding minimum N/C ratio, maximum number of oxygens, mass tolerance, and the nitrogen rule to make assignments of low-mass mass peaks.

Above 300 m/z, where non-unique mass peaks are no longer within the instrument's resolving power (Gautier et al., 2014), the program uses lower mass peak assignments to choose best fit assignments.

As in previous analyses (Moran et al., 2020; Vuitton et al., 2021), we calculate the elemental composition of the tholin sample from Orbitrap measurements using *idmol* peak assignments weighted by the spectral intensity. We perform a correction to the intensity weighted elemental composition by multiplying the lowest 10% intensities by 10 to account for differing ionization yields of oxygen molecules, as was shown by Hörst (2011) to mitigate differences between Orbitrap and combustion derived elemental compositions. We also calculate the non-intensity weighted elemental composition, as ionization efficiency may prevent a direct proportionality to molecular concentration. For further discussion regarding ionization efficiencies of various chemical species, including as a function of positive and negative polarities, see Vuitton et al. (2021).

4.3 Results

In this section, we present the results of the production rate, our elemental, mass spectrometry, and Fourier Transform Infrared (FTIR) spectroscopy analysis. Broadly, CO from the initial gas mixture profoundly influences both the resulting composition and spectra of the solid particles. First, we discuss production rate of haze as a function of CO and CH_4 mixing ratios. Then we focus on the bulk composition as determined by both combustion and high resolution mass spectrometry (HRMS). Next we delve deeper into the composition and specific molecular identifications enabled by HRMS, and finally we examine the Triton tholin FTIR spectra for signs of the novel chemistry that may be observable by remote sensing.

4.3.1 Production Rate of Triton Tholin Particles

In Figure 4.2, we show the production rates of our Triton tholin experiment compared to that of our standard Titan gas mixture (5% CH_4 in N_2) with varying CO percentages (He et al., 2017). While the production rates measured by He et al. (2017) found that varying CO from 0% to 5% with 5% CH_4 did not impact the production rate within the limits of experimental error (0.20 mg/hr), our Triton experiment made markedly less haze, at only 3.93±0.2 mg/hr compared to the Titan-like production rates of 7.25-7.42 mg/hr. We also show the production rates (L. Jovanović, personal communication) of tholin experiments for Pluto gas composition from the PAMPRE experimental set-up (Alcouffe et al., 2009; Szopa et al., 2006) at LATMOS, which used 500 ppm CO in N_2 with either 1% CH_4 to simulate Pluto's atmosphere at altitude of 400 km or 5% CH_4 for an altitude of 600 km (Jovanović et al., 2020), though at room temperature. Like our Triton and Titan results, the Pluto-like results show a much higher production rate when the methane mixing ratio is higher (14.6 mg/hr with 1% CH_4 compared to 24.3 mg/hr with 5% CH_4.) While the differing experimental set-ups prevent a direct comparison between the absolute production rates seen in PHAZER and PAMPRE, a trend is suggested. The much lower starting mixing ratio of methane in the Triton mixture (0.1%) and low-altitude Pluto composition mixture (1%) results in much less haze compared to that of our Titan experiments or high-altitude Pluto-like experiments with 5% methane.

Other investigations of N_2-CH_4 mixtures have shown that aerosol mass loading is always higher with 2% CH_4 than with 0.1% CH_4 using a spark discharge energy source, though the opposite is observed when the energy source is a UV lamp (Hörst & Tolbert, 2013). Given the Triton and Titan PHAZER experiments, our glow discharge is thus likely more analogous to the spark discharge, where the larger methane gas mixing ratio allows for the production of more solid material. In a later experiment with the same set-up, the total abundance of gas phase products also increased with

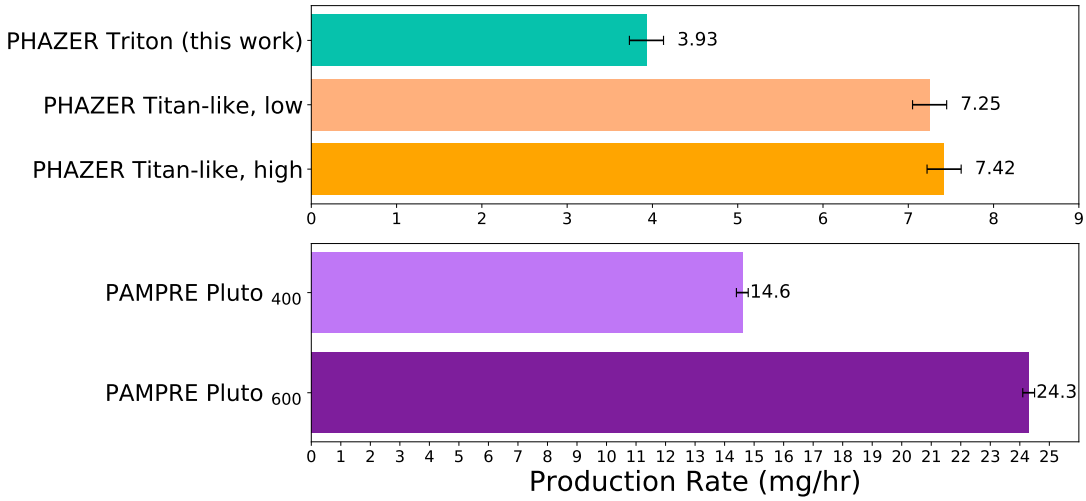

Figure 4.2. Top: PHAZER production rates (in mg/hr) of the amount of solid produced from the Triton gas mixture (CO = 0.5%; CH_4 = 0.1%; top bar in turquoise) compared to our Titan-like tholin (CH_4 = 5%; CO in varying mixing ratios from 0% to 5%; He et al. 2017, middle and lower orange bars). Bottom: PAMPRE production rates from the room temperature Pluto-like tholin (CO = 500ppm; CH_4 = 1%, upper light purple bar and CH_4 = 5%, lower purple bar) of Jovanović et al. (2020). Note that due to differing experimental set-ups, the absolute production rates between the PHAZER and PAMPRE apparatus cannot be directly compared and have different x-axis limits. While CO alters the haze chemistry, higher methane mixing ratios generate larger amounts of haze material in both experimental set-ups.

higher methane mixing ratios in the initial gas mixture (Hörst et al., 2018c). PHAZER exoplanet atmospheric studies have also shown that higher initial methane mixing ratios can increase solid material production (Hörst et al., 2018a), though the third highest observed production rate of those experimental conditions did not include an initial gas phase inventory of methane at all. Additional Pluto-like composition experiments (of 500 ppm CO in N_2) observed significantly thicker thin films were produced under 5% CH_4 conditions than with 0.5% or 1% CH_4 (Jovanović et al., 2021). Prior work has shown that Titan's methane mixing ratio, represented in the laboratory by an intial gas phase methane concentration at 5%, appears to most efficiently convert gas precursors to tholin solids due to competing solid growth mechanisms when CH_4 increases beyond this percentage (Sciamma-O'Brien et al., 2010). While we clearly demonstrate in later sections that the haze chemistry changes under the influence of very small amounts of CO, the literature suggests CH_4 may play a larger part in the ultimate aerosol mass loading. Current trends in the literature when combining CO and CH_4 remain tentative or contradictory and could benefit from further study (see e.g., Hörst & Tolbert, 2014). While we identify the methane mixing ratio as the driver behind increased production, it remains unclear if any carbon source in high enough quantities could serve to generate substantial haze (see, e.g, He et al. (2018a) and He et al. (2020b), Hörst et al. (2018a). However, the trends we observe with PHAZER – that a smaller CH_4 mixing ratio with small amounts of CO generates less solid aerosol – fit reasonably with the optically thicker haze observed on Pluto as compared to Triton (Hillier et al., 2021).

4.3.2 Composition of Triton Tholin Particles

4.3.2.1 Bulk Composition and Differences in Ion Polarities

We observe first that despite CO being present at only a 0.5% mixing ratio in the initial gas mixture, the bulk solid is approximately 10% oxygen. From the combustion

analysis, we determine that H, O, C, and N are present at 5.29±0.06%, 10.3±0.3%, 43.7±0.4%, and 40.7±0.4% respectively. The bulk composition as calculated from the combined positive and negative ions of the soluble fraction of the tholin from Orbitrap is 5.4±0.7% H, 9.8±4.3% O, 47.4±1.7% C, and 37.4±2.8% N. The bulk composition from the Orbitrap agrees to within 2% or better with the combustion analysis. As seen in previous work (Hörst, 2011), oxygen is primarily detected in the negatively ionized products from the Orbitrap, which is consistent with the identification of carboxylic acid groups (discussed further in the following subsections) which are efficient proton donors (Vuitton et al., 2021). The bulk values obtained for negative, positive, and combined ions from Orbitrap, as well as from combustion analysis, are shown in Figure 4.3.

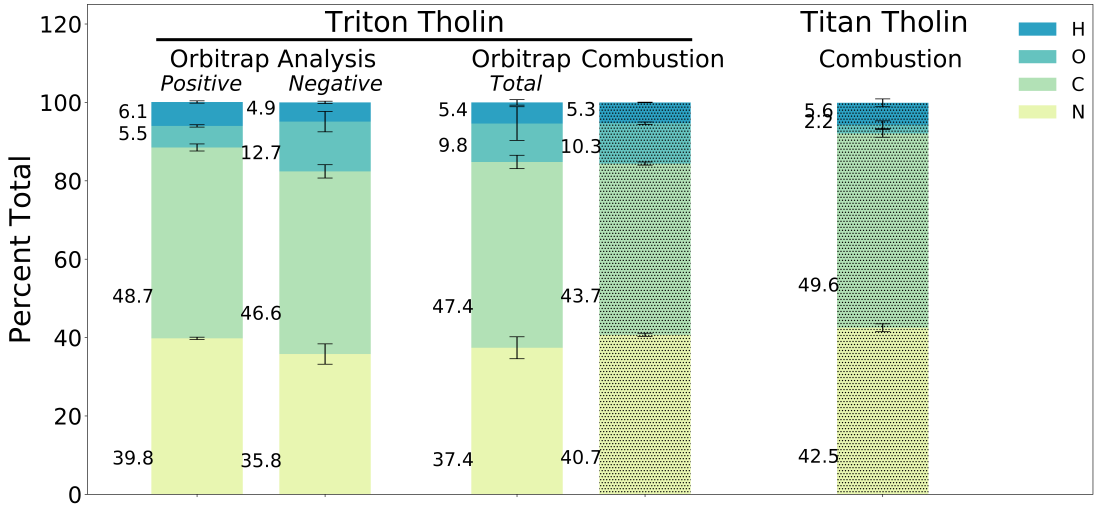

Figure 4.3. Average elemental composition of Triton tholin from positive, negative, and combined ions, as determined by Orbitrap MS analysis (left three bars), combustion analysis (fourth bar), and comparison to standard PHAZER Titan values from combustion analysis (right). Triton tholin more strongly incorporates oxygen, apparently through carbon depletion. Hatching on the right two bars indicates these results come from combustion analysis.

Titan tholin produced without CO from the same experimental set-up contains ∼2% oxygen (likely due to minor water adsorption during measurements) compared to the Triton tholin with ∼10% oxygen (Figure 4.3). Previous PHAZER CO experiments

(He et al., 2017) have included up to 5% CO in N_2-CH_4 mixtures, yet never observe more than 8% oxygen in the solid and indeed measure only 5% oxygen in mixtures with starting CO at 0.5% as in this work. Importantly, these prior experiments were conducted with constant CH_4 gas mixing ratios of 5% and thus demonstrate how much more strongly oxygen can be incorporated into the solid when CO $\geqslant$ CH_4 in the starting gas mixture. Hydrogen contents remain at approximately 5% across varying CO/CH_4 starting ratios (He et al., 2017), and our Triton results here support this trend. Our elemental analysis results in a bulk N/C ratio for the Triton tholin of 0.93, which is higher than that of "standard" PHAZER Titan tholin at N/C = 0.85. This result is surprising, considering that past work with N_2-CH_4-CO mixtures has postulated that the competition between N_2 and CO chemistry results in oxygen incorporation primarily at the expense of nitrogen incorporation (He et al., 2017; Jovanović et al., 2020). Here, instead, carbon appears depleted with respect to the Titan tholin structure. This result is more in line with previous work that explored the addition of CO_2 and O_2 in N_2-CH_4 atmospheres (Hörst et al., 2018b), which found increasingly oxidized gas mixtures increased nitrogen fixation in the solid. Nitrogen's role in haze formation has been the subject of several studies, where it has been observed to make up considerable mass of tholin despite production under UV sources which cannot directly break N≡N bonds (Hörst et al., 2018c; Trainer et al., 2012), which has defied conclusive explanation. However, recent theoretical calculations show that intermolecular energy exchange from excited carbon monoxide molecules can exceed the contribution of direct excitation by photoelectrons on nitrogen dissociation – i.e., collisional break-up (Kirillov, 2020), potentially providing an explanation for how nitrogen incorporation happens in UV lamp-driven tholin studies. While a previous Triton experiment also showed stronger nitrogen incorporation compared to Titan tholin (McDonald et al., 1994), that experiment contained no CO and likely simply reflects the lower methane mixing ratio of the starting gas mixture. For PHAZER

Titan tholin, the C/O ratio of the bulk solid is 22.5 but the Triton tholin's bulk C/O is only 4.2. Even the previous PHAZER CO experimental series with the highest starting CO/CH_4 gas ratio (1:1) resulted in a C/O ratio for the tholin of ~6, considerably higher than we observe for the Triton tholin.

4.3.2.2 Molecules in the Triton Sample from HRMS

Following our characterization of the bulk Triton haze analogue sample and its bulk soluble fraction, we examined the mass spectral data for specific molecular formulas of interest. The positive and negative mass spectra are shown in Figure 4.4. We detect thousands of individual peaks across both ionization polarities, indicating the high complexity of the Triton tholin as is the case with its Titan, Pluto, and exoplanet counterparts (e.g., Gautier et al., 2016; He et al., 2017; Jovanović et al., 2020; Moran et al., 2020). Distinct periodicity is observed in the peak groupings, with a repeating pattern between 13 and 14 amu across both the positive and negative ions. Positive ions have peak group periods that average to 13.57 amu; negative ions cluster in peak groupings with average spacing of 13.66 amu. These values are quite close to the 13.5 amu observed by Hörst (2011) and consistent with the frequently observed 12 to 16 amu spacing (averaging to 14 amu) in Titan and Pluto tholin produced in various set-ups (Cable et al., 2012; Gautier et al., 2014; Gautier et al., 2017; Imanaka et al., 2004; Jovanović et al., 2020). These peak spacings display quite regular but not exact amu periodicity. Therefore, these groupings likely indicate repeating chemical units of co-added and substituted monomers (such as HCN, CH_2, etc.) (Gautier et al., 2017).

We report in Table 4.I a small subset of the thousands of molecular formulas of species identified from Orbitrap MS with intensities $\geqslant 10^3$. These molecular formulas are consistent with those of various prebiotic molecules, though we stress that without structural information (which is not possible with the measurements conducted in this work), we cannot confirm that the formula we identify is in fact the isomer of

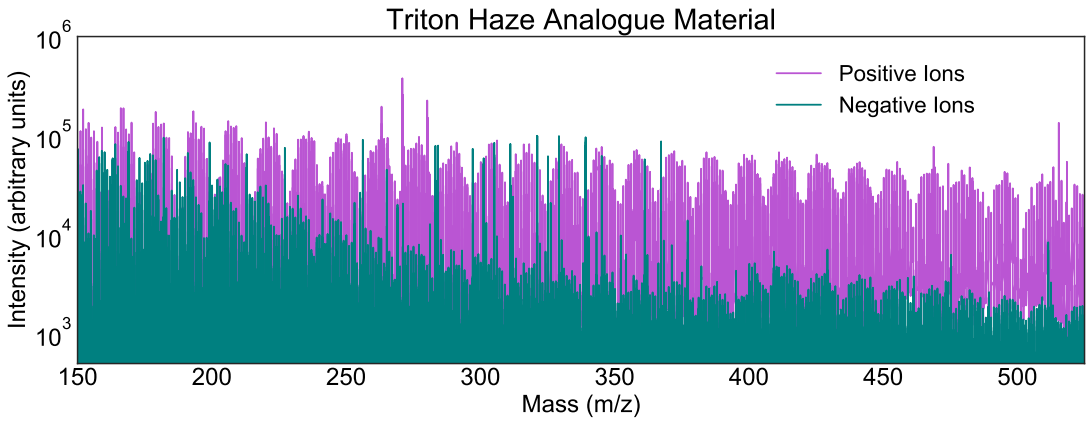

Figure 4.4. Positive (teal) and negative (purple) ion mode mass spectra of the Triton haze analogue particles from 150 to 525 m/z. Due to differing ionization efficiencies, the negative ion mode intensities are systematically lower. Peak groupings of ∼13.5 amu repeat across the oberved mass range.

the prebiotic species indicated in Table 4.I. We detect the formulas for all biologically relevant nucleotide bases (adenine, $C_5H_5N_5$; cytosine, $C_4H_5N_3O$; guanine, $C_5H_5N_5O$; thymine, $C_5H_6N_2O_2$; and uracil, $C_4H_4N_2O_2$) and one non-biologic nucleotide base (xanthine, $C_5H_4N_4O_2$). We note that while we include the formulas for uracil and thymine because they represent the remaining nucleotide bases, they are present only at 10^2 intensities. Each of these species has been previously identified and confirmed through alternate measurement techniques in prior tholin produced from N_2-CH_4-CO mixtures (Hörst et al., 2012; Sebree et al., 2018), raising the likelihood that the formulas we identify in the Triton tholin could be the prebiotic species in question. We also identify numerous formulas consistent with isomers of amino acids and their derivatives. Nearly all of these formulas are also present as at least one ion in HRMS data of tholin produced under CO-free Titan conditions with the PHAZER set-up, as indicated in the far right column of Table 4.I. In contrast and most notably, we detect here the formula $C_3H_6O_3$ with a potential isomer of glyceraldehyde, the simplest possible monosaccharide. This species' formula is unique to the Triton tholin among all N_2-CH_4-CO experiments to which we compare our results. Only prior tholin work considering significantly more oxidizing atmospheres has previously observed sugar

m/z ±	Δppm	Ion Formula	Intensity	Potential Molecule	In Titan Sample?
90.0312	0.18	$C_3H_6O_3^-$	9.4 x 10^3	Glyceraldehyde	**No**
111.043	-0.45	$C_4H_5N_3O^+$	1.8 x 10^4	Cytosine	Yes
112.027	0.18	$C_4H_4N_2O_2^-$	6.9 x 10^2	Uracil	Yes
126.043	0.21	$C_5H_6N_2O_2^-$	8.0 x 10^2	Thymine	Yes
135.054	-0.97	$C_5H_5N_5^+$	1.6 x 10^4	Adenine	No
	0.43	$C_5H_5N_5^-$	9.3 x 10^3		Yes
151.049	-1.56	$C_5H_5N_5O^+$	9.0 x 10^3	Guanine	No
	-0.10	$C_5H_5N_5O^-$	7.4 x 10^4		Yes
151.063	0.90	$C_8H_9NO_2^-$	2.5 x 10^3	2-phenylglycine	No
152.033	-2.27	$C_5H_4N_4O_2^-$	1.3 x 10^3	Xanthine	Yes
155.069	-1.45	$C_6H_9N_3O_2^+$	9.2 x 10^3	Histidine	Yes
	-0.41	$C_6H_9N_3O_2^-$	1.0 x 10^4		Yes
156.065	-0.74	$C_5H_8N_4O_2^+$	1.2 x 10^4	1,2,4-triazole-3-alanine	Yes
	-0.04	$C_5H_8N_4O_2^-$	1.4 x 10^4		Yes
160.048	0.57	$C_5H_8N_2O_4^-$	4.1 x 10^3	Thymine glycol	No
167.069	-0.68	$C_7H_9N_3O_2^-$	6.4 x 10^3	β-pyrazinyl-L-alanine	Yes
169.085	0.18	$C_7H_{11}N_3O_2^+$	1.4 x 10^4	3-methylhistidine	Yes
	-0.78	$C_7H_{11}N_3O_2^-$	6.0 x 10^3		Yes
171.064	0.15	$C_6H_9N_3O_3^-$	3.2 x 10^3	β-hydroxyhistidine	Yes
172.096	0.05	$C_6H_{12}N_4O_2^+$	2.7 x 10^4	Iminoarginine	Yes
	0.55	$C_6H_{12}N_4O_2^-$	1.2 x 10^3		No
182.080	0.72	$C_7H_{10}N_4O_2^+$	1.8 x 10^4	Lathyrine	Yes
	0.54	$C_7H_{10}N_4O_2^-$	1.4 x 10^4		Yes
193.074	0.32	$C_{10}H_{11}NO^-$	1.3 x 10^3	Phenylglycine, m-acetyl	No
206.080	0.76	$C_9H_{10}N_4O_2^-$	6.2 x 10^3	Benzotriazolylalanine	Yes
226.107	-0.26	$C_9H_{14}N_4O_3^-$	2.8 x 10^3	Alanylhistidine	Yes
246.100	-1.85	$C_{13}H_{14}N_2O_3^-$	1.6 x 10^3	Acetyltryptophan	No

Table 4.I. Molecular formulas of prebiotic interest detected in the Triton tholin by HRMS.

relevant formulas (Moran et al., 2020). Again, this result underscores the impact of a starting CO/CH_4 mixing ratio over unity. If confirmed, the existing co-presence of nucleotide bases, amino groups, and sugar molecules in the complex solids that make up this haze should significantly advance Triton as a target of astrobiological interest. For each identified formula in Table 4.I, we confirm that it is not present in the Orbitrap data of the blank solvent above the noise level (intensities $\geqslant 10^1$).

In Figure 4.5, we show the Double Bond Equivalent of the molecules identified in both ionization products of the Orbitrap. The Double Bond Equivalent (DBE), also

called the degree of unsaturation, is a measure of how many rings and double bonds are in a molecule and helps elucidate the overall structure of the material with respect to its hydrogen bonding environment. For C, H, O, N-containing materials, the DBE is calculated by

$$DBE = c + \frac{n}{2} - \frac{h}{2} + 1 \tag{4.2}$$

where c is the number of carbons, n is the number of nitrogens, and h is the number of hydrogens in the molecule. In both positive and negative ion modes, the DBE linearly increases with mass, as has been previously observed for Titan tholin (Sarker et al., 2003). In both ionization modes, the molecules at low masses have DBE between 1 and 5 (saturated), which increases up to 10 to 15 (increasingly unsaturated) at the high end of the mass range. Previous N_2-CH_4-CO mixtures with large CO mixing ratios also produced largely unsaturated tholins (He et al., 2017), which could point to hydrogen atoms in higher masses bonding to nitrogen or oxygen atoms in the form of O-H or N-H, which we return to in our discussion of the Triton tholin spectra.

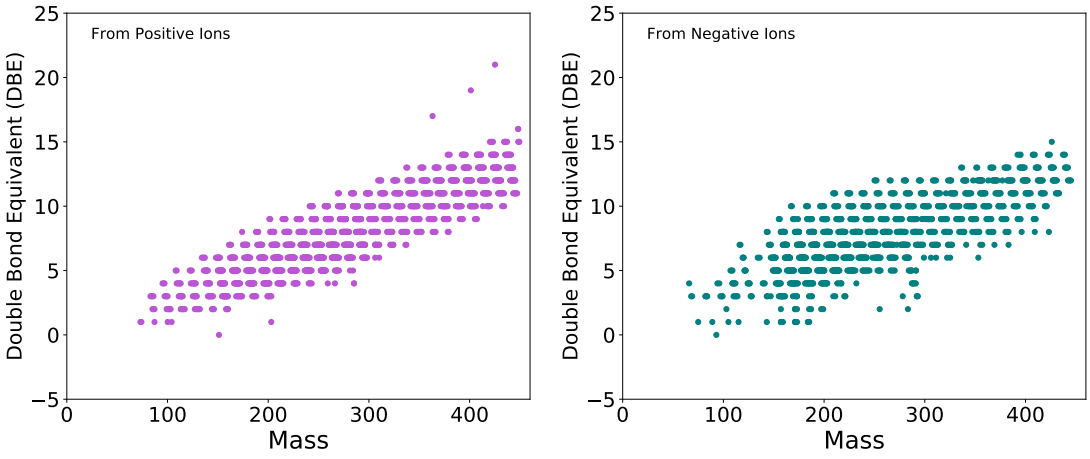

Figure 4.5. Double Bond Equivalent (DBE) versus mass. Left (in magenta) is derived from positive ion measurement; right (teal) from negative ion measurement. As in seen previous Titan tholin characterization, the degree of unsaturation increases with mass.

In Figure 4.6, we present Van Krevelen diagrams of both H/C vs. O/C ratios

of the identified molecules, which are widely used to understand the structures of complex organic matter on Earth (e.g., Kim et al., 2003), and H/C vs. N/C ratios of the identified molecules, which are a modification frequently used in the planetary literature to study complex organic materials like tholin (e.g., Gautier et al., 2014; Hörst, 2011; Jovanović et al., 2020). We separate the molecular ratios by whether they were seen in positive or negative ion mode. The difference in clustering between ion polarities clearly demonstrates that both are needed to understand the full chemical nature of the tholin. Strongly oxygenated molecules clearly favor negative ionization while more heavily nitrogenated molecules increase in positive ionization mode. We compare our results to PHAZER Titan tholin produced without CO. The Titan Van Krevelen diagrams use molecular assignments performed with slightly different software, *Attributor*, (Orthous-Daunay et al., 2020), but which has been benchmarked against *idmol* and reliably produces comparable results at masses $\leqslant$300 m/z (Bonnet et al., 2013; Hörst, 2011).

Unsurprisingly, the Triton tholin reach much higher O/C ratios across all H/C ratios compared to the Titan tholin. Oxygen species are always more prevalent in the negative ionization data and consequently reach larger O/C ratio in both samples. We show in Figure 4.7 an empty Van Krevelen diagram that shows the regions in which particular molecular functional groups fall, for reference. Molecules in the Titan tholin are primarily confined to H/C $\leqslant$ 1.0 and O/C $\leqslant$ 0.3, indicative of hydrocarbon aromatic species. In contrast, the Triton tholin distinctly cluster above an H/C of 1.0, the demarcation of oxidation reactions and more highly unsaturated species. From the elemental analysis, however, we know that the overall hydrogen content is comparable between the two samples, reiterating our previous interpretation that oxygen is incorporated into the solid at the expense of carbon. The Triton tholin exhibit a shift away from simple unsaturated hydrocarbons to long chain carboxylic acids (fatty acids), bounded by H/C ratios of 1.0 – 2.0 and an O/C ratio $\leqslant$ 0.4.

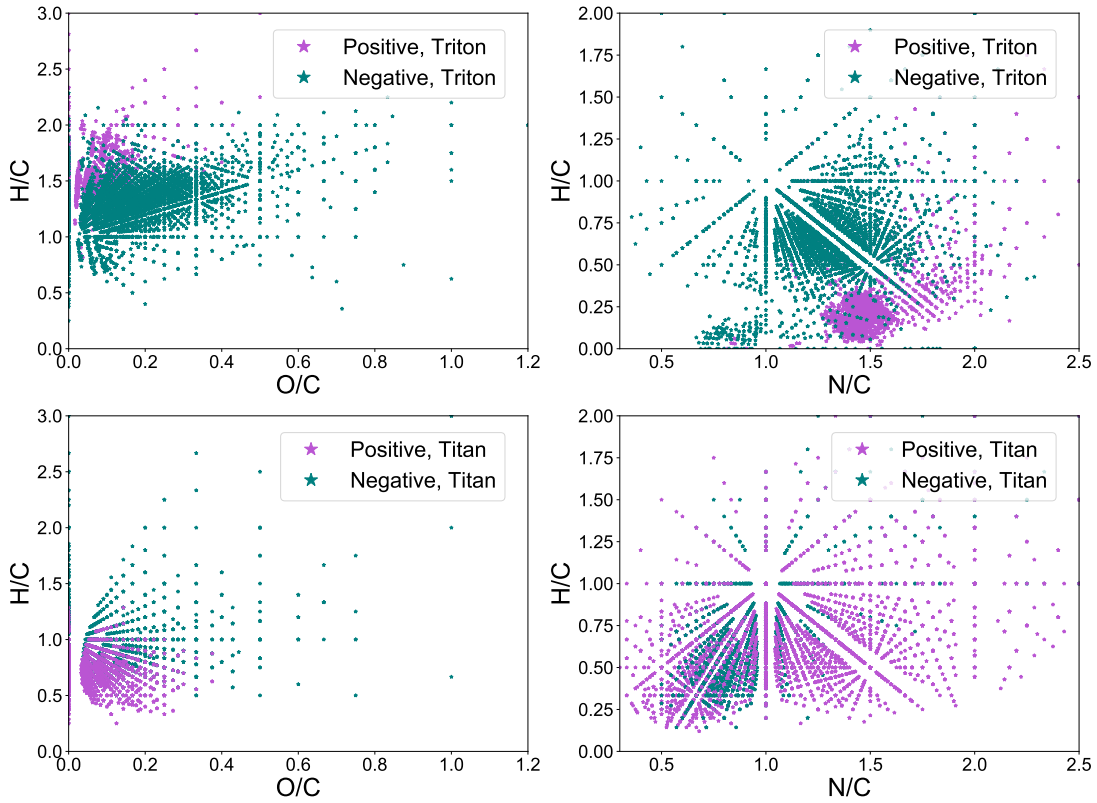

Figure 4.6. Van Krevelen diagrams of the PHAZER Triton haze analogues (top) and PHAZER Titan haze analogues (bottom). Left shows the more typical H/C vs O/C; right shows H/C vs N/C common in other tholin studies. The molecular character clearly differs between negative and positive ionizations, underscoring the need for both to understand the sample's chemistry. The nitrogen incorporation also clearly differs between the Titan sample and the Triton sample produced from a gas mix with CO dominant over CH_4. Note that the axis limits differ between the left (O/C) and right (N/C) columns.

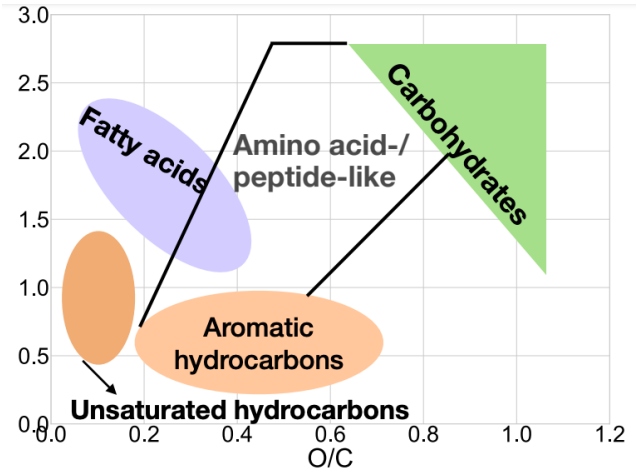

Figure 4.7. An empty Van Krevelen diagram showing H/C vs O/C with shaded, labeled regions denoting where particular molecular functional groups tend to cluster, following Ruf et al. (2018).

Additionally, the Triton tholin displays a larger clustering of molecules consistent with amino acid and peptide-like species ($1.0 \geqslant \mathrm{H/C} \leqslant 2.0$; $0.2 \geqslant \mathrm{O/C} \leqslant 0.8$) compared to the Titan tholin. Finally, the Triton tholin, due to its increased oxidation, shows greater clustering above H/C of 1.5 and O/C of 0.8, where carbohydrate species fall on Van Krevlen diagrams (Ruf et al., 2018).

In H/C vs. N/C space, the Titan tholin is relatively similar between positive and negative ionization, but the Triton tholin is dramatically different. While the negatively ionized molecules from the Triton tholin are qualitatively similar to Titan in this visualization, the nitrogenation of the Triton tholin is clearly enhanced above that of the Titan tholin as seen in the intense clustering of molecules above an N/C of 1.0. These results are also in strong contrast to the results of Jovanović et al. (2020), who studied varying CO-containing N_2-CH_4 mixtures for Pluto atmospheric composition. Jovanović et al. (2020) found, like with our Titan tholin, a preference for molecules with N/C ratios less than one, suggesting that oxygen is incorporated into the solid at the expense of nitrogen. As discussed in our elemental analysis results, we find instead that carbon depletion is associated with the addition of oxygen atoms into the tholin while nitrogen comparatively increases. These results strongly suggest

an alternative chemical pathway is at work in the production of the solids when CO gas $\geqslant$ CH_4. The shift to a more oxidizing atmosphere increasing nitrogen fixation has precedence in early Earth studies with CO_2 and O_2 (Gavilan et al., 2018; Hörst et al., 2018b). Morever, unlike our PHAZER Titan tholin, the positively ionized molecules in our PHAZER Triton tholin are remarkably tightly confined between N/C ratios of 1.2 and 1.5 and H/C ratios of 0 to 0.5. Combined with the increase in unsaturation and oxidation, this tight clustering is likely demonstrating that hydrogen atoms preferentially bond to nitrogen and oxygen atoms. As postulated in Hörst and Tolbert (2014) and He et al. (2017), these reactions may occur due to oxygen radicals from CO efficiently removing hydrogen atoms and molecules from CH_4 along the pathway to solid haze formation.

4.3.3 Transmission and Reflectance Spectra of the Triton Tholin

4.3.3.1 Functional Groups from VIS to NIR

We show in Figure 4.8 the transmittance and reflectance spectra of the Triton tholin from visible to near-infrared wavelengths, 0.4 to 5 μm (25000 cm^{-1} to 2000 cm^{-1}). In visible wavelengths, the most noticeable characteristic of the tholin is its sharp downward slope from 15000 cm^{-1} in transmission, which is observable to the eye as the tholin's brown-ish orange color, well known from Titan tholin studies. In the near-IR, we attribute the variety of features observed to a combination of N-H, C-H, C$\equiv$N, C=C, and O-H bonds. Amine (N-H and N-H_2) features are well described in Titan and Pluto tholin in the 3500 cm^{-1} to 3000 cm^{-1} regions (e.g., Imanaka et al., 2004; Jovanović et al., 2020), but given the prevalence of O species identified in the mass spectral data and combustion analysis, we assign a subset of these features tentatively to O-H alcohol bonds in addition to amines. We also see features attributable to O-H bonds between 2600 and 2400 cm^{-1}, which have not been seen in previous tholin

spectra. These features derive from carboxylic acid species with O-H bonds, which is consistent with the clustering we describe above in the Van Krevelen diagrams. In the 3000 to 2600 cm^{-1} region, we identify several features consistent with various C-H bonds, namely alkenes, alkanes, and aldehydes. Between 2300 and 2000 cm^{-1}, we see some combination of nitrile, alkyne, and imine functional groups. Overall, this plethora of features underscores the complex nature of tholin. We provide a complete list of potential attributions of the spectra in Table 4.II. We also observe some weak features likely indicative of adsorption from ambient atmosphere or residuals in the spectrometer (∼1 hPa) when the sample is briefly exposed to air (water at 3900-3700 cm^{-1} and carbon dioxide at 2370 cm^{-1}), which is also seen in Pluto-like tholin (Jovanović et al., 2020).

Unfortunately, due to our quartz substrate which strongly absorbs in the mid-IR, we are not sensitive to wavelengths beyond 5 μm (2000 cm^{-1}), where carbonyl groups (C=O) have prominent spectral features. The only O bonds we can readily detect are O-H bonds, which could be alcohols or carboxylic acids. Both of these have clusters in the relevant regions of our V-K diagrams (Figure 4.6, upper left panel), but considerably more molecules fall in the carboxylic acid region (where the line with intercept at H/C = 2.0 has a slope of -1) than in the alcohol region (where the line with intercept at H/C = 2.0 has a slope of 0). The spectral features we are able to observe at wavenumbers above 2000 cm^{-1} add credence to the molecules we identify from the HRMS data (including the detection of $C_3H_6O_3$, the formula of glyceraldehyde) but as with the HRMS data itself, they cannot confirm the presence of these isomers of the formula assignments due to the complexity of the tholin.

4.3.3.2 Comparison to Other Tholin Spectra

We compare our measured transmission spectrum of Triton tholin to a collection of literature-reported values for tholin generated from nitrogen/methane atmospheres.

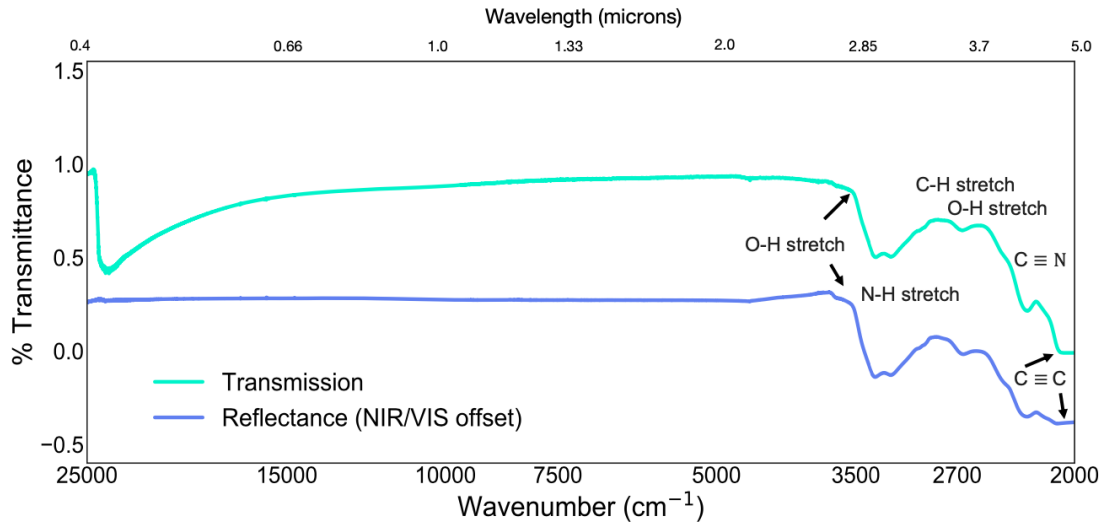

Figure 4.8. Transmittance (teal) and reflectance (periwinkle) of the Triton tholin. A downward slope is visible from 15000 cm^{-1} in transmission and features from O-H, N-H, C-H, C=C, and C≡N are present from 4000 to 2000 cm^{-1} in both transmittance and reflectance spectra. The relfectance spectrum has been offset from the transmittance spectrum in the NIR by 0.4 for clarity.

We do not report every single tholin experiment to date, but select experiments which contain CO or have a Triton-focus. We also generally include only those data published originally as spectra, rather than including each set of published optical constants. We make an exception for the work of Khare et al. due to their widespread use. The Titan optical constants of Khare et al. (1984) and the Triton-specific optical constants of Khare et al. (1994) provide the complex refractive indices, n and k, which they derive from their measured spectra. To convert these values back to spectra for comparison here, we follow their method, given by

$$R = \frac{(n-1)^2 + k^2}{(n+1)^2 + k^2} \tag{4.3}$$

$$T = (1-R)e^{\lambda/4t\pi}e^{-k} \tag{4.4}$$

where R and T are the reflectance and transmittance, respectively, n is the real refractive index, k is the imaginary refractive index, λ is the wavelength in microns,

Frequency (cm^{-1})	**Wavelength (μm)**	**Potential functional group (bond, type)**	**Feature (extent, strength)**
3775 - 3584	2.64	O-H stretching (alcohol)	sharp, medium
3900 - 3700	2.56 - 2.7	H_2O adsorption (contaminant)	broad, weak
3580 - 3575	2.79	O-H stretching (alcohol)	shoulder
3560 - 2889	2.8 - 3.46	N-H stretching (amine)	broad, strong
3337	2.99	$–NH_2$ asymmetric stretching, –NH– stretching (amines)	sharp, strong
3260	3.07	N-H stretching (amine)	sharp, strong
3200 - 3190	3.12 - 3.13	–NH– stretching, overtone of $–NH_2$ bending (amines)	sharp, strong
3004 - 2906	3.32 - 3.44	$–CH_3$, $–CH_2–$ asymmetric stretching (alkenes, alkanes)	shoulder, weak
2924 - 2736	3.41 - 3.65	O-H stretching (carboxylic acids)	broad, strong
2663	3.75	C-H stretching (aldehyde), O-H stretching (alcohol) ?	sharp, strong
2631 - 2450	3.8 - 4.08	O-H stretching (carboxylic acids)	broad, strong
2370	4.21	CO_2 adsorption (contaminant)	shoulder
2340 - 2215	4.27 - 4.51	-C≡N stretching (nitrile)	broad, weak
2210	4.52	C≡C stretching (alkyne), -C≡N stretching (aromatic nitrile)	sharp, strong
2145	4.66	–C≡N stretching (nitrile), –N=C=N– (carbodiimide), CO fundamental	shoulder
2096	4.77	C≡C stretching (alkyne), C=C=N stretching (ketene imines)	weak

Table 4.II. Spectral features observed in the Triton tholin by FTIR.

and t is the film thickness, which in the region of interest (0.4 μm - 5 μm) is approximately 1 μm. We affirm that the reflectance spectrum we derive from the given complex refractive indices in Khare et al. (1984) is identical to their Fig. 5.

A general summary of the experimental conditions used to generate each set of tholin spectra discussed here is found in Table 4.III. Note that a more detailed

discussion of most experimental conditions, as well as the wider range of experiments used to measure optical constants of (Titan) tholin, can be found in the review by Brassé et al. (2015).

We present a comparison of our Triton tholin transmittance spectra, PHAZER Titan transmittance spectra (He et al., 2021), and the other experimental data to which we compare our results in Figure 4.9. The PHAZER Titan tholin spectra has wider absorption at the blue visible edge (0.4 μm) compared to our Triton spectra, consistent with the slightly bluer cast of Triton's haze compared to Titan's, which is known from photometry (Hillier et al., 2021). The most noticeable similarity amongst all the spectra is the broad feature between 3600 and 3200 cm^{-1}, which results from N-H bonds in the form of primary and secondary amines. The most overall similar spectra are the PHAZER Titan (He et al., 2021) and Triton (this work) spectra, which is not surprising given the known effect of different experimental set-ups on resulting tholin properties (e.g., Brassé et al., 2015; Cable et al., 2012). Our Triton tholin spectra have broad, wide features in the 3600 to 3200 cm^{-1} region, which could also be due to the inclusion of oxygen in the chemical structure of the tholin, which could add O-H stretching from alcohols. This broadening is apparent even in comparison to the PHAZER Titan data, which has absorption neither as wide nor as deep at these wavelengths.

The second commonality to most spectra (except McDonald et al. (1994) and Khare et al. (1994) likely due to their very low starting methane mixing ratios) is a narrower feature at $\sim$ 2200 cm^{-1} (4.5 μm). This absorption is likely from some combination of C≡C (alkyne) or C≡N (nitrile) bonds. Our Triton tholin, PHAZER Titan tholin (He et al., 2021), Imanaka et al. (2004) tholin, and Tran et al. (2008) tholin all have features at ∼3000 cm^{-1}, which are indicative of C-H bonds in the form of alkenes or alkanes. These features are notably absent in the spectra of Jovanović et al. (2020). He et al. (2021), Imanaka et al. (2004), and Tran et al. (2008) all

produced tholin from much higher methane mixing ratios (or in the case of Tran et. al, higher mixing ratios of other hydrocarbon species) than either Jovanović et al. (2020) or our Triton tholin. This suggests the features we see in the Triton tholin spectra in this region (∼3000 to 2500 cm^{-1}) could derive from additional O-H bonds from alcohols and carboxylic acids that are not present in the Pluto composition tholin of Jovanović et al. (2020) because of the smaller amount of CO in their starting gas mixture. In a follow-up study, Jovanović et al. (2021) measured optical constants for Pluto analogue aerosols as well, varying the CH_4 mixing ratio but holding CO steady. In effect, this explored the importance of CO as it competes with CH_4. In agreement with our results here, their optical constants results show that N- and O-bearing molecules increase and generate additional absorption in the visible and near-IR with lower methane mixing ratios. Their study extended into the UV as well, finding that this absorption due to N and O molecules also affects shorter wavelengths (Jovanović et al., 2021).

We also note that many of the spectra to which we compare have their strongest identifying features at slightly longer wavelengths and into the fingerprint region, from roughly 5 to 15 μm (1700 to 700 cm^{-1}). This region is highly complex because of the multitude of features found there, but it can also provide much needed context to the VIS-NIR wavelength spectra explored here, particularly regarding the oxygen-bonding environment of tholin or haze particles. Carbonyl (C=O) species including aldehydes, ketones, esters, amides, and carboxylic acids all have prominent peaks from 1800 to 1600 cm^{-1} (5.55 to 6.25 μm), and in fact have been observed in other studies with relatively larger CO starting fractions (Tran et al., 2008). Additionally, a study which examined the effect of CO_2 in N_2-CH_4 gas mixtures also found significant enhancement in both N- and O-bearing functional groups as CO_2 increased (Gavilan et al., 2018). This study examined both shorter (UV, down to 0.13 μm) and longer (MIR, 6-10 μm) wavelengths, reitering the importance of wide wavelength coverage in understanding

increasingly oxidized aerosols.

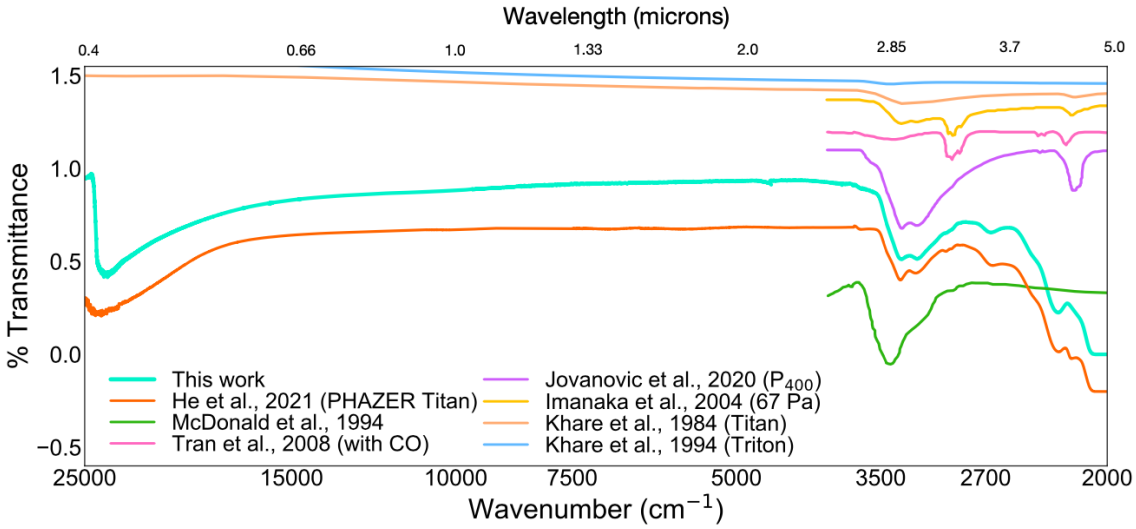

Figure 4.9. Transmittance spectra of various tholins produced from N_2-CH_4 mixtures. The full details of each experiment can be found in Table 4.III. Some features are present in all tholin. In the Triton tholin of this work, we attribute some of the broadening between 3500 and 3200 cm^{-1} and additional absorption between 3000 and 2500 cm^{-1} to be due uniquely to O-H bonds. These bonds likely result from $CO > CH_4$ in the initial gas mixture. All spectra have been offset vertically for clarity.

Reference/Body	Gas mixture	Temperature	Pressure	Energy Source
This work *Triton*	99.3% N_2 0.5% CO 0.2% CH_4	90 K	∼1 mbar	AC plasma discharge
He et al., submitted *Titan*	95% N_2 5% CH_4	90 K	∼1 mbar	AC plasma discharge
McDonald et al., 1994 *Triton*	99.9% N_2 0.1% CH_4	room temp (294 K)	∼1 mbar	RF ICP discharge
Tran et al., 2008 *Titan*	98% N_2 1.8% CH_4 0.2% H_2 400 ppm C_2H_2 300 ppm C_2H_4 20 ppm HC_3N 0.3% CO	297 K	900 mbar	Mercury lamp
Jovanovic et al., 2020 *Pluto*	99% N_2 1% CH_4 500 ppm CO	room temp (294 K)	∼1 mbar	RF CCP discharge
Imanaka et al., 2004 *Titan*	90% N_2 10% CH_4	room temp (294 K)	0.67 mbar	RF ICP discharge
Khare et al., 1984 *Titan*	90% N_2 10% CH_4	room temp (294 K)	0.2 mbar	DC plasma discharge
Khare et al., 1994 *Triton*	99.9% N_2 0.1% CH_4	room temp (294 K)	0.86 mbar	DC plasma discharge

Table 4.III. Previous relevant experimental work. *Key. AC: Alternating current. RF ICP: Radio frequency inductively coupled plasma. RF CCP: Radio frequency capacitively coupled plasma. DC: Direct current.*

4.4 Discussion

4.4.1 Comparison to Existing Observations of Triton

4.4.1.1 Voyager 2 Atmospheric Observations

In situ observations of Triton's atmosphere are mainly limited to visible and UV photometry rather than spectra, preventing a true direct comparison of our experimental tholin results. Voyager 2 imaging and visible photometry observations of Triton's atmosphere suggest optically thin hazes (Smith et al., 1989), with scattering optical depths between 0.001–0.01 that increase with shorter wavelengths (Pollack et al., 1990; Rages & Pollack, 1992) and particle sizes of around 100-200 nm (Pollack et al., 1990; Rages & Pollack, 1992). UV occultation data from Voyager 2 suggests significantly higher (0.024) scattering optical depths, reiterating the wavelength dependent nature of the haze scattering and suggesting even smaller particles (30 nm) in the Rayleigh regime (Herbert & Sandel, 1991). At visible wavelengths, the haze is strongly forward scattering and requires particles larger than 200 nm (Hillier et al., 1991). To meet these observational signatures of higher scattering in the blue (small particles) and large forward scattering (large particles) simultaneously, the hazes have been suggested to be fractal aggregrates (Lavvas et al., 2020; Ohno et al., 2021). Aggregrates also explain the haze properties of both Titan (Tomasko et al., 2008) and Pluto (Cheng et al., 2017; Gao et al., 2017a; Gladstone et al., 2016), though the fractal dimension and growth rate is not settled (Kutsop et al., 2021). This range of particle sizes well fits with those we produce in the PHAZER chamber (e.g., He et al., 2018b; He et al., 2017), though these particle sizes may in part result from the physical size of the chamber itself, which inhibits further growth. Material characterization of PHAZER Titan tholin particles suggests, however, that the necessary particle sizes and fractals to match observations through coagulation and growth is consistent with this size range (Yu et al., 2017). More generally, tholin particles produced in a variety of setups

seem to easily coagulate and form aggregrates (Cable et al., 2012).

4.4.1.2 Seasonal Changes from Space- and Ground-Based Observations

Ground-based observations were responsible for the initial confirmed detection of CO in Triton's atmosphere (Lellouch et al., 2010). However, earlier Hubble Space Telescope (HST) data using the Space Telescope Imaging Spectrograph (STIS) also provided upper limits on CO that differed from the initial Voyager 2 data and suggested strong surface absorption at UV wavelengths, which could be attributable to photochemical products from the atmosphere settling to the surface (Krasnopolsky & Cruikshank, 1995; Stern et al., 1995). Both the ground- and space-based data indicate that CO levels in the atmosphere can change over seasonal timescales. Further HST STIS observations showed that Triton's UV albedo brightened between the Voyager 2 flyby and 1999, evidence of ongoing seasonal cycling in the form of volatile transport between the surface and atmosphere or plume activity (Young & Stern, 2001). Later HST and ground-based observations continued to find surface reflectivity changes in the UV, as well as in visible and NIR wavelengths which probe methane abundances, suggestive of continued seasonal volatile transport on sub-decadal timescales (Bauer et al., 2010; Buratti et al., 2011). Additionally, both thermal and pressure changes have been observed from ground-based solar occultations (Elliot et al., 1998; Olkin et al., 1997), demonstrating that the atmosphere undergoes substantial interaction with the surface. The surface is predominately N_2 ice, with contributions from diluted CO ice (Merlin et al., 2018). This CO ice and N_2 ice experience greater longitudinal and temporal variation than does CH_4 ice present on the surface (Grundy et al., 2002; Grundy et al., 2010), including over diurnal timescales (Holler et al., 2016).

Given our results regarding the importance of the exact CO/CH_4 mixing ratio in determining both the nitrogenation and oxidation of haze particles, these observations suggest that large shifts can happen in the dominant haze chemistry over Triton's

seasonal cycle, as may also be occuring on Pluto (Bertrand & Forget, 2017). In their study of Pluto tholin optical constants, Jovanović et al. (2021) found that the real refractive index n increased when CO mixing ratios in the gas increased, and oxidation of the aerosols promoted both UV and visible absorption. Therefore, our experimental results combined with past observations suggests a complicated set of processes likely controls Triton's atmospheric and surface properties. Ices sublimate, change the overall atmospheric abundances, shift haze chemistry, and these hazes settle or condense out onto the surface again.

4.4.2 Comparison to Other Experimental Results

We demonstrate above that the formulas for a variety of astrobiologically interesting molecules (amino acids, nucleobases, and a simple sugar) are present in our tholin, and subsequent sedimentation of this putative haze material likely coats the icy surface of Triton, as also likely occurs on Pluto (Grundy et al., 2018; Protopapa et al., 2020). However, amino acids may be subject to further photolysis on icy surfaces, suggesting that they are rapidly destroyed unless this material quickly reaches the subsurface (Johnson et al., 2012), though Triton's atmosphere attenuates more UV radiation than Johnson et al. (2012)'s experiment simulated. Complementing our atmospheric study, Triton surface ice chemistry by photolysis can also produce chemically complex material from N_2-CH_4-CO ice mixtures (Hodyss et al., 2011; Moore & Hudson, 2003). The products of these surface ice experiments with CO/CH_4 $\sim$1 include many of the molecular species and spectral features we identify here, including carboxylic acids, alcohols, ketones, aldehydes, amines, and nitriles in addition to having similar nitrogen, carbon, and oxygen abundances overall (Materese et al., 2015; Materese et al., 2014). Additionally, potential interactions of these ices and tholin-like materials could further react with water ice deposits present on Triton's surface (Cruikshank et al., 2000) to generate molecules of additional prebiotic complexity and interest (Cruikshank et al.,

2019). Given the seasonal cycling through sublimation and condensation of volatile ices combined with the products of photochemistry both in the atmosphere and on the surface, Triton holds great interest for future study.

4.4.3 Haze Formation and Ice Condensation

Efforts to model the haze formation process on Pluto and Triton have shown previously that the CO and CH_4 mixing ratios in the atmosphere act as a strong control on the overall composition of haze (Krasnopolsky, 2012; Krasnopolsky & Cruikshank, 1995; Strobel & Zhu, 2017), in agreement with our laboratory results. These models have noted that ethylene, C_2H_4, as a product of the haze formation process is likely to condense the most readily of all photochemical products considered (Krasnopolsky et al., 1992; Wong et al., 2017). The hazes of the upper atmosphere can act as thermal controls of both the atmosphere and surface (Zhang et al., 2017), which is critically dependent on the exact composition and optical properties of the material. Recent coupled photochemical and microphysical modeling suggests that coagulation of ice particles and hydrocarbon (C_2-based) hazes (Luspay-Kuti et al., 2017) or ice condensation onto haze particle condensation nuclei (dominated by HCN cores) may better explain the observations of both Pluto and Triton's atmosphere (Lavvas et al., 2020), where C_2H_4 would dominate the composition of these heterogeneous, coated particles on Triton (Krasnopolsky, 2020). Both spherical and fractal aggregate particles can explain Triton observations using heterogeneous haze-ice particles, though fractals are preferred (Ohno et al., 2021).

In fact, Lavvas et al. (2020) argues that Titan, Pluto, and Triton lie along a continuum of haze formation outcomes, with Titan at the "molecular growth" end and Triton on the "condensate growth" end, with Pluto in the middle. However, these comparisons primarily used the optical constants of Khare et al. (1984) Titan tholin and photochemical models driven by methane photolysis where CO is less important

(Lavvas et al., 2020), despite CO being a potential driver of increased haze growth (He et al., 2018a; He et al., 2020b; He et al., 2017; Hörst & Tolbert, 2014; Hörst et al., 2018a). More recent optical constants of purely photochemical Pluto tholin (from CO-containing mixtures) provide better agreements to existing New Horizons data (Jovanović et al., 2021), but there may still be a substantial contribution from condensed ices onto the hazes (see, e.g., Fayolle et al. (2021). Our results, which show increased nitrogenation and oxidation even over that observed by Jovanović et al. (2021), Jovanović et al. (2020), may further resolve observational discrepancies. Further radiative transfer modeling has suggested that perhaps the redder Pluto and Titan hazes are more similar to each other in comparison to Triton, which is bluer. Such differences could be either chemical, perhaps due to higher CO/CH_4 mixing ratios as we have shown here, or physical, potentially due to the increased contribution from ice condensates in Triton's atmosphere (Hillier et al., 2021). However, to pinpoint the cause of the similarities and differences between the hazes of these three worlds, further measurements to obtain optical constants of the spectra we provide here, as well as laboratory measurements of the formation and properties of heterogeneous haze-ice condensate particles across multiple haze chemistries, is required.

4.4.4 Future Triton Missions

While ground- and space-based observations have furthered our understanding of Triton in the years since the Voyager 2 flyby (e.g., Bauer et al., 2010; Lellouch et al., 2010; Stansberry et al., 2015; Stern et al., 1995; Young & Stern, 2001), *in situ* missions would dramatically improve our knowledge of the atmosphere, surface, and interior processes of the moon (Christophe et al., 2012; Fletcher et al., 2020; Hofstadter et al., 2019; Masters et al., 2014). Several proposed missions in various states of development would visit Triton, with complementary goals. Trident, a Discovery class mission that was downselected as a finalist, though not ultimately chosen for flight in the Discovery

15 and 16 competition, would perform a single flyby of Triton (Prockter et al., 2019). The Neptune Odyssey mission concept, a Flagship class orbiter and probe under study for the 2023 Planetary Science and Astrobiology Decadal Survey, would orbit the Neptune-Triton system with a four year prime mission and would perform ∼monthly flybys of Triton itself (Rymer et al., 2020). Triton Hopper is a mission concept under study by the NASA Innovative Advanced Concepts (NIAC) program, which would act as a lander capable of producing its own propellant from surface ices in order to perform short flights across the surface (Landis et al., 2019; Oleson & Landis, 2018).

Trident's major scientific goals would be to confirm the presence of a subsurface ocean and infer whether it interacts with the surface, sample the ionosphere, and perform repeated surface imaging to characterize its composition and geology (Prockter et al., 2019). To achieve these goals, Trident would be equipped with, among other instruments, a plasma spectrometer and a high-resolution infrared spectrometer with spectral range up to 5 μm. In the context of the study we have performed here, the Trident mission could clearly benefit our understanding of ionospheric processes driving haze formation by providing better constraints on the ion energies of the upper atmosphere. On Titan, for example, haze formation in the upper atmosphere is more strongly influenced by the Saturnian magnetosphere and solar EUV while longwave solar UV photons primarily dominate haze formation processes below 500 km (Lavvas et al., 2008). In laboratory measurements, plasma or spark discharge energy sources compared to UV lamps produce tholin which differs in composition and observable spectra (Cable et al., 2012), illustrating this dual haze formation process. A better understanding of the Triton ionosphere could similarly help guide future laboratory experiments and modeling efforts to describe the haze formation process for Triton specifically. Trident's infrared spectrometer would have the same range as the spectral measurements we have performed in this study (out to 5 μm) and would clearly advance our understanding of Triton's surface and atmosphere-surface

interactions (Prockter et al., 2019). However, as we have shown above, the presence of CO as both a surface ice and and as a minor atmospheric component should induce significant oxygen chemistry. Such chemistry could be best probed with measurements that encompass carbonyl groups out past 6 μm, which could be taken into account with future development of the Trident concept.

The Triton Hopper concept study explored the ability of its design to generate propellant from the primarily nitrogen-ice surface of the moon, but also considered a wide instrument package to enable scientific characterization of Triton's surface and atmosphere (Landis et al., 2019; Oleson & Landis, 2018). These instruments include a quadrupole mass spectrometer and a gas chromatograph (based on SAM, Sample Analysis at Mars) a V/UV/NIR spectrometer, a meteorological package, and an X-ray spectrometer. In context of increased oxidation of sedimented haze materials on the surface suggested by our results, the ability of the Hopper concept to use surface materials as propellant may be impacted. Recent efforts to use Pluto-like tholin to match the New Horizons surface observations of dark reddish material suggest highly porous structures of surface ice mixed with aerosols (Fayolle et al., 2021). If similar porous ice-aerosol structure is present on Triton, or if aerosol is entrained with the surface ice or snow, the oxidized refractory organic materials that make up the haze could prevent efficient intake of N_2 to melt for propellant.

Neptune Odyssey, as a Flagship class concept, would be equipped with an extensive suite of instrumentation to enable its wide-ranging science goals, *à la* a Cassini for the Neptune system (Rymer et al., 2020). In terms of Triton science, Odyssey would investigate whether Triton is an ocean world, the source of its plumes, and broad scale compositional and dynamical processes of the atmosphere, surface, and interior. Relevant to our laboratory study here, this mission would carry imaging spectrometers in the UV and VIS-NIR, an ion and neutral mass spectrometer, a thermal plasma spectrometer, and an energetic charged particle detector. Such a mission would enable

not only significant comparison to the Saturn-Titan system but also a far deeper understanding of Triton and Neptune than we currently possess. Nevertheless, the concept study also only studied a VIS-NIR spectrometer with range up to 5 μm and an ion and neutral mass spectrometer with range up to 100 amu (Rymer et al., 2020). Here we have shown that significantly large and complex molecules with significant oxygen incorporation can be produced under Triton atmosphere conditions, which could be best explored with spectroscopy beyond 5 μm and mass spectrometry up to and beyond 450 amu. Lessons learned about the complex atmospheric chemistry of Titan and its unveiling (and the new questions uncovered) with Cassini should inform future mission development to explore and understand the correspondingly complex chemistry of Triton's atmosphere and surface.

4.5 Conclusion

We simulated haze formation in Triton's atmosphere using the PHAZER chamber and apparatus with a starting gas mixture of 0.5% CO and 0.2% CH_4 in N_2 at 90 K. We then measured the production rate, composition, and spectra of the haze analogues produced with combustion analysis, very high resolution mass spectrometry, and transmittance and reflectance spectroscopy.

We find that:

1) Oxygen is incorporated into the elemental composition of the solid tholin particles at approximately 10% by mass despite its inclusion in the form of CO in the original gas mixture at just 0.5%.

2) When taking our Triton results and comparing them to previous PHAZER N_2-CH_4-CO experiments, the increase of CO over that of CH_4 in the original gas mixture shifts the elemental composition away from carbon and toward a more nitrogen-rich structure, though more CH_4 may generate larger absolute amounts of solid.

3) From very high resolution mass spectrometry measurements, we detect, as in previous studies, molecular formulas consistent with all 5 biological nucleotide bases, one non-biological nucleotide base, and several amino acid derivatives. Additionally, we observe the formula for glyceraldehyde, the simplest monosaccharide, for the first time from a N_2-CH_4-CO atmospheric experiment.

4) Transmission and reflectance spectra of the Triton tholin produce features attributable to O-H, N-H, C-H, C≡N, and C≡C bonding. Most of these are also seen in spectra of similar tholin experimental data, but we also observe additional features as well as deeper and broader features attributable to oxygen bonds.

5) To take full advantage of the chemistry we observe in our laboratory setting, future Triton missions should carry instrumentation capable of probing high molecular weight compounds, such as mass spectrometers with high mass range ($\geqslant$450 amu), and carbon-oxygen bonds, such as NIR spectrometers with spectral range out to at least 6.5 μm.

6) The exact CO/CH_4 mixing ratio in N_2 atmospheres can dramatically affect the resulting haze chemistry. Since both Triton and Pluto undergo substantial atmospheric changes through sublimation of surface ices, their haze chemistry may also experience seasonal dependence.

Given our results along with the existing body of literature for Titan and Pluto, additional study is clearly motivated into the exact chemical pathways for haze formation between these three similar, yet distinct planetary bodies. The nature of this haze chemistry can affect the prebiotic inventories of these worlds, their climates and radiative balance, and seasonal cycling between their atmospheres and surfaces. As three worlds with N_2-CH_4-CO atmospheres under different energetic regimes, Triton, Titan, and Pluto are themselves a fruitful laboratory for understanding carbon monoxide's dramatic influence on atmospheric chemistry.

Chapter 5

Discussion and Conclusions

"To learn which questions are unanswerable, and *not to answer them*: this skill is most needful in times of stress and darkness."

— Ursula K. Le Guin, *The Left Hand of Darkness*

5.1 Summary

In this dissertation, I have made the first few steps in connecting the results of laboratory experiments to atmospheric models for exoplanet hazes, as well as performed a deeper dive into the haze chemistry of the oft-neglected moon of Neptune, Triton. My work has been driven in part by the new discoveries of the plethora of exoplanets we now know are out in the universe, which demand exploration. Over the course of this work, new molecules and gases have been discovered in both exoplanetary as well as Solar System atmospheres, pushing us to piece together how atmospheric chemistry functions on distant worlds. I summarize in the following sections a few of the implications my work has for this understanding of (exo)planetary atmospheric physics and chemistry.

5.2 Hazy, Hydrogen-Rich Terrestrial Atmospheres

In Chapter 2, I began the process of linking very fundamental measurements from the laboratory – particle size and haze production rate – into simple parametrized atmospheric models for exoplanets. Thanks in large part to our *in situ* data from Solar System atmospheres in addition to remote sensing observations, I was able to provide the first physically motivated treatment of these simple parametric scalings. I showed that the often invoked very large multiplicative factors of "haze amplitudes" are, at least for terrestrial exoplanet atmospheres, likely unphysical.

I specifically explored whether we can explain *Hubble* observations of the TRAPPIST-1 planets with hazy hydrogen-rich atmospheres. The amount of haze produced in a hydrogen-rich atmosphere is simply not enough to generate the intensely flat transmission spectra observed. Taking these conclusions beyond TRAPPIST-1, additional studies of planetary systems with sub-Neptune and terrestrial worlds have built on this methodology in atmospheric models with hazy constituents (Pidhorodetska et al., 2021).

5.3 Cloud Decks and Secondary Atmospheres

I also reproduced in Chapter 2 the well-known degeneracy between simple grey clouds and metallicity (or mean molecular weight) in dampening spectral features in transmission. I showed that, particularly for the *Hubble* G141 grism which centers on the water feature at 1.4 μm, increasing water content and moving clouds higher in the atmosphere cannot be disentangled from each other with only near-IR measurements. Treating clouds more realistically or extending measurements into longer wavelengths can both overcome this problem. I demonstrate the latter in my part of the follow-up work on TRAPPIST-1 g, published in Wakeford et al. (2019a).

5.4 Characterization of Terrestrial Atmospheres

Finally, my work in Chapter 2 and the publications which followed it demonstrates – in agreement with much of the literature – that bigger, next-generation observatories (starting with JWST) are necessary to truly understand the composition of exoplanet atmospheres below $\sim$1.6 $R_\oplus$. The transit depth precisions required to observe secondary, small atmospheres around these planets are on the order of 15 to 20 ppm, well beyond what is reasonable for small planets by current observatories.

5.5 Exoplanet Tholin Composition

In Chapter 3, I provide the first laboratory measurements about the chemical composition of exoplanet hazes, using analogue materials produced in the PHAZER (Planetary HAZE Research) chamber. In particular, my work demonstrated that for planets on the inner edge of the Habitable Zone and warmer, oxygen is strongly incorporated into the haze particles, at proportions of up to 20%. These measurements strongly diverge from the proxy hazes previous literature used to represent hazes in exoplanet atmospheric models, which are frequently based on (outdated) Titan tholin or soots, neither of which are oxygen-rich. The first attempts to account for this greater chemical diversity in hazes, based upon my work, have recently been published in a study of the planetary system L 98-59 (Pidhorodetska et al., 2021).

5.6 Haze-Cloud Interactions

As part of my work in Chapter 3, I stumbled upon the solubility behavior of exoplanet hazes as a function of the polarity of the solvent. Given the greater likelihood of soluble particles being better cloud condensation nuclei (CCN), I suggested that these exoplanet hazes (for 300 K to 600 K atmospheres between 100$\times$ and 10000$\times$ metallicity) could act as efficient cloud seeds for polar condensibles, like water, in

exoplanet atmospheres. More recent and in-depth study about the surface energy of these exoplanet laboratory hazes has confirmed quantitatively that they are likely to be good cloud condensation nuclei (CCN) under some conditions (Yu et al., 2021). This result may help explain the beginnings of trends we observe for hazy versus clear atmospheres in exoplanets of this temperature regime.

Moreover, in Chapter 4, I also find that oxygen due to CO is incorporated at higher rates than expected into Triton-like haze particles. Given recent scholarship (Lavvas et al., 2020; Ohno et al., 2021) suggesting an ice cloud component in the moon's atmosphere to explain observations, my work on the composition of the haze should be taken into account for future studies. Oxygen content may both affect the observed characteristics of Triton's haze, as well as alter the haze's ability to act as efficient cloud condensation nuclei.

5.7 Hazy, Oxygenated Atmospheres as a Source of Prebiotic Molecules

In both Chapters 3 and 4, I detect a multitude of molecular formulas with prebiotic roles, including those for nucleotide bases, amino acids, and simple sugars. Given the high amounts of CHON-bearing molecules that form these hazes, such a result is perhaps unsurprising. Previous, Titan-focused work has already shown that nucleotide bases and amino acids can readily form under these upper atmosphere-like conditions (Hörst et al., 2012; Sebree et al., 2018). However, the experiments here show that additional oxygen into the system does not create such an oxidizing environment that formation of these prebiotic species cannot proceed, and in fact, this additional oxygen could enable the generation of simple monosaccharides.

While confirmation of molecular structure, and not merely formula, is absolutely required to confirm my results, my work again reiterates the importance of upper atmospheres as a prebiotic pathway both in the Solar System and beyond. The

exact mechanisms that lead to such molecules, how and whether they are generated in substantial enough quantities to enable further prebiotic and ultimately biotic chemistry, and the specific locations across the universe where such reactions have or can occur is left to future work by other researchers.

5.8 Trace Species and Alternate Haze Formation Pathways

While I showed conclusively the powerful role oxygen can play in haze formation throughout Chapter 3 and 4, a further revelation from these experiments is the importance of the specific bonding environment of the oxygen-bearing molecules, as well as that of other elements like nitrogen and carbon. In Chapter 3, I show that nitrogen in the form of ammonia in the gas phase can substantially alter the solubility of the haze particles, with implications for the ability of cooler planets to form water clouds. Chapter 3 also demonstrates that the hottest of our experimental water-rich atmospheres, at 600 K, generates the most oxygen-rich hazes despite having the least oxygen by weight percentage in the starting gas mixture. Of the water-rich cases, this experiment alone contains carbon monoxide in addition to water and carbon dioxide vapor. We hypothesize, therefore, that carbon monoxide acts as a more efficient seed to build up eventual haze particles than the dissociation of water molecules.

In Chapter 4, I also demonstrate that the mixing ratio of carbon monoxide to methane gas in the starting mixture is critical to the ultimate oxygen content of the haze particles. Again, the mechanism for the greater oxygen inclusion in the haze may follow from building on top of carbon monoxide rather than breaking up methane, but further work is needed to elucidate the exact pathway of this chemical process.

On the note of haze formation pathways, Chapter 3 and 4 clearly break the "conventional" wisdom long assumed in both exoplanetary and solar system atmospheric photochemical and parameterized models that only methane or hydrocarbons are

the dominant precursors to haze formation. In addition to my work here, further exoplanet experiments in the PHAZER lab have shown that carbon monoxide and carbon dioxide (He et al., 2020b), as well as sulfur-bearing hydrogen sulfide (He et al., 2020a), can generate substantial organic and organosulfur hazes (Vuitton et al., 2021). Clearly, more work is needed to understand the many potential chemistries to create hazes in planetary atmospheres, as well as their ultimate effect on the climates of these worlds.

5.9 Observational Tracers of Haze Chemistry

In Chapter 4, I present transmittance and reflectance spectra of the Triton analogue hazes, clearly showing that oxygen-bearing molecules create observable spectral features for future observations and missions to search for in the atmosphere. I also demonstrate that a true understanding of the haze is likely best achieved with longer wavelength observations, where carbonyl features are located out near 6 μm. Given the high oxygen contents of the exoplanet tholin described in Chapter 2, I expect similar probes of the haze chemistry will be enabled if exoplanet hazes are present at sufficient quantities in the atmosphere. In Chapter 2, I utilized the small particle sizes observed in the laboratory to suggest strong scattering slopes in the optical, in agreement with previous studies (e.g., Wakeford & Sing, 2015). In this way, shortwavelengh observations may offer insight into the physics while longer wavelengths open up the chemistry of planetary clouds and hazes.

5.10 Remaining Questions

I have tackled a number of the questions with which I began, as well as found the answers to questions I did not think to have. However, many remain. These include:

- What do exoplanet hazes actually look like? Are there spectral features indicative

of exoplanet hazes, which JWST and future observatories can search for?

• What are all the possible and/or likely drivers of haze formation in exoplanets? Are oxygen-bearing molecules as important as my results suggest?

• Do the laboratory hazes we make and analyze here actually share the important physical and chemical properties of actual hazes in planetary atmospheres?

• How tightly coupled is haze and cloud formation? How do these two processes interact with each other in the outer Solar System and on exoplanets?

• How can we best treat clouds and hazes in (exo)planetary atmospheres? What is the right level of complexity that balances physical reality with computational expense and effort?

• How does our understanding of haze composition and production depend on the host star?

5.11 Final Thoughts

While I have pushed forward our understanding of both exoplanetary and Triton clouds and hazes, we have much more learn, as the above list of outstanding questions suggests. The now months away launch of JWST, along with future observatories and future outer Solar System missions to Titan (like Dragonfly) and hopefully the Ice Giant systems, will illuminate whether the work started here is on the right track, or whether we must throw it all out and start anew. So it goes. Planets and their atmospheres constantly defy expectations, and I'm (mostly) ever grateful that I can be part of the story.

Here, at the end of it, I also must grapple with that most fundamental question:

Why study this at all?[1] The study of planetary atmospheres outside our own may not seem the most important of subjects.[2] But, to me, this pursuit of knowledge is one of the things that makes us human. No, I'm not curing cancer or developing vaccines or building better infrastructure. I could give you the clichés about how learning about other climates teaches us ultimately about our own, or a screed about the Golden Goose awards and the importance of fundamental research, but honestly, that's not why I'm here. I'm here as part of an endeavor as noble as any artistic quest. We're looking for meaning beyond ourselves, bits of discarded stardust yearning to understand its own atoms – the universe working to know itself. It's a privilege beyond measure that I can ask those questions and work toward making something like an answer to a small few of them. Art is worthwhile because it makes us human; it's an outlet for the deepest loneliness we hold in our souls. Science of the kind performed here is no different, really. So why is this important? Because looking for the beauty in a gravity wave as it sculpts a cloud deck on another world is the same as writing a great novel. Because searching for the colors of a distant sky is as human as painting a masterpiece. Because the shadow of a far-off sun as it streaks across a landscape some tens of lightyears away is no less than the poetry of the universe at work. Because "we are all in the gutter, but some of us are looking at the stars."[3]

[1] a rant; a soapbox moment of cheese because it's *my* goddamn dissertation, dammit.
[2] After all, there's people that are dying, Kim.
[3] –Oscar Wilde

References

Ackerman, A. S., & Marley, M. S. (2001). Precipitating Condensation Clouds in Substellar Atmospheres. *ApJ*, *556*, 872–884. https://doi.org/10.1086/321540

Adams, D., Gao, P., de Pater, I., & Morley, C. V. (2019). Aggregate Hazes in Exoplanet Atmospheres. *The Astrophysical Journal*, *874*(1), Article 61, 61. https://doi.org/10.3847/1538-4357/ab074c

Agnor, C. B., & Hamilton, D. P. (2006). Neptune's capture of its moon Triton in a binary-planet gravitational encounter. *Nature*, *441*(7090), 192–194. https://doi.org/10.1038/nature04792

Alberti, T., Carbone, V., Lepreti, F., & Vecchio, A. (2017). Comparative Climates of the Trappist-1 Planetary System: Results from a Simple Climate-vegetation Model. *ApJ*, *844*, Article 19, 19. https://doi.org/10.3847/1538-4357/aa78a2

Alcouffe, G., Cavarroc, M., Cernogora, G., Ouni, F., Jolly, A., Boufendi, L., & Szopa, C. (2009). Capacitively coupled plasma used to simulate titan's atmospheric chemistry. *Plasma Sources Science and Technology*, *19*(1), 015008.

Arney, G. N., Meadows, V. S., Domagal-Goldman, S. D., Deming, D., Robinson, T. D., Tovar, G., Wolf, E. T., & Schwieterman, E. (2017). Pale Orange Dots: The Impact of Organic Haze on the Habitability and Detectability of Earthlike Exoplanets. *ApJ*, *836*, Article 49, 49. https://doi.org/10.3847/1538-4357/836/1/49

Bar-Nun, A., & Podolak, M. (1979). The photochemistry of hydrocarbons in Titan's atmosphere. *Icarus*, *38*(1), 115–122. https://doi.org/10.1016/0019-1035(79)90091-5

Barstow, J. K., & Irwin, P. G. J. (2016). Habitable worlds with JWST: transit spectroscopy of the TRAPPIST-1 system? *MNRAS*, *461*, L92–L96. https://doi.org/10.1093/mnrasl/slw109

Barstow, J. K. (2020). Unveiling cloudy exoplanets: the influence of cloud model choices on retrieval solutions. *MNRAS*, *497*(4), 4183–4195. https://doi.org/10.1093/mnras/staa2219

Batalha, N. E., Kempton, E. M.-R., & Mbarek, R. (2017). Challenges to Constraining Exoplanet Masses via Transmission Spectroscopy. *ApJ Letters*, *836*, Article L5, L5. https://doi.org/10.3847/2041-8213/aa5c7d

Batalha, N. E., Lewis, N. K., Line, M. R., Valenti, J., & Stevenson, K. (2018). Strategies for Constraining the Atmospheres of Temperate Terrestrial Planets with JWST. *ApJ Letters*, *856*, Article L34, L34. https://doi.org/10.3847/2041-8213/aab896

Batalha, N. E., Lewis, T., Fortney, J. J., Batalha, N. M., Kempton, E., Lewis, N. K., & Line, M. R. (2019). The Precision of Mass Measurements Required for Robust Atmospheric Characterization of Transiting Exoplanets. *ApJ Letters*, *885*(1), Article L25, L25. https://doi.org/10.3847/2041-8213/ab4909

Batalha, N. E., & Line, M. R. (2017). Information Content Analysis for Selection of Optimal JWST Observing Modes for Transiting Exoplanet Atmospheres. *AJ*, *153*, Article 151, 151. https://doi.org/10.3847/1538-3881/aa5faa

Bauer, J. M., Buratti, B. J., Li, J.-Y., Mosher, J. A., Hicks, M. D., Schmidt, B. E., & Goguen, J. D. (2010). Direct Detection of Seasonal Changes on Triton with Hubble Space Telescope. *Astrophysical Journal*, *723*(1), L49–L52. https://doi.org/10.1088/2041-8205/723/1/L49

Benneke, B., Knutson, H. A., Lothringer, J., Crossfield, I. J. M., Moses, J. I., Morley, C., Kreidberg, L., Fulton, B. J., Dragomir, D., & Howard, A. W. (2019a). A sub-Neptune exoplanet with a low-metallicity methane-depleted atmosphere and Mie-scattering clouds. *Nature Astronomy*, 361. https://doi.org/10.1038/s41550-019-0800-5

Benneke, B., Wong, I., Piaulet, C., Knutson, H. A., Lothringer, J., Morley, C. V., Crossfield, I. J. M., Gao, P., Greene, T. P., Dressing, C., Dragomir, D., Howard, A. W., McCullough, P. R., Kempton, E. M. .-R., Fortney, J. J., & Fraine, J. (2019b). Water Vapor and Clouds on the Habitable-zone Sub-Neptune Exoplanet K2-18b. *ApJ Letters*, *887*(1), Article L14, L14. https://doi.org/10.3847/2041-8213/ab59dc

Bernard, J. .-M., Coll, P., Coustenis, A., & Raulin, F. (2003). Experimental simulation of Titan's atmosphere: Detection of ammonia and ethylene oxide. *Planetary and Space Science*, *51*(14-15), 1003–1011. https://doi.org/10.1016/j.pss.2003.05.009

Berry, J. L., Ugelow, M. S., Tolbert, M. A., & Browne, E. C. (2019). The Influence of Gas-phase Chemistry on Organic Haze Formation. *ApJ Letters*, *885*(1), Article L6, L6. https://doi.org/10.3847/2041-8213/ab4b5b

Bertrand, T., & Forget, F. (2017). 3D modeling of organic haze in Pluto's atmosphere. *Icarus*, *287*, 72–86. https://doi.org/10.1016/j.icarus.2017.01.016

Bolmont, E., Selsis, F., Owen, J. E., Ribas, I., Raymond, S. N., Leconte, J., & Gillon, M. (2017). Water loss from terrestrial planets orbiting ultracool dwarfs: implications for the planets of TRAPPIST-1. *MNRAS*, *464*, 3728–3741. https://doi.org/10.1093/mnras/stw2578

Bonnet, J.-Y., Thissen, R., Frisari, M., Vuitton, V., Quirico, É., Orthous-Daunay, F.-R., Dutuit, O., Le Roy, L., Fray, N., Cottin, H., Hörst, S. M., & Yelle, R. V. (2013). Compositional and structural investigation of HCN polymer through high resolution mass spectrometry. *International Journal of Mass Spectrometry*, *354*, 193–203. https://doi.org/10.1016/j.ijms.2013.06.015

Borucki, W. J., Koch, D., Basri, G., Batalha, N., Brown, T., Caldwell, D., Caldwell, J., Christensen-Dalsgaard, J., Cochran, W. D., DeVore, E., Dunham, E. W., Dupree, A. K., Gautier, T. N., Geary, J. C., Gilliland, R., Gould, A., Howell, S. B., Jenkins, J. M., Kondo, Y., ... Prsa, A. (2010). Kepler Planet-Detection Mission: Introduction and First Results. *Science*, *327*(5968), 977. https://doi.org/10.1126/science.1185402

Bourrier, V., de Wit, J., Bolmont, E., Stamenković, V., Wheatley, P. J., Burgasser, A. J., Delrez, L., Demory, B. .-O., Ehrenreich, D., Gillon, M., Jehin, E., Leconte, J., Lederer, S. M., Lewis, N., Triaud, A. H. M. J., & Van Grootel, V. (2017). Temporal Evolution of the High-energy Irradiation and Water Content of TRAPPIST-1 Exoplanets. *AJ*, *154*, Article 121, 121. https://doi.org/10.3847/1538-3881/aa859c

Brassé, C., Muñoz, O., Coll, P., & Raulin, F. (2015). Optical constants of Titan aerosols and their tholins analogs: Experimental results and modeling/observational data. *Planetary and Space Science*, *109*, 159–174. https://doi.org/10.1016/j.pss.2015.02.012

Brown, T. M. (2001). Transmission Spectra as Diagnostics of Extrasolar Giant Planet Atmospheres. *ApJ*, *553*(2), 1006–1026. https://doi.org/10.1086/320950

Buratti, B. J., Bauer, J. M., Hicks, M. D., Hillier, J. K., Verbiscer, A., Hammel, H., Schmidt, B., Cobb, B., Herbert, B., Garsky, M., Ward, J., & Foust, J. (2011). Photometry of Triton 1992-2004: Surface volatile transport and discovery of a remarkable opposition surge. *Icarus*, *212*(2), 835–846. https://doi.org/10.1016/j.icarus.2011.01.012

Cable, M. L., Hörst, S. M., Hodyss, R., Beauchamp, P., Smith, M. A., & Willis, P. (2012). Titan Tholins: Simulating Titan Organic Chemistry in the Cassini-Huygens Era. *Chemical Reviews*, *3*, Article 112, 1882–1909. https://doi.org/10.1021/cr200221x

Callahan, M. P., Smith, K. E., Cleaves, H. J., Ruzicka, J., Stern, J. C., Glavin, D. P., House, C. H., & Dworkin, J. P. (2011). Carbonaceous meteorites contain a wide range of extraterrestrial nucleobases. *Proceedings of the National Academy of Science*, *108*(34), 13995–13998. https://doi.org/10.1073/pnas.1106493108

Carrasco, N., Schmitz-Afonso, I., Bonnet, J. .-Y., Quirico, E., Thissen, R., Dutuit, O., Bagag, A., Laprévote, O., Buch, A., Giulani, A., Adand é, G., Ouni, F., Hadamcik, E., Szopa, C., & Cernogora, G. (2009). Chemical Characterization of Titan's Tholins: Solubility, Morphology and Molecular Structure Revisited. *Journal of Physical Chemistry A*, *113*, 11195–11203. https://doi.org/10.1021/jp904735q

Charbonneau, D., Brown, T. M., Noyes, R. W., & Gilliland, R. L. (2002). Detection of an Extrasolar Planet Atmosphere. *ApJ*, *568*(1), 377–384. https://doi.org/10.1086/338770

Charnay, B., Meadows, V., Misra, A., Leconte, J., & Arney, G. (2015). 3D Modeling of GJ1214b's Atmosphere: Formation of Inhomogeneous High Clouds and Observational Implications. *ApJ Letters*, *813*(1), Article L1, L1. https://doi.org/10.1088/2041-8205/813/1/L1

Cheng, A. F., Summers, M. E., Gladstone, G. R., Strobel, D. F., Young, L. A., Lavvas, P., Kammer, J. A., Lisse, C. M., Parker, A. H., Young, E. F., Stern, S. A., Weaver, H. A., Olkin, C. B., & Ennico, K. (2017). Haze in Pluto's atmosphere. *Icarus*, *290*, 112–133. https://doi.org/10.1016/j.icarus.2017.02.024

Christophe, B., Spilker, L. J., Anderson, J. D., André, N., Asmar, S. W., Aurnou, J., Banfield, D., Barucci, A., Bertolami, O., Bingham, R., Brown, P., Cecconi, B., Courty, J. .-M., Dittus, H., Fletcher, L. N., Foulon, B., Francisco, F., Gil, P. J. S., Glassmeier, K. H., ... Wolf, P. (2012). OSS (Outer Solar System): a fundamental and planetary physics mission to Neptune, Triton and the Kuiper Belt. *Experimental Astronomy*, *34*(2), 203–242. https://doi.org/10.1007/s10686-012-9309-y

Chubb, K. L., Rocchetto, M., Yurchenko, S. N., Min, M., Waldmann, I., Barstow, J. K., Mollière, P., Al-Refaie, A. F., Phillips, M. W., & Tennyson, J. (2021). The ExoMolOP database: Cross sections and k-tables for molecules of interest in high-temperature exoplanet atmospheres. *A&A*, *646*, Article A21, A21. https://doi.org/10.1051/0004-6361/202038350

Civis, S., Szabla, R., Szyja, B. M., Smykowski, D., Ivanek, O., Knizek, A., Kubelik, P., Sponer, J., Ferus, M., & Sponer, J. E. (2016). TiO_2-catalyzed synthesis of sugars from formaldehyde in extraterrestrial impacts on the early Earth. *Scientific Reports*, *6*, Article 23199, 23199. https://doi.org/10.1038/srep23199

Cleaves, I., H. James. (2008). The prebiotic geochemistry of formaldehyde. *Precambrian Research*, *164*(3-4), 111–118. https://doi.org/10.1016/j.precamres.2008.04.002

Cloutier, R., & Menou, K. (2019). Evolution of the radius valley around low mass stars from *Kepler* and *K*2. *arXiv e-prints*, Article arXiv:1912.02170, arXiv:1912.02170.

Coll, P., Bernard, J.-M., Navarro-González, R., & Raulin, F. (2003). Oxirane: An Exotic Oxygenated Organic Compound on Titan? *Astrophysical Journal*, *598*(1), 700–703. https://doi.org/10.1086/378792

Conrath, B., Flasar, F. M., Hanel, R., Kunde, V., Maguire, W., Pearl, J., Pirraglia, J., Samuelson, R., Gierasch, P., Weir, A., Bezard, B., Gautier, D., Cruikshank, D., Horn, L., Springer, R., & Shaffer, W. (1989). Infrared Observations of the Neptunian System. *Science*, *246*(4936), 1454–1459. https://doi.org/10.1126/science.246.4936.1454

Cooper, G., Kimmich, N., Belisle, W., Sarinana, J., Brabham, K., & Garrel, L. (2001). Carbonaceous meteorites as a source of sugar-related organic compounds for the early Earth. *Nature*, *414*(6866), 879–883. https://doi.org/10.1038/414879A

Cooper, G., Rios, A. C., & Nuevo, M. (2018). Monosaccharides and their derivatives in carbonaceous meteorites: A scenario for their synthesis and onset of enantiomeric excesses. *Life*, *8*(3). https://doi.org/10.3390/life8030036

Crossfield, I. J. M., & Kreidberg, L. (2017). Trends in Atmospheric Properties of Neptune-size Exoplanets. *AJ*, *154*(6), Article 261, 261. https://doi.org/10.3847/1538-3881/aa9279

Cruikshank, D. P., Materese, C. K., Pendleton, Y. J., Boston, P. J., Grundy, W. M., Schmitt, B., Lisse, C. M., Runyon, K. D., Keane, J. T., Beyer, R. A., Summers, M. E., Scipioni, F., Stern, S. A., Dalle Ore, C. M., Olkin, C. B., Young, L. A., Ennico, K., Weaver, H. A., & Bray, V. J. (2019). Prebiotic Chemistry of Pluto. *Astrobiology*, *19*(7), 831–848. https://doi.org/10.1089/ast.2018.1927

Cruikshank, D. P., Roush, T. L., Owen, T. C., Geballe, T. R., de Bergh, C., Schmitt, B., Brown, R. H., & Bartholomew, M. J. (1993). Ices on the Surface of Triton. *Science*, *261*(5122), 742–745. https://doi.org/10.1126/science.261.5122.742

Cruikshank, D. P., Schmitt, B., Roush, T. L., Owen, T. C., Quirico, E., Geballe, T. R., de Bergh, C., Bartholomew, M. J., Dalle Ore, C. M., Douté, S., & Meier, R. (2000). Water Ice on Triton. *Icarus*, *147*(1), 309–316. https://doi.org/10.1006/icar.2000.6451

Damasso, M., Bonomo, A. S., Astudillo-Defru, N., Bonfils, X., Malavolta, L., Sozzetti, A., Lopez, E., Zeng, L., Haywood, R. D., Irwin, J. M., Mortier, A., Vanderburg, A., Maldonado, J., Lanza, A. F., Affer, L., Almenara, J. .-M., Benatti, S., Biazzo, K., Bignamini, A., ... Wünsche, A. (2018). Eyes on K2-3: A system of three likely sub-Neptunes characterized with HARPS-N and HARPS. *A&A*, *615*, Article A69, A69. https://doi.org/10.1051/0004-6361/201732459

de Marcellus, P., Meinert, C., Myrgorodska, I., Nahon, L., Buhse, T., d'Hendecourt, L. L. S., & Meierhenrich, U. J. (2015). Aldehydes and sugars from evolved precometary ice analogs: Importance of ices in astrochemical and prebiotic evolution. *Proceedings of the National Academy of Science*, *112*, 965–970. https://doi.org/10.1073/pnas.1418602112

de Wit, J., Wakeford, H. R., Lewis, N. K., Delrez, L., Gillon, M., Selsis, F., Leconte, J., Demory, B.-O., Bolmont, E., Bourrier, V., Burgasser, A. J., Grimm, S., Jehin, E., Lederer, S. M., Owen, J. E., Stamenković, V., & Triaud, A. H. M. J. (2018). Atmospheric reconnaissance of the habitable-zone Earth-sized planets orbiting TRAPPIST-1. *Nature Astronomy*, *2*, 214–219. https://doi.org/10.1038/s41550-017-0374-z

Demory, B.-O., Gillon, M., de Wit, J., Madhusudhan, N., Bolmont, E., Heng, K., Kataria, T., Lewis, N., Hu, R., Krick, J., Stamenković, V., Benneke, B., Kane, S., & Queloz, D.

(2016). A map of the large day-night temperature gradient of a super-Earth exoplanet. *Nature*, *532*(7598), 207–209. https://doi.org/10.1038/nature17169

Dobson, C. M., Ellison, G. B., Tuck, A. F., & Vaida, V. (2000). Atmospheric aerosols as prebiotic chemical reactors. *Proceedings of the National Academy of Science*, *97*(22), 11864–11868. https://doi.org/10.1073/pnas.200366897

Dong, C., Jin, M., Lingam, M., Airapetian, V. S., Ma, Y., & van der Holst, B. (2018). Atmospheric escape from the TRAPPIST-1 planets and implications for habitability. *Proceedings of the National Academy of Science*, *115*, 260–265. https://doi.org/10.1073/pnas.1708010115

Dragomir, D., Benneke, B., Pearson, K. A., Crossfield, I. J. M., Eastman, J., Barman, T., & Biddle, L. I. (2015). Rayleigh Scattering in the Atmosphere of the Warm Exo-Neptune GJ 3470b. *Astrophysical Journal*, *814*, Article 102, 102. https://doi.org/10.1088/0004-637X/814/2/102

Eistrup, C., Walsh, C., & van Dishoeck, E. F. (2018). Molecular abundances and C/O ratios in chemically evolving planet-forming disk midplanes. *A&A*, *613*, Article A14, A14. https://doi.org/10.1051/0004-6361/201731302

Elkins-Tanton, L. T., & Seager, S. (2008). Ranges of Atmospheric Mass and Composition of Super-Earth Exoplanets. *ApJ*, *685*(2), 1237–1246. https://doi.org/10.1086/591433

Elliot, J. L., Hammel, H. B., Wasserman, L. H., Franz, O. G., McDonald, S. W., Person, M. J., Olkin, C. B., Dunham, E. W., Spencer, J. R., Stansberry, J. A., Buie, M. W., Pasachoff, J. M., Babcock, B. A., & McConnochie, T. H. (1998). Global warming on Triton. *Nature*, *393*(6687), 765–767. https://doi.org/10.1038/31651

Fayolle, M., Quirico, E., Schmitt, B., Jovanovic, L., Gautier, T., Carrasco, N., Grundy, W., Vuitton, V., Poch, O., Protopapa, S., Young, L., Cruikshank, D., Dalle Ore, C., Bertrand, T., & Stern, A. (2021). Testing tholins as analogues of the dark reddish material covering pluto's cthulhu region. *Icarus*, *367*, 114574. https://doi.org/https://doi.org/10.1016/j.icarus.2021.114574

Ferus, M., Pietrucci, F., Saitta, A. M., Ivanek, O., Knizek, A., Kubelik, P., Krus, M., Juha, L., Dudzak, R., Dostal, J., Pastorek, A., Petera, L., Hrncirova, J., Saeidfirozeh, H., Shestivska, V., Sponer, J., Sponer, J. E., Rimmer, P., Civis, S., & Cassone, G. (2019). Prebiotic synthesis initiated in formaldehyde by laser plasma simulating high-velocity impacts. *A&A*, *626*, Article A52, A52. https://doi.org/10.1051/0004-6361/201935435

Fletcher, L. N., Helled, R., Roussos, E., Jones, G., Charnoz, S., André, N., Andrews, D., Bannister, M., Bunce, E., Cavalié, T., Ferri, F., Fortney, J., Grassi, D., Griton, L., Hartogh, P., Hueso, R., Kaspi, Y., Lamy, L., Masters, A., ... Turrini, D. (2020). Ice Giant Systems: The scientific potential of orbital missions to Uranus and Neptune. *Planetary and Space Science*, *191*, Article 105030, 105030. https://doi.org/10.1016/j.pss.2020.105030

Fleury, B., Gudipati, M. S., Henderson, B. L., & Swain, M. (2019). Photochemistry in Hot H_2-dominated Exoplanet Atmospheres. *ApJ*, *871*(2), Article 158, 158. https://doi.org/10.3847/1538-4357/aaf79f

Forget, F., & Lebonnois, S. (2013). Global Climate Models of the Terrestrial Planets. In S. J. Mackwell, A. A. Simon-Miller, J. W. Harder, & M. A. Bullock (Eds.), *Comparative climatology of terrestrial planets* (p. 213). https://doi.org/10.2458/azu_uapress_9780816530595-ch010

Fortney, J. J., Mordasini, C., Nettelmann, N., Kempton, E. M. .-R., Greene, T. P., & Zahnle, K. (2013). A Framework for Characterizing the Atmospheres of Low-mass Low-density

Transiting Planets. *ApJ*, *775*(1), Article 80, 80. https://doi.org/10.1088/0004-637X/775/1/80

France, K., Froning, C. S., Linsky, J. L., Roberge, A., Stocke, J. T., Tian, F., Bushinsky, R., Désert, J.-M., Mauas, P., Vieytes, M., & Walkowicz, L. M. (2013). The Ultraviolet Radiation Environment around M dwarf Exoplanet Host Stars. *ApJ*, *763*, Article 149, 149. https://doi.org/10.1088/0004-637X/763/2/149

Freedman, R. S., Lustig-Yaeger, J., Fortney, J. J., Lupu, R. E., Marley, M. S., & Lodders, K. (2014). Gaseous Mean Opacities for Giant Planet and Ultracool Dwarf Atmospheres over a Range of Metallicities and Temperatures. *ApJ Supplements*, *214*, Article 25, 25. https://doi.org/10.1088/0067-0049/214/2/25

Freedman, R. S., Marley, M. S., & Lodders, K. (2008). Line and Mean Opacities for Ultracool Dwarfs and Extrasolar Planets. *ApJ Supplements*, *174*, 504–513. https://doi.org/10.1086/521793

Fressin, F., Torres, G., Charbonneau, D., Bryson, S. T., Christiansen, J., Dressing, C. D., Jenkins, J. M., Walkowicz, L. M., & Batalha, N. M. (2013). The False Positive Rate of Kepler and the Occurrence of Planets. *Astrophysical Journal*, *766*, Article 81, 81. https://doi.org/10.1088/0004-637X/766/2/81

Fulton, B. J., & Petigura, E. A. (2018). The California-Kepler Survey. VII. Precise Planet Radii Leveraging Gaia DR2 Reveal the Stellar Mass Dependence of the Planet Radius Gap. *AJ*, *156*(6), Article 264, 264. https://doi.org/10.3847/1538-3881/aae828

Fulton, B. J., Petigura, E. A., Howard, A. W., Isaacson, H., Marcy, G. W., Cargile, P. A., Hebb, L., Weiss, L. M., Johnson, J. A., Morton, T. D., Sinukoff, E., Crossfield, I. J. M., & Hirsch, L. A. (2017). The California-Kepler Survey. III. A Gap in the Radius Distribution of Small Planets. *AJ*, *154*(3), Article 109, 109. https://doi.org/10.3847/1538-3881/aa80eb

Furukawa, Y., Chikaraishi, Y., Ohkouchi, N., Ogawa, N. O., Glavin, D. P., Dworkin, J. P., Abe, C., & Nakamura, T. (2019). Extraterrestrial ribose and other sugars in primitive meteorites. *Proceedings of the National Academy of Sciences*. https://doi.org/10.1073/pnas.1907169116

Gao, P., & Benneke, B. (2018). Microphysics of KCl and ZnS Clouds on GJ 1214 b. *ApJ*, *863*(2), Article 165, 165. https://doi.org/10.3847/1538-4357/aad461

Gao, P., Fan, S., Wong, M. L., Liang, M. C., Shia, R.-L., Kammer, J. A., Yung, Y. L., Summers, M. E., Gladstone, G. R., Young, L. A., Olkin, C. B., Ennico, K., Weaver, H. A., Stern, S. A., & New Horizons Science Team. (2017a). Constraints on the microphysics of Pluto's photochemical haze from New Horizons observations. *Icarus*, *287*, 116–123. https://doi.org/10.1016/j.icarus.2016.09.030

Gao, P., Marley, M. S., Zahnle, K., Robinson, T. D., & Lewis, N. K. (2017b). Sulfur Hazes in Giant Exoplanet Atmospheres: Impacts on Reflected Light Spectra. *AJ*, *153*(3), Article 139, 139. https://doi.org/10.3847/1538-3881/aa5fab

Gao, P., Thorngren, D. P., Lee, E. K. H., Fortney, J. J., Morley, C. V., Wakeford, H. R., Powell, D. K., Stevenson, K. B., & Zhang, X. (2020). Aerosol composition of hot giant exoplanets dominated by silicates and hydrocarbon hazes. *Nature Astronomy*, *4*, 951–956. https://doi.org/10.1038/s41550-020-1114-3

Gao, P., Wakeford, H. R., Moran, S. E., & Parmentier, V. (2021). Aerosols in Exoplanet Atmospheres. *Journal of Geophysical Research (Planets)*, *126*(4), Article e06655, e06655. https://doi.org/10.1029/2020JE006655

Gautier, T., Carrasco, N., Schmitz-Afonso, I., Touboul, D., Szopa, C., Buch, A., & Pernot, P. (2014). Nitrogen incorporation in Titan's tholins inferred by high resolution orbitrap mass spectrometry and gas chromatography-mass spectrometry. *Earth and Planetary Science Letters*, *404*, 33–42. https://doi.org/10.1016/j.epsl.2014.07.011

Gautier, T., Schmitz-Afonso, I., Touboul, D., Szopa, C., Buch, A., & Carrasco, N. (2016). Development of HPLC-Orbitrap method for identification of N-bearing molecules in complex organic material relevant to planetary environments. *Icarus*, *275*, 259–266. https://doi.org/10.1016/j.icarus.2016.03.007

Gautier, T., Sebree, J. A., Li, X., Pinnick, V. T., Grubisic, A., Loeffler, M. J., Getty, S. A., Trainer, M. G., & Brinckerhoff, W. B. (2017). Influence of trace aromatics on the chemical growth mechanisms of Titan aerosol analogues. *Planetary and Space Science*, *140*, 27–34. https://doi.org/10.1016/j.pss.2017.03.012

Gavilan, L., Broch, L., Carrasco, N., Fleury, B., & Vettier, L. (2017). Organic Aerosols in the Presence of CO_2 in the Early Earth and Exoplanets: UV-Vis Refractive Indices of Oxidized Tholins. *ApJ Letters*, *848*(1), Article L5, L5. https://doi.org/10.3847/2041-8213/aa8cc4

Gavilan, L., Carrasco, N., Vrønning Hoffmann, S., Jones, N. C., & Mason, N. J. (2018). Organic Aerosols in Anoxic and Oxic Atmospheres of Earth-like Exoplanets: VUV-MIR Spectroscopy of CHON Tholins. *ApJ*, *861*, Article 110, 110. https://doi.org/10.3847/1538-4357/aac8df

Gillon, M., Triaud, A. H. M. J., Demory, B. O., Jehin, E., Agol, E., Deck, K. M., Lederer, S. M., de Wit, J., Burdanov, A., Ingalls, J. G., Bolmont, E., Leconte, J., Raymond, S. N., Selsis, F., Turbet, M., Barkaoui, K., Burgasser, A., Burleigh, M. R., Carey, S. J., ... Queloz, D. (2017). Seven temperate terrestrial planets around the nearby ultracool dwarf star TRAPPIST-1. *Nature*, *542*, 456–460. https://doi.org/10.1038/nature21360

Gladstone, G. R., Stern, S. A., Ennico, K., Olkin, C. B., Weaver, H. A., Young, L. A., Summers, M. E., Strobel, D. F., Hinson, D. P., Kammer, J. A., Parker, A. H., Steffl, A. J., Linscott, I. R., Parker, J. W., Cheng, A. F., Slater, D. C., Versteeg, M. H., Greathouse, T. K., Retherford, K. D., ... Zirnstein, E. (2016). The atmosphere of Pluto as observed by New Horizons. *Science*, *351*(6279), Article aad8866, aad8866. https://doi.org/10.1126/science.aad8866

Gordon, I. E., Rothman, L. S., Hill, C., Kochanov, R. V., Tan, Y., Bernath, P. F., Birk, M., Boudon, V., Campargue, A., Chance, K. V., Drouin, B. J., Flaud, J. .-M., Gamache, R. R., Hodges, J. T., Jacquemart, D., Perevalov, V. I., Perrin, A., Shine, K. P., Smith, M. .-A. H., ... Zak, E. J. (2017). The HITRAN2016 molecular spectroscopic database. *Journal of Molecular Spectroscopy*, *203*, 3–69. https://doi.org/10.1016/j.jqsrt.2017.06.038

Gordon, S., & McBride, B. (1996). Computer Program for Calculation of Complex Chemical Equilibrium Compositions and Applications. *NASA Reference Publication*, *1311*.

Goyal, J. M., Mayne, N., Sing, D. K., Drummond, B., Tremblin, P., Amundsen, D. S., Evans, T., Carter, A. L., Spake, J., Baraffe, I., Nikolov, N., Manners, J., Chabrier, G., & Hebrard, E. (2018). A library of ATMO forward model transmission spectra for hot Jupiter exoplanets. *MNRAS*, *474*(4), 5158–5185. https://doi.org/10.1093/mnras/stx3015

Grimm, S. L., Demory, B.-O., Gillon, M., Dorn, C., Agol, E., Burdanov, A., Delrez, L., Sestovic, M., Triaud, A. H. M. J., Turbet, M., Bolmont, É., Caldas, A., Wit, J. d., Jehin, E., Leconte, J., Raymond, S. N., Grootel, V. V., Burgasser, A. J., Carey,

S., ... Queloz, D. (2018). The nature of the TRAPPIST-1 exoplanets. *A&A*, *613*, Article A68, A68. https://doi.org/10.1051/0004-6361/201732233

Gronoff, G., Lilensten, J., & Modolo, R. (2009). Ionization processes in the atmosphere of Titan. II. Electron precipitation along magnetic field lines. *Astronomy and Astrophysics*, *506*(2), 965–970. https://doi.org/10.1051/0004-6361/200912125

Gronoff, G., Mertens, C., Lilensten, J., Desorgher, L., Flückiger, E., & Velinov, P. (2011). Ionization processes in the atmosphere of Titan. III. Ionization by high-Z nuclei cosmic rays. *Astronomy and Astrophysics*, *529*, Article A143, A143. https://doi.org/10.1051/0004-6361/201015675

Grundy, W. M., Bertrand, T., Binzel, R. P., Buie, M. W., Buratti, B. J., Cheng, A. F., Cook, J. C., Cruikshank, D. P., Devins, S. L., Dalle Ore, C. M., Earle, A. M., Ennico, K., Forget, F., Gao, P., Gladstone, G. R., Howett, C. J. A., Jennings, D. E., Kammer, J. A., Lauer, T. R., ... Zhang, X. (2018). Pluto's haze as a surface material. *Icarus*, *314*, 232–245. https://doi.org/10.1016/j.icarus.2018.05.019

Grundy, W. M., Buie, M. W., & Spencer, J. R. (2002). Spectroscopy of Pluto and Triton at 3-4 Microns: Possible Evidence for Wide Distribution of Nonvolatile Solids. *AJ*, *124*(4), 2273–2278. https://doi.org/10.1086/342933

Grundy, W. M., Young, L. A., Stansberry, J. A., Buie, M. W., Olkin, C. B., & Young, E. F. (2010). Near-infrared spectral monitoring of Triton with IRTF/SpeX II: Spatial distribution and evolution of ices. *Icarus*, *205*(2), 594–604. https://doi.org/10.1016/j.icarus.2009.08.005

Guillot, T. (2010). On the radiative equilibrium of irradiated planetary atmospheres. *A&A*, *520*, Article A27, A27. https://doi.org/10.1051/0004-6361/200913396

Gupta, A., & Schlichting, H. E. (2019). Sculpting the valley in the radius distribution of small exoplanets as a by-product of planet formation: the core-powered mass-loss mechanism. *MNRAS*, *487*(1), 24–33. https://doi.org/10.1093/mnras/stz1230

Hammond, N. P., Parmenteir, E. M., & Barr, A. C. (2018). Compaction and Melt Transport in Ammonia-Rich Ice Shells: Implications for the Evolution of Triton. *Journal of Geophysical Research (Planets)*, *123*(12), 3105–3118. https://doi.org/10.1029/2018JE005781

Hansen, C. J., McEwen, A. S., Ingersoll, A. P., & Terrile, R. J. (1990). Surface and Airborne Evidence for Plumes and Winds on Triton. *Science*, *250*(4979), 421–424. https://doi.org/10.1126/science.250.4979.421

Hansen, C. J., & Paige, D. A. (1992). A thermal model for the seasonal nitrogen cycle on Triton. *Icarus*, *99*(2), 273–288. https://doi.org/10.1016/0019-1035(92)90146-X

Hardegree-Ullman, K. K., Zink, J. K., Christiansen, J. L., Dressing, C. D., Ciardi, D. R., & Schlieder, J. E. (2020). Scaling K2. I. Revised Parameters for 222,088 K2 Stars and a K2 Planet Radius Valley at 1.9 $R_{\oplus}$. *arXiv e-prints*, Article arXiv:2001.11511, arXiv:2001.11511.

Harman, C. E., Kasting, J. F., & Wolf, E. T. (2013). Atmospheric Production of Glycolaldehyde Under Hazy Prebiotic Conditions. *Origins of Life and Evolution of the Biosphere*, *43*(2), 77–98. https://doi.org/10.1007/s11084-013-9332-7

Hartle, R. E., Sittler, E. C., Neubauer, F. M., Johnson, R. E., Smith, H. T., Crary, F., McComas, D. J., Young, D. T., Coates, A. J., Simpson, D., Bolton, S., Reisenfeld, D., Szego, K., Berthelier, J. J., Rymer, A., Vilppola, J., Steinberg, J. T., & Andre, N. (2006). Initial interpretation of Titan plasma interaction as observed by the Cassini

plasma spectrometer: Comparisons with Voyager 1. *Planetary and Space Science*, *54*(12), 1211–1224. https://doi.org/10.1016/j.pss.2006.05.029

Hartwick, V. L., Toon, O. B., & Heavens, N. G. (2019). High-altitude water ice cloud formation on Mars controlled by interplanetary dust particles. *Nature Geoscience*, *12*(7), 516–521. https://doi.org/10.1038/s41561-019-0379-6

Hasenkopf, C. A., Beaver, M. R., Trainer, M. G., Langley Dewitt, H., Freedman, M. A., Toon, O. B., McKay, C. P., & Tolbert, M. A. (2010). Optical properties of Titan and early Earth haze laboratory analogs in the mid-visible. *Icarus*, *207*(2), 903–913. https://doi.org/10.1016/j.icarus.2009.12.015

He, C., Hörst, S. M., Lewis, N. K., Moses, J. I., Kempton, E. M. .-R., Marley, M. S., Morley, C. V., Valenti, J. A., & Vuitton, V. (2019). Gas Phase Chemistry of Cool Exoplanet Atmospheres: Insight from Laboratory Simulations. *ACS Earth Space Chem*, *3*, 39–50. https://doi.org/10.1021/acsearthspacechem.8b00133

He, C., Hörst, S. M., Lewis, N. K., Yu, X., Moses, J. I., Kempton, E. M. .-R., Marley, M. S., McGuiggan, P., Morley, C. V., Valenti, J. A., & Vuitton, V. (2018a). Photochemical Haze Formation in the Atmospheres of Super-Earths and Mini-Neptunes. *AJ*, *156*, Article 38, 38. https://doi.org/10.3847/1538-3881/aac883

He, C., Hörst, S. M., Lewis, N. K., Yu, X., Moses, J. I., Kempton, E. M. .-R., McGuiggan, P., Morley, C. V., Valenti, J. A., & Vuitton, V. (2018b). Laboratory Simulations of Haze Formation in the Atmospheres of Super-Earths and Mini-Neptunes: Particle Color and Size Distribution. *ApJ*, *856*, Article L3, L3. https://doi.org/10.3847/2041-8213/aab42b

He, C., Hörst, S. M., Lewis, N. K., Yu, X., Moses, J. I., McGuiggan, P., Marley, M. S., Kempton, E. M. .-R., Moran, S. E., Morley, C. V., & Vuitton, V. (2020a). Sulfur-driven haze formation in warm CO_2-rich exoplanet atmospheres. *Nature Astronomy*, *4*, 986–993. https://doi.org/10.1038/s41550-020-1072-9

He, C., Hörst, S. M., Lewis, N. K., Yu, X., Moses, J. I., McGuiggan, P., Marley, M. S., Kempton, E. M. .-R., Morley, C. V., Valenti, J. A., & Vuitton, V. (2020b). Haze Formation in Warm H_2-rich Exoplanet Atmospheres. *The Planetary Science Journal*, *1*(2), Article 51, 51. https://doi.org/10.3847/PSJ/abb1a4

He, C., Hörst, S. M., Radke, M. J., & Yant, M. (2021). Optical Constants of Titan Haze Analogue from 0.4 to 3.5 μm: Determined Using Vacuum Spectroscopy. *Astrophysical Journal Letters*, *submitted*.

He, C., Hörst, S. M., Riemer, S., Sebree, J. A., Pauley, N., & Vuitton, V. (2017). Carbon Monoxide Affecting Planetary Atmospheric Chemistry. *ApJ*, *841*, Article L31, L31. https://doi.org/10.3847/2041-8213/aa74cc

He, C., & Smith, M. A. (2014). Solubility and Stability Investigation of Titan Aerosol Analogues: New Insight from NMR Analysis. *Icarus*, *232*, Article 54, 54–59. https://doi.org/10.1016/j.icarus.2014.01.007

Helling, C. (2019). Exoplanet Clouds. *Annual Review of Earth and Planetary Sciences*, *47*, 583–606. https://doi.org/10.1146/annurev-earth-053018-060401

Herbert, F., & Sandel, B. R. (1991). CH_4 and haze in Triton's lower atmosphere. *Journal of Geophysical Research*, *96*, 19241–19252. https://doi.org/10.1029/91JA01821

Hillier, J., Helfenstein, P., Verbiscer, A., & Veverka, J. (1991). Voyager photometry of Triton: Haze and surface photometric properties. *Journal of Geophysical Research*, *96*, 19203–19209. https://doi.org/10.1029/91JA01736

Hillier, J. H., Buratti, B. J., Hofgartner, J. D., Hicks, M. D., Devins, S., & Kivrak, L. (2021). Characteristics of Pluto's Haze and Surface from an Analytic Radiative Transfer Model. *The Planetary Science Journal*, *2*(1), Article 11, 11. https://doi.org/10.3847/PSJ/abbdaf

Hodyss, R., Howard, H. R., Johnson, P. V., Goguen, J. D., & Kanik, I. (2011). Formation of radical species in photolyzed CH $_4$:N $_2$ ices. *Icarus*, *214*(2), 748–753. https://doi.org/10.1016/j.icarus.2011.05.023

Hofstadter, M., Simon, A., Atreya, S., Banfield, D., Fortney, J. J., Hayes, A., Hedman, M., Hospodarsky, G., Mandt, K., Masters, A., Showalter, M., Soderlund, K. M., Turrini, D., Turtle, E., Reh, K., Elliott, J., Arora, N., Petropoulos, A., & Ice Giant Mission Study Team. (2019). Uranus and Neptune missions: A study in advance of the next Planetary Science Decadal Survey. *Planetary and Space Science*, *177*, Article 104680, 104680. https://doi.org/10.1016/j.pss.2019.06.004

Holler, B. J., Young, L. A., Grundy, W. M., & Olkin, C. B. (2016). On the surface composition of Triton's southern latitudes. *Icarus*, *267*, 255–266. https://doi.org/10.1016/j.icarus.2015.12.027

Hollis, J. M., Lovas, F. J., & Jewell, P. R. (2000). Interstellar Glycolaldehyde: The First Sugar. *ApJ Letters*, *540*(2), L107–L110. https://doi.org/10.1086/312881

Hörst, S. M. (2011). *Post-Cassini Investigations of Titan Atmospheric Chemistry* (Doctoral dissertation). PhD Thesis, University of Arizona. 2011. Advisor: Yelle, Roger V.

Hörst, S. M. (2017). Titan's atmosphere and climate. *Journal of Geophysical Research (Planets)*, *122*(3), 432–482. https://doi.org/10.1002/2016JE005240

Hörst, S. M., & Tolbert, M. A. (2013). In Situ Measurements of the Size and Density of Titan Aerosol Analogs. *ApJ Letters*, *770*(1), Article L10, L10. https://doi.org/10.1088/2041-8205/770/1/L10

Hörst, S. M., & Tolbert, M. A. (2014). The Effect of Carbon Monoxide on Planetary Haze Formation. *Astrophysical Journal*, *781*(1), Article 53, 53. https://doi.org/10.1088/0004-637X/781/1/53

Hörst, S. (2016). Clouds and haze and dust, oh my!

Hörst, S. M., He, C., Lewis, N. K., Kempton, E. M. .-R., Marley, M. S., Morley, C. V., Moses, J. I., Valenti, J. A., & Vuitton, V. (2018a). Haze production rates in super-Earth and mini-Neptune atmosphere experiments. *Nature Astronomy*, 2. https://doi.org/10.1038/s41550-018-0397-0

Hörst, S. M., He, C., Ugelow, M. S., Jellinek, A. M., Pierrehumbert, R. T., & Tolbert, M. A. (2018b). Exploring the Atmosphere of Neoproterozoic Earth: The Effect of O_2 on Haze Formation and Composition. *ApJ*, *858*, Article 119, 119. https://doi.org/10.3847/1538-4357/aabd7d

Hörst, S. M., Yelle, R. V., Buch, A., Carrasco, N., Cernogora, G., Dutuit, O., Quirico, E., Sciamma-O'Brien, E., Smith, M. A., Somogyi, A., & Szopa, C. (2012). Formation of amino acids and nucleotide bases in a Titan atmosphere simulation experiment. *Astrobiology*, *12*(9), 809. https://doi.org/10.1089/ast.2011.0623

Hörst, S. M., Yoon, Y. H., Ugelow, M. S., Parker, A. H., Li, R., de Gouw, J. A., & Tolbert, M. A. (2018c). Laboratory investigations of Titan haze formation: In situ measurement of gas and particle composition. *Icarus*, *301*, 136–151. https://doi.org/10.1016/j.icarus.2017.09.039

Howe, A. R., & Burrows, A. S. (2012). Theoretical Transit Spectra for GJ 1214b and Other "Super-Earths". *ApJ*, *756*, Article 176, 176. https://doi.org/10.1088/0004-637X/756/2/176

Hu, Q., Noll, R. J., Li, H., Makarov, A., Hardman, M., & Graham Cooks, R. (2005). The orbitrap: A new mass spectrometer. *Journal of Mass Spectrometry*, *40*(4), 430–443. https://doi.org/10.1002/jms.856

Hu, R., & Seager, S. (2014). Photochemistry in Terrestrial Exoplanet Atmospheres. III. Photochemistry and Thermochemistry in Thick Atmospheres on Super Earths and Mini Neptunes. *ApJ*, *784*(1), Article 63, 63. https://doi.org/10.1088/0004-637X/784/1/63

Hubbard, W. B., Fortney, J. J., Lunine, J. I., Burrows, A., Sudarsky, D., & Pinto, P. (2001). Theory of Extrasolar Giant Planet Transits. *ApJ*, *560*(1), 413–419. https://doi.org/10.1086/322490

Imanaka, H., & Smith, M. A. (2010). Abiological Nitrogen: Formation of Nitrogenated Organic Aerosols in the Titan Upper Atmosphere. *Astrobiology Science Conference 2010: Evolution and Life: Surviving Catastrophes and Extremes on Earth and Beyond*, *1538*, 5186.

Imanaka, H., Khare, B. N., Elsila, J. E., Bakes, E. L. O., McKay, C. P., Cruikshank, D. P., Sugita, S., Matsui, T., & Zare, R. N. (2004). Laboratory experiments of Titan tholin formed in cold plasma at various pressures: implications for nitrogen-containing polycyclic aromatic compounds in Titan haze. *Icarus*, *168*(2), 344–366. https://doi.org/10.1016/j.icarus.2003.12.014

Imanaka, H., & Smith, M. A. (2007). Role of photoionization in the formation of complex organic molecules in Titan's upper atmosphere. *Geophysical Research Letters*, *34*(2), Article L02204, L02204. https://doi.org/10.1029/2006GL028317

Jalbout, A. F., Abrell, L., Adamowicz, L., Polt, R., Apponi, A. J., & Ziurys, L. M. (2007). Sugar Synthesis from a Gas-Phase Formose Reaction. *Astrobiology*, *7*(3), 433–442. https://doi.org/10.1089/ast.2006.0083

Johnson, P. V., Hodyss, R., Chernow, V. F., Lipscomb, D. M., & Goguen, J. D. (2012). Ultraviolet photolysis of amino acids on the surface of icy Solar System bodies. *Icarus*, *221*(2), 800–805. https://doi.org/10.1016/j.icarus.2012.09.005

Jovanović, L., Gautier, T., Broch, L., Protopapa, S., Bertrand, T., Rannou, P., Fayolle, M., Quirico, E., Johann, L., En Naciri, A., & Carrasco, N. (2021). Optical constants of Pluto aerosol analogues from UV to near-IR. *Icarus*, *362*, Article 114398, 114398. https://doi.org/10.1016/j.icarus.2021.114398

Jovanović, L., Gautier, T., Vuitton, V., Wolters, C., Bourgalais, J., Buch, A., Orthous-Daunay, F.-R., Vettier, L., Flandinet, L., & Carrasco, N. (2020). Chemical composition of Pluto aerosol analogues. *Icarus*, *346*, Article 113774, 113774. https://doi.org/10.1016/j.icarus.2020.113774

Kasting, J. F., Whitmire, D. P., & Reynolds, R. T. (1993). Habitable Zones around Main Sequence Stars. *Icarus*, *101*, 108–128. https://doi.org/10.1006/icar.1993.1010

Kawashima, Y., & Ikoma, M. (2019). Theoretical Transmission Spectra of Exoplanet Atmospheres with Hydrocarbon Haze: Effect of Creation, Growth, and Settling of Haze Particles. II. Dependence on UV Irradiation Intensity, Metallicity, C/O Ratio, Eddy Diffusion Coefficient, and Temperature. *Astrophysical Journal*, *877*(2), Article 109, 109. https://doi.org/10.3847/1538-4357/ab1b1d

Kempton, E. M.-R., Lupu, R., Owusu-Asare, A., Slough, P., & Cale, B. (2017). Exo-Transmit: An Open-Source Code for Calculating Transmission Spectra for Exoplanet Atmospheres of Varied Composition. *Publications of the Astronomical Society of the Pacific*, *129*(4), 044402. https://doi.org/10.1088/1538-3873/aa61ef

Khare, B. N., Sagan, C., Arakawa, E. T., Suits, F., Callcott, T. A., & Williams, M. W. (1984). Optical constants of organic tholins produced in a simulated Titanian atmosphere: From soft x-ray to microwave frequencies. *Icarus*, *60*(1), 127–137. https://doi.org/10.1016/0019-1035(84)90142-8

Khare, B. N., Sagan, C., Heinrich, M., Thompson, W. R., Arakawa, E. T., Tuminello, P. S., & Clark, M. (1994). Optical Constants of Triton Tholin: Preliminary Results. *AAS/Division for Planetary Sciences Meeting Abstracts #26*, *26*, Article 30.03, 30.03.

Kim, S., Kramer, R. W., & Hatcher, P. G. (2003). Graphical method for analysis of ultrahigh-resolution broadband mass spectra of natural organic matter, the van krevelen diagram [PMID: 14710810]. *Analytical Chemistry*, *75*(20), 5336–5344. https://doi.org/10.1021/ac034415p

Kirillov, A. S. (2020). Study of the Kinetics of Metastable Molecular Nitrogen in the Atmospheres of the Earth, Triton, Titan, and Pluto. *Solar System Research*, *54*(1), 28–33. https://doi.org/10.1134/S0038094620010062

Kislyakova, K. G., Noack, L., Johnstone, C. P., Zaitsev, V. V., Fossati, L., Lammer, H., Khodachenko, M. L., Odert, P., & Guedel, M. (2017). Magma oceans and enhanced volcanism on TRAPPIST-1 planets due to induction heating. *Nature Astronomy*, *1*, 878–885. https://doi.org/10.1038/s41550-017-0284-0

Kite, E. S., & Barnett, M. N. (2020). Exoplanet secondary atmosphere loss and revival. *Proceedings of the National Academy of Science*, *117*, 18264–18271.

Kitzmann, D., & Heng, K. (2018). Optical properties of potential condensates in exoplanetary atmospheres. *MNRAS*, *475*, 94–107. https://doi.org/10.1093/mnras/stx3141

Knutson, H. A., Dragomir, D., Kreidberg, L., Kempton, E. M.-R., McCullough, P. R., Fortney, J. J., Bean, J. L., Gillon, M., Homeier, D., & Howard, A. W. (2014a). Hubble Space Telescope Near-IR Transmission Spectroscopy of the Super-Earth HD 97658b. *ApJ*, *794*, Article 155, 155. https://doi.org/10.1088/0004-637X/794/2/155

Knutson, H. A., Benneke, B., Deming, D., & Homeier, D. (2014b). A featureless transmission spectrum for the Neptune-mass exoplanet GJ436b. *Nature*, *505*, 66–68. https://doi.org/10.1038/nature12887

Koll, D. D. B., & Abbot, D. S. (2016). Temperature Structure and Atmospheric Circulation of Dry Tidally Locked Rocky Exoplanets. *ApJ*, *825*(2), Article 99, 99. https://doi.org/10.3847/0004-637X/825/2/99

Kopetzki, D., & Antonietti, M. (2011). Hydrothermal formose reaction. *New Journal of Chemistry*, *35*, 1787–1794. https://doi.org/10.1039/C1NJ20191C

Kopparapu, R. k., Wolf, E. T., Arney, G., Batalha, N. E., Haqq-Misra, J., Grimm, S. L., & Heng, K. (2017). Habitable Moist Atmospheres on Terrestrial Planets near the Inner Edge of the Habitable Zone around M Dwarfs. *ApJ*, *845*, Article 5, 5. https://doi.org/10.3847/1538-4357/aa7cf9

Krasnopolsky, V. A., Sandel, B. R., & Herbert, F. (1992). Properties of haze in the atmosphere of Triton. *Journal of Geophysical Research*, *97*(E7), 11695–11700. https://doi.org/10.1029/92JE00945

Krasnopolsky, V. A., Sandel, B. R., Herbert, F., & Vervack, R. J. (1993). Temperature, N_2, and N density profiles of Triton's atmosphere: Observations and model. *Journal of Geophysical Research*, *98*(E2), 3065–3078. https://doi.org/10.1029/92JE02680

Krasnopolsky, V. A. (2012). Titan's photochemical model: Further update, oxygen species, and comparison with Triton and Pluto. *Planetary and Space Science*, *73*(1), 318–326. https://doi.org/10.1016/j.pss.2012.08.013

Krasnopolsky, V. A. (2020). A photochemical model of Pluto's atmosphere and ionosphere. *Icarus*, *335*, Article 113374, 113374. https://doi.org/10.1016/j.icarus.2019.07.008

Krasnopolsky, V. A., & Cruikshank, D. P. (1995). Photochemistry of Triton's atmosphere and ionosphere. *Journal of Geophysical Research*, *100*, 21, 271, 286.

Kreidberg, L., Bean, J. L., Désert, J.-M., Benneke, B., Deming, D., Stevenson, K. B., Seager, S., Berta-Thompson, Z., Seifahrt, A., & Homeier, D. (2014a). Clouds in the atmosphere of the super-Earth exoplanet GJ1214b. *Nature*, *505*, 69–72. https://doi.org/10.1038/nature12888

Kreidberg, L., Bean, J. L., Désert, J.-M., Line, M. R., Fortney, J. J., Madhusudhan, N., Stevenson, K. B., Showman, A. P., Charbonneau, D., McCullough, P. R., Seager, S., Burrows, A., Henry, G. W., Williamson, M., Kataria, T., & Homeier, D. (2014b). A Precise Water Abundance Measurement for the Hot Jupiter WASP-43b. *ApJ*, *793*, Article L27, L27. https://doi.org/10.1088/2041-8205/793/2/L27

Kreidberg, L., Koll, D. D. B., Morley, C., Hu, R., Schaefer, L., Deming, D., Stevenson, K. B., Dittmann, J., Vanderburg, A., Berardo, D., Guo, X., Stassun, K., Crossfield, I., Charbonneau, D., Latham, D. W., Loeb, A., Ricker, G., Seager, S., & Vand erspek, R. (2019). Absence of a thick atmosphere on the terrestrial exoplanet LHS 3844b. *Nature*, *573*(7772), 87–90. https://doi.org/10.1038/s41586-019-1497-4

Krimigis, S. M., Armstrong, T. P., Axford, W. I., Bostrom, C. O., Cheng, A. F., Gloeckler, G., Hamilton, D. C., Keath, E. P., Lanzerotti, L. J., Mauk, B. H., & van Allen, J. A. (1989). Hot Plasma and Energetic Particles in Neptune's Magnetosphere. *Science*, *246*(4936), 1483–1489. https://doi.org/10.1126/science.246.4936.1483

Kutsop, N. W., Hayes, A. G., Buratti, B. J., Corlies, P. M., Ennico, K., Fan, S., Gladstone, R., Helfenstein, P., Hofgartner, J. D., Hicks, M., Lemmon, M., Lunine, J. I., Moore, J., Olkin, C. B., Parker, A. H., Stern, S. A., Weaver, H. A., & Young, L. A. (2021). Pluto's haze abundance and size distribution from limb scatter observations by MVIC. *The Planetary Science Journal*, *2*(3), 91. https://doi.org/10.3847/psj/abdcaf

Kwok, S. (2016). Complex organics in space from Solar System to distant galaxies. *The Astronomy and Astrophysics Review*, *24*, Article 8, 8. https://doi.org/10.1007/s00159-016-0093-y

Lacis, A. A., & Oinas, V. (1991). A description of the correlated-k distribution method for modelling nongray gaseous absorption, thermal emission, and multiple scattering in vertically inhomogeneous atmospheres. *Journal of Geophysical Research*, *96*, 9027–9064. https://doi.org/10.1029/90JD01945

Landis, G., Oleson, S., Abel, P., Bur, M. J. C., Colozza, A. J., Faller, B., James, Fittje, Gyekenyesi, J., Hartwig, J., Jones, R., Lantz, N. J., McCarty, S. L., Thomas, Packard, Schmitz, P., Smith, D., Turnbull, E., Izenberg, N., ... O'brien. (2019). Missions to triton and pluto using a hopper vehicle with in-situ refueling. *70th International Astronautical Congress*.

Lavvas, P., & Koskinen, T. (2017). Aerosol Properties of the Atmospheres of Extrasolar Giant Planets. *The Astrophysical Journal*, *847*, Article 32, 32. https://doi.org/10.3847/1538-4357/aa88ce

Lavvas, P., Lellouch, E., Strobel, D. F., Gurwell, M. A., Cheng, A. F., Young, L. A., & Gladstone, G. R. (2020). A major ice component in Pluto's haze. *Nature Astronomy*. https://doi.org/10.1038/s41550-020-01270-3

Lavvas, P. P., Coustenis, A., & Vardavas, I. M. (2008). Coupling photochemistry with haze formation in Titan's atmosphere, Part II: Results and validation with Cassini/Huygens data. *Planetary and Space Science*, *56*(1), 67–99. https://doi.org/10.1016/j.pss.2007.05.027

Lecavelier Des Etangs, A., Pont, F., Vidal-Madjar, A., & Sing, D. (2008). Rayleigh scattering in the transit spectrum of HD 189733b. *A&A*, *481*, L83–L86. https://doi.org/10.1051/0004-6361:200809388

Leconte, J. (2021). Spectral binning of precomputed correlated-k coefficients. *A&A*, *645*, Article A20, A20. https://doi.org/10.1051/0004-6361/202039040

Leconte, J., Forget, F., & Lammer, H. (2015). On the (anticipated) diversity of terrestrial planet atmospheres. *Experimental Astronomy*, *40*(2-3), 449–467. https://doi.org/10.1007/s10686-014-9403-4

Lee, G., Helling, C., Dobbs-Dixon, I., & Juncher, D. (2015). Modelling the local and global cloud formation on HD 189733b. *A&A*, *580*, Article A12, A12. https://doi.org/10.1051/0004-6361/201525982

Lehmer, O. R., & Catling, D. C. (2017). Rocky Worlds Limited to ∼1.8 Earth Radii by Atmospheric Escape during a Star's Extreme UV Saturation. *ApJ*, *845*(2), Article 130, 130. https://doi.org/10.3847/1538-4357/aa8137

Lellouch, E., de Bergh, C., Sicardy, B., Ferron, S., & Käufl, H. .-U. (2010). Detection of CO in Triton's atmosphere and the nature of surface-atmosphere interactions. *Astronomy and Astrophysics*, *512*, Article L8, L8. https://doi.org/10.1051/0004-6361/201014339

Lewis, B., Stansberry, J., Holler, B., Grundy, W., Schmitt, B., Protopapa, S., Lisse, C., Stern, S. A., Young, L., Weaver, H., Olkin, C., Ennico, K., & the New Horizons Science Team. (2020). Distribution and Energy Balance of Pluto's Nitrogen Ice, as seen by New Horizons in 2015. *Icarus*, *in press*. https://doi.org/10.1016/j.icarus.2020.113633

Lincowski, A. P., Meadows, V. S., Crisp, D., Robinson, T. D., Luger, R., Lustig-Yaeger, J., & Arney, G. N. (2018). Evolved Climates and Observational Discriminants for the TRAPPIST-1 Planetary System. *ArXiv e-prints*.

Line, M. R., Knutson, H., Deming, D., Wilkins, A., & Desert, J.-M. (2013a). A Near-infrared Transmission Spectrum for the Warm Saturn HAT-P-12b. *ApJ*, *778*, Article 183, 183. https://doi.org/10.1088/0004-637X/778/2/183

Line, M. R., Knutson, H., Wolf, A. S., & Yung, Y. L. (2014). A Systematic Retrieval Analysis of Secondary Eclipse Spectra. II. A Uniform Analysis of Nine Planets and their C to O Ratios. *ApJ*, *783*, Article 70, 70. https://doi.org/10.1088/0004-637X/783/2/70

Line, M. R., Wolf, A. S., Zhang, X., Knutson, H., Kammer, J. A., Ellison, E., Deroo, P., Crisp, D., & Yung, Y. L. (2013b). A Systematic Retrieval Analysis of Secondary Eclipse Spectra. I. A Comparison of Atmospheric Retrieval Techniques. *ApJ*, *775*, Article 137, 137. https://doi.org/10.1088/0004-637X/775/2/137

Lodders, K. (2003). Solar System Abundances and Condensation Temperatures of the Elements. *ApJ*, *591*, 1220–1247. https://doi.org/10.1086/375492

Lopez, E. D., & Fortney, J. J. (2014). Understanding the Mass-Radius Relation for Sub-neptunes: Radius as a Proxy for Composition. *ApJ*, *792*, Article 1, 1. https://doi.org/10.1088/0004-637X/792/1/1

Lothringer, J. D., Benneke, B., Crossfield, I. J. M., Henry, G. W., Morley, C., Dragomir, D., Barman, T., Knutson, H., Kempton, E., Fortney, J., McCullough, P., & Howard, A. W. (2018). An HST/STIS Optical Transmission Spectrum of Warm Neptune GJ 436b. *Astronomical Journal*, *155*, Article 66, 66. https://doi.org/10.3847/1538-3881/aaa008

Loyd, R. O. P., Shkolnik, E. L., Schneider, A. C., Richey-Yowell, T., Barman, T. S., Peacock, S., & Pagano, I. (2020). Current Population Statistics Do Not Favor Photoevaporation over Core-powered Mass Loss as the Dominant Cause of the Exoplanet Radius Gap. *ApJ*, *890*(1), Article 23, 23. https://doi.org/10.3847/1538-4357/ab6605

Lu, Y., & Freeland, S. (2006). Testing the Potential for Computational Chemistry to Quantify Biophysical Properties of the Non-Proteinaceous Amino Acids. *Astrobiology*, *6*(4), 606–624. https://doi.org/10.1089/ast.2006.6.606

Luger, R., Sestovic, M., Kruse, E., Grimm, S. L., Demory, B.-O., Agol, E., Bolmont, E., Fabrycky, D., Fernandes, C. S., Van Grootel, V., Burgasser, A., Gillon, M., Ingalls, J. G., Jehin, E., Raymond, S. N., Selsis, F., Triaud, A. H. M. J., Barclay, T., Barentsen, G., ... Queloz, D. (2017). A seven-planet resonant chain in TRAPPIST-1. *Nature Astronomy*, *1*, Article 0129, 0129. https://doi.org/10.1038/s41550-017-0129

Luspay-Kuti, A., Mandt, K., Jessup, K.-L., Kammer, J., Hue, V., Hamel, M., & Filwett, R. (2017). Photochemistry on Pluto - I. Hydrocarbons and aerosols. *MNRAS*, *472*(1), 104–117. https://doi.org/10.1093/mnras/stx1362

Lyons, J. R., Yung, Y. L., & Allen, M. (1992). Solar Control of the Upper Atmosphere of Triton. *Science*, *256*(5054), 204–206. https://doi.org/10.1126/science.11540928

Madhusudhan, N. (2019). Exoplanetary Atmospheres: Key Insights, Challenges, and Prospects. *Annual Review of Astronomy and Astrophysics*, *57*, 617–663. https://doi.org/10.1146/annurev-astro-081817-051846

Maillard, J., Carrasco, N., Schmitz-Afonso, I., Gautier, T., & Afonso, C. (2018). Comparison of soluble and insoluble organic matter in analogues of Titan's aerosols. *Earth and Planetary Science Letters*, *495*, 185–191. https://doi.org/10.1016/j.epsl.2018.05.014

Marley, M. S., Ackerman, A. S., Cuzzi, J. N., & Kitzmann, D. (2013). Clouds and hazes in exoplanet atmospheres. *Comparative climatology of terrestrial planets* (pp. 367–391). University of Arizona Press. https://doi.org/10.2458/azu_uapress_9780816530595-ch15

Masters, A., Achilleos, N., Agnor, C. B., Campagnola, S., Charnoz, S., Christophe, B., Coates, A. J., Fletcher, L. N., Jones, G. H., Lamy, L., Marzari, F., Nettelmann, N., Ruiz, J., Ambrosi, R., Andre, N., Bhardwaj, A., Fortney, J. J., Hansen, C. J., Helled, R., ... Volwerk, M. (2014). Neptune and Triton: Essential pieces of the Solar System puzzle. *Planetary and Space Science*, *104*, 108–121. https://doi.org/10.1016/j.pss.2014.05.008

Materese, C. K., Cruikshank, D. P., Sandford, S. A., Imanaka, H., & Nuevo, M. (2015). Ice Chemistry on Outer Solar System Bodies: Electron Radiolysis of N2-, CH4-, and CO-Containing Ices. *ApJ*, *812*(2), Article 150, 150. https://doi.org/10.1088/0004-637X/812/2/150

Materese, C. K., Cruikshank, D. P., Sandford, S. A., Imanaka, H., Nuevo, M., & White, D. W. (2014). Ice Chemistry on Outer Solar System Bodies: Carboxylic Acids, Nitriles, and Urea Detected in Refractory Residues Produced from the UV Photolysis of

N_2:CH_4:CO-Containing Ices. *ApJ*, *788*(2), Article 111, 111. https://doi.org/10.1088/0004-637X/788/2/111

McDonald, G. D., Thompson, W. R., Heinrich, M., Khare, B. N., & Sagan, C. (1994). Chemical Investigation of Titan and Triton Tholins. *Icarus*, *108*(1), 137–145. https://doi.org/10.1006/icar.1994.1046

McKinnon, W. B. (1984). On the origin of Triton and Pluto. *Nature*, *311*(5984), 355–358. https://doi.org/10.1038/311355a0

Meinert, C., Myrgorodska, I., de Marcellus, P., Buhse, T., Nahon, L., Hoffmann, S. V., d'Hendecourt, L. L. S., & Meierhenrich, U. J. (2016). Ribose and related sugars from ultraviolet irradiation of interstellar ice analogs. *Science*, *352*(6282), 208–212. https://doi.org/10.1126/science.aad8137

Merlin, F., Lellouch, E., Quirico, E., & Schmitt, B. (2018). Triton's surface ices: Distribution, temperature and mixing state from VLT/SINFONI observations. *Icarus*, *314*, 274–293. https://doi.org/10.1016/j.icarus.2018.06.003

Miller, S. L. (1953). A Production of Amino Acids under Possible Primitive Earth Conditions. *Science*, *117*(3046), 528–529. https://doi.org/10.1126/science.117.3046.528

Miller, S. L., & Urey, H. C. (1959). Organic Compound Synthesis on the Primitive Earth. *Science*, *130*(3370), 245–251. https://doi.org/10.1126/science.130.3370.245

Miller-Ricci Kempton, E., Zahnle, K., & Fortney, J. J. (2012). The Atmospheric Chemistry of GJ 1214b: Photochemistry and Clouds. *ApJ*, *745*, Article 3, 3. https://doi.org/10.1088/0004-637X/745/1/3

Moore, M. H., & Hudson, R. L. (2003). Infrared study of ion-irradiated N $_2$-dominated ices relevant to Triton and Pluto: formation of HCN and HNC. *Icarus*, *161*(2), 486–500. https://doi.org/10.1016/S0019-1035(02)00037-4

Moran, S. E., Hörst, S. M., Batalha, N. E., Lewis, N. K., & Wakeford, H. R. (2018). Limits on Clouds and Hazes for the TRAPPIST-1 Planets. *AJ*, *156*(6), Article 252, 252. https://doi.org/10.3847/1538-3881/aae83a

Moran, S. E., Hörst, S. M., Vuitton, V., He, C., Lewis, N. K., Flandinet, L., Moses, J. I., North, N., Orthous-Daunay, F.-R., Sebree, J., Wolters, C., Kempton, E. M. .-R., Marley, M. S., Morley, C. V., & Valenti, J. A. (2020). Chemistry of Temperate Super-Earth and Mini-Neptune Atmospheric Hazes from Laboratory Experiments. *The Planetary Science Journal*, *1*(1), Article 17, 17. https://doi.org/10.3847/PSJ/ab8eae

Morley, C. V., Fortney, J. J., Kempton, E. M. .-R., Marley, M. S., Visscher, C., & Zahnle, K. (2013). Quantitatively Assessing the Role of Clouds in the Transmission Spectrum of GJ 1214b. *ApJ*, *775*, Article 33, 33. https://doi.org/10.1088/0004-637X/775/1/33

Morley, C. V., Fortney, J. J., Marley, M. S., Zahnle, K., Line, M., Kempton, E., Lewis, N., & Cahoy, K. (2015). Thermal Emission and Reflected Light Spectra of Super Earths with Flat Transmission Spectra. *ApJ*, *815*, Article 110, 110. https://doi.org/10.1088/0004-637X/815/2/110

Morley, C. V., Knutson, H., Line, M., Fortney, J. J., Thorngren, D., Marley, M. S., Teal, D., & Lupu, R. (2017a). Forward and Inverse Modeling of the Emission and Transmission Spectrum of GJ 436b: Investigating Metal Enrichment, Tidal Heating, and Clouds. *AJ*, *153*(2), Article 86, 86. https://doi.org/10.3847/1538-3881/153/2/86

Morley, C. V., Kreidberg, L., Rustamkulov, Z., Robinson, T., & Fortney, J. J. (2017b). Observing the Atmospheres of Known Temperate Earth-sized Planets with JWST. *ApJ*, *850*, Article 121, 121. https://doi.org/10.3847/1538-4357/aa927b

Moses, J. I., Line, M. R., Visscher, C., Richardson, M. R., Nettelmann, N., Fortney, J. J., Barman, T. S., Stevenson, K. B., & Madhusudhan, N. (2013). Compositional Diversity in the Atmospheres of Hot Neptunes, with Application to GJ 436b. *ApJ*, *777*(1), Article 34, 34. https://doi.org/10.1088/0004-637X/777/1/34

Neish, C. D., Somogyi, Á., & Smith, M. A. (2010). Titan's Primordial Soup: Formation of Amino Acids via Low-Temperature Hydrolysis of Tholins. *Astrobiology*, *10*(3), 337–347. https://doi.org/10.1089/ast.2009.0402

Neri, F., Saitta, G., & Chiofalo, S. (1987). A simple procedure to remove the interference fringes from optical spectra. *Journal of Physics E Scientific Instruments*, *20*(7), 894–896. https://doi.org/10.1088/0022-3735/20/7/015

Nimmo, F., & Spencer, J. R. (2015). Powering Triton's recent geological activity by obliquity tides: Implications for Pluto geology. *Icarus*, *246*, 2–10. https://doi.org/10.1016/j.icarus.2014.01.044

Nuevo, M., Cooper, G., & Sandford, S. A. (2018). Deoxyribose and deoxysugar derivatives from photoprocessed astrophysical ice analogues and comparison to meteorites. *Nature Communications*, *9*, Article 5276, 5276. https://doi.org/10.1038/s41467-018-07693-x

Ohno, K., & Kawashima, Y. (2020). Super-Rayleigh Slopes in Transmission Spectra of Exoplanets Generated by Photochemical Haze. *ApJ Letters*, *895*(2), Article L47, L47. https://doi.org/10.3847/2041-8213/ab93d7

Ohno, K., & Okuzumi, S. (2018). Microphysical Modeling of Mineral Clouds in GJ1214 b and GJ436 b: Predicting Upper Limits on the Cloud-top Height. *ApJ*, *859*(1), Article 34, 34. https://doi.org/10.3847/1538-4357/aabee3

Ohno, K., Zhang, X., Tazaki, R., & Okuzumi, S. (2021). Haze formation on triton. *The Astrophysical Journal*, *912*(1), 37. https://doi.org/10.3847/1538-4357/abee82

Oleson, S. R., & Landis, G. (2018). Triton Hopper: Exploring Neptune's Captured Kuiper Belt Object. In V. Badescu & K. Zacny (Eds.), *Outer solar system* (p. 367). https://doi.org/10.1007/978-3-319-73845-1_9

Olkin, C. B., Elliot, J. L., Hammel, H. B., Cooray, A. R., McDonald, S. W., Foust, J. A., Bosh, A. S., Buie, M. W., Millis, R. L., Wasserman, L. H., Dunham, E. W., Young, L. A., Howell, R. R., Hubbard, W. B., Hill, R., Marcialis, R. L., McDonald, J. S., Rank, D. M., Holbrook, J. C., & Reitsema, H. J. (1997). The Thermal Structure of Triton's Atmosphere: Results from the 1993 and 1995 Occultations. *Icarus*, *129*(1), 178–201. https://doi.org/10.1006/icar.1997.5757

O'Malley-James, J. T., & Kaltenegger, L. (2017). UV surface habitability of the TRAPPIST-1 system. *MNRAS*, *469*, L26–L30. https://doi.org/10.1093/mnrasl/slx047

Orthous-Daunay, F.-R., Thissen, R., & Vuitton, V. (2020). Measured mass to stoichoimetric formula through exhaustive search. In F. Salama & H. Linnartz (Eds.), *Laboratory astrophysics: From observations to interpretation* (pp. 193–199). https://doi.org/10.1017/S1743921319008032

Owen, J. E., & Wu, Y. (2016). Atmospheres of Low-mass Planets: The "Boil-off". *ApJ*, *817*(2), Article 107, 107. https://doi.org/10.3847/0004-637X/817/2/107

Peacock, S., Barman, T., Shkolnik, E. L., Hauschildt, P. H., & Baron, E. (2019). Predicting the Extreme Ultraviolet Radiation Environment of Exoplanets around Low-mass Stars: The TRAPPIST-1 System. *ApJ*, *871*(2), Article 235, 235. https://doi.org/10.3847/1538-4357/aaf891

Perry, R. H., Cooks, R. G., & Noll, R. J. (2008). Orbitrap mass spectrometry: Instrumentation, ion motion and applications. *Mass Spectrometry Reviews*, *27*(6), 661–699. https://doi.org/10.1002/mas.20186

Pestunova, O., Simonov, A., Snytnikov, V., Stoyanovsky, V., & Parmon, V. (2005). Putative mechanism of the sugar formation on prebiotic Earth initiated by UV-radiation. *Advances in Space Research*, *36*(2), 214–219. https://doi.org/10.1016/j.asr.2005.02.049

Pidhorodetska, D., Moran, S. E., Schwieterman, E. W., Barclay, T., Fauchez, T. J., Lewis, N. K., Quintana, E. V., Villanueva, G. L., Domagal-Goldman, S. D., Schlieder, J. E., Gilbert, E. A., Kane, S. R., & Kostov, V. B. (2021). L 98-59: a Benchmark System of Small Planets for Future Atmospheric Characterization. *arXiv e-prints*, Article arXiv:2106.00685, arXiv:2106.00685.

Pollack, J. B., Schwartz, J. M., & Rages, K. (1990). Scatterers in Triton's Atmosphere: Implications for the Seasonal Volatile Cycle. *Science*, *250*(4979), 440–443. https://doi.org/10.1126/science.250.4979.440

Pont, F., Knutson, H., Gilliland, R. L., Moutou, C., & Charbonneau, D. (2008). Detection of atmospheric haze on an extrasolar planet: the 0.55-1.05 μm transmission spectrum of HD 189733b with the HubbleSpaceTelescope. *MNRAS*, *385*(1), 109–118. https://doi.org/10.1111/j.1365-2966.2008.12852.x

Porco, C. C., Baker, E., Barbara, J., Beurle, K., Brahic, A., Burns, J. A., Charnoz, S., Cooper, N., Dawson, D. D., Del Genio, A. D., Denk, T., Dones, L., Dyudina, U., Evans, M. W., Fussner, S., Giese, B., Grazier, K., Helfenstein, P., Ingersoll, A. P., ... West, R. (2005). Imaging of Titan from the Cassini spacecraft. *Nature*, *434*(7030), 159–168. https://doi.org/10.1038/nature03436

Prockter, L. M., Mitchell, K. L., Howett, C. J. A., Smythe, W. D., Sutin, B. M., Bearden, D. A., & Frazier, W. E. (2019). Exploring Triton with Trident: A Discovery Class Mission. *Lunar and Planetary Science Conference*, Article 3188, 3188.

Protopapa, S., Olkin, C. B., Grundy, W. M., Li, J.-Y., Verbiscer, A., Cruikshank, D. P., Gautier, T., Quirico, E., Cook, J. C., Reuter, D., Howett, C. J. A., Stern, A., Beyer, R. A., Porter, S., Young, L. A., Weaver, H. A., Ennico, K., Dalle Ore, C. M., Scipioni, F., & Singer, K. (2020). Disk-resolved Photometric Properties of Pluto and the Coloring Materials across its Surface. *AJ*, *159*(2), Article 74, 74. https://doi.org/10.3847/1538-3881/ab5e82

Quarles, B., Quintana, E. V., Lopez, E., Schlieder, J. E., & Barclay, T. (2017). Plausible Compositions of the Seven TRAPPIST-1 Planets Using Long-term Dynamical Simulations. *ApJ*, *842*, Article L5, L5. https://doi.org/10.3847/2041-8213/aa74bf

Rackham, B., Espinoza, N., Apai, D., López-Morales, M., Jordán, A., Osip, D. J., Lewis, N. K., Rodler, F., Fraine, J. D., Morley, C. V., & Fortney, J. J. (2017). ACCESS I: An Optical Transmission Spectrum of GJ 1214b Reveals a Heterogeneous Stellar Photosphere. *ApJ*, *834*, Article 151, 151. https://doi.org/10.3847/1538-4357/aa4f6c

Rackham, B. V., Apai, D., & Giampapa, M. S. (2018). The Transit Light Source Effect: False Spectral Features and Incorrect Densities for M-dwarf Transiting Planets. *ApJ*, *853*, Article 122, 122. https://doi.org/10.3847/1538-4357/aaa08c

Rages, K., & Pollack, J. B. (1992). Voyager imaging of Triton's clouds and hazes. *Icarus*, *99*(2), 289–301. https://doi.org/10.1016/0019-1035(92)90147-Y

Ranjan, S., Wordsworth, R., & Sasselov, D. D. (2017). The Surface UV Environment on Planets Orbiting M Dwarfs: Implications for Prebiotic Chemistry and the Need for

Experimental Follow-up. *ApJ*, *843*, Article 110, 110. https://doi.org/10.3847/1538-4357/aa773e

Reed, N. W., Browne, E. C., & Tolbert, M. A. (2020). Impact of Hydrogen Sulfide on Photochemical Haze Formation in Methane/Nitrogen Atmospheres. *ACS Earth and Space Chemistry*, *4*(6), 897–904. https://doi.org/10.1021/acsearthspacechem.0c00086

Ricker, G. R., Winn, J. N., Vanderspek, R., Latham, D. W., Bakos, G. Á., Bean, J. L., Berta-Thompson, Z. K., Brown, T. M., Buchhave, L., Butler, N. R., Butler, R. P., Chaplin, W. J., Charbonneau, D., Christensen-Dalsgaard, J., Clampin, M., Deming, D., Doty, J., De Lee, N., Dressing, C., ... Villasenor, J. (2014). Transiting Exoplanet Survey Satellite (TESS). *Proceedings of the SPIE*, *9143*, Article 914320, 914320. https://doi.org/10.1117/12.2063489

Rimmer, P. B., Xu, J., Thompson, S. J., Gillen, E., Sutherland, J. D., & Queloz, D. (2018). The origin of RNA precursors on exoplanets. *Science Advances*, *4*, eaar3302. https://doi.org/10.1126/sciadv.aar3302

Robinson, T. D., & Catling, D. C. (2014). Common 0.1bar tropopause in thick atmospheres set by pressure-dependent infrared transparency. *Nature Geoscience*, *7*, 12–15. https://doi.org/10.1038/ngeo2020

Robinson, T. D., & Catling, D. C. (2012). An Analytic Radiative-Convective Model for Planetary Atmospheres. *ApJ*, *757*, Article 104, 104. https://doi.org/10.1088/0004-637X/757/1/104

Robinson, T. D., Maltagliati, L., Marley, M. S., & Fortney, J. J. (2014). Titan solar occultation observations reveal transit spectra of a hazy world. *Proceedings of the National Academy of Science*, *111*, 9042–9047. https://doi.org/10.1073/pnas.1403473111

Rogers, L. A. (2015). Most 1.6 Earth-radius Planets are Not Rocky. *ApJ*, *801*, Article 41, 41. https://doi.org/10.1088/0004-637X/801/1/41

Ruf, A., Le Sergeant d'Hendecourt, L., & Schmitt-Kopplin, P. (2018). Data-driven astrochemistry: One step further within the origin of life puzzle. *Life*, *8*, 18. https://doi.org/10.3390/life8020018

Rymer, A. M., Clyde, B., Runyon, K., & the Neptune-Odyssey team. (2020). Neptune Odyssey: Mission to the Neptune-Triton System. *LPI Contributions*, *2547*, Article 6031, 6031.

Sarker, N., Somogyi, A., Lunine, J. I., & Smith, M. A. (2003). Titan Aerosol Analogues: Analysis of the Nonvolatile Tholins. *Astrobiology*, *3*(4), 719–726. https://doi.org/10.1089/153110703322736042

Schaefer, L., Lodders, K., & Fegley, B. (2012). Vaporization of the Earth: Application to Exoplanet Atmospheres. *ApJ*, *755*(1), Article 41, 41. https://doi.org/10.1088/0004-637X/755/1/41

Schenk, P. M., & Zahnle, K. (2007). On the negligible surface age of Triton. *Icarus*, *192*(1), 135–149. https://doi.org/10.1016/j.icarus.2007.07.004

Schwartz, A. W. (2007). Intractable mixtures and the origin of life. *Chemistry & Biodiversity*, *4*(4), 656–664. https://doi.org/10.1002/cbdv.200790056

Schwartz, A. W., Voet, A. B., & van der Veen, M. (1984). Recent Progress in the Prebiotic Chemistry of HCN. *Origins of Life*, *14*(1-4), 91–98. https://doi.org/10.1007/BF00933644

Sciamma-O'Brien, E., Carrasco, N., Szopa, C., Buch, A., & Cernogora, G. (2010). Titan's atmosphere: An optimal gas mixture for aerosol production? *Icarus*, *209*(2), 704–714. https://doi.org/10.1016/j.icarus.2010.04.009

Seager, S., & Sasselov, D. D. (2000). Theoretical Transmission Spectra during Extrasolar Giant Planet Transits. *ApJ*, *537*(2), 916–921. https://doi.org/10.1086/309088

Sebree, J. A., Roach, M. C., Shipley, E. R., He, C., & Hörst, S. M. (2018). Detection of Prebiotic Molecules in Plasma and Photochemical Aerosol Analogs Using GC/MS/MS Techniques. *ApJ*, *865*(2), Article 133, 133. https://doi.org/10.3847/1538-4357/aadba1

Seinfeld, J., & Pandis, S. (1998). *Atmospheric chemistry and physics: From air pollution to climate change*. Wiley.

Sing, D. K., Fortney, J. J., Nikolov, N., Wakeford, H. R., Kataria, T., Evans, T. M., Aigrain, S., Ballester, G. E., Burrows, A. S., Deming, D., Désert, J. M., Gibson, N. P., Henry, G. W., Huitson, C. M., Knutson, H. A., Lecavelier Des Etangs, A., Pont, F., Showman, A. P., Vidal-Madjar, A., ... Wilson, P. A. (2016). A continuum from clear to cloudy hot-Jupiter exoplanets without primordial water depletion. *Nature*, *529*, 59–62. https://doi.org/10.1038/nature16068

Smith, B. A., Soderblom, L. A., Banfield, D., Barnet, C., Basilevksy, A. T., Beebe, R. F., Bollinger, K., Boyce, J. M., Brahic, A., Briggs, G. A., Brown, R. H., Chyba, C., Collins, S. A., Colvin, T., Cook, A. F., Crisp, D., Croft, S. K., Cruikshank, D., Cuzzi, J. N., ... Veverka, J. (1989). Voyager 2 at Neptune: Imaging Science Results. *Science*, *246*(4936), 1422–1449. https://doi.org/10.1126/science.246.4936.1422

Somogyi, A., Thissen, R., Orthous-Daunay, F.-R., & Vuitton, V. (2016). The role of ultra-high resolution fourier transform mass spectrometry (ft-ms) in astrobiology-related research: Analysis of meteorites and tholins. *International Journal of Molecular Sciences*, *17*, 439. https://doi.org/10.3390/ijms17040439

Stansberry, J. A., Spencer, J., & Linscott, I. (2015). Voyager IRIS Measurements of Triton's Thermal Emission: Implications for Pluto? *AAS/Division for Planetary Sciences Meeting Abstracts #47*, Article 210.32, 210.32.

Stern, S. A., Bagenal, F., Ennico, K., Gladstone, G. R., Grundy, W. M., McKinnon, W. B., Moore, J. M., Olkin, C. B., Spencer, J. R., Weaver, H. A., Young, L. A., Andert, T., Andrews, J., Banks, M., Bauer, B., Bauman, J., Barnouin, O. S., Bedini, P., Beisser, K., ... Zirnstein, E. (2015). The Pluto system: Initial results from its exploration by New Horizons. *Science*, *350*(6258), Article aad1815, aad1815. https://doi.org/10.1126/science.aad1815

Stern, S. A., & McKinnon, W. B. (2000). Triton's Surface Age and Impactor Population Revisited in Light of Kuiper Belt Fluxes: Evidence for Small Kuiper Belt Objects and Recent Geological Activity. *Astronomical Journal*, *119*(2), 945–952. https://doi.org/10.1086/301207

Stern, S. A., Trafton, L. M., & Flynn, B. (1995). Rotationally Resolved Studies of the Mid-Ultraviolet Spectrum of Triton. II. HST Surface and Atmospheric Results. *Astronomical Journal*, *109*, 2855. https://doi.org/10.1086/117491

Stone, E. C., Cummings, A. C., Looper, M. D., Selesnick, R. S., Lal, N., McDonald, F. B., Trainor, J. H., & Chenette, D. L. (1989). Energetic Charged Particles in the Magnetosphere of Neptune. *Science*, *246*(4936), 1489–1494. https://doi.org/10.1126/science.246.4936.1489

Strobel, D. F., & Summers, M. E. (1995). Triton's upper atmosphere and ionosphere. *Neptune and Triton*, 1107–1148.

Strobel, D. F., & Zhu, X. (2017). Comparative planetary nitrogen atmospheres: Density and thermal structures of Pluto and Triton. *Icarus*, *291*, 55–64. https://doi.org/10.1016/j.icarus.2017.03.013

Suissa, G., & Kipping, D. (2018). TRAPPIST-1e Has a Large Iron Core. *Research Notes of the American Astronomical Society*, *2*, Article 31, 31. https://doi.org/10.3847/2515-5172/aac32f

Sullivan, P. W., Winn, J. N., Berta-Thompson, Z. K., Charbonneau, D., Deming, D., Dressing, C. D., Latham, D. W., Levine, A. M., McCullough, P. R., Morton, T., Ricker, G. R., Vanderspek, R., & Woods, D. (2015). The Transiting Exoplanet Survey Satellite: Simulations of Planet Detections and Astrophysical False Positives. *ApJ*, *809*, Article 77, 77. https://doi.org/10.1088/0004-637X/809/1/77

Szopa, C., Cernogora, G., Boufendi, L., Correia, J. J., & Coll, P. (2006). Pampre: A dusty plasma experiment for titan's tholins production and study. *Planetary and Space Science*, *54*(4), 394–404. https://doi.org/https://doi.org/10.1016/j.pss.2005.12.012

Tamayo, D., Rein, H., Petrovich, C., & Murray, N. (2017). Convergent Migration Renders TRAPPIST-1 Long-lived. *ApJ*, *840*, Article L19, L19. https://doi.org/10.3847/2041-8213/aa70ea

Telfer, M. W., Parteli, E. J. R., Radebaugh, J., Beyer, R. A., Bertrand, T., Forget, F., Nimmo, F., Grundy, W. M., Moore, J. M., Stern, S. A., Spencer, J., Lauer, T. R., Earle, A. M., Binzel, R. P., Weaver, H. A., Olkin, C. B., Young, L. A., Ennico, K., Runyon, K., & aff12. (2018). Dunes on Pluto. *Science*, *360*(6392), 992–997. https://doi.org/10.1126/science.aao2975

Tennyson, J., & Yurchenko, S. N. (2012). ExoMol: molecular line lists for exoplanet and other atmospheres. *MNRAS*, *425*(1), 21–33. https://doi.org/10.1111/j.1365-2966.2012.21440.x

Thompson, W. R., Singh, S. K., Khare, B. N., & Sagan, C. (1989). Triton: Stratospheric molecules and organic sediments. *Geophyscal Research Letters*, *16*(8), 981–984. https://doi.org/10.1029/GL016i008p00981

Tomasko, M. G., Doose, L., Engel, S., Dafoe, L. E., West, R., Lemmon, M., Karkoschka, E., & See, C. (2008). A model of Titan's aerosols based on measurements made inside the atmosphere. *Planetary and Space Science*, *56*(5), 669–707. https://doi.org/10.1016/j.pss.2007.11.019

Trainer, M. G., Pavlov, A. A., Dewitt, H. L., Jimenez, J. L., McKay, C. P., Toon, O. B., & Tolbert, M. A. (2006). Inaugural Article: Organic haze on Titan and the early Earth. *Proceedings of the National Academy of Science*, *103*(48), 18035–18042. https://doi.org/10.1073/pnas.0608561103

Trainer, M. G., Jimenez, J. L., Yung, Y. L., Toon, O. B., & Tolbert, M. A. (2012). Nitrogen Incorporation in CH4-N2Photochemical Aerosol Produced by Far Ultraviolet Irradiation. *Astrobiology*, *12*(4), 315–326. https://doi.org/10.1089/ast.2011.0754

Trainer, M. G., Pavlov, A. A., Curtis, D. B., McKay, C. P., Worsnop, D. R., Delia, A. E., Toohey, D. W., Toon, O. B., & Tolbert, M. A. (2004). Haze Aerosols in the Atmosphere of Early Earth: Manna from Heaven. *Astrobiology*, *4*, 409–419. https://doi.org/10.1089/ast.2004.4.409

Tran, B. N., Force, M., Briggs, R. G., Ferris, J. P., Persans, P., & Chera, J. J. (2008). Titan's atmospheric chemistry: Photolysis of gas mixtures containing hydrogen cyanide and carbon monoxide at 185 and 254 nm. *Icarus*, *193*(1), 224–232. https://doi.org/10.1016/j.icarus.2007.09.010

Tsiaras, A., Waldmann, I. P., Tinetti, G., Tennyson, J., & Yurchenko, S. N. (2019). Water vapour in the atmosphere of the habitable-zone eight-Earth-mass planet K2-18 b. *Nature Astronomy*, *3*, 1086–1091. https://doi.org/10.1038/s41550-019-0878-9

Turbet, M., Bolmont, E., Leconte, J., Forget, F., Selsis, F., Tobie, G., Caldas, A., Naar, J., & Gillon, M. (2018). Modeling climate diversity, tidal dynamics and the fate of volatiles on TRAPPIST-1 planets. *A&A*, *612*, Article A86, A86. https://doi.org/10.1051/0004-6361/201731620

Tyler, G. L., Sweetnam, D. N., Anderson, J. D., Borutzki, S. E., Campbell, J. K., Eshleman, V. R., Gresh, D. L., Gurrola, E. M., Hinson, D. P., Kawashima, N., Kursinski, E. R., Levy, G. S., Lindal, G. F., Lyons, J. R., Marouf, E. A., Rosen, P. A., Simpson, R. A., & Wood, G. E. (1989). Voyager Radio Science Observations of Neptune and Triton. *Science*, *246*(4936), 1466–1473. https://doi.org/10.1126/science.246.4936.1466

Ugelow, M. S., De Haan, D. O., Hörst, S. M., & Tolbert, M. A. (2018). The Effect of Oxygen on Organic Haze Properties. *The Astrophysical Journal Letters*, *859*(1), Article L2, L2. https://doi.org/10.3847/2041-8213/aac2c7

Unterborn, C. T., Hinkel, N. R., & Desch, S. J. (2018a). Updated Compositional Models of the TRAPPIST-1 Planets. *Research Notes of the American Astronomical Society*, *2*, Article 116, 116. https://doi.org/10.3847/2515-5172/aacf43

Unterborn, C. T., Desch, S. J., Hinkel, N. R., & Lorenzo, A. (2018b). Inward migration of the TRAPPIST-1 planets as inferred from their water- rich compositions. *Nature Astronomy*, *2*, 297–302. https://doi.org/10.1038/s41550-018-0411-6

Vida, K., & Roettenbacher, R. M. (2018). Finding flares in Kepler data using machine learning tools. *ArXiv e-prints*, Article arXiv:1806.00334, arXiv:1806.00334.

Vuitton, V., Yelle, R. V., Klippenstein, S. J., Hörst, S. M., & Lavvas, P. (2019). Simulating the density of organic species in the atmosphere of Titan with a coupled ion-neutral photochemical model. *Icarus*, *324*, 120–197. https://doi.org/10.1016/j.icarus.2018.06.013

Vuitton, V., Bonnet, J.-Y., Frisari, M., Thissen, R., Quirico, E., Dutuit, O., Schmitt, B., Le Roy, L., Fray, N., Cottin, H., Sciamma-O'Brien, E., Carrasco, N., & Szopa, C. (2010). Very high resolution mass spectrometry of HCN polymers and tholins. *Faraday Discussions*, *147*, 495. https://doi.org/10.1039/c003758c

Vuitton, V., Briois, C., & Makarov, A. e. (2014). The Orbitrap mass analyzer as a space instrument for the understanding of prebiotic chemistry in the Solar System. *40th COSPAR Scientific Assembly*, *40*, Article B0.6-2-14, B0.6-2–14.

Vuitton, V., Moran, S. E., He, C., Wolters, C., Flandinet, L., Orthous-Daunay, F.-R., Moses, J. I., Valenti, J. A., Lewis, N. K., & Hörst, S. M. (2021). H_2SO_4 and Organosulfur Compounds in Laboratory Analogue Aerosols of Warm High-metallicity Exoplanet Atmospheres. *The Planetary Science Journal*, *2*(1), Article 2, 2. https://doi.org/10.3847/PSJ/abc558

Wakeford, H. R., Lewis, N. K., Fowler, J., Bruno, G., Wilson, T. J., Moran, S. E., Valenti, J., Batalha, N. E., Filippazzo, J., Bourrier, V., Hörst, S. M., Lederer, S. M., & de Wit, J. (2019a). Disentangling the Planet from the Star in Late-Type M Dwarfs: A Case Study of TRAPPIST-1g. *AJ*, *157*(1), Article 11, 11. https://doi.org/10.3847/1538-3881/aaf04d

Wakeford, H. R., & Sing, D. K. (2015). Transmission spectral properties of clouds for hot Jupiter exoplanets. *Astronomy & Astrophysics*, *573*, Article A122, A122. https://doi.org/10.1051/0004-6361/201424207

Wakeford, H. R., Sing, D. K., Kataria, T., Deming, D., Nikolov, N., Lopez, E. D., Tremblin, P., Amundsen, D. S., Lewis, N. K., Mandell, A. M., Fortney, J. J., Knutson, H., Benneke, B., & Evans, T. M. (2017). HAT-P-26b: A Neptune-mass exoplanet with a

well-constrained heavy element abundance. *Science*, *356*, 628–631. https://doi.org/10.1126/science.aah4668

Wakeford, H. R., Wilson, T. J., Stevenson, K. B., & Lewis, N. K. (2019b). Exoplanet Atmosphere Forecast: Observers Should Expect Spectroscopic Transmission Features to be Muted to 33%. *Research Notes of the American Astronomical Society*, *3*, Article 7, 7. https://doi.org/10.3847/2515-5172/aafc63

Wheatley, P. J., Louden, T., Bourrier, V., Ehrenreich, D., & Gillon, M. (2017). Strong XUV irradiation of the Earth-sized exoplanets orbiting the ultracool dwarf TRAPPIST-1. *MNRAS*, *465*, L74–L78. https://doi.org/10.1093/mnrasl/slw192

Wolf, E. T. (2017). Assessing the Habitability of the TRAPPIST-1 System Using a 3D Climate Model. *ApJ*, *839*, Article L1, L1. https://doi.org/10.3847/2041-8213/aa693a

Wolters, C., Flandinet, L., He, C., Isa, J., Orthous-Daunay, F.-R., Thissen, R., Hörst, S., & Vuitton, V. (2020). Enhancing data acquisition for the analysis of complex organic matter in direct-infusion orbitrap mass spectrometry using micro-scans [e8818 RCM-20-0022.R2]. *Rapid Communications in Mass Spectrometry*, *34*(15), e8818. https://doi.org/https://doi.org/10.1002/rcm.8818

Wong, M. L., Fan, S., Gao, P., Liang, M.-C., Shia, R.-L., Yung, Y. L., Kammer, J. A., Summers, M. E., Gladstone, G. R., Young, L. A., Olkin, C. B., Ennico, K., Weaver, H. A., Stern, S. A., & New Horizons Science Team. (2017). The photochemistry of Pluto's atmosphere as illuminated by New Horizons. *Icarus*, *287*, 110–115. https://doi.org/10.1016/j.icarus.2016.09.028

Yelle, R. V., Lunine, J. I., Pollack, J. B., & Brown, R. H. (1995). Lower atmospheric structure and surface-atmosphere interactions on Triton. *Neptune and Triton*, 1031–1105.

Young, L. A., & Stern, S. A. (2001). Ultraviolet Observations of Triton in 1999 with the Space Telescope Imaging Spectrograph: 2150-3180 Å Spectroscopy and Disk-integrated Photometry. *Astronomical Journal*, *122*(1), 449–456. https://doi.org/10.1086/322062

Youngblood, A., France, K., Loyd, R. O. P., Brown, A., Mason, J. P., Schneider, P. C., Tilley, M. A., Berta-Thompson, Z. K., Buccino, A., Froning, C. S., Hawley, S. L., Linsky, J., Mauas, P. J. D., Redfield, S., Kowalski, A., Miguel, Y., Newton, E. R., Rugheimer, S., Segura, A., ... Vieytes, M. (2017). The MUSCLES Treasury Survey. IV. Scaling Relations for Ultraviolet, Ca II K, and Energetic Particle Fluxes from M Dwarfs. *ApJ*, *843*(1), Article 31, 31. https://doi.org/10.3847/1538-4357/aa76dd

Yu, X., He, C., Zhang, X., Hörst, S. M., Dymont, A. H., McGuiggan, P., Moses, J. I., Lewis, N. K., Fortney, J. J., Gao, P., Kempton, E. M.-R., Moran, S. E., Morley, C. V., Powell, D., Valenti, J. A., & Vuitton, V. (2021). Haze Evolution in Temperate Exoplanet Atmospheres Through Surface Energy Measurements. *Nature Astronomy*.

Yu, X., Hörst, S. M., He, C., McGuiggan, P., & Bridges, N. T. (2017). Direct Measurement of Interparticle Forces of Titan Aerosol Analogs ("Tholin") Using Atomic Force Microscopy. *Journal of Geophysical Research (Planets)*, *122*(12), 2610–2622. https://doi.org/10.1002/2017JE005437

Yu, X., Hörst, S. M., He, C., McGuiggan, P., Kristiansen, K., & Zhang, X. (2020). Surface Energy of the Titan Aerosol Analog "Tholin". *ApJ*, *905*(2), Article 88, 88. https://doi.org/10.3847/1538-4357/abc55d

Zahnle, K., Marley, M. S., Morley, C. V., & Moses, J. I. (2016). Photolytic Hazes in the Atmosphere of 51 Eri b. *ApJ*, *824*(2), Article 137, 137. https://doi.org/10.3847/0004-637X/824/2/137

Zahnle, K. J., & Catling, D. C. (2017). The Cosmic Shoreline: The Evidence that Escape Determines which Planets Have Atmospheres, and what this May Mean for Proxima Centauri B. *ApJ*, *843*(2), Article 122, 122. https://doi.org/10.3847/1538-4357/aa7846

Zahnle, K. J., Lupu, R., Catling, D. C., & Wogan, N. (2020). Creation and Evolution of Impact-generated Reduced Atmospheres of Early Earth. *The Planetary Science Journal*, *1*(1), Article 11, 11. https://doi.org/10.3847/PSJ/ab7e2c

Zhang, M., Chachan, Y., Kempton, E. M. .-R., Knutson, H. A., & Chang, W. ((2020). PLATON II: New Capabilities and a Comprehensive Retrieval on HD 189733b Transit and Eclipse Data. *ApJ*, *899*(1), Article 27, 27. https://doi.org/10.3847/1538-4357/aba1e6

Zhang, X. (2020). Atmospheric regimes and trends on exoplanets and brown dwarfs. *Research in Astronomy and Astrophysics*, *20*(7), Article 099, 099. https://doi.org/10.1088/1674-4527/20/7/99

Zhang, X., Strobel, D. F., & Imanaka, H. (2017). Haze heats Pluto's atmosphere yet explains its cold temperature. *Nature*, *551*, 352–355. https://doi.org/10.1038/nature24465

Zhang, Z., Zhou, Y., Rackham, B., & Apai, D. (2018). The Near-Infrared Transmission Spectra of TRAPPIST-1 Planets b, c, d, e, f, and g and Stellar Contamination in Multi-Epoch Transit Spectra. *ArXiv e-prints*, Article arXiv:1802.02086, arXiv:1802.02086.

Sarah E. Moran

3400 N Charles St., Earth and Planetary Sciences, Johns Hopkins University, Baltimore, MD 21218
smoran14@jhu.edu | moran.sarahe@gmail.com | 816-739-9348
ORCID: 0000-0002-6721-3284 | Twitter: @Of_FallingStars | sarahemoran.com

Education

Johns Hopkins University, Baltimore, MD — June 2021
PhD, Planetary Sciences
Dissertation: *In Search of Clearer Skies?*
Linking Planetary Clouds and Hazes from the Laboratory to Atmospheric Models
Advisor: Prof. Sarah M. Hörst
Master of Arts, Planetary Sciences — May 2018

Barnard College, Columbia University, New York, NY — May 2015
Bachelor of Arts, Astrophysics; *cum laude*
Science & Public Policy minor

Research Experience

Director's Postdoctoral Fellow — starting from January 2022
Lunar and Planetary Laboratory, University of Arizona, *Tucson, AZ*
Modeling of planetary, exoplanetary, and brown dwarf atmospheres
Advisor: Dr. Mark S. Marley

Postdoctoral Research Associate — Sept 2021 – Dec 2021
NASA Ames Research Center/Bay Area Environmental Research Institute, *Mountain View, CA*
Aerosol/microphysical modeling for transiting planetary atmospheric observations
Supervisor: Dr. Natasha E. Batalha

Graduate Research Assistant — June 2017 – Aug 2021
Space Telescope Science Institute, *Baltimore, MD*
Exoplanet atmospheric modeling, STARGATE collaboration
Advisor: Prof. Nikole K. Lewis (Cornell University, Dept. of Astronomy and Carl Sagan Institute)

Graduate Research Assistant/NASA Earth and Space Science Fellow — Jan 2017 – Aug 2021
Johns Hopkins University, *Earth & Planetary Sciences, Baltimore, MD*
PHAZER Laboratory: atmospheric chamber experiments and FTIR for planetary atmospheres
Advisor: Prof. Sarah M. Hörst

Visiting Researcher — Jan 2017 – Sept 2018
Institute for Planetology & Astrophysics of Grenoble*, Grenoble, France*
High resolution mass spectrometry of atmospheric haze analogues
Supervisor: Dr. Véronique Vuitton

NSF REU Researcher — Summer 2014
Georgetown University, *Materials Physics*, *Washington, D.C*
Computational study of 2-D materials for electronics/solar cells with Quantum Espresso
Advisor: Prof. Amy Liu

NSF REU Researcher — Summer 2013
University of Utah*, Physics and Astronomy, Salt Lake City, UT*
Data analysis of SDSS BOSS BAL quasar spectroscopy and photometry with IDL
Advisor: Prof. Kyle S. Dawson

Policy Experience

Lloyd V. Berkner Space Policy Intern Fall 2019
Space Studies Board, National Academies of Sciences, Engineering, and Medicine, Washington, DC
Projects: *Solar and Space Physics Midterm Report; Astro2020; Committee on Solar and Space Physics Rideshare Opportunity Short Report; Committee on Astrobiology and Planetary Science Decadal Survey planning*

Additional Training

ComSciCon-SciWri, Penn State University, State College, PA — October 2019
Cloud Academy, Les Houches School of Physics, Les Houches, France — September 2018
Johns Hopkins University SafeZone training, Baltimore, MD — August 2017
Software Carpentry Coding Bootcamp, JHU EPS, Baltimore, MD — August 2016

Grants, Fellowships, and Selected Competitive Observing Programs

Co-I, 4 JWST Cycle 1 Programs – 108.8 total hours — 2021 – present
GO Program 1981 (PI Kevin Stevenson & Jacob Lustig-Yaeger), 75.6 hours
Tell Me How I'm Supposed to Breathe with No Air: Measuring the Prevalence and Diversity of M-Dwarf Planet Atmospheres
GO Program 2288 (PI Joshua Lothringer & Jeff Valenti), 7.4 hours
Formation and Impact of Silicate Clouds on L Dwarfs
GO Program 2594 (PI Jessica Spake & Zafar Rustamkulov), 16.6 hours
The Twin Paradox: Assessing Planetary Radius Evolution with a CH_4 Thermometer
GO Program 2667 (PI Hannah Wakeford), 9.2 hours
Good Vibrations: Directly Measuring Exoplanet Aerosol Compositions with MIRI Spectroscopy

Co-I, NASA Exoplanet Research Program 2018 2 (PI Chao He) — 2020 – present
Laboratory Exploration of Hazes in Atmospheres of Rocky Planets around M-dwarfs

Co-I, Hubble Space Telescope Cycle 27 Program, PI Jessica Spake, 16 orbits — 2019 – present
GO Program 15838, *How Hot Is the Inside of a Young Planet?*

Fellow, NASA Earth and Space Science Fellowship, Astrophysics — 2018 – 2021
The Role of Hazes in the Atmospheres of Temperate Planets in M-Dwarf Systems

Service and Leadership

Reviewer; *Nature Astronomy, Icarus* — Spring 2021 –
NASA Review Panel Executive Secretary — Spring 2021
JHU EPS Buddy System, Co-Founder and Inaugural Head Buddy — June 2020 – July 2021
JHU EPS Bromery Speaker Seminar Organizational Committee — July 2020 – August 2021
Science team, exoplanet working group, Odyssey mission to Neptune concept study — February 2020 – August 2020
JHU EPS Equity, Diversity, and Inclusion committee — Fall 2019 – August 2021
EPS Course Guide Curator — Fall 2019 – Fall 2020
EPS Graduate Student President — Fall 2018 – Fall 2019
Graduate Council Department Representative, Johns Hopkins University — Fall 2017 – Fall 2018

Outreach

Delaware Teen Science Café Featured Scientist, Delaware Museum of Natural History — February 2021
AAS Congressional Visits Day 2020 — September 2020
Presentation, Johns Hopkins Center for Talented Youth, (35 MS/HS students) — June 2019
Skype a Scientist, (~20 MS students) — January 2019
Volunteer, 2018 USA Science & Engineering Festival, AAAS, Washington, D.C. — April 2018
Catalyzing Advocacy for Scientists and Engineers Workshop, AAAS, Washington, D.C. — March 2018
St. Teresa's Academy eMentor, STEM careers — Spring 2017 – present

Honors, and Awards

AAS Rodger Doxsey Travel Prize	January 2021
J. Brien Key Fund Travel Award, Johns Hopkins University	December 2018
Women in Astronomy IV Conference Travel Grant, NRAO	June 2017
EPS Summer Field Research Grant, Johns Hopkins University	June 2017
*Cum Laud*e, Barnard College	May 2015
Dean's List, Barnard College	Fall 2011 – Spring 2015

Publications

[11] **Moran, S.E.**, Hörst, S. M., He, C., Radke, M.J., Izenberg, N.R., Sebree, J. A., Vuitton, V., Flandinet, L., Orthous-Daunay, F.-R., Wolters, C. "*Triton Haze Analogues: the Role of Carbon Monoxide in Haze Formation*," submitted to the Journal of Geophysical Research – Planets, June 2021

[10] Pidhorodetska, D., **Moran, S.E.**, Schwieterman, E.W., Fauchez, T.J., Barclay, T.F., Quintana, E.V., Domagal-Goldman, S.D., Lewis, N.K., Villanueva, G.L., Schlieder, J.E., Gilbert, E.A., Kostov, V.B. *L 98-59: a Benchmark System of Small Planets for Future Atmospheric Characterization*, Astrophysical Journal, accepted May 2021

[9] Yu, X., Zhang, X., Hörst, S.M., He, C., Dymont, A. H., McGuiggan, P., Lewis, N.K., Moses, J.I., Fortney, J.J., Gao, P., Kempton, E.M.-R., **Moran, S.E.**, Morley, C.V., Powell, D., Valenti, J.A., Vuitton, V. *Haze Evolution in Temperate Exoplanet Atmospheres through Surface Energy Measurements*, Nature Astronomy, accepted March 2021

[8] Rymer, A., Runyon, K., Clyde, B., and 69 coauthors, including **Moran, S.E.** *Neptune Odyssey Flagship Concept for the Exploration of the Neptune-Triton System*, Planetary Science Journal, (Special Issue – "Planetary Mission Concept Studies"), resubmitted March 2021

[7] Gao, P., Wakeford, H.R., **Moran, S.E.,** Parmentier, V. *Aerosols in Exoplanet Atmospheres*, Journal of Geophysical Research – Planets, *126* **(Invited Review for Special Issue, "Exoplanets: The Nexus of Astronomy and Geoscience"),** DOI: 10.1029/2020JE006655. 2021.

[6] Vuitton, V., **Moran, S.E.,** He, C., Wolters, C., Flandinet, L., Orthous-Daunay, F.-R., Moses, J. I., Valenti, J.A., Lewis, N.K., Hörst, S.M. *H_2SO_4 and Organosulfur Compounds in Laboratory Analogue Aerosols of Warm High Metallicity Exoplanet Atmospheres*, Planetary Science Journal, 2 (2). DOI: 10.3847/PSJ/abc558. 2021.

[5] **Moran, S.E.,** Hörst, S.M., Vuitton, V., He, C., Lewis, N.K., Flandinet, L., Moses, J.I., North, N., Orthous-Daunay, F.-R., Sebree, J., Wolters, C., M-R. Kempton, E., Marley, M.S., Morley, C.V., Valenti, J.A. *Chemistry of Temperate Super-Earth and Mini-Neptune Atmospheric Hazes from Laboratory Experiments*, Planetary Science Journal, 1, (17). DOI: 10.3847/PSJ/ab8eae. 2020.

[4] He, C., Hörst, S.M., Lewis, N.K., Yu, X., Moses, J.I., McGuiggan, P., Marley, M.S., Kempton, E. M.-R., **Moran, S.E.**, Morley, C.V., Vuitton, V. *Sulfur-driven Haze Formation in Warm CO_2-rich Exoplanet Atmospheres*, Nature Astronomy, 4, [986-993]. DOI: 10.1038/s41550-020-1072-9. 2020.

[3] Wakeford, H.R., Lewis, N.K., Fowler, J., Bruno, G., Wilson, T.J., **Moran, S.E.,** Valenti, J., Batalha, N.E., Filippazzo, J., Bourrier, V., Hörst, S.M., Lederer, S.M., de Wit, J. *Disentangling the planet from the star in late type M dwarfs: A case study of TRAPPIST-1g*, Astronomical Journal, *157* (1), [11]. DOI: 10.3847/1538-3881/aaf04d. 2018.

[2] **Moran, S.E.**, Hörst, S.M., Batalha, N.E., Lewis, N.K., Wakeford, H.R. *Limits on Clouds and Hazes for the TRAPPIST-1 Planets*, Astronomical Journal, *156* (6), [252]. DOI: 10.3847/1538-3881/aae83a (**Research Highlight in *Nature Astronomy;* Research Highlight in *AAS Nova*).** 2018.

[1] Harris, D. W., Jensen, T. W., Suzuki, N., Bautista, J. E., Dawson, K. S., Vivek, M., Brownstein, J. R., Ge, J., Hamann, F., Herbst, H., Jiang, L., **Moran, S. E**., Myers, A. D., Olmstead, M. D., Schneider, D. P. *The Composite Spectrum of Boss Quasars Selected for Studies of the Lyα Forest*., Astronomical Journal, *151* (6), [155]. DOI: 10.3847/0004-6256/151/6/155. 2016.

Invited Seminars and Colloquia

Johns Hopkins University/Space Telescope Science Institute Summer Talks Series	June 2021
Geological Society of Washington, Exoplanets and Super-Earths Themed Meeting	May 2021
MIT, Astronomy Brown Bag Lunch Seminar	April 2021
NASA Goddard Space Flight Center, Exoplanet Series Seminar	December 2020
University of California, Santa Cruz, Planetary Lunch Seminar	November 2020
University of Maryland, College Park, Planetary and Exoplanetary Astronomy Seminar	October 2020
Caltech, Planetary Science Seminar	May 2020

Teaching Experience

The Johns Hopkins University

Teaching Assistant, AS.270.114 Guided Tour: The Planets — Spring 2021

Guest Lecturer (1 lecture), AS.270.423 Planetary Atmospheres — Spring 2020
Atmospheric Chemistry

Guest Lecturer (1 lecture), AS.270.328 Planetary Exploration: Techniques and Data Analysis — Fall 2018
Exoplanet Detection Techniques

Skills

Programming languages:	Python, IDL, Fortran, Matlab
Software:	LaTeX/Overleaf, HTML, CHIMERA, Pandexo, MS Office suite, Keynote
Operating systems:	Macintosh, Unix/Linux, Windows
Laboratory Instrumentation:	ESI-Orbitrap MS, FTIR
Laboratory Skills:	vacuum techniques, machine shop; technical theatre production
Languages:	elementary proficiency in Latin, Italian; beginning proficiency in French
Communication:	excellent creative/professional writing, organizational, and communication skills

Technical Non-refereed Publications

[4] *Neptune and Triton: A Flagship for Everyone,* Rymer, A., Runyon, K. and 40 coauthors, including **Moran, S.E.** White Paper for the Planetary Science and Astrobiology Decadal Survey 2023-2032. 2020.

[3] *Neptune Odyssey: Mission to the Neptune-Triton System*, Rymer, A., Clyde, B., Runyon, K., and 70 coauthors, including **Moran, S.E.** NASA Planetary Mission Concept Study for the Astrobiology and Planetary Science Decadal Survey 2023-2032. 2020.

[2] *Enabling Effective Exoplanet / Planetary Collaborative Science*, Marley, M.S., Harman, C. Hammel, H.B., Bryne, P.K., Fortney, J.J., Accomazzi, A., **Moran, S.E.,** Way, M.J., Christiansen, J.L., Izenberg, N.R. Holt, T., Vahidinia, S., Kohler, E., Brugman, K.K. White Paper for the Planetary Science and Astrobiology Decadal Survey 2023-2032. 2020.

[1] *The Importance of Prioritizing Exoplanet Experimental Facilities*, Kohler, E., He, C., **Moran, S.E.,** Dan Shim, S.-H., Brugman, K.K., Johnson, A.C., Vergeli, P.C., Thompson, M.A., Graham, H. White Paper for the Planetary Science and Astrobiology Decadal Survey 2023-2032. 2020.

1st Author Conference and Workshop Presentations

[18] *Clouds in the Lab*, **Moran, S.E.,** CloudNineCon (**Invited Keynote Speaker)**. Virtual Meeting. August 2021.

[17] *The Complexity of Oxygenated Planetary Hazes Near and Far*, **Moran, S.E.,** et al., Emerging Researchers in Exoplanet Science 2021. Virtual Meeting. May 2021. Plenary Oral Presentation.

[16] *In Search of Clearer Skies? Linking Exoplanet Clouds and Hazes from the Laboratory to Atmospheric Models*, **Moran, S.E.,** Hörst, S.M., Lewis, N.K. AAS 237, 413.05 D. Virtual Meeting. January 2021. Oral Presentation (Dissertation Talk).

[15] *Triton's Haze Properties as Characterized in the Lab*, **Moran, S.E.,** Hörst, S.M., He, C., Radke, M.J., Sebree, J., Izenberg, N.R., Vuitton, V., Flandinet, L., Orthous-Daunay, F.-R., Wolters, C. AGU , P066-0016, Virtual Meeting. December 2020. Poster.

[14] *Chemical Composition and Behavior of Super-Earth and Mini-Neptune Exoplanet Hazes*, **Moran, S.E.,** Hörst, S. M., Vuitton, V., He, C., Lewis, N.K., Bishop, N., Flandinet, L., Moses, J., Orthous-Daunay, F.-R., Sebree, J., Wolters, C. DPS 52, 213.02. Virtual Meeting. October 2020. Oral Presentation.

[13] ****Chemistry of Exoplanet Hazes from the Lab,* **Moran, S.E.,** Hörst, S. M., Vuitton, V., He, C., Lewis, N.K., Bishop, N., Flandinet, L., Moses, J., Orthous-Daunay, F.-R., Sebree, J., Wolters, C. Cloud Academy II, Les Houches School of Physics, Les Houches, France. March 2020. Oral Presentation.
** postponed to March 2022 due to COVID-19 outbreak

[12] *Chemistry of Laboratory Exoplanet Hazes,* **Moran, S.E.,** Hörst, S. M., Vuitton, V., He, C., Lewis, N.K., Bishop, N., Flandinet, L., Moses, J., Orthous-Daunay, F.-R., Sebree, J., Wolters, C. Exoplanets in Our Backyard, Planetary Atmospheres Thick and Thin #3030, Lunar and Planetary Institute, Houston, TX. February 2020. Oral Presentation.

[11] *Chemistry of Temperate Exoplanet Hazes from the Laboratory,* **Moran, S.E.,** Hörst, S. M., Vuitton, V., He, C., Lewis, N.K., Flandinet, L., Moses, J., Orthous-Daunay, F.-R., Sebree, J., Wolters, C. AAS 235, 248.04, Honolulu, HI. January 2020. Oral Presentation.

[10] *Chemistry of Exoplanet Haze Analogues from the Laboratory,* **Moran, S.E.,** Hörst, S. M., Vuitton, V., He, C., Lewis, N.K., Bishop, N., Flandinet, L., Moses, J., Orthous-Daunay, F.-R., Sebree, J., Wolters, C. Chesapeake Bay Area Exoplanet Meeting, University of Delaware, Newark, DE. September 2019. Oral Presentation.

[9] *Chemistry of Exoplanet Haze Analogues from the Lab,* **Moran, S.E.,** Hörst, S. M., Vuitton, V., He, C., Lewis, N.K., Bishop, N., Flandinet, L., Moses, J., Orthous-Daunay, F.-R., Sebree, J., Wolters, C. Exoclimes V, Oxford, UK. August 2019. Poster.

[8] *Exoplanet Hazes in the Laboratory and Atmospheric Models*, **Moran, S.E,** et al., Emerging Researchers in Exoplanet Science 2019, Cornell University, Ithaca, NY. June 2019. Oral Presentation.

[7] *Atmospheric Hazes of M-Dwarf Temperate Planets*, **Moran, S.E**., Hörst, S.M., Lewis, N.K. NESSF Special Session, AAS 233, 215.14, Seattle, Washington. January 2019. Oral Presentation.

[6] *Limits on Clouds and Hazes for the TRAPPIST-1 Planets: Insight from the laboratory and models***, Moran, S.E**., Hörst, S.M., Batalha, N.E., Lewis, N.K., Wakeford, H.R. AAS 233, 103.04, Seattle, Washington. January 2019. Oral Presentation.

[5] *Insights into the atmospheres of the TRAPPIST-1 planets from the laboratory and models*, **Moran, S.E.**, Hörst, S.M., Batalha, N.E., Lewis, N.K., Wakeford, H.R. AGU, P44B-06, Washington, D.C. December 2018. Oral Presentation.

[4] *Limits on Clouds and Hazes for the TRAPPIST-1 Planets,* **Moran, S.E**., Hörst, S.M., Batalha, N.E., Lewis, N.K., Wakeford, H.R. Cloud Academy, Les Houches School of Physics, Les Houches, France. September 2018. Poster.

[3] *Super-Earth and mini-Neptune laboratory haze analogues and their effects on exoplanetary atmospheric modeling***, Moran, S. E**., et al. Exoplanets II, Cambridge, UK. July 2018. Oral Presentation.

[2] *Modeling Exoplanetary Haze and Cloud Effects for Transmission Spectroscopy of the TRAPPIST-1 System*, **Moran, S.E**., Hörst, S.M., Lewis, N.K., Batalha, N.E., de Wit, J. AAS 231, 148.39, Washington, DC. January 2018. Poster.

[1] *Laboratory Studies of Planetary Hazes: composition of cool exoplanet atmospheric aerosols with very high resolution mass spectrometry*, **Moran, S.E.**, Hörst, S.M., Lewis, N.K., He, C., Flandinet, L., Moses, J.I., Orthous-Daunay, F-R., Vuitton, V., Wolters, C. DPS 49, 416.25, Provo, UT. October 2017. Poster.

Co-Author Conference and Workshop Presentations

[12] *L 98-59: a Benchmark System of Small Planets for Future Atmospheric Characterization*, D. Pidhorodetska, **Moran, S.E.,** Fauchez, T., Schwieterman, E., Barclay, T., Quintana, E., Domagal-Goldman, S., Lewis, N.K., Villanueva, G., Schlieder, J. AAS 237, 437.05. Virtual Meeting. January 2021.

[11] *Hazes and Exoplanetary Atmospheres in the Lab*, Hörst, S.M., He, C., Lewis, N.K., Moses, J.I., Yu, X., Vuitton, V., McGuiggan, P., Marley, M., Kempton, E.M.-R., Valenti, J.A., Morley, C.V., Sebree, J., **Moran, S.E.** AGU, INV14. Virtual Meeting. December 2020.

[10] *Laboratory Investigation of Haze Formation in Exoplanet Atmospheres: Implication for Habitability and Biosignatures*, He, C., Hörst, S.M., Lewis, N.K., **Moran, S.E.,** Yu, X., Moses, J.I. AGU, P018-03. Virtual Meeting. December 2020.

[9] *Sulfur Promotes Haze Formation in Warm CO_2-Rich Exoplanet Atmospheres*, He, C., Hörst, S.M., Lewis, N.K., Yu, X., Moses, J.I., McGuiggan, P., Marley, M.S., Kempton, E. M.-R., **Moran, S.E.**, Morley, C.V., Vuitton, V. DPS 52, 403.04.Virtual Meeting. October 2020.

[8] *L 98-59: A Benchmark System of Terrestrial Planets for Future Atmospheric Characterization*, Pidhorodetska, D., **Moran, S. E**., Fauchez, T., Kopparapu, R. K., Colon, K., Quintana, E., Villanueva, G., Domagal-Goldman, S. Exoplanets in Our Backyard, Lunar and Planetary Institute, Houston, TX. February 2020.

[7] *Orbitrap mass spectrometry of synthetic exoplanetary particles,* Wolters, C, Vuitton, V., Flandinet, L., **Moran, S.E.,** He, C., Orthous-Daunay, F.-R., Hörst, S.M. EPSC-DPS Meeting 2019- L2.122. Geneva, Switzerland. September 2019.

[6] *Orbitrap mass spectrometry of synthetic (exo-)planetary organic haze,* Vuitton, V., Flandinet, L., **Moran, S.E.,** He, C., Orthous-Daunay, F.-R., Wolters, C., Hörst, S.M. EPSC-DPS Joint Meeting 2019-38. Geneva, Switzerland. September 2019.

[5] *Comparison of Molecular Complexity Between Chondrites, Martian Meteorite and Lunar Soils,* Orthous-Daunay, F.-R., Wolters, C., Flandinet, L., Vuitton, V., Beck, P., Bonal, L., Isa, J., Moynier, F., Voisin, D., **Moran, S.E.,** Hörst, S.M., Danger, G., Vinogradoff, V., Piani, L., Bekaert, D., Tissandier, L., Isono, Y., Tachibana, S., Naraoka, H., Thissen, R. MetSoc2019, Sapporo, Japan. July 2019.

[4] *Liquid Chromatography Orbitrap Mass Spectrometry Study of Synthetic and Chrondritic Organic Mixtures,* Wolters, C., Vuitton, V., Orthous-Daunay, F.-R., Flandinet, L., He, C., **Moran, S.E.**, Hörst, S.M., Bekaert, D., Tissandier, L., Marty, B., Piani L. MetSoc2019, Sapporo, Japan. July 2019.

[3] *Laboratory Investigation of the Molecular Composition of (Exo-)Planetary Organic Aerosols*, Vuitton, V., Flandinet, L., Orthous-Daunay, F.-R., Wolters, C., Ayoub, H., Hörst, S.M., He, C., and **Moran, S.E.** AbSciCon2019, Bellevue, Washington. June 2019.

[2] *Disentangling the Planet from the Star in Late-type M Dwarfs: A Case Study of TRAPPIST-1g,* Wakeford, H.R., Lewis, N.K., Fowler, J. , Bruno, G., Wilson, T.J., **Moran, S.E.,** Valenti, J., Batalha, N.E., Filippazzo, J., Bourrier, V., Hörst, S.M., Lederer, S.M., de Wit, J. AAS 233, 103.05, Seattle, Washington. January 2019. Oral Presentation.

[1] *Titan's Oxygen Chemistry and its Impact on Haze Formation*, Vuitton, V., He, C., **Moran, S.E.,** Wolters, C., Flandinet, L., Orthous-Daunay, F.-R., Thissen, R., Hörst, S.M. AAS 232, 123.02, Denver, CO. June 2018. iPoster.

Professional Affiliations

Division for Planetary Sciences – American Astronomical Society
Laboratory Astrophysics Division – American Astronomical Society
American Geophysical Union
American Association for the Advancement of Science